TRƯỜNG ĐẠI HỌC THỦ ĐÔ HÀ NỘI
HANOI METROPOLITAN UNIVERSITY

TẠP CHÍ KHOA HỌC

SCIENCE JOURNAL OF HANOI METROPOLITAN UNIVERSITY

ISSN 2354-1504

SỐ 24 – KHOA HỌC TỰ NHIÊN VÀ CÔNG NGHỆ

THÁNG 6 – 2018

TẠP CHÍ KHOA HỌC TRƯỜNG ĐẠI HỌC THỦ ĐÔ HÀ NỘI
SCIENTIFIC JOURNAL OF HANOI METROPOLITAN UNIVERSITY
(Tạp chí xuất bản định kì 1 tháng/số)

Giấy phép hoạt động báo chí số 571/GP-BTTTT cấp ngày 26/10/2015
In 200 cuốn tại Trường ĐH Thủ đô Hà Nội. In xong và nộp lưu chiểu tháng 6/2018

MỤC LỤC

Trang

GALERKIN METHOD WITH CUBIC B - SPLINE FOR SOLUTION OF THE GRLW EQUATION

Nguyen Van Tuan[1], Nguyen Thu Thuy[2]
[1]*Hanoi Metropolitan University*
[2]*Hanoi Metropolitan University*

Abstract: *In this paper, numerical solution of the generalized regularized long wave (GRLW) equations are obtained by using Galerkinmethod with cubic B – splines. Applying the von – Neumann stability analysis, the proposed method is shown to be unconditionallystable. The numerical algorithm is applied to some test problems consisting of a single solitary wave for the GRLW equation and the RLW equation. The numerical result shows that the present method is a successful numerical technique for solving the GRLW equations.*

Keywords: *Galekin method; GRLW equation; RLW equation; cubic B-spline; finite difference.*

Email: nvtuan@daihocthudo.edu.vn
Received 16 April 2018
Accepted for publication 20 May 2018

1. INTRODUCTION

In this work, we consider the solution of the GRLW equation

$$u_t + \alpha u_x + \varepsilon u^p u_x - \mu u_{xxt} = 0, \tag{1}$$

$x \in [a, b], t \in [0, T]$, with the initial condition

$$u(x, 0) = f(x), x \in [a, b], \tag{2}$$

and the boundary condition

$$\begin{cases} u(a, t) = 0, u(b, t) = 0 \\ u_x(a, t) = u_x(a, t) = 0, \end{cases} \tag{3}$$

where $\alpha, \varepsilon, \mu, p$ are constants, $\mu > 0, \varepsilon > 0, p$ is an positive integer.

The equation (1)is called the generalized equal with wave (GEW) equation if $\alpha = 0$, the regularized long wave (RLW) equation or Benjamin – Bona – Mohony (BBM) equation if $\mu = 1, p = 1$, etc.

Equation (1) describes the mathematical model of wave formation and propagation in fluid dynamics, turbulence, acoustics, plasma dynamics, ect. So in recent years, researchers solve the GRLW and RLW equation by both analytic and numerical methods.

In this present work, we have applied Galerkin method with cubic B – spline to the GRLW equation and the RLW equation. This work is built as follow: in Section 2, numerical scheme is presented. The stability analysis of the method is established in Section 3. The numerical results are discussed in Section 4. In the last Section, Section 5, conclusion is presented.

2. GALERKINMETHOD WITH CUBIC B – SPLINE

The interval $[a, b]$ is partitioned in to a mesh of uniform length $h = x_{i+1} - x_i$ by the knots $x_i, i = \overline{0, N}$ such that

$$a = x_0 < x_1 < \cdots < x_{N-1} < x_N = b.$$

Our numerical study for the GRLW equation using the Galerkin method with cubic B-spline is to find an approximate solution $U(x, t)$ to exact solution $u(x, t)$ in the form

$$U(x,t) = \sum_{i=-1}^{N+1} \delta_i(t) B_i(x), \tag{4}$$

$B_i(x)$ are the quintic B-spline basis functions at knots, given by [10].

$$B_i(x) = \frac{1}{h^3}\begin{cases} (x - x_{i-2})^3, & x_{i-2} \le x \le x_{i-1} \\ h^3 + 3h^2(x - x_{i-1}) + 3h(x - x_{i-1})^2 - 3(x - x_{i-1})^3, & x_{i-1} \le x \le x_i \\ h^3 + 3h^2(x_{i+1} - x) + 3h(x_{i+1} - x)^2 - 3(x_{i+1} - x)^3, & x_i \le x \le x_{i+1} \\ (x_{i+2} - x)^3, & x_{i+1} \le x \le x_{i+2} \\ 0, & \text{otherwise.} \end{cases} \tag{5}$$

The value of $B_i(x)$ and its derivatives may be tabulated as in Table 1.

$$U_i = \delta_{i-1} + 4\delta_i + \delta_{i+1}$$

$$U'_i = \frac{3}{h}(-\delta_{i-1} + \delta_{i+1})$$

$$U''_i = \frac{6}{h^2}(\delta_{i-1} - 2\delta_i + \delta_{i+1}).$$

Table 1. *B_i, B'_i, and B''_i at the node points*

x	x_{i-2}	x_{i-1}	x_i	x_{i+1}	x_{i+2}
$B_i(x)$	0	1	4	1	0
$B'_i(x)$	0	$\frac{3}{h}$	0	$-\frac{3}{h}$	0
$B''_i(x)$	0	$\frac{6}{h^2}$	$-\frac{12}{h^2}$	$\frac{6}{h^2}$	0

From (5) we see that, for cubic B – spline $B_i(x)$ covers four finite interval, so each interval $[x_i, x_{i+1}]$is covered by four splines. Assumethat $h\eta = x - x_i,\ \eta \in [0,1]$. Hence, the cubic B – spline (5) depending on variable $\eta \in [0,1]$ are defined

$$\begin{cases} B_{i-1}(\eta) = (1-\eta)^3, B_i(\eta) = 1 + 3(1-\eta) + 3(1-\eta)^2 - 3(1-\eta)^3 \\ B_{i+1}(\eta) = 1 + 3\eta + 3\eta^2 - 3\eta^3, B_{i+2}(\eta) = \eta^3. \end{cases} \quad (6)$$

Now, each interval $[x_i, x_{i+1}], i = 0, \ldots, N-1$ we have

$$U(\eta, t) = \sum_{j=i-1}^{i+2} \delta_j(t) B_j(\eta),\ i = 0, \ldots, N-1, \eta \in [0,1]\,. \quad (7)$$

The nodal values of element of U, U', U'' are defined as follows

$$U_i = \delta_{i-1} + 4\delta_i + \delta_{i+1}$$
$$U'_i = 3(-\delta_{i-1} + \delta_{i+1})$$
$$U''_i = 6(\delta_{i-1} - 2\delta_i + \delta_{i+1}).$$

When applying the Galerkin's approach with weight function w(x) to Eq. (1), we get

$$\int_a^b w(u_t + \alpha u_x + \varepsilon u^p u_x - \mu u_{xxt})dx = 0. \quad (8)$$

Implementing the change of variable x to integral (6), we have

$$\int_0^1 w\left(u_t + \frac{\alpha}{h}u_\eta + \frac{\varepsilon}{h}u^p u_\eta - \frac{\mu}{h^2}u_{\eta\eta t}\right)d\eta = 0. \quad (9)$$

Applying partial integration one to (7), this leads to the following equality:

$$\int_0^1 w\left(u_t + \frac{\alpha+\gamma}{h}u_\eta + \beta w_\eta u_{\eta t}\right)d\eta = \beta w\, u_{\eta t}\Big|_0^1, \quad (10)$$

where $\gamma = \varepsilon u^p, \beta = \frac{\mu}{h^2}$. Substituting cubic B – splines (6) instead of the weigh function w(x) and trial function (7) into (10), we get

$$\sum_{j=m-1}^{m+2}\left[\left(\int_0^1 B_i B_j + \beta B'_i B'_j\right)d\eta - \beta B_i B'_j\Big|_0^1\right]\dot{\delta}_j^e + \sum_{j=m-1}^{m+2}\left(\frac{\alpha+\gamma}{h}\int_0^1 B_i B'_j d\eta\right)\delta_j^e = 0, \quad (11)$$

where m = 0, …, N-1. Assume that $\delta^e = (\delta_{m-1}, \delta_m, \delta_{m+1}, \delta_{m+2})^T, m = 0, \ldots, N-1$, and the dot states differentiation to t, which can be written in matrix form by

$$[A^e + \beta(B^e - C^e)]\dot{\delta}_j^e + \frac{\alpha+\gamma}{h}D^e\delta^e = 0, \quad (12)$$

where

$$A_{ij}^e = \int_0^1 B_i B_j d\eta = \frac{1}{140}\begin{pmatrix} 20 & 129 & 60 & 1 \\ 129 & 1188933 & & 60 \\ 60 & 9331188 & & 129 \\ 1 & 60 & 129 & 20 \end{pmatrix}$$

$$B_{ij}^e = \int_0^1 B'_i B'_j d\eta = \frac{1}{10}\begin{pmatrix} 18 & 21 & -36 & -3 \\ 21 & 102-87 & & -36 \\ -36 & -87102 & & 21 \\ -3 & -36 & 21 & 18 \end{pmatrix}$$

$$C_{ij}^e = B_i B'_j \Big|_0^1 = \frac{1}{140}\begin{pmatrix} 1 & 0 & -1 & 0 \\ 4 & -1 & -4 & 1 \\ 1 & -4 & -1 & 4 \\ 0 & -1 & 0 & 1 \end{pmatrix}$$

$$D_{ij}^e = \int_0^1 B_i B'_j d\eta = \frac{1}{140}\begin{pmatrix} -10 & -9 & 18 & 1 \\ -71 & -150 & 183 & 38 \\ -38 & -183 & 150 & 71 \\ -1 & -18 & 9 & 10 \end{pmatrix}$$

i, j = m – 1, m, m + 1, m + 2, $\gamma = \varepsilon\left(\frac{u_{m+1}+u_m}{2}\right)^p = \frac{\varepsilon}{2^p}(\delta_{m-1} + 4\delta_m + \delta_{m+1})^p$.

From Eq. (12), $m = 0, \dots, N-1$, we can see that

$$[A + \beta(B - C)]\dot{\delta}^e + \frac{\alpha+\gamma}{h} D^e \delta^e = 0, \tag{13}$$

where $\delta = (\delta_{-1}, \dots, \delta_{N+1})^T$. The A, B, C and D are septadiagonal matrices and their line of m is

$$A = \frac{1}{140}(1,120,1191,2416,1191,120,1), B = \frac{1}{10}(-3,-72,-45,240,-45,-72,-3)$$

$$C = (0,0,0,0,0,0,0), \qquad D = \frac{1}{20}(-1,-56,-245,0,245,56,1)$$

$$\gamma D = \frac{1}{20}(-\gamma_1, -18\gamma_1 - 38\gamma_2, -9\gamma_1 - 183\gamma_2 - 71\gamma_3, 10\gamma_1 + 150\gamma_2 - 150\gamma_3 - 10\gamma_4, 71\gamma_2 + 183\gamma_3 - 9\gamma_4, 38\gamma_3 + 14\gamma_4, \gamma_4)$$

where

$$\gamma_1 = \frac{\varepsilon}{2^p}(\delta_{m-2} + 5\delta_{m-1} + 5\delta_m + \delta_{m+1})^p, \gamma_2 = \frac{\varepsilon}{2^p}(\delta_{m-1} + 5\delta_m + 5\delta_{m+1} + \delta_{m+2})^p,$$

$$\gamma_3 = \frac{\varepsilon}{2^p}(\delta_m + 5\delta_{m+1} + 5\delta_{m+2} + \delta_{m+3})^p, \gamma_4 = \frac{\varepsilon}{2^p}(\delta_{m+1} + 5\delta_{m+2} + 5\delta_{m+3} + \delta_{m+4})^p.$$

Because $\dot{\delta} = \frac{1}{\Delta t}(\delta^{n+1} - \delta^n), \delta = \frac{1}{2}(\delta^{n+1} + \delta^n)$, from (13) we obtain the matrix system

$$\left[A + \beta(B - C) + \frac{(\alpha+\gamma)\Delta t}{2h} D\right]\delta^{n+1} = \left[A + \beta(B - C) - \frac{(\alpha+\gamma)\Delta t}{2h} D\right]\delta^n. \tag{14}$$

Using the boundary conditions given by Eq. (3), the $(N + 3) \times (N + 3)$system (14) is reduced to $(N + 1) \times (N + 1)$ matrix system. Since the row m of A, B, C and D has seven element, we have

$$a_1\delta_{m-3}^{n+1} + a_2\delta_{m-2}^{n+1} + a_3\delta_{m-1}^{n+1} + a_4\delta_m^{n+1} + a_5\delta_{m+1}^{n+1} + a_6\delta_{m+2}^{n+1} + a_7\delta_{m+3}^{n+1} = \\ = a_7\delta_{m-3}^n + a_6\delta_{m-2}^n + a_5\delta_{m-1}^n + a_4\delta_m^n + a_3\delta_{m+1}^n + a_2\delta_{m+2}^n + a_1\delta_{m+3}^n \tag{15}$$

where

$$a_1 = \frac{1}{140} - \frac{3\beta}{10} + \frac{(\alpha+\gamma_1)\Delta t}{40h}, a_2 = \frac{120}{140} - \frac{72\beta}{10} - \frac{(56\alpha + 18\gamma_1 + 38\gamma_2)\Delta t}{40h}$$

$$a_3 = \frac{1191}{140} - \frac{45\beta}{10} + \frac{(-245\alpha + 9\gamma_1 - 183\gamma_2 - 71\gamma_3)\Delta t}{40h}$$

$$a_4 = \frac{2416}{140} + \frac{240\beta}{10} + \frac{(10\gamma_1 + 150\gamma_2 - 150\gamma_3 - 10\gamma_4)\Delta t}{40h}$$

$$a_5 = \frac{1191}{140} - \frac{45\beta}{10} + \frac{(245\alpha + 71\gamma_2 + 183\gamma_3 - 9\gamma_4)\Delta t}{40h}$$

$$a_6 = \frac{120}{140} - \frac{72\beta}{10} - \frac{(56\alpha + 18\gamma_4 + 38\gamma_3)\Delta t}{40h}$$

$$a_7 = \frac{1}{140} - \frac{3\beta}{10} + \frac{(\alpha+\gamma_4)\Delta t}{40h}.$$

The algorithm is then used to solve the system (7). We apply first the intial condition

$$U(x,0) = \sum_{i=-1}^{N+1} \delta_i^0 B_i(x), \tag{16}$$

then we need that the approximately solution is satisfied folowing conditions

$$\begin{cases} U(x,0) = f(x) \\ U(a,t) = 0, U(b,t) = 0 \\ U_x(a,t) = U_x(a,t) = 0, \end{cases} \tag{17}$$

Eliminating $\delta_{-1}^0, \delta_{N+1}^0$ from the system (17), we get

$$E\delta^0 = r,$$

where E is the three-diagonal matrix given by

$$E = \begin{pmatrix} 2 & 1 & 0 & 0 & 0 & 0 & \dots & 0 \\ 1 & 4 & 1 & 0 & 0 & 0 & \dots & 0 \\ 0 & 1 & 4 & 1 & 0 & 0 & \dots & 0 \\ \dots & & \dots & & & \dots & & \\ \dots & & \dots & & & \dots & & \\ 0 & \dots & 0 & 0 & 1 & 4 & 1 & 0 \\ 0 & \dots & 0 & 0 & 0 & 1 & 4 & 1 \\ 0 & \dots & 0 & 0 & 0 & 0 & 1 & 2 \end{pmatrix}.$$

and $\delta^0 = (\delta_0^0, \delta_1^0, \dots, \delta_N^0)^T, r = (f(x_0), f(x_1), \dots, f(x_N))^T$.

3. STABILITY ANALYSIS

To apply the Von-Neumann stability for the system (6), we must first linearize this system.

We have

$$\delta_j^n = \xi^n \exp(i\theta jh), i = \sqrt{-1}, \tag{18}$$

where θ is the mode number and h is the element size.

Being applicable to only linear schemes the nonlinear term U^pU_x is linearized by taking U as a locally constant. The linearized form of proposed scheme is given as

$$a_1\xi^{n+1}e^{i(m-3)\theta h} + a_2\xi^{n+1}e^{i(m-2)\theta h} + a_3\xi^{n+1}e^{i(m-1)\theta h} + a_4\xi^{n+1}e^{im\theta h} + a_5\xi^{n+1}e^{i(m+1)\theta h} + a_6\xi^{n+1}e^{i(m+2)\theta h} + a_7\xi^{n+1}e^{i(m+3)\theta h} = a_7\xi^n e^{i(m-3)\theta h} + a_6\xi^n e^{i(m-2)\theta h} + a_5\xi^n e^{i(m-1)\theta h} + a_4\xi^n e^{im\theta h} + a_3\xi^n e^{i(m+1)\theta h} + a_2\xi^n e^{i(m+2)\theta h} + a_1\xi^n e^{i(m+3)\theta h} \tag{19}$$

Simplifying Eq. (13), we get

$$\xi = \frac{A_1 - iB_1}{A_1 + iB_1},$$

where

$$A_1 = (a_7 + a_1)\cos(3\phi) + (a_6 + a_2)\cos(2\phi) + (a_5 + a_3)\cos\phi + a_4,$$
$$B_1 = (a_7 - a_1)\cos(3\phi) + (a_6 - a_2)\cos(2\phi) + (a_5 - a_3)\cos\phi.$$
$$\phi = \theta h.$$

It is clear that $|\xi| = 1$.

Therefore, the linearized numerical scheme for the GRLW equation is unconditionally stable.

4. NUMERICAL EXAMPLE

We now obtain the numerical solution of the GRLW equation for some problems. To show the efficiency of the present method for our problem in comparison with the exact solution, we report L_∞ and L_2 using formula

$$L_\infty = \max_i |U(x_i, t) - u(x_i, t)|,$$
$$L_2 = \left(h\sum_i |U(x_i, t) - u(x_i, t)|^2\right)^{\frac{1}{2}},$$

where U is numerical solution and u denotes exact solution.

Three invariants of motion which correspond to the conservation of mass, momentum, and energy are given as

$$I_1 = \int_a^b u dx, I_2 = \int_a^b (u^2 + \mu u_x^2) dx, I_3 = \int_a^b (u^4 - \mu u_x^2) dx.$$

The exact solution of the GRLW is [5]

$$u(x,t) = \left[\frac{(p+1)(p+2)(c-\alpha)}{2\varepsilon} \operatorname{sech}^2 \left(\frac{p}{2} \sqrt{\frac{c-\alpha}{\mu c}} (x - x_0 - ct) \right) \right]^{\frac{1}{p}},$$

where c is positive constant, x_0 is arbitrary constant.

In the tests problems, we choose$f(x) = u(x, 0)$.

We take $p = 2, \alpha = 1, \varepsilon = 6, \mu = 1, a = 0, b = 100, x_0 = 40, \Delta t = 0.025 h = 0.2, c = 2, t \in [0, 10]$.The values of the variants and the error norms at several times are listed in Table 2. From Table 2, we see that, changes of variants I_1, I_2 and $I_3$from their initial value are less than 0.02, 0.02 and 0.03, respectively. The error nomrs L_2, L_∞ are less than 0.008 and 0.004, respectively. Error graphs are shown in figure 1 at t = 0, 5 and t = 10.

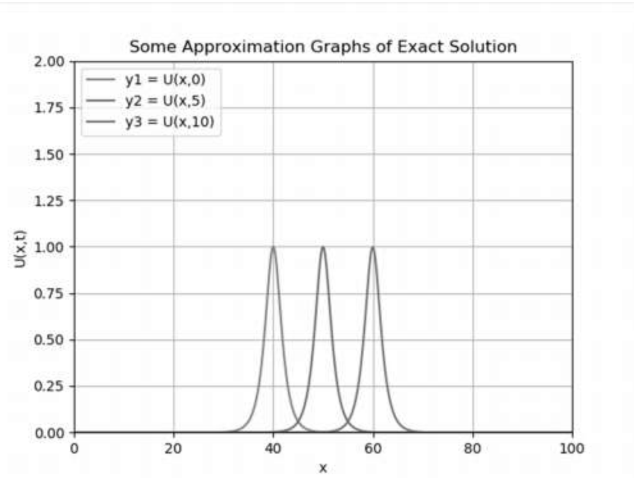

Figure 1*. Single solitary wave with*

$p = 2, c = 2, \alpha = 1, \varepsilon = 6, a = 0, b = 100, x_0 = 40, \Delta t = 0.025$, *t = 0, 5, 10*

When $p = 2, \alpha = 1, \varepsilon = 6, \mu = 1, a = 0, b = 100, x_0 = 40, \Delta t = 0.01 h = 0.1, c = 1.3, t \in [0, 20]$. The values of the variants and the error norms at several times are listed in Table 3.In Table 3, changes changes of variants $I_1 \times 10^4, I_2 \times 10^3$ and $I_3 \times 10^4$from their initial value are less than 0.9, 0.1 and 0.1, respectively. The error nomrs L_2, L_∞ are less than 0.30499×10^{-3} and 0.6×10^{-4}, respectively. The plot of the estimated solution at time t = 0, 5, 10 in figure 2.

***Table 2**. Variants and error norms of the GRLW equation with* $p = 2, \alpha = 1,$
$\varepsilon = 6, \mu = 1, a = 0, b = 100, x_0 = 40, \Delta t = 0.025, h = 0.2, t \in [0, 10]$

t	0	2	4	6	8	10
I_1	4.442883	4.440755	4.438610	4.436467	4.434329	4.432197
I_2	2.847283	2.843751	2.840609	2.837706	2.834883	2.832098
I_3	1.866762	1.863292	1.859375	1.855237	1.851048	1.846854
$L_2 \times 10^3$	0	1.692562	2.750986	5.967200	11.330402	18.583061
$L_\infty \times 10^3$	0	1.107770	1.782894	4.073369	7.272741	11.376977

***Table 3**. Variants and error norms of the GRLW equation with* $p = 2, \alpha = 1,$
$\varepsilon = 6, \mu = 1, a = 0, b = 100, x_0 = 40, \Delta t = 0.01, h = 0.1, t \in [0, 20]$

t	0	4	8	12	16	20
I_1	3.581967	3.851952	3.581937	3.581923	3.581908	3.581893
I_2	1.249960	1.249937	1.249916	1.249900	1.249885	1.249871
I_3	0.248839	0.248845	0.248849	0.248848	0.248845	0.248842
$L_2 \times 10^4$	0	1.1928760	1.854964	2.335763	2.726010	3.049922
$L_\infty \times 10^4$	0	0.734902	1.003855	1.207699	1.378303	1.525412

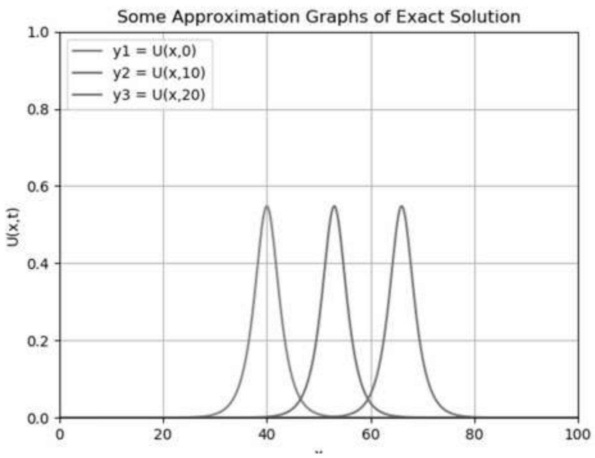

***Figure 2**. Single solitary wave with*

$$p = 2, c = 1.3, h = 0.1, \alpha = 1, \varepsilon = 6, \mu = 1, a = 0,$$

$$b = 100, x_0 = 40, \Delta t = 0.01, t = 0, 5, 10$$

We take $p = 3, c = 1.8, h = 0.2, \alpha = 1.5, \varepsilon = 7, \mu = 1, a = 0, b = 100, x_0 = 40, \Delta t = 0.025$. The variants and error norms are listed in Table 4. In this table, we get, the changes of variants $I_1 \times 10^2, I_2 \times 10$ and $I_3 \times 10$ from their initial values are less than 0.5, 0.1 and 0.2, respectively. The error nomrs $L_2$and L_∞ are less than 5.242345×10^{-4} and0.602344×10^{-4}, respectively.

When we choose the parameters $p = 3, c = 1.21, h = 0.1, \alpha = 1.2, \varepsilon = 278, \mu = 1, a = 0, b = 100, x_0 = 40, \Delta t = 0.01.$ The values of the variants and the error norms at several times are listed in Table 5. From Table 5, we see that, the changes of variants $I_1 \times 10^2, I_2 \times 10^2$and $I_3 \times 10^2$from their initial values are less than 0.2, 0.3 and 0.2, respectively. The error nomrs L_2 and L_∞ are less than 0.2×10^{-2} and 0.7×10^{-3}, respectively.

Table 4*. Variants and error norms of the GRLW equation with* $p = 3, \alpha = 1.5, \varepsilon = 7, \mu = 1, a = 0, b = 100, x_0 = 40, \Delta t = 0.025, h = 0.2, t \in [0, 10]$

t	0	2	4	6	8	10
I_1	5.179062	5.178759	5.178455	5.178149	5.177842	5.177535
I_2	2.408354	2.407931	2.407505	2.407103	2.406719	2.406346
I_3	0.880978	0.880785	0.800624	0.800422	0.880186	0.879923
$L_2 \times 10^3$	0	0.802979	1.347870	1.734118	1.999404	2.156209
$L_\infty \times 10^3$	0	0.546362	0.799050	0.968823	1.085402	1.153859

Table 5*. Variants and error norms of the GRLW equation with* $p = 3, \alpha = 1.2, \varepsilon = 278, \mu = 1, a = 0, b = 100, x_0 = 40, \Delta t = 0.01, h = 0.1, t \in [0, 20]$

t	0	4	8	12	16	20
I_1	2.156002	2.169113	2.181860	2.192123	2.196968	2.193693
I_2	0.095914	0.095967	0.096024	0.096076	0.096103	0.096081
I_3	0.000312	0.000312	0.000112	0.000312	0.000312	0.000312
$L_2 \times 10^3$	0.866147	2.332274	5.071251	7.637045	9.587245	10.992184
$L_\infty \times 10^3$	2.703610	3.629625	3.871343	3.611625	3.109749	2.862487

We choose thequantitiesp $= 8, c = 1.03, h = 0.1, \alpha = 1, \varepsilon = 6, \mu = 1, a = 0, b = 100, x_0 = 40, \Delta t = 0.01.$ The numerical computation are done up to t = 20. The obtained results are given in Table 6 which clearly shows that the changes of the variants $I_1 \times 10, I_2 \times 10^3$ and $I_3 \times 10^6$from their initial value are less than 0.5, 0.2 and 0.3, respectively. The error nomrs L_2, L_∞ are less than 0.011 and 0.0012, respectively. Solitary wave profiles are depicted at time levels in Figure 3.

Table 6. Error norms for single solitary wave for the wave of the GRLW equation with $p = 8, \alpha = 1, \varepsilon = 6, \mu = 1, a = 0, b = 100, x_0 = 40, \Delta t = 0.01, t \in [0, 20]$

t	0	5	10	15	20
I_1	11.310061	11.315842	11.321569	11.326921	11.327968
I_2	5.291757	5.291739	5.291719	5.291698	5.291671
I_3	2.181899	2.181908	2.181954	2.182018	2.182092
$L_2 \times 10^3$	0.307304	1.202922	2.554735	3.682438	4.489347
$L_\infty \times 10^3$	0.971254	1.535357	1.626896	1.467989	1.257064

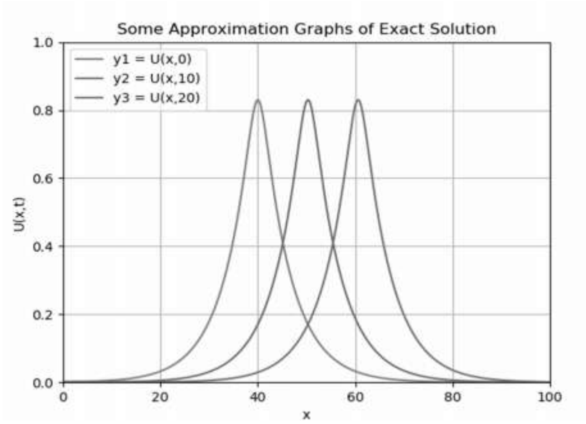

Figure 3*. Single solitary wave with* $p = 8, c = 1.03, h = 0.1, \alpha = 1, \mu = 1, \varepsilon = 6, a = 0, b = 100, x_0 = 40, \Delta t = 0.01$*, t = 0, 5, 10*

Finally, we choose thethe parametersp $= 1, c = 1.03, h = 0.1, \alpha = 1, \varepsilon = 6, \mu = 1, a = 0, b = 100, x_0 = 40, \Delta t = 0.01$, for solving the RLW equation. The numerical computation are done up to t = 20. The variants and error norms are listed in Table 7. In this table, we get, the changes of variants $I_1 \times 10^5, I_2 \times 10^5$and $I_3 \times 10^6$from their initial values are less than 0.3, 0.3 and 0.4, respectively. The error nomrs L_2 and L_∞ are less than 1.8×10^{-5} and 0.8×10^{-5}, respectively.

t	0	4	8	12	16	20
I_1	1.248999	1.248999	1.248999	1.248998	1.248998	1.248997
I_2	0.124958	0.124957	0.124957	0.124957	0.124957	0.124956
I_3	0.001869	0.001869	0.001869	0.001869	0.001869	0.001869
$L_2 \times 10^6$	0	8.549214	14.228561	18.383282	22.266543	26.328942
$L_\infty \times 10^6$	0	3.537749	5.399335	7.024708	9.034782	11.037470

5. CONCLUSIONS

In this work, we have used the Galerkin method with cubic B - spline for solution of the GRLW equation and the RLW equation. We tasted our scheme through single solitary wave and the obtained results are tabulaces. These tables show that, the changes of variants are quite small. The error norms L_2, L_∞ for the GRLW equation are acceptable. So the present method is more capable for solving these equations.

REFERENCES

1. S. S. Askar and A. A. Karawia (2015), "On solving pentadiagonal linear systems via transformations", *Mathematical Problems in Engineering*, Vol. **2015**, pp. 1-9.
2. S. Battal Gazi Karakoça, Halil Zeybek (2016), "A cubic B – spline Galerkin approach for the numerical simulation of the GEW equation", *Statistics, Optimization and Information Computing*, Vol. **4**, pp. 30-41.
3. D. J. Evans and K. R. Raslan (2005), "Solitary waves for the generalized equal width (GEW) equation", *International J. of Computer Mathematics*, Vol. **82(4)**, pp. 445-455.
4. C. M. García - Lospez, J. I. Ramos (2012), "Effects of convection on a modified GRLW equation", *Applied Mathematics and Computation*, Vol. **219**, pp. 4118-4132.
5. C. M. García - Lospez, J. I. Ramos(2015), "Solitari waves generated by bell - shaped initial conditions in the invicis and viscous GRLW equations", *Applied Mathematical Modelling*, Vol. **39 (21)**, pp. 6645-6668.
6. S. Islam, F. Haq and I. A. Tirmizi (2010), "Collocation method using quartic B-spline for numerical solution of the modified equal width wave equation", *J. Appl. Math.Inform.*, Vol. **28(3 - 4)**, pp. 611-624.
7. A. G. Kaplan, Y. Dereli (2017), "Numerical solutions of the GEW equation using MLS collocation method", *International Journal of Modern Physics C*, Vol. **28(1), 1750011**, pp. 1-23.
8. M. Mohammadi, R. Mokhtari(2011), "Solving the generalized regularized long wave equation on the basis of a reproducing kernel space", *J. of Computation and Applied Mathematics*, Vol. **235**, pp. 4003-4014.
9. E. Pindza and E. Maré (2014), "Solving the generalized regularized long wave equation using a distributed approximating functional method", *International Journal of Computational Mathematics*, Vol. **2014**, pp. 1-12.
10. P. M. Prenter (1975), "Splines and Variational Methods", *Wiley, New York*.
11. T. Roshan(2011), "A Petrov – Galerkin method for solving the generalized equal width (GEW) equation", *J. Comput. Appl. Math.*, Vol. **235**, pp. 1641-1652.
12. T. Roshan (2012), "A Petrov – Galerkin method for solving the generalized regularized long wave (GRLW) equation", *Computers and Mathematics with Applications*, Vol. **63**, pp. 943-956.

13. M. Zarebnia and R. Parvaz (2013), "Cubic B-spline collocation method for numerical solution of the Benjamin - Bona - Mahony - Burgers equation", *International Journal of Mathematical, Computational, Physical, Electrical and Computer Engineering*, Vol. **7 (3)**, pp. 540-543.

14. H. Zeybek and S. Battal Gazi Karakoça (2017), "Application of the collocation method with B - spline to the GEW equation", *Electronic Transactions on Numerical Analysis*, Vol. **46**, pp. 71-88.

15. L. Zhang (2005), "A finite difference scheme for generalized regularized long wave equation", *Applied Mathematics and Computation*, Vol. **168**, pp. 962-972.

PHƯƠNG PHÁP GALERKIN VỚI B – SPLINE BẬC 3 GIẢI PHƯƠNG TRÌNH GRLW

Tóm tắt: *Trong bài báo này, nghiệm số của phương trình GRLW, RLW sẽ tìm được dựa trên cơ sở phương pháp galerin với B – spline bậc 3. Sử dụng phương pháp Von – Neumann chứng minh được hệ phương trình sai phân ổn định vô điều kiện. Thuật toán được với sóng đơn được áp dụng giải một số ví dụ. Kết quả số chứng tỏ phương pháp đưa ra hữu hiệu để giải các loại phương trình trên.*

Từ khóa: *Phương trình GRLW, phương trình RLW, spline bậc 3, phương pháp Galerkin, phương pháp sai phân hữu hạn.*

DIAGONALIZING SQUARE MATRICES BASING ON LINEAR OPERATORS

Hoang Ngoc Tuyen
Hanoi Metropolital University

Abstract: *When studying about structures of vector spaces, we do not study separately but consider them in relations. The tools to define these relations are linear mappings. And, the effective tools contributing in defining linear mappings are matrices.*

There is a class of self-linear mappings of a vector space (with finite generation). It is said to be linear Operator or linear Transformation. Linear Operators and Matrices are closedly related since linear operators are defined by matrices. Conversely, for each square matric, there is a linear operator having a represented matrix which is the original square matric.

In this article, we mention the simplest square matrics (diagonal form) and the problem of diagonalizing a square matric as well as the condition for a square matric to be diagonalizable basing on linear operator. We show that the above relation is a ring isomorphism among linear operators of space L(E) and rings of square matrices $Mat_n(K)$.

Keywords: *Operator, Matric, basis, diagonalization...*

Email: hntuyen@daihocthudo.edu.vn
Received 22 April 2018
Accepted for publication 25 May 2018

1. INTRODUCTION

In this article, we assume E and F are vetor spaces (with finite generation) over some field K.

2. SOME EFECTIVE KNOWLEDGE

2.1. Linear mapping

Each mapping: $\varphi : E \to F$ is said to be linear if

$$\varphi(x+y) = \varphi(x) + \varphi(y)$$
$$\varphi(ax) = a\varphi(x); \forall x, y \in E, a \in K$$

Therefore, linear mappings preserve addition and scalar product.

Examples:

The followings are linear mappings

1. Identity mapping:

$$id_E : E \to E$$
$$id_E(x) = x; \forall x \in E$$

2. Mapping $\varphi : K^n \to K^m, (n \geq m)$ satisfying

$$\varphi(a_1,...,a_n) = (a_1,...,a_m)$$

Is the projection from K^n on K^m

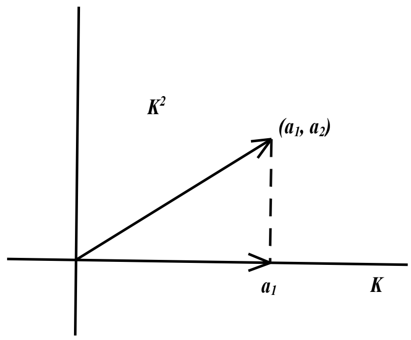

Figure 1: The projection from K^2 on K

3. Mapping $\varphi : K^n \to K^n$ satisfying

$$\varphi(a_1,...,a_i,...,a_j,...,a_n) = (a_1,...,a_j,...,a_i,...,a_n)$$

Is a face reflection $a_i = a_j$ of the space K^n

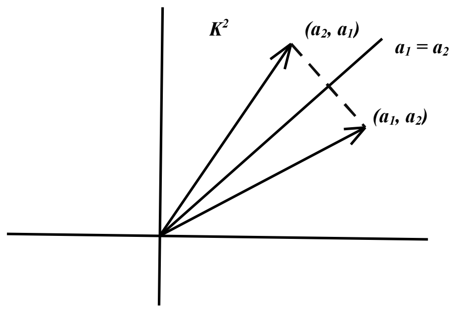

Figure 2: The reflection K^2 over face $a_1 = a_2$

2.2. Matrices of linear mappings

Assume $\varphi : E \to F$ is a linear mapping. Fix 2 basises $S \subset E; T \subset F$:

$$S = (s_1,...,s_n); T = (t_1,....t_m)$$

The image set $\varphi(S)$: $\varphi(s_1) = a_{11}t_1 + ... + a_{m1}t_m$

....

$$\varphi(s_n) = a_{1n}t_1 + ... + a_{mn}t_m$$

We say that $m \times n$ matrices $A := (a_{ij}); i = 1,...,m; j = 1,...,n$ are represented matrixes of φ (according 2 basises S and T).

Hence, to define the represented matrix of φ (according S and T), we just need to combine coordinate columns according T of image vector in the set φ(S):

$$A = \begin{bmatrix} a_{11} & ... & a_{1n} \\ ... & ... & ... \\ a_{m1} & ... & a_{mn} \end{bmatrix}$$

Examples:

1. The represented matrix of identity mapping id_E is the unit matric with respect to any basis of E.

$$[id_E] = \begin{bmatrix} 1 & 0 & ... & 0 \\ 0 & 1 & ... & ... \\ ... & ... & ... & 0 \\ 0 & 0 & ... & 1 \end{bmatrix}$$

2. The projection mapping $\varphi : K^n \to K^m, (n \geq m)$ satisfying:

$\varphi(a_1,...,a_n) = (a_1,...,a_m)$

Let S and T be 2 basises of K^n and K^m

Then:

$$\begin{cases} \varphi(e_i) = t_i; & i = 1,...,m \\ \varphi(e_i) = 0; & i = m+1,...,n \end{cases}$$

And the matric of φ is:

$$[\varphi] = \begin{bmatrix} 1 & 0 & ... & 0 & ... & 0 \\ 0 & 1 & ... & 0 & ... & 0 \\ ... & ... & ... & ... & ... & ... \\ 0 & 0 & ... & 1 & ... & 0 \end{bmatrix} \text{(order } m \times n\text{)}$$

Comment: If we identify the elements of E and F with their coordinate columns on the basis of S and T, then all linear maps from E to F are defined by the multiplication of the matrix represented by the vector of E.

Theorem 2.2.1

Let A be a matric. We have $\varphi(x) = Ax$ for all $x \in E$ if and only if A is represented matrix of φ.

Proof: If A is represented matrix of φ then $\varphi(x_j)$ is j –th column of A (j = 1,..,n). Then $\varphi(x_j) = Ax_j$. For all $x \in E;\ x = a_1x_1 + ... + a_nx_n$, we have:

$$\begin{aligned}\varphi(x) &= a_1\varphi(x_1) + ... + a_n\varphi(x_n)\\ &= a_1(Ax_1) + ... + a_n(Ax_n)\\ &= A(a_1x_1) + ... + A(a_nx_n) = Ax\end{aligned}$$

Conversely, assume $A = (a_{ij})$ and $\varphi(x) = Ax$, for all $x \in E$

Since x_j has the coordinate on S which is $x_j = (0,...,1,...,0)$ (1 is the j-th) then Ax_j has result at j-th column of A. Then:

$$\varphi(x_j) = a_{1j}y_1 + ... + a_{mj}y_m; (j = 1,...,n)$$

Basing on the definition, A is the represented matrix of φ

2.3. Linear operator and represented matrix of linear operator

Each linear mapping from the space E on E is called a linear operator of E.

A linear operator of E is also said to be a linear transformation on E.

Then, linear operator is the special case of linear mapping when E = F.

To define matrices of linear operators of the space E, we just need fix a basis $S \subset E$. If dimE = n then we also say that the square matric $\left[a_{ij}\right] / (i; j = 1,...,n)$ is the represented matrix of φ according the basis S

Examples

Linear operators and Represented matrix es.

1. Identity mapping in the above examples and its represented matrix is the unit matric order n with respect to any basis of E

$$\begin{bmatrix} 1 & 0 & ... & 0\\ 0 & 1 & ... & 0\\ 0 & 0 & ... & 0\\ 0 & 0 & ... & 1 \end{bmatrix}$$

2. The projection on the line $a_2 = 0$ of the space K^2:

$$\varphi(a_1;a_2) = (a_1;0)$$

The matric of the projection according basis systems of the plane K^2 is

$$\begin{bmatrix} 1 & 0 \\ 0 & 0 \end{bmatrix}$$

3. The reflection over the line $a_1 = a_2$ of the space K^2:

$$\varphi(a_1;a_2) = (a_2;a_1)$$

The matric of φ *according the basis of* K^2 is

$$\begin{bmatrix} 0 & 1 \\ 1 & 0 \end{bmatrix}$$

Theorem 2.3.1

The correspondence among linear operators and their matrices is an isomorphism amoL(E) and $Mat_n(K)$

Proof: Since L (E) and $Mat_n(K)$ are two vector spaces, dimL(E) = dim$Mat_n(K)$= n^2 then the above correspondence defines an isomorphism among two spaces. This correspondence preserves the multiplication and the matrix of the product of the two linear operators, which is the product of the two matrixes of the linear operators.

However, the matrix of a linear operator also changes as we change the basis.

Theorem 2.3.2

Let S and T be two basis of the vector space E and P is the matric transformed from S to T. If A and B are presented matrix of the linear operator φ of E then.

$$B = P^{-1}AP$$

Proof: This is the special case of linear mapping when $E = F$

and $S_1 = S_2 = S$, $T_1 = T_2 = T$ with $P_1 = P_2 = P$

Example

Let φ be a linear operator of the space E. The represented matrix of φ with respect to $S = (x_1, x_2)$ is:

$$A = \begin{bmatrix} 4 & 3 \\ -1 & 1 \end{bmatrix}$$

Assume $T = (y_1, y_2)$ is also a basis of E

$$y_1 = x_1 - 2x_2$$
$$y_2 = -x_1 + x_2$$

Now, we want to find represented matrix of φ with respect to basis T.

By presenting vectors in T according S, we have the matric changing basis from S to T:

$$P = \begin{bmatrix} 1 & -1 \\ -2 & 1 \end{bmatrix}$$

And the inverse of P:

$$P^{-1} = -\begin{bmatrix} 1 & 1 \\ 2 & 1 \end{bmatrix} = \begin{vmatrix} -1 & -1 \\ -2 & -1 \end{vmatrix}$$

And the represented matrix of φ in basis T:

$$B = P^{-1}AP = \begin{bmatrix} -1 & -1 \\ -2 & -1 \end{bmatrix}\begin{bmatrix} 4 & 3 \\ -1 & 1 \end{bmatrix}\begin{bmatrix} 1 & -1 \\ -2 & 1 \end{bmatrix} = \begin{bmatrix} 5 & -1 \\ 7 & 0 \end{bmatrix}$$

The above theorem allows us to classify the matrix of linear operators by the following concept:

2.4. Concept of similar matrices

Two square matrices A and B with same order is said to be similar (Denoted by $A \approx B$) If there exists an inversible matric P such that

$$B = P^{-1}AP$$

Similar relation is an equivalent relation among matrices.

According the above examples, 2 matrices

$$A = \begin{bmatrix} 4 & 3 \\ -1 & 1 \end{bmatrix} \text{ and } B = \begin{bmatrix} 5 & -1 \\ 7 & 0 \end{bmatrix}$$

Is similar (over K)

Two square matrices is similar if and only if they are represented matrixes of the same operator.

Indeed, if A and B are represented matrix es of the same operator then $A \approx B$ basing on theorem 1.3.2

Conversely, assume $B = P^{-1}AP$ for P is inversible.

Let A be the represented matrix of the linear operator φ of space E according a basis S. Then, we can choose a basis T in E such that matric transformed from S to T is P. Basing on the theorem 1.3.2 then B must be the represented matrix of φ according the basis T.

The above concept gives us an interesting view of the relation among two matrices of a linear operator in two different basises.

For each linear operator of E, when fixing a basis $(S) \subset E$ we can identify φ with a matric, A: $\forall x \in E : \varphi(x) = Ax$

3. STRUCTURE OF LINEAR OPERATOR

3.1. Stable space

Let $\varphi : E \to E$ be a linear operator of E.

The study over the whole space E is difficult (since E is too large). To resolve that, we restrict φ on a subspace E' of E. However, to preserve that φ still is the linear operator of the space E', the subspace E' must have a special property. It's a stable subspace:

The subspace E' of E is called a stable space with respect to φ if $\varphi(E') \subseteq E'$.

For any linear operator $\varphi : E \to E$ then then the following subspaces are stable: $\{0\}; E$, they are trivial subspaces of φ. The problem is to define which stably nontrivial subspaces φ has.

By the definition we can see that E is stable with respect to φ since $\varphi(E) = E$. Moreover, Kernel space $\mathrm{Ker}\varphi = \{x \in E : \varphi(x) = 0\}$ is also stable with respect to φ. If φ is not automorphic then $\mathrm{Ker}\varphi \neq \{0\}$ is a stably nontrivial subspace of φ.

Also, φ has other stable subspaces.

Example:

1. If we have a projection on a line, then that line is a stably nontrivial subspace.

2. If we have a reflection over a line, then that line and its orthogonal line are stably nontrivial subspaces.

The following criterion allows us to check whether a subspace is stable with respect to φ: The subspace $E' \subseteq E$ is stable if and only if the image of a generation of E' is in E'.

Indeed, by the definition of stable subspaces, we just need to prove the converse part. Assume that S' is a generation of E' and $\varphi(S') \subseteq E'$. Since any $x \in E'$ is a linear combination of S' then $\varphi(x)$ is also a linear combination of $\varphi(S')$. Hence, $\varphi(x) \in E'$.

The concept of stable subspace plays an important role in finding a simpler form for the matrices of the linear operators. The above statement is confirmed by the following theorem:

Theorem 3.1.1. Assume $E = E_1 \oplus \ldots \oplus E_r$ is the direct sum of stable subspaces $E_1, \ldots, E_r$. Let $S, S_1, \ldots, S_r$ be basises of $E, E_1, \ldots, E_r$ such that $S = S_1 \cup \ldots \cup S_r$. Let A be the matric of the linear operator φ according S, $A_1, \ldots, A_r$ are respectively matrices of φ restricted on $E_1, \ldots, E_r$ according $S_1, \ldots, S_r$. We have:

$$A = \begin{bmatrix} A_1 & 0 & \ldots & 0 \\ 0 & A_2 & \ldots & 0 \\ \ldots & \ldots & \ldots & \ldots \\ 0 & 0 & 0 & A_r \end{bmatrix}$$

We arrange S in the order of the elements in S_1, then similarize to the elements in S_2, ... and finally to the elements in S_r. Then A will have the above form.

Matrix A is the simplest form if the matrices $A_1, \ldots, A_r$ have the smallest order. That means, we must find an analysis of E as the direct sum of the stable subspaces such that these spaces have the smallest possible dimension.

This problem leads to finding one-dimensional stably subspaces. And every one-dimensional subspace of E is generated by a vector $x \neq 0$ and represented as $E_x = \{ax / a \in K\}$.

Lemma 3.1.2

E_x is a stable subspace of linear operator φ if and only of there exists a number $c \in K$ such that $\varphi(x) = cx$.

Proof. If E_x is a stable subspace then $\varphi(x) \in E_x$. That means there exists $c \in K$ such that $\varphi(x) = cx$.

Conversely, if $\varphi(x) = cx$ then $\varphi(ax) = a\varphi(x) = acx \in E_x$ for all $a \in K$.

The numbers c in this lemma play an important role in analyzing E as the direct sum of the stable subspaces.

3.2. Eigen vector and Eigen value

A number $c \in K$ is said to be an eigen value of φ if there exists a vector $x \neq 0$ of E such that $\varphi(x) = cx$. Vector $x \neq 0$ is said to be eigen vector of φ with respect to c. The set of all eigen values of φ is said to be the spectrum of φ.

Examples:

1. The identity mapping id_E has unique eigen value 1 and any vector $x \neq 0$ is eigen vector.

2. If φ is not auto-isomorphic then φ has an eigen value 0 and $\mathrm{Ker}\varphi - \{0\}$ is the set of corresponding eigen vectors.

3. Let φ be the projection $\varphi(a_1,...,a_n) = (a_1,...,a_m,0,...,0); \quad (m < n)$. Then $c(a_1,...,a_n) = (a_1,...,a_m,0,...,0)$ if and only if $a_1 = ... = a_m = 0$ or c = 1, $a_{m+1} = ... = a_n = 0$.

Hence, φ has 2 eigen values which are 0 and 1 and the set of corresponding eigen vectors is:

$$\{(a_1,...,a_n) \in K^n : a_1 = ... = a_m = 0\} - \{0\}$$
$$\{(a_1,...,a_n) \in K^n : a_{m+1} = ... = a_n = 0\} - \{0\}$$

3.3. Matrices diagonalization and diagonalizable linearly operators

In application or computation, instead of working with the linear operator φ, we work on its represented matrix. To reduce the work, for every linear operator $\varphi: E \to E$, if possible, we want to find a basis S in E such that the represented matrix of φ according S has the simplest form (diagonal form). That means:

$$[\varphi]\Big|_S = \begin{bmatrix} a_{11} & 0 & \dots & 0 \\ 0 & a_{22} & \dots & 0 \\ \dots & \dots & \dots & \dots \\ 0 & 0 & 0 & a_{nn} \end{bmatrix} (a_{\mathrm{ij}} = 0; i \neq j)$$

Finding a basis of E in such in this basis, the represented matrix of φ is diagonal, is called diagonalizing φ. If there exists such a basis, we also assert that the linear operator φ is diagonal.

When studying about the structure of a linear operator, beyond finding a basis of space such that its represented matrix is diagonal, an interesting problem is the condition for a linear operator to be diagonalizable.

Let the represented matric of φ according a given basis be:

$$A = \begin{bmatrix} a_{11} & a_{12} & \dots & a_{1n} \\ a_{21} & a_{22} & \dots & a_{2n} \\ \dots & \dots & \dots & \dots \\ a_{n1} & a_{n2} & \dots & a_{nn} \end{bmatrix}$$

A is said to be diagonalizable if A is similar to a diagonal matric:

$$B = \begin{bmatrix} a_{11} & 0 & \dots & 0 \\ 0 & a_{22} & \dots & 0 \\ \dots & \dots & \dots & \dots \\ 0 & 0 & 0 & a_{nn} \end{bmatrix} (a_{\mathrm{ij}} = 0; i \neq j)$$

However, A and B are similar if and only if they are represented matrices of the same linear operator. That means according a basis S, the represented matric of φ is diagonal. It means φ is diagonalizable

$$[\varphi]\Big|_S := B = \begin{bmatrix} a_{11} & 0 & \dots & 0 \\ 0 & a_{22} & \dots & 0 \\ \dots & \dots & \dots & \dots \\ 0 & 0 & 0 & a_{nn} \end{bmatrix} (a_{\mathrm{ij}} = 0; i \neq j)$$

The linear operator φ of the vector space E is called diagonalizable if it can be represented by a diagonal matrix.

Example: The projection $\varphi(a_1,...,a_n) = (a_1,...,a_m,0,...,0); \quad (m < n)$

is diagonalizable since matric of φ according the natural basis of K^n has the form

$$A = \begin{bmatrix} 1 & .. & 0 & .. & 0 \\ .. & .. & .. & .. & .. \\ 0 & .. & 1 & .. & 0 \\ .. & .. & .. & .. & .. \\ 0 & .. & .. & .. & 0 \end{bmatrix}$$

The following theorem shows that a linear operator is diagonalizable if and only if E has a basis including eigen vectors of φ.

Theorem 3.3.1. Let $S = \{x_1,...,x_n\}$ be a basis of E. The matrix of the linear operator φ according S is a diagonal matrix if and only if $x_1,...,x_n$ are eigen vectors of φ. Then the components on the diagonal of the matrices are eigen values $x_1,...,x_n$

Proof. A matric of the linear operator φ according S is diagonal if and only if there exist numbers $c_i \in K$ such that $\varphi(x_i) = c_i x_i$ for all i = 1,...,n.

That means c_i is an eigen value and x_i is the corresponding eigen vector.

We have the following condition for the system of linearly independent vectors: Let $x_1,...,x_r$ be eigen vectors of the linear operator φ and $c_1,...,c_r$ are corresponding eigen values. If $c_1,...,c_r$ are totally different then $x_1,...,x_r$ are linearly independent.

Indeed, If r = 1 then $x_1 \neq 0$ is linearly independent.

For r > 1, assume we have the linear relation

$$a_1x_1 + ... + a_rx_r = 0$$

Since $\varphi(x_i) = c_i x_i$ then

$$a_1c_1x_1 + ... + a_rc_rx_r = a_1\varphi(x_1) + ... + a_r\varphi(x_r) = \varphi(a_1x_1 + ... + a_rx_r) = 0$$

Subtract the right-handed side of the above formula for the product of c_r with the right-handed side of the originally linear relation, we obtain:

$$a_1(c_1 - c_r)x_1 + ... + a_{r-1}(c_{r-1} - c_r)x_{r-1} = 0$$

By induction, we may assume that $x_1,...,x_{r-1}$ is linearly independent. Hence

$$a_1(c_1 - c_r) = ... = a_{r-1}(c_{r-1} - c_r) = 0$$

Since $c_1,...,c_r$ are totally different then $a_1 = ... = a_{r-1} = 0$

It implies $a_r x_r = 0$. Since $x_r \neq 0$ then we also have $a_r = 0$

Therefore, $x_1,...,x_r$ are linearly independent.

The above theorem gives an assertion: If dimE = n then each linear operator of E has at most n distinct eigen values.

Indeed, since φ can only have at most n linearly independent eigen vectors, then φ can only have at most n distinct eigen values.

And if dimE = n and the linear operator φ has n distinct values then φ is diagonalizable.

For examples:

1. The reflection $\varphi(a_1, a_2) = (a_2, a_1)$. The matric of φ according the natural basis of K^2 is

$$\begin{bmatrix} 0 & 1 \\ 1 & 0 \end{bmatrix}$$

If $\varphi(a_1, a_2) = (a_2, a_1) = c(a_1, a_2)$ then $a_1 = ca_2$; $a_2 = ca_1$

It implies that $c^2 = 1$. We see that φ has 2 eigen values which are 1 and -1. Therefore φ is diagonalizable and based on the definition 2.1.1 then φ can be represented as the diagonal matric

$$\begin{bmatrix} 1 & 0 \\ 0 & -1 \end{bmatrix}$$

On the other hand, a matric A is said to be diagonalizable if A is similar to a diagonal matric. Moreover, 2 matrices are similar if they are represented matrices of the same linear operator. Then

$$\begin{bmatrix} 0 & 1 \\ 1 & 0 \end{bmatrix} \text{and} \begin{bmatrix} 1 & 0 \\ 0 & -1 \end{bmatrix} \text{ are similar.}$$

In the other words, $\begin{bmatrix} 0 & 1 \\ 1 & 0 \end{bmatrix}$ is diagonalizable

2. The matric $\begin{bmatrix} 8 & -5 \\ 10 & -7 \end{bmatrix}$ is also diagonalizable since it is similar to $\begin{bmatrix} -2 & 0 \\ 0 & 3 \end{bmatrix}$

3. The linear operator φ of K^3 has the represented matric according the natural basis which is

$$A = \begin{bmatrix} 1 & 2 & -2 \\ 1 & 0 & 3 \\ 1 & 3 & 0 \end{bmatrix}$$

The question is whether there exists a diagonal matric which is similar to the matric A?

Since A is the represented matric of φ then we can represent φ by the formula $\varphi(x) = Ax$. Hence φ and A have the same sets of eigen values and eigen vectors.

The characteristic equation of A:

$$\det(A - \lambda I) = 0$$

Has 3 solutions which are -3; 1 and 3. They are eigen values of φ and A.

The sets of corresponding eigen vector are $cx_1 = \{c(6,-7,5)\}$; $cx_2 = \{c(-2,1,1)\}$ and $cx_3 = \{c(0,1,1)\}$

Since 3 eigen values are different then the system of eigen vectors x_1, x_2, x_3 is linearly independent and is a basis of K^3. Since φ is diagonalizable then the reprentation matric of φ according the basis system x_1, x_2, x_3 is a diagonal matric B which is similar to A. That means A is diagonalizable.

$$A \approx B = \begin{bmatrix} -3 & 0 & -0 \\ 0 & 1 & 0 \\ 0 & 0 & 3 \end{bmatrix}$$

Comment:

We also have $E_1 =< x_1 >= \{c(6,-7,5)\}$; $E_2 =< x_2 >= \{c(-2,1,1)\}$và $E_3 =< x_3 >= \{c(0,1,1)\}$ for $c \in K$ are one-dimentional stable subspaces of E with respect to φ and $E = E_1 \oplus E_2 \oplus E_3$

4. CONCLUSION

The article is about the problem of matrix diagonalization but is mentioned from the linear operator of the vector space point of view. The reason is that the two concepts of square matrices and linear operators are closely related. The above correspondence is a ring isomorphism between L(E) and L (E).

REFERENCES

1. Nguyễn Duy Thuận (2004), *Linear Algebra*, - Pulishing House of Hanoi National University of Education.
2. Nguyễn Hữu Việt Hưng (2001), *Linear Algebra*, - Pulishing House of Vietnam National University.
3. Lê Tuấn Hoa (2001), *Modern Algebra*, - Pulishing House of Vietnam National University.
4. Trần Văn Hạo (1977), *Premium algebra* (Volume 1. Modern Algebra), - Educational Publishing House.
5. Ngô Thúc Lanh (1982), *Linear Algebra*, - Publishing House of Colleges and Universities.

CHÉO HÓA MA TRẬN VUÔNG DƯỚI GÓC ĐỘ TOÁN TỬ TUYẾN TÍNH

Tóm tắt: *Khi nghiên cứu cấu trúc của không gian véc tơ ta không nghiên cứu chúng một cách đơn lẻ mà đặt chúng trong mối liên hệ với nhau. Công cụ để xác lập mối liên hệ đó là các ánh xạ tuyến tính. Tuy nhiên, ngôn ngữ hữu hiệu giúp cho việc mô tả các ánh xạ tuyến tính chính là ma trận.*

Có một lớp các tự ánh xạ tuyến tính của một không gian véc tơ (hữu hạn sinh), gọi là Toán tử tuyến tính hay phép biến đổi tuyến tính. Toán tử tuyến tính và ma trận có một mối liên hệ chặt chẽ. Bởi Toán tử tuyến tính xác định bởi ma trận và ngược lại, với mỗi ma trận vuông ắt sẽ có một Toán tử tuyến tính nhận ma trận đó là ma trận biểu diễn.

Bài viết này, đề cập tới ma trận vuông dạng đơn giản nhất (đó là dạng đường chéo) và bài toán chéo hóa một ma trận vuông cũng như điều kiện để một ma trận vuông chéo hóa được dưới góc độ Toán tử tuyến tính như một khẳng định đã có: Mối tương ứng trên là một sự đẳng cấu giữa vành các Toán tử tuyến tính của không gian L(E) và vành các ma trận vuông $Mat_n(K)$.

Từ khóa: *Toán tử, ma trận,cơ sở, chéo hóa...*

UNPARTICLE EFFECTS ON DARK MATTER FERMIONS PRODUCTION IN e^+e^- COLLISIONS

Ha Huy Bang[1], Ngan Van Thap[2], Mai Thi Dieu[3], Sa Thi Lan Anh[4]
Faculty of Physics, Ha Noi University of Sciences, Viet Nam National University, 334 Nguyen Trai Street, Ha Noi, Viet Nam
Email: 1hahuybang@hus.edu.vn, 2nganvanthap_t59@hus.edu.vn, 3maithidieu_t59@hus.edu.vn, 4lananhkhtn@gmail.com.

Abstract: *In this paper, we investigate the effects of the vector unparticle on* $e^+e^- \to \chi\bar{\chi}$ *processes. The numerical results show that the cross-section with unparticle effects should be about* 10^{17} *time larger than the ove without unparticle effects. This could have important implications for dark matter searches*

Keywwords: *Unparticle, dark matter, cross-section,* e^+e^-*collisions.*

Email: hahuybang@hus.edu.vn
Received 22 April 2018
Accepted for publication 25 May 2018

1. INTRODUCTION

As well known, astrophysical observations have shown that Dark Matter (DM) exists in our universe. In several extensions of the standard Model, dark matter fermions are postulated [1-5]. On the other hand, searching for the new physics effects, the e^+e^- linear colliders have an exceptional advantageons for its appealing clean background, and the possibilitty for the options of eγ and $\gamma\gamma$ colliders based on it.

Very recently, we have investigated unparticle effects on Bhabha scattering [6] and on axion-like particles production in e^+e^- collisions [7]. In this paper, we extend the previons study [4] to obtain the production of dark matter fermion in the annihilation of the electron - positron pair via unparticle exchange.

2. THE CROSS SECTIONS

We need to note that the unparticle electron - positron vertex

$$V_{Ue^+e^-} = \frac{1}{\Lambda_U^{d_U-1}}(c_1\gamma_\mu + c_2\gamma_\mu\gamma_5) \qquad (1)$$

and unparticle - dark matter fermion χ- antidark matter fermion $\bar{\chi}$ vertex

$$V_{U\chi\bar{\chi}} = \frac{1}{\Lambda_U^{d_U-1}}(\lambda_1\gamma_\mu + \lambda_2\gamma_\mu\gamma_5). \tag{2}$$

The propagator of a vector unparticle has the form

$$\frac{iA_{d_U}}{2\sin(d_U\pi)}(-g^{\mu\nu} + \frac{p^\mu p^\nu}{P^2})(-P^2 - i\epsilon)^{d_U-2}, \tag{3}$$

$$A_{d_U} = \frac{16\pi^{5/2}\Gamma(d_U + 1/2)}{(2\pi^{2d_U})\Gamma(d_U - 1)\Gamma(2d_U)}. \tag{4}$$

Now, let us investigate the effects of unparticle on $e^+(k_2)e^-(k_1) \xrightarrow{U} \chi(q_1)\,\bar{\chi}(q_2)$ process. This process is described by the Feynman diagram presented in Figure 1.

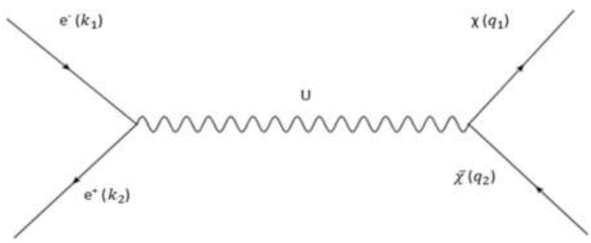

Figure 1. *Feynman diagram for $e^+e^- \to \chi\bar{\chi}$ process via a vector unparticle.*

The amplitude for this process is given by

$$\begin{aligned} iM =&\bar{v}(k_2)\left(\frac{1}{\Lambda_u^{d_u-1}}(c_1\gamma_\mu + c_2\gamma_\mu\gamma_5)\right)u(k_1) \\ &\frac{iA_{d_u}}{2sin(d_u\pi)}\Big(-g^{\mu\nu} + \frac{p^\mu p^\nu}{P^2}\Big)(-p^2 - i\epsilon)^{d_u-2} \\ &\times \bar{u}(q_1)\left(\frac{1}{\Lambda_u^{d_u-1}}(\lambda_1\gamma_\nu + \lambda_2\gamma_\nu\gamma_5)\right)v(q_2). \end{aligned} \tag{5}$$

By putting $F = -\frac{iA_{d_U}}{\Lambda_U^{2d_U-2}2\sin(d_U\pi)}(-P^2 - i\epsilon)^{d_U-2}$ and $\gamma_5 = \gamma^5$.

We have

$$iM = F.[\bar{v}(k_2)\,(c_1\gamma_\mu + c_2\gamma_\mu\gamma_5)\,u(k_1)]\times[\bar{u}(q_1)\,\big(\lambda_1\gamma^\mu + \lambda_2\gamma^\mu\gamma^5\big)\,v(q_2)]. \tag{6}$$

So, the matrix element square is

$$\begin{aligned} |M|^2 =& 16\,|F|^2\Big\{2(c_1^2 + c_2^2)(\lambda_1^2 + \lambda_2^2)\Big[(k_1q_1) \times (k_2q_2) + (k_1q_2)(k_2q_1) - (k_1k_2)(q_1q_2)\Big] \\ &+ 2\lambda_1^2(c_1^2 + c_2^2)(m_\chi^2 + q_1q_2)k_1k_2 - 2\lambda_2^2(c_1^2 + c_2^2)(m_\chi^2 - q_1q_2)k_1k_2 \\ &+ 8c_1c_2\lambda_1\lambda_2\Big[(k_1q_1)(k_2q_2) - (k_1q_2)(k_2q_1)\Big]\Big\}. \end{aligned} \tag{7}$$

In center of mass frame, four-momenta of particles are defined

$k_1 = (E,\mathrm{k})$; $k_2 = (E,-\mathrm{k})$;

$q_1 = (E,\mathrm{q})$; $q_2 = (E,-\mathrm{q})$;

$p^2 = (k_1 + k_2)^2 = 4E^2 = s$,

where s is the center of mass energy. The differential cross-section can be obtained as follows

$$\frac{d\sigma}{d\Omega} = \frac{s}{32\pi^2}|F|^2\sqrt{1-\frac{4m_\chi^2}{s}}.\Bigg\{(c_1^2+c_2^2)(\lambda_1^2+\lambda_2^2)\times\left[\frac{1}{2}\left[1+\left(1-\frac{4m_\chi^2}{s}\right)cos^2\theta\right]\right.$$
$$\left.-\left(1-\frac{2m_\chi^2}{s}\right)\right]+\lambda_1^2(c_1^2+c_2^2)+\lambda_2^2(c_1^2+c_2^2)\left(1-\frac{4m_\chi^2}{s}\right)$$
$$-4c_1c_2\lambda_1\lambda_2\sqrt{1-\frac{4m_\chi^2}{s}}cos\theta\Bigg\}. \tag{8}$$

From (8), we get the total cross section is

$$\sigma = 4\pi\alpha^2.|F|^2.\sqrt{1-\frac{4m_\chi^2}{s}}\left[\frac{s}{3}(c_1^2+c_2^2)(\lambda_1^2+\lambda_2^2)\times\left(1-\frac{m_\chi^2}{s}\right)-m_\chi^2(c_1^2+c_2^2)(\lambda_2^2-\lambda_1^2)\right]. \tag{9}$$

3. NUMERICAL RESULTS AND DISENSSIONS

Let us now turn to the numerical analysis. We take $c_1 = c_2 = \frac{1}{\sqrt{2}}$, $\Lambda_U = 1TeV$, $m_\chi = 30MeV$, $\lambda_1 = \lambda_2 = 414.3$ as input parameters.

Let us plot $\frac{d\sigma}{d\Omega}$ thewith respect to $\cos\theta$ for $\sqrt{s} = 100GeV$ (Figure 2).

We give the numerical values of variation of differential cross-section as function of $\cos\theta$ fors $\sqrt{s} = 100GeV$ in Table 1 and with respect to $\sqrt{s}$ for $\cos\theta = -1$ (Figure 3).

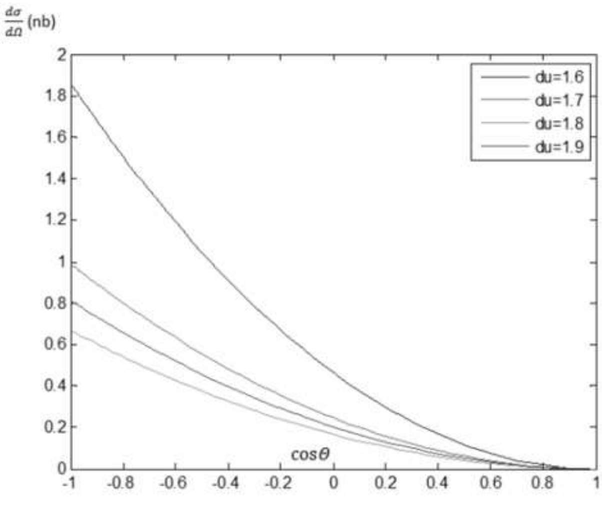

Figure 2. *The variation of differential crosssection as function of cosθ for* $\sqrt{s} = 100GeV$

Table 1. *The variation of differential crosssection as function of cosθ for $\sqrt{s}$ = 100GeV.*

cosΘ	$\frac{d\sigma}{d\Omega}$ (nb)			
	du=1.6	du=1.7	du=1.8	du=1.9
-0.9	1.678	0.891	0.602	0.732
-0.6	1.190	0.632	0.427	0.519
-0.3	0.786	0.417	0.282	0.343
0	0.465	0.247	0.167	0.203
0.3	0.228	0.121	0.082	0.099
0.6	0.074	0.040	0.027	0.032
0.9	0.005	0.003	0.002	0.185

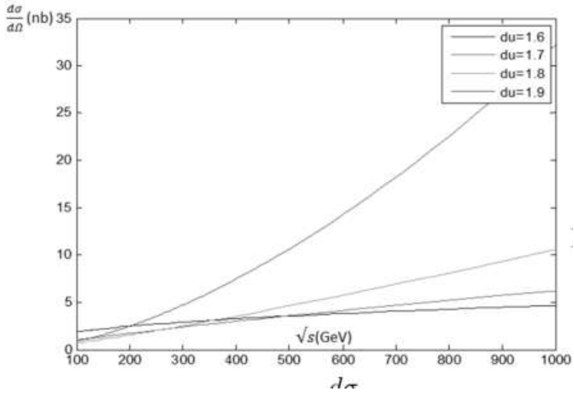

Figure 3. *The variation of $\frac{d\sigma}{d\Omega}$ as function of $\sqrt{s}$ for cosθ = −1.*

Table 2. *The variation of $\frac{d\sigma}{d\Omega}$ as function of $\sqrt{s}$ for cosθ = −1.*

√s (GeV)	$\frac{d\sigma}{d\Omega}$ (nb)			
	du=1.6	du=1.7	du=1.8	du=1.9
100	1.859	0.987	0.987	0.987
200	2.454	1.718	1.718	1.718
300	2.886	2.376	2.376	2.376
400	3.237	2.991	2.991	2.991
500	3.540	3.576	3.576	3.576
600	3.808	4.137	4.137	4.137
700	4.050	4.680	4.680	4.680
800	4.272	5.208	5.208	5.208
900	4.478	5.723	5.723	5.723
1000	4.671	6.226	6.226	6.226

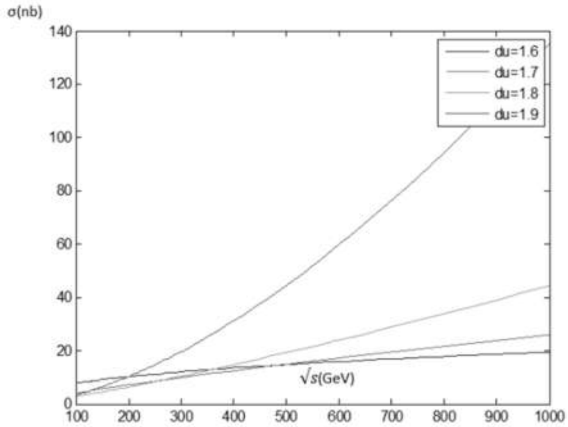

Figure 4. *The variation of σ as function of $\sqrt{s}$*

As we can observe from Figure 2 and Figure 3, thedecreases with cosθ and increases with $\sqrt{s}$.

Next, we present the variation of σ as a function of $\sqrt{s}$ (Figure 4).

In Ref. [8], the authors determined the differential cross-section and total crosssection on process $e^+e^-\chi\bar{\chi}$ via photo are as follows

$$\frac{d\sigma_\gamma}{d\Omega} = \frac{\alpha}{16s\pi}\sqrt{1-\frac{4m_\chi^2}{s}} \times \left\{\mu_\chi^2\left[s(1-cos^2\theta)+4m_\chi^2(1+cos^2\theta)\right]+d_\chi^2(1-cos^2\theta)(s-4m_\chi^2)\right\}, \quad (10)$$

$$\sigma_\gamma = \frac{\alpha}{6s}\sqrt{1-\frac{4m_\chi^2}{s}}\left\{\mu_\chi^2(s+8m_\chi^2)+d_\chi^2(s-4m_\chi^2)\right\} \quad (11)$$

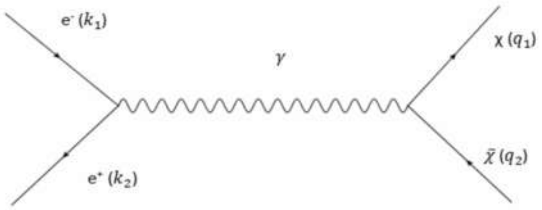

Figure 5. *Feynman diagram for* $e^+e^- \to \chi\bar{\chi}$ *process through a photon..*

Table 3. *The total cross-section σ of* $e^+e^- \to \chi\bar{\chi}$ *process with unparticle effects.*

√s(GeV)	σ(nb)			
	du=1.6	du=1.7	du=1.8	du=1.9
100	7.789	4.133	2.795	3.396
200	10.277	7.196	6.421	10.295
300	12.087	9.954	10.446	19.696
400	13.561	12.530	14.752	31.209
500	14.827	14.978	19.282	44.601
600	15.949	17.330	23.998	59.708
700	16.963	19.605	28.874	76.409
800	17.894	21.815	33.892	94.609
900	18.757	23.971	39.037	114.229
1000	19.564	26.079	44.298	135.203

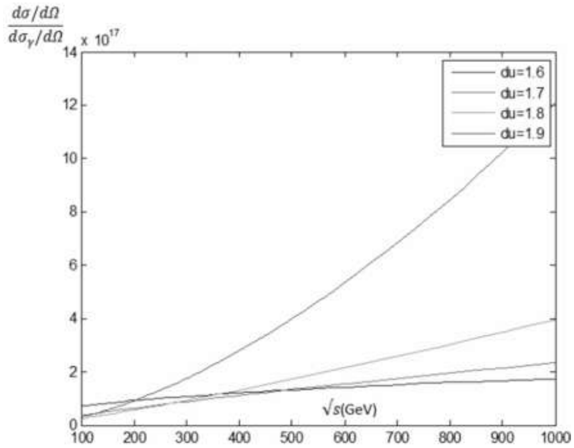

Figure 6. *The ratio of differential crosssection with unparticle effects to one without unparticle effects at cosθ = 0.*

Table 4. *The ratio of differential crosssection with unparticle effects to one without unparticle effects at cosθ = 0.*

√s (GeV)	$\frac{d\sigma/d\Omega}{d\sigma_\gamma/d\Omega}$ (x 10^{-17})			
	du=1.6	du=1.7	du=1.8	du=1.9
100	0.697	0.370	0.250	0.304
200	0.920	0.644	0.575	0.922
300	1.082	0.891	0.935	1.763
400	1.214	1.122	1.321	2.794
500	1.327	1.341	1.726	3.992
600	1.428	1.551	2.148	5.345
700	1.519	1.755	2.585	6.840
800	1.602	1.953	3.034	8.469
900	1.679	2.146	3.494	10.225
1000	1.751	2.334	3.965	12.103

Next, we give the numerical values of the ratio of the differential cross-section with unparticle effects $\frac{d\sigma}{d(\Omega}$ of (9) to the $\frac{d\sigma}{d(\Omega_\gamma}$ of (10) at different energies in Figure 6 and Table 4.

So, direct computations have showed that the about differential cross-section of (8) should be about 10^{17} times larger than the one in (10). In exactly the same way, we have obtained the ratio of the total cross-section with unparticle effects σ of (9) to the total crosssection without unparticle effects σ_γ of (11) at different energies in Figure 7 and Table 5.

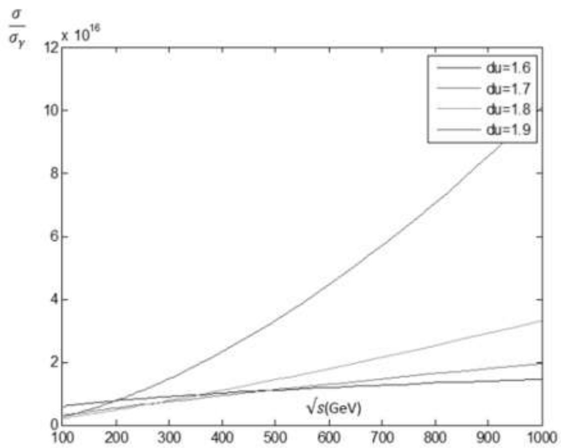

Figure 7. *The ratio of cross-section with unparticle effects to one without unparticle effects at cosθ = 0.*

Table 5. *The ratio of cross-section with unparticle effects to one without unparticle effects.*

√s(GeV)	$\frac{\sigma}{\sigma_\gamma}$ (x10 $^{-16}$)			
	du=1.6	du=1.7	du=1.8	du=1.9
100	0.581	0.308	0.209	0.253
200	0.767	0.537	0.479	0.768
300	0.902	0.743	0.779	1.469
400	1.012	0.935	1.101	2.328
500	1.106	1.117	1.438	3.327
600	1.190	1.293	1.790	4.454
700	1.265	1.463	2.154	5.700
800	1.335	1.627	2.528	7.057
900	1.399	1.788	2.912	8.521
1000	1.459	1.945	3.305	10.086

The results above show that the total crosssection of (9) is larger than the one in (11) by 15 - 17 order of magnitudes.

In summary, we have examined the unparticle effects at $e^+e^- \to \chi\bar{\chi}$ From numerical results, we have found that the effects of the unparticle on the cross-sections can be very strong. If the measurement is carried out at $\sqrt{s}$ = 100GeV -1000GeV, thenthe cross-section for the process $e^+e^- \to \chi\bar{\chi}$ should be detectable. These could have important implications for the dark matter fermion and unparticle searches at futurecolliders. Our work can be extended forother scatterings, for example $e^+e^- \to \phi\phi$ process, here ϕ is the dark matter scalar.

REFERENCES

1. Y. Mambrini and T. Toma, Eur. Phys. J. C75 no. 12 (2015) 570.
2. The CMS Collaboration, arXiv:1 701.02042 [hep-ph].
3. R. Bartels, D. Gaggero, and Ch. Weniger, arXiv:1703.02546 [astro-ph.HE].
4. Guha, Selvaganapathy J, and P. K. Das, Phys. Rev. D 95, 015001(2017).
5. P. H. Gu and X. G. He, Phys. Lett. B 778, 292(2018).
6. S. T. L. Anh, H. H. Bang et al., Can. J. Phys. 96:3, 268(2018).
7. S. T. L. Anh, H. H. Bang et al., Int. J. Theor. Phys. 149(2018),
8. https://doi.org/101007/s10773-018-3727-1.
9. Atanu Guha et al. arXiv:1509.05901 [hep-ph]

ẢNH HƯỞNG CỦA U-HẠT LÊN VIỆC SẢN SINH CÁC HẠT VẬT CHẤT TỐI TRONG TÁN XẠ E^+E^-

Tóm tắt: *Bài báo nghiên cứu về những tác động của vec-tơ U-hạt trong quá trình* $e^+e^- \to \chi\bar{\chi}$*. Kết quả cho thấy mặt cắt ngang bởi những tác động của U-hạt có thể là lơn hơn* 10^{17} *lần so với lúc khi không có sự tác động của U-hạt. Đây là những chỉ số quan trong các nghiên cứu về vật chất tối.*

Từ khóa: *U-hạt, vật chất tối, mặt cắt ngang, tán xạ* e^+e^-*.*

UNPARTICLE EFFECTS ON PHOTON AXION LIKE SCATTERINGS

Ha Huy Bang[1], Mai Thi Thuy[2], Ngan Van Thap[3], Truong Minh Anh polytechnic[4]

Faculty of Physics, Ha Noi University of Sciences, Viet Nam National University, 334 Nguyen Trai Street, Ha Noi, Viet Nam

Email: [1]hahuybang@hus.edu.vn; [2]maithithuy_t59@hus.edu.vn; [3]nganvanthap_t59@hus.edu.vn; [4]anh.truongminh@hust.edu.vn

Abstract: *We study the effects of unparticle physics on the photon axion like scatterings and calculate the production cross sections. Interestingly, from the numerical results, we have found that the effects of the unparticle can be strong and should be detectable.*

Keywword: *Unparticle, photon, effect, cross-section*

Email: hahuybang@hus.edu.vn
Received 22 April 2018
Accepted for publication 25 May 2018

1. INTRODUCTION

A decade ago, Georgi [1] made an interesting observation that a nontrial scale invarianve sector of scale dimention d_u might manifest itself at low energy as a non intergral number d_u of invisible massless particle, dubbed unparticle. If unparticles exist, their phenomenological implications should be discussed. In the literature, there have been many discussions which investigate various features of unparticle physics [2-13]. In the some of these researches several unparticle effects on processes have been studied.

Recently, by considering not only the self-interactions of unparticle but also all the other possible contributions, which are dominant, a detailed study of the processes, within a scalar unparticle scenario $pp \rightarrow 4\gamma$, $pp \rightarrow 2\gamma\ 2g$, $pp \rightarrow 4e$, $pp \rightarrow 4u$, and $pp \rightarrow 2\mu$ at $\sqrt{S} = 14\ TeV$ at the LHC has been carried out in Ref. [11]. A search for dark matter and unparticle production at the LHC has been performed in Ref. [12].

On the other hand, there are many works describing the theoretical motivations for axion like particles (ALPs), which are spin-zero, neutral and extremely light bosons [14-16]. Recently, in Ref. [17] the authors have proposed new searches for axion like particles produced in flavor changing neutral current processes. Interestingly, the products of invisibly-decaying ALPs at lepton colliders arise from processes $e^+e^- \to \gamma a$, $a \to$ invisible via the ALP coupling to $\gamma\gamma$ and γZ have been considered in Ref. [18].

In Refs. [19-21] we have investigated the effects of the unparticle and radion on → processes, Bhabha scattering and → processes.

In this work, we consider the effects of the spin 1 unparticle on $\gamma\gamma \to \gamma\gamma$ processes. Bhabha scattering and $e^+e^- \to \gamma a$ processes.

In this work, we consider the effects of the spin 1 unparticle on $\gamma a \to \gamma a$ processes.

2. THE CROSS SECTIONS

The $\gamma a \to \gamma a$ process via a vector unparticle is described by the Feynman diagram presented in Fig. 1.

In this process, the ALPs and photon annihilate into an unparticle U which then converts into ALPs and photon. The unparticle operator coupling effectively to the ALPs and photon is [14]

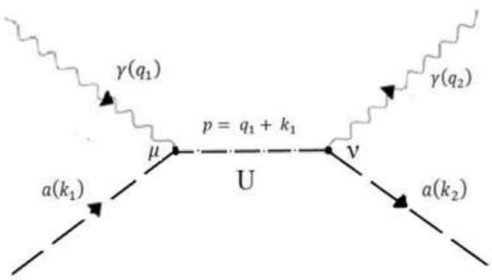

Figure 1. *Feynman diagram for $\gamma a \to \gamma a$ process through a vector unparticle*

$$\frac{c_V^{a\gamma}}{\Lambda^{d_U}} a F_{\mu\nu} \partial^\mu O_U^\nu + \frac{c_V^{a\gamma}}{\Lambda^{d_U}} a \tilde{F}_{\mu\nu} \partial^\mu O_U^\nu, \tag{1}$$

where $F_{\mu\nu} = \partial_\mu A_\nu - \partial_\nu A_\mu$ is the photon field strength and $\tilde{F}^{\mu\nu}$ its dual, is the axion-like particle.

The propagator of the vector unparticle has form [15,16].

$$D^{\mu\nu}(x) = \int d^4x e^{iPx} \left\langle 0 \,|\, T[O_U^\mu(\mathrm{x}) O_U^\nu(0)] |0\right\rangle = \frac{iA_{d_U}}{2\sin(d_U\pi)} \left(-g^{\mu\nu} + \frac{P^\mu P^\nu}{P^2}\right) \left(-P^2 - i\varepsilon\right)^{d_U-2}, \tag{2}$$

where p = $q_1 + k_1$ and

$$A_{d_U} = \frac{16\pi^{5/2}}{(2\pi)^{2d_U}} \frac{\Gamma(d_U + 1/2)}{\Gamma(d_U - 1)\Gamma(2d_U)}. \tag{3}$$

The vector operator is assumed to satisfy the transverse condition $\partial_U O_U^\mu = 0$. The amplitude (M) for this process is given by

$$iM = F \times \begin{bmatrix} \frac{C_1}{\Lambda_U^{du}}\left(q_{1\alpha}\varepsilon_\mu(q_1) - q_{1\mu}\varepsilon_\alpha(q_1)\right) \\ +2\frac{C_2}{\Lambda_U^{du}}\varepsilon_{\alpha\mu\rho\sigma}q_1^\rho\varepsilon^\sigma(q_1) \end{bmatrix} \times p^\alpha \times \begin{bmatrix} \frac{C_1}{\Lambda_U^{du}}\left(q_{2\beta}\varepsilon^{\mu*}(q_2) - q_2^\upsilon\varepsilon_\beta^*(q_2)\right) \\ +2\frac{C_2}{\Lambda_U^{du}}\varepsilon_{\beta\upsilon\gamma\theta}q_2^\gamma\varepsilon^{\theta*}(q_2)g^{\mu\upsilon} \end{bmatrix} \times p^\beta, \tag{4}$$

With

$$F = \frac{(-i)\times A_{du}}{2\sin(\mathrm{du}\,\pi)} \times \left(-p^2 - i\varepsilon\right)^{du-2}. \tag{5}$$

Hence

$$|M|^2 = F^2\frac{\left(C_1^2 + 4C_2^2\right)^2}{\Lambda_U^{4du}}\begin{bmatrix} 2(q_1p)^2(q_2p)^2 \\ -2p^2(q_1p)(q_2p)(q_1q_2) \\ +p^4(q_1q_2)^2 \end{bmatrix}, \tag{6}$$

In center of mass frame, four - momenta of particles are defined

$$q_1 = (E, \mathbf{q}); q_2 = (E, \mathbf{k}), \tag{7}$$

$$k_1 = (E, -\mathbf{q}); \mathrm{k}_2 = (E, -\mathbf{k}), \tag{8}$$

$$\text{and} \quad S = P^2 = (q_1 + k_1)^2 = 4E^2, \tag{9}$$

where S is the center of mass energy

Finally,we get

$$|M|^2 = F^2\frac{\left(C_1^2 + 4C_2^2\right)^2}{\Lambda_U^{4du}}\frac{S^4}{16}\left(1 + \cos^2\theta\right). \tag{10}$$

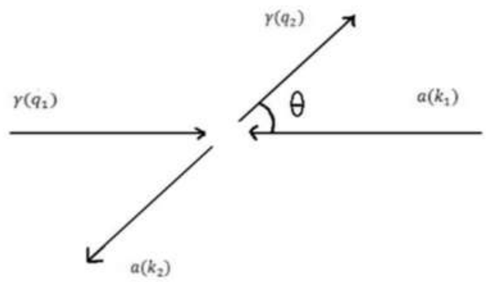

Figure 2.

The differential cross section can be obtained as follows

$$\frac{d\sigma}{d\Omega} = \frac{1}{64\pi^2 S}|M|^2 = \frac{F^2 S^3}{1024\pi^2}\frac{\left(C_1^2 + 4C_2^2\right)^2}{\Lambda_U^{4du}}\left(1 + \cos^2\theta\right). \tag{11}$$

From this, we get the total cross section is

$$\sigma = \frac{F^2 S^3}{192\pi} \frac{\left(C_1^2 + 4C_2^2\right)^2}{\Lambda_U^{4du}}. \tag{12}$$

Therefore

$$\frac{d\sigma}{\sigma d\Omega} = \frac{3}{16\pi}\left(1 + \cos^2\theta\right). \tag{13}$$

3. NUMERICAL RESULTS AND DISCUSSIONS

Let us now turn to the numerical analysis.We take $C_1 = C_2 = =1$, $\Lambda_u = 1TeV$, $\sqrt{S} = 1TeV$ as input parameters.

In the figure 3, 4 we plot the differential cross section for unparticle contribution for different values of the scaling parameter d_u.

As we can observe from Fig.3 the $\frac{d\sigma}{d\Omega}$ has a minimum for cosθ = 0.

Next, the behaviour of the $\frac{d\sigma}{d\Omega}$ as function of the center of mass energy is shown in Fig. 4.

This $\frac{d\sigma}{d\Omega}$ strongly increase with increasing $\sqrt{S}$.

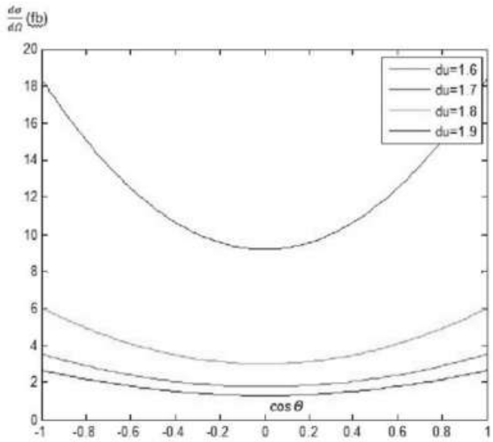

Figure 3. *The differential cross section for unparticle contribution at $\sqrt{S} = 1TeV$. Here we assumed $C_1 = C_2 = =1$, $\Lambda_u = 1TeV$.*

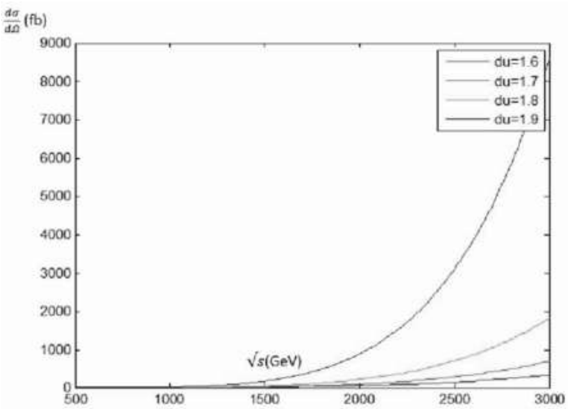

Figure 4. *The differential cross section. Due to unparticle contribution depending on the center of mass energy. Here we assume $C_1 = C_2 = =1$, $\Lambda_u = 1TeV$.*

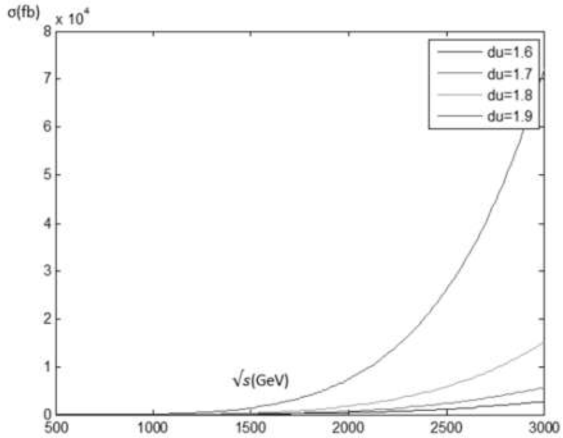

Figure 5. *The total cross sections due to unparticle contribution depending on the center of mass energy. Here we assume $C_1 = C_2 = =1$, $\Lambda_u = 1TeV$.*

In the following, let us present the variation of σ as a function of $\sqrt{S}$ (Fig. 5). The dependence of σ on $\sqrt{S}$ is in general similar to that of the $\frac{d\sigma}{d\Omega}$.

Finally, we give the numerical values of the differential cross sections in Table 1,2 and the total cross sections in Table 3.

Table 1. *The differential cross section with unparticle effects at* $\sqrt{S} = 1TeV$, *$C_1 = C_2 = =1$, Λ_u =1TeV.*

cosθ	$\frac{d\sigma}{d\Omega}$ (fb)			
	d_u=1.6	d_u=1.7	d_u=1.8	d_u=1.9
-1	265.73x10^{-2}	354.21x10^{-2}	601.68x10^{-2}	183.64x10^{-1}
-0.8	217.9x10^{-2}	290.46x10^{-2}	493.38x10^{-2}	150.58x10^{-1}
-0.6	180.7x10^{-2}	240.87x10^{-2}	409.14x10^{-2}	124.87x10^{-1}
-0.4	154.12x10^{-2}	205.44x10^{-2}	348.97x10^{-2}	106.51x10^{-1}
-0.2	138.18x10^{-2}	184.19x10^{-2}	312.87x10^{-2}	954.93x10^{-2}
0	132.87x10^{-2}	177.11x10^{-2}	300.84x10^{-2}	918.2x10^{-2}
0.2	138.18x10^{-2}	184.19x10^{-2}	312.87x10^{-2}	954.93x10^{-2}
0.4	154.12x10^{-2}	205.44x10^{-2}	348.97x10^{-2}	106.51x10^{-1}
0.6	180.7x10^{-2}	240.87x10^{-2}	409.14x10^{-2}	124.87x10^{-1}
0.8	217.9x10^{-2}	290.46x10^{-2}	493.38x10^{-2}	150.58x10^{-1}
1	265.73x10^{-2}	354.21x10^{-2}	601.68x10^{-2}	183.64x10^{-1}

Table 2. *he differential cross section for the unparticle contribution $C_1 = C_2 = =1$, Λ_u =1TeV.*

√s(GeV)	$\frac{d\sigma}{d\Omega}$ (fb)			
	d_u=1.6	d_u=1.7	d_u=1.8	d_u=1.9
500	12.59x10^{-2}	12.72x10^{-2}	21.023x10^{-2}	40.122x10^{-1}
1000	265.73x10^{-2}	354.21x10^{-2}	612.5x10^{-2}	0.1842x10^{2}
1500	158.21x10^{-1}	248.03x10^{-1}	495.11x10^{-1}	1.7791x10^{2}
2000	561.02x10^{-1}	986.75x10^{-1}	2.2112x10^{2}	8.9072x10^{2}
2500	497.54x10^{-1}	2.8799x10^{2}	7.0581x10^{2}	3.1077x10^{3}
3000	3.3402x10^{2}	6.9095x10^{2}	1.8214x10^{3}	8.6268x10^{3}

We see from these Tables that the differential cross sections are about 0.12 – 8.6×10^3.fb and the total cross sections are about 1.1 – 7.2×10^4 fb.

In Ref. [22] the authors computed the cross section for the αγ → αγ scattering through a photon and found that $\sigma < 10^{-69}\left(\frac{S}{GeV^2}\right) cm^2$.

Table 3. *The total cross section for the unparticle contribution $C_1 = C_2 = =1$, Λ_u =1TeV.*

√s(GeV)	σ (fb)			
	d_u=1.6	d_u=1.7	d_u=1.8	d_u=1.9
500	110.1x10^{-2}	110.03x10^{-2}	120.11x10^{-2}	312.31x10^{-2}
1000	223.01x10^{-1}	297.1x10^{-1}	500.2x10^{-1}	1.54x10^{2}
1500	1.325x10^{2}	2.078x10^{2}	4.15x10^{2}	1.490x10^{3}
2000	4.70x10^{2}	8.267x10^{2}	1.853x10^{3}	7.462x10^{3}
2500	1.2546x10^{3}	2.4127x10^{3}	5.913x10^{3}	2.6035x10^{4}
3000	2.7983x10^{3}	5.7885x10^{3}	1.5259x10^{4}	7.2271x10^{4}

So, direct computations have showed that the cross sections with unparticle effect is larger than the one in Ref. [22] by 30 – 34 order of magnitudes. If the measurement is carried out at $\sqrt{S}$ = 500 GeV – 3000 GeV, then the cross sections for the photon axion like scatterings should be detectable. We hope that axion – like can be observed at LHC or ILC. Our work can be extended for other scatterings, for example $\alpha\gamma \to f\bar{f}$ here, f is a generic fermion.

REFERENCES

1. H. Georgi, Phys. Rev. Lett. 98(2007), 221601.
2. H. Georgi, Phys. Lett. B 650(2007), 275.
3. K. Cheung, W – Y. Keung and T – C. Yuan,, Phys. Rev. D 76(2007), 055003.
4. Sahin and B. Sahin, arXiv: 0711.1665 [hep-ph].
5. O. Cakir and K. O. Ozansoy, arXiv: 0712.3814 [hep–ph].
6. T. Kikuchi, N. Okada and M. Takenchi, arXiv: 0801.0018 [hep-ph].
7. C. F. Chang and T. C. Yuan, arXiv: 0801.2843 [hep-ph].
8. S. Dutta and A. Goyal, arXiv: 0705.3946 [hep-ph].
9. O. Cakir and K. O. Ozansoy, arXiv: 0906.2728 [hep-ph]
10. S-L Chen and X-G He, arXiv:0705.3946 [hep-ph]
11. T. MAlievetal, arXiv:1701.00498 [hep-ph].
12. The CMS collaboration, arXiv:1701.02042 [hep-ph].
13. T. Q. Trang and H. H. Bang, Mod. Phys. Lett A 30 19(2015), 1550095.
14. E. Witten, Phys. Lett. B 149(1984) 351.
15. E. Masso and R. Toldra, Phys. Rev. D52 (1995) 1775 arXiv:9503293 [hep-ph].
16. J. Jaeckel, E. Masso. J. Rendondo, A. Ringwald and F. Takahashi, Phys. Rev. D 75 (2007) 013004 arXiv:0610203 [hep-hp].
17. K. Mimasu and V. Sanz, JHEP 06 (2015) 173.
18. M. J. Dolan, F. Kahlhoefer, C. McCabe and K. Schimidt-Hoberg, JHEP 03 (2015) 171.
19. T. Q. Trang, H. H. Bang, N. T. Huong and S. T. L. Anh, J. Mod. Phys. Vol 6. No 13(2015) 1798
20. Int. J. Theor. Phys. (2018) doi.10.1007/s10773 – 018 – 3727 - 1
21. S. T. L. Anh, T. Q. Trang, N. T. Huong and H. H. Bang, accepted for publication in Canadian J. Phys. (2017), http:/doi.org/10.1139/cjp-2016-0955.
22. M. Roncadelli, arXiv:1704.00144 [astro-ph.HE].

TÁC ĐỘNG CỦA U-HẠT LÊN HẠT CƠ BẢN PHOTON QUA CÁC TÁN XẠ

Tóm tắt: *Bài báo nghiên cứu về tác động của U-hạt lên hạt cơ bản photon qua các tán xạ và tính toán việc sản sinh ra các mặt cắt ngang. Thật thú vị khi kết quả mà chúng tôi thu được cho thấy U-hạt có thể đã tác động rất mạnh và cũng có thể thực hiện được.*

Từ khóa: *U-hạt, hạt photon, tác động, mặt cắt ngang.*

HYBRIDONS IN A FREE QUANTUM WIRE

Đang Tran Chien[1*], Ta Anh Tan[2]
[1]*Hanoi University of Natural Resources and Environment*
[2]*Hanoi Metropolitan University*

Abstract: *The confinement of optical modes of vibration in a free quantum wire is described by a theory involving the triple hybridization of Longitudinal-Optical phonons (LO), Interface Polariton 1 (IP1), and Interface Polariton 2 (IP2) modes. The resulting hybrids satisfy both mechanical and electromagnetic boundary conditions. A free-stanhding quantum wire was applied to investigate so the continuous boundary condition shifts to zero at the boundary of the wire. Using the second quantization theory, we obtained hybridons and found their dispersion patterns. From the numerical results, the energy of the electron is a function of the wave vector* $\boldsymbol{q_z}$ *and it decreases rapidly to zero for those with a smaller radius. For larger wires, the energy of the electron decreases more slowly.*

Keywords: *Hybridons, LO, IP1, IP2, wave vector* $\boldsymbol{q_z}$.

Email: dtchien@hunre.edu.vn
Received 22 April 2018
Accepted for publication 25 May 2018

1. INTRODUCTION

The previous works have shown that when expressing the properties of the confinement of optical modes in a free quantum wire, it is necessary to consider the hybridization of the optical modes in the wire by linear combination of three LO, TO and IP modes. The resulting hybrids satisfy both mechanical and electromagnetic boundary conditions [1]. The hybrid of the LO, TO and IP components describes very well the vibrational patterns in solids and the electron-hybridon interaction as well as the dielectric, electron mobility in the wires and quantum wells [2].

In this work, a free-stanhding quantum wire was applied to investigate so the boundary condition shifts to zero at the boundary of the wire. Using the second quantization theory, we obtained hybridons and found their dispersion patterns. From the numerical results, the energy of the electron is a function of the wave vector $\mathbf{q_z}$ and it decreases rapidly to zero for those with a smaller radius. For larger wires, the energy of the electron decreases more slowly.

2. CALCULATION

2.1. Hybrid modes

The hybrid modes were described some where in [3]:

$$\begin{cases} u_r = \left\{ A_{sp} \dfrac{-i\mathbf{q}_{s,p}^{L}}{\mathbf{q}_z} \mathbf{J}_s^{'}\left(\mathbf{q}_{s,p}^{L} r\right) + B_{sp}\mathbf{I}_s(\mathbf{q}_z r) + C_r \mathbf{I}_s(\mathbf{q}_z r) \right\} e^{is\varphi} e^{i\mathbf{q}_z z} \\ u_\varphi = \left\{ \begin{array}{l} A_{sp} \dfrac{s}{\mathbf{q}_z r} \mathbf{J}_s\left(\mathbf{q}_{s,p}^{L} r\right) + B_{sp} \dfrac{is\mathbf{I}_s\left(\mathbf{q}_z R\right)}{\eta} \mathbf{I}_s(\mathbf{q}_z r) + \\ + C_{sp} \dfrac{i}{s} \dfrac{\eta}{\mathbf{I}_s\left(\mathbf{q}_z R_0\right)} \mathbf{I}_s(\mathbf{q}_z r) \end{array} \right\} e^{is\varphi} e^{i\mathbf{q}_z z} \\ u_z = \left\{ A_{sp}\mathbf{J}_s\left(\mathbf{q}_{s,p}^{L} r\right) + B_{sp} \dfrac{i}{\mathbf{q}_z R_0} \dfrac{\left[\eta^2 - s^2\mathbf{I}_s^2\left(\mathbf{q}_z R_0\right)\right]}{\Gamma_2 \mathbf{I}_s\left(\mathbf{q}_z R_0\right)} \mathbf{I}_s(\mathbf{q}_z r) \right\} e^{is\varphi} e^{i\mathbf{q}_z z} \end{cases} \tag{1}$$

The boundary condition was applied for a free quantum wire (a vacuum was around the wire) so every shifts to zero at the boundary of the wire. Therefore, a system of equations was found as following:

$$\begin{cases} -A_{sp} \dfrac{i}{(\mathbf{q}_z R_0)} \left[s\mathbf{J}_s\left(\mathbf{q}_{s,p}^{L} R_0\right) - \mathbf{q}_{s,p}^{L} R_0 J_{s+1}\left(\mathbf{q}_{s,p}^{L} R_0\right) \right] + B_{sp}\mathbf{I}_s(\mathbf{q}_z R) + C_{sp}\mathbf{I}_s(\mathbf{q}_z R_0) = 0 \quad (a) \\ A_{sp} \dfrac{s}{(\mathbf{q}_z R_0)} \mathbf{J}_s\left(\mathbf{q}_{s,p}^{L} R_0\right) + B_{sp} \dfrac{is\mathbf{I}_s(\mathbf{q}_z R_0)}{\eta} \mathbf{I}_s(\mathbf{q}_z R_0) + C_{sp} \dfrac{i}{s} \dfrac{\eta}{\mathbf{I}_s(\mathbf{q}_z R_0)} \mathbf{I}_s(\mathbf{q}_z R_0) = 0 \quad (b) \\ A_{sp}\mathbf{J}_s\left(\mathbf{q}_{s,p}^{L} R_0\right) + B_{sp} \dfrac{i}{(\mathbf{q}_z R_0)} \dfrac{\left[\eta^2 - s^2\mathbf{I}_s^2(\mathbf{q}_z R_0)\right]}{\eta \mathbf{I}_s(\mathbf{q}_z R_0)} \mathbf{I}_s(\mathbf{q}_z R_0) = 0 \quad (c) \end{cases}$$

(2)

From equation (2a)

$$A_{sp}\mathbf{J}_s\left(\mathbf{q}_{s,p}^{L} R_0\right) + B_{sp} \frac{i}{(\mathbf{q}_z R_0)} \frac{\left[\eta^2 - s^2\mathbf{I}_s^2(\mathbf{q}_z R_0)\right]}{\eta \mathbf{I}_s(\mathbf{q}_z R_0)} \mathbf{I}_s(\mathbf{q}_z R_0) = 0 \tag{3}$$

We found

$$A_{sp} = -B_{sp} \frac{i}{(\mathbf{q}_z R_0)} \frac{\left[\eta^2 - s^2\mathbf{I}_s^2(\mathbf{q}_z R_0)\right]}{\eta \mathbf{J}_s\left(\mathbf{q}_{s,p}^{L} R_0\right)} \tag{4}$$

Place this result into equation (2b), we got

$$C_{sp} = B_{sp} s^2 \frac{\left[\eta^2 - s^2\mathbf{I}_s^2\left(\mathbf{q}_z R_0\right)\right] - \mathbf{q}_Z^2 R_0^2 \mathbf{I}_s^2\left(\mathbf{q}_z R_0\right)}{\mathbf{q}_Z^2 R_0^2 \eta^2} \tag{5}$$

Relations of the shift of the hybrid modes were represented via the unique constant as follows:

$$\begin{cases} u_r = B_{sp}\left\{ \begin{aligned} & -\frac{\mathbf{q}_{s,p}^L}{\mathbf{q}_Z^2 R_0}\frac{\left[\eta^2 - s^2\mathbf{I}_s^2\left(\mathbf{q}_z R_0\right)\right]}{\eta \mathbf{J}_s\left(\mathbf{q}_{s,p}^L R_0\right)}\mathbf{J}_s'\left(\mathbf{q}_{s,p}^L r\right) + \mathbf{I}_s\left(\mathbf{q}_z r\right) + \\ & + s^2\frac{\left[\eta^2 - s^2\mathbf{I}_s^2\left(\mathbf{q}_z R_0\right)\right] - \mathbf{q}_Z^2 R^2 \mathbf{I}_s^2\left(\mathbf{q}_z R_0\right)}{\mathbf{q}_Z^2 R_0^2 \eta^2}\mathbf{I}_s\left(\mathbf{q}_z r\right) \end{aligned} \right\} e^{is\varphi} e^{i\mathbf{q}_z z} \\ u_\varphi = -B_{sp}\frac{is}{\mathbf{q}_Z^2 R_0 \eta}\left[\eta^2 - s^2\mathbf{I}_s^2\left(\mathbf{q}_z R_0\right)\right]\left\{\frac{1}{r}\frac{\mathbf{J}_s\left(\mathbf{q}_{s,p}^L r\right)}{\mathbf{J}_s\left(\mathbf{q}_{s,p}^L R_0\right)} - \frac{1}{R_0}\frac{\mathbf{I}_s\left(\mathbf{q}_z r\right)}{\mathbf{I}_s\left(\mathbf{q}_z R_0\right)}\right\} e^{is\varphi} e^{i\mathbf{q}_z z} \\ u_z = -B_{sp}\frac{i}{\mathbf{q}_z R_0 \eta}\left[\eta^2 - s^2\mathbf{I}_s^2\left(\mathbf{q}_z R_0\right)\right]\left\{\frac{\mathbf{J}_s\left(\mathbf{q}_{s,p}^L r\right)}{\mathbf{J}_s\left(\mathbf{q}_{s,p}^L R_0\right)} - \frac{\mathbf{I}_s\left(\mathbf{q}_z r\right)}{\mathbf{I}_s\left(\mathbf{q}_z R_0\right)}\right\} e^{is\varphi} e^{i\mathbf{q}_z z} \end{cases} \tag{6}$$

where B_{sp} constant of the hybrid mode was calculated via the standardization condition.

2.2. Standardization constant of the hybrid modes

The standardization energy method was applied to obtain standardization constant. The hybrids were quantized to get hybridons. The hybridons were named hybrid phonons. They are referred to as harmonic oscillating grains with generalized coordinates in the second quantization as follows:

$$\mathbf{X} = \left(\frac{\hbar}{2\overline{M}\omega_{sp}}\right)^{\frac{1}{2}}\left\{\hat{a}^+ + \hat{a}\right\} \tag{7}$$

Energy of harmonic oscillator:

$$U = \frac{1}{2}\overline{M}\omega_{sp}^2\mathbf{X}^2 \tag{8}$$

The energy of the hybrid modes was calculated via the shifts of the lattice nodes:

$$U = \frac{1}{2}\frac{\overline{M}\omega_{sp}^2}{V_0}\int_0^{R_0}\int_0^{2\pi}\int_0^{L}\mathbf{u}^*.\mathbf{u}dV + \frac{1}{2}\varepsilon(\omega)\int_0^{R_0}\int_0^{2\pi}\int_0^{L}\mathbf{E}^*.\mathbf{E}dV \tag{9}$$

The first term in equation 9 is the mechanical energy of the hybrid modes. The second term is the electric energy of the hybrid modes. The mechanical energy of the hybrid modes come from the contribution of LO mode, IP modes donates the electromagnetic energy [1, 4].

From equation (8) and (9), we found:

$$\frac{\bar{M}\omega_{sp}^2}{V_0}\int_0^{R_0}\int_0^{2\pi}\int_0^{L}\mathbf{u_L}^*.\mathbf{u_L}dV+\varepsilon(\omega)\int_0^{R_0}\int_0^{2\pi}\int_0^{L}\mathbf{E_P}^*.\mathbf{E_P}dV=\bar{M}\omega_{sp}^2\mathbf{X}^2 \tag{10}$$

Standardization constant is calculated:

$$B_{sp}^2=\frac{\pi L\left[\eta^2-s^2I_s^2(\mathbf{q}_zR_0)\right]^2}{\mathbf{q}_z^2\eta^2}\begin{Bmatrix}\dfrac{\overline{M}\omega_{sp}^2}{V_0}\left(\dfrac{\mathbf{q}_L^2}{\mathbf{q}_z^2}+1\right)\dfrac{\mathbf{J}_{s+1}^2(\mathbf{q}_LR_0)}{\mathbf{J}_s^2(\mathbf{q}_LR_0)}+\\ +\varepsilon(\omega)\rho_p^2\left(\begin{matrix}\dfrac{\left(\mathbf{q}_Z^2R_0^2+s^2\right)^2}{\mathbf{q}_Z^2R_0^2\eta^2}+\\+\dfrac{\left(s^2+\mathbf{q}_zR_0\right)\eta}{\mathbf{I}_s^2(\mathbf{q}_zR_0)}\end{matrix}\right)\mathbf{I}_{s+1}^2(\mathbf{q}_zR_0)\end{Bmatrix}=\bar{M}\omega_{sp}^2\mathbf{X}^2 \tag{11}$$

$$B_{sp}=\omega_{sp}\mathbf{X}\sqrt{\frac{\bar{M}}{\pi L\Theta}} \tag{12}$$

with

$$\Theta=\frac{\left[\eta^2-s^2\mathbf{I}_s^2(\mathbf{q}_zR_0)\right]^2}{\mathbf{q}_z^2\eta^2}\begin{Bmatrix}\dfrac{\bar{M}\omega_{sp}^2}{V_0}\left(\dfrac{\left(\mathbf{q}_{s,p}^L\right)^2}{\mathbf{q}_z^2}+1\right)\dfrac{\mathbf{J}_{s+1}^2(\mathbf{q}_{s,p}^LR_0)}{\mathbf{J}_s^2\left(\mathbf{q}_{s,p}^LR_0\right)}+\\ +\varepsilon(\omega)\rho_p^2\left(\dfrac{\left(\mathbf{q}_Z^2R_0^2+s^2\right)^2}{\mathbf{q}_Z^2\omega_{sp}^2\eta^2}+\dfrac{\left(s^2+\mathbf{q}_zR_0\right)\eta}{\mathbf{I}_s^2(\mathbf{q}_zR_0)}\right)\mathbf{I}_{s+1}^2(\mathbf{q}_zR_0)\end{Bmatrix} \tag{13}$$

2.3. Dispersion relation of the hybrid modes

Place $A_{\mathbf{sp}}$ and C_{sp} constants in equation (2c)

$$\begin{aligned}&-B_{sp}\frac{1}{\mathbf{q}_zR_0}\frac{1}{\mathbf{q}_zR_0}\frac{\left[\eta^2-s^2\mathbf{I}_s^2(\mathbf{q}_zR_0)\right]}{\eta\mathbf{J}_s\left(\mathbf{q}_{s,p}^LR_0\right)}\boldsymbol{\xi}+B_{sp}\mathbf{I}_s(\mathbf{q}_zR_0)+\\&+B_{sp}s^2\frac{\left[\eta^2-s^2\mathbf{I}_s^2(\mathbf{q}_zR_0)\right]-\mathbf{q}_Z^2R^2\mathbf{I}_s^2(\mathbf{q}_zR_0)}{\mathbf{q}_Z^2\omega_{sp}^2\eta^2}\mathbf{I}_s(\mathbf{q}_zR_0)=0\end{aligned} \tag{14}$$

From equation 7, we found the dispersion relatio for hybrid modes:

$$\xi\eta-\left(s^2+\mathbf{q}_Z^2\omega_{sp}^2\right)\mathbf{I}_s(\mathbf{q}_zR_0)\mathbf{J}_s\left(\mathbf{q}_{s,p}^LR_0\right)=0 \tag{15}$$

where

$$\xi=\left[s\mathbf{J}_s\left(\mathbf{q}_{s,p}^LR_0\right)-\mathbf{q}_{s,p}^LR_0\mathbf{J}_{s+1}\left(\mathbf{q}_{s,p}^LR_0\right)\right]$$

$$\begin{bmatrix} s\mathbf{J}_s\left(\mathbf{q}_{s,p}^L R_0\right) - \\ -\mathbf{q}_{s,p}^L R_0 \mathbf{J}_{s+1}\left(\mathbf{q}_{s,p}^L R_0\right) \end{bmatrix} \begin{bmatrix} (s+1)\mathbf{I}_s\left(\mathbf{q}_z R_0\right) - \\ -C_{\mathbf{r}} R_0 \mathbf{q}_z \mathbf{I}_{s+1}\left(\mathbf{q}_z R_0\right) \end{bmatrix} - \left(s^2 + \mathbf{q}_Z^2 \omega_{sp}^2\right)\mathbf{I}_s(\mathbf{q}_z R_0)\mathbf{J}_s\left(\mathbf{q}_{s,p}^L R_0\right) = 0 \quad (16)$$

In this work, we calculated the dispersion relation with S = 0,1,2

For mode S=0, we get:

$$-\sqrt{\left(\omega_L^2 - \omega_{sp}^2\right)\beta^{-2} - \mathbf{q}_z^2}\, R_0 \mathbf{J}_1\left(\mathbf{q}_{s,p}^L R_0\right)\left[\mathbf{I}_0\left(\mathbf{q}_z R_0\right) - R_0 \mathbf{q}_z \mathbf{I}_1\left(\mathbf{q}_z R_0\right)\right] - \mathbf{q}_Z^2 \omega_{sp}^2 \mathbf{I}_0(\mathbf{q}_z R_0)\mathbf{J}_0\left(\mathbf{q}_{s,p}^L R_0\right) = 0$$

or

$$\begin{gathered} -\sqrt{\left(\omega_L^2 - \omega_{sp}^2\right)\beta^{-2} - k_z^2}\, R_0 \mathbf{J}_1\left(\sqrt{\left(\omega_L^2 - \omega_{sp}^2\right)\beta^{-2} - \mathbf{q}_z^2}\, R_0\right)\left[\mathbf{I}_0\left(k_z R_0\right) - R_0 \mathbf{q}_z \mathbf{I}_1\left(\mathbf{q}_z R_0\right)\right] - \\ - \mathbf{q}_Z^2 R_0^2 \mathbf{I}_0(\mathbf{q}_z R_0)\mathbf{J}_0\left(\sqrt{\left(\omega_L^2 - \omega_{sp}^2\right)\beta^{-2} - \mathbf{q}_z^2}\, R_0\right) = 0 \end{gathered} \quad (17)$$

For mode S=1

$$\begin{gathered} \left[\mathbf{J}_1\left(\mathbf{q}_{s,p}^L R_0\right) - \sqrt{\left(\omega_L^2 - \omega_{sp}^2\right)\beta^{-2} - \mathbf{q}_z^2}\, R_0\left(\frac{2}{\mathbf{q}_{s,p}^L R_0}\mathbf{J}_1\left(\mathbf{q}_{s,p}^L R_0\right) - \mathbf{J}_0\left(\mathbf{q}_{s,p}^L R_0\right)\right)\right] \times \\ \times\left[2\mathbf{I}_1\left(\mathbf{q}_z R_0\right) - R_0 \mathbf{q}_z\left(\frac{2}{\mathbf{q}_z r}\mathbf{I}_1\left(\mathbf{q}_z R_0\right) - \mathbf{I}_0\left(\mathbf{q}_z R_0\right)\right)\right] - \left(1 + \mathbf{q}_Z^2 R_0^2\right)\mathbf{I}_1(\mathbf{q}_z R_0)\mathbf{J}_1\left(\mathbf{q}_{s,p}^L R_0\right) = 0 \end{gathered} \quad (18)$$

2.4. The dispersion graph

We calculate and draw the dispersion graph for GaAs semiconductor wire with $\omega_L = 292.8\ cm^{-1}$; $\beta = 4.73.10^5\ cm.s^{-1}$ and radius $R_o = 30, 40, 50, 60, 70...$ Å for mode S = 0,1.

Mode S = 0, dispersion equation:

$$\begin{gathered} -\sqrt{\left(\omega_L^2 - \omega_{sp}^2\right)\beta^{-2} - k_z^2}\, R_0 \mathbf{J}_1\left(\sqrt{\left(\omega_L^2 - \omega_{sp}^2\right)\beta^{-2} - \mathbf{q}_z^2}\, R_0\right)\left[\mathbf{I}_0\left(k_z R_0\right) - R_0 \mathbf{q}_z \mathbf{I}_1\left(\mathbf{q}_z R_0\right)\right] - \\ - \mathbf{q}_Z^2 R_0^2 \mathbf{I}_0(\mathbf{q}_z R_0)\mathbf{J}_0\left(\sqrt{\left(\omega_L^2 - \omega_{sp}^2\right)\beta^{-2} - \mathbf{q}_z^2}\, R_0\right) = 0 \end{gathered}$$

The graph for this mode with radius of the wires R_0 =30, 60, 70,90, 120, 150 Å are shown in Fig 1,2,3.

Graph for mode S=1

$$\begin{gathered} \left[\mathbf{J}_1\left(\mathbf{q}_{s,p}^L R_0\right) - \sqrt{\left(\omega_L^2 - \omega_{sp}^2\right)\beta^{-2} - \mathbf{q}_z^2}\, R_0\left(\frac{2}{\mathbf{q}_{s,p}^L R_0}\mathbf{J}_1\left(\mathbf{q}_{s,p}^L R_0\right) - \mathbf{J}_0\left(\mathbf{q}_{s,p}^L R_0\right)\right)\right] \times \\ \times\left[2\mathbf{I}_1\left(\mathbf{q}_z R_0\right) - R_0 \mathbf{q}_z\left(\frac{2}{\mathbf{q}_z r}\mathbf{I}_1\left(\mathbf{q}_z R_0\right) - \mathbf{I}_0\left(\mathbf{q}_z R_0\right)\right)\right] - \left(1 + \mathbf{q}_Z^2 R_0^2\right)\mathbf{I}_1(\mathbf{q}_z R_0)\mathbf{J}_1\left(\mathbf{q}_{s,p}^L R_0\right) = 0 \end{gathered}$$

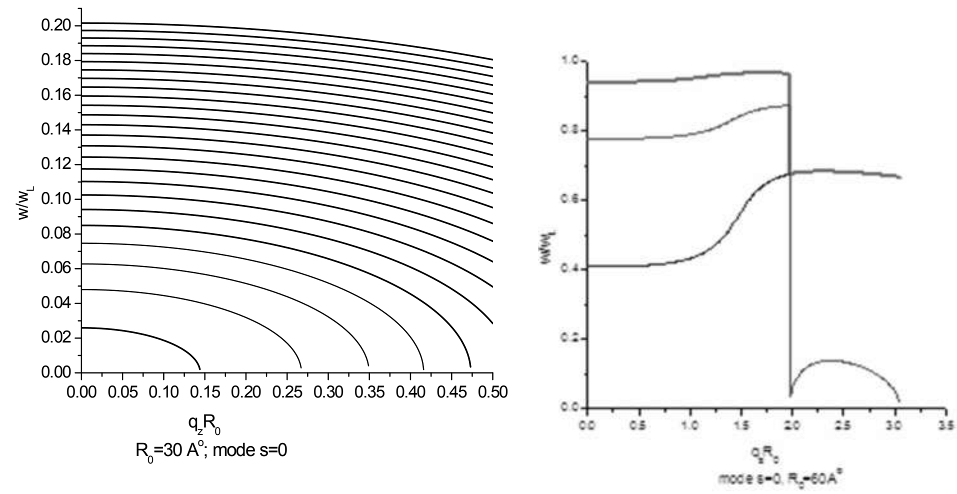

Figure 1

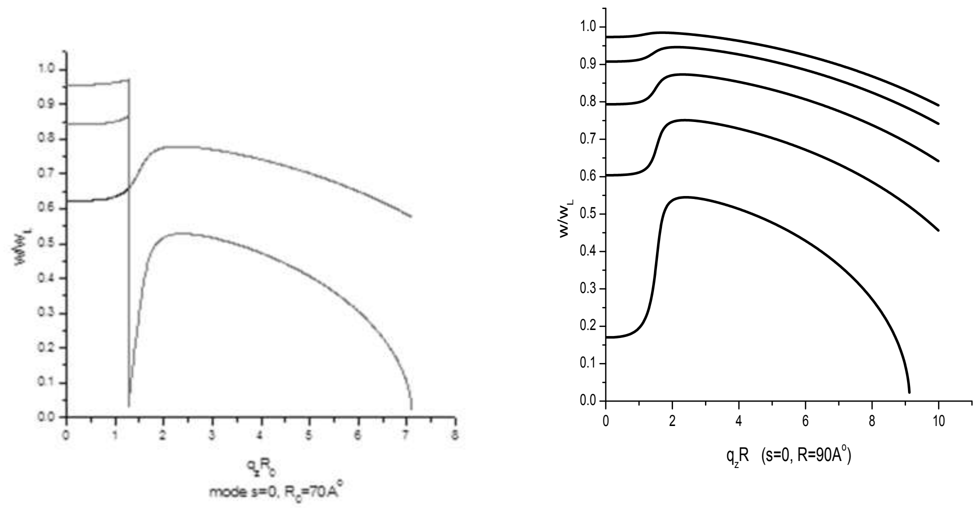

Figure 2

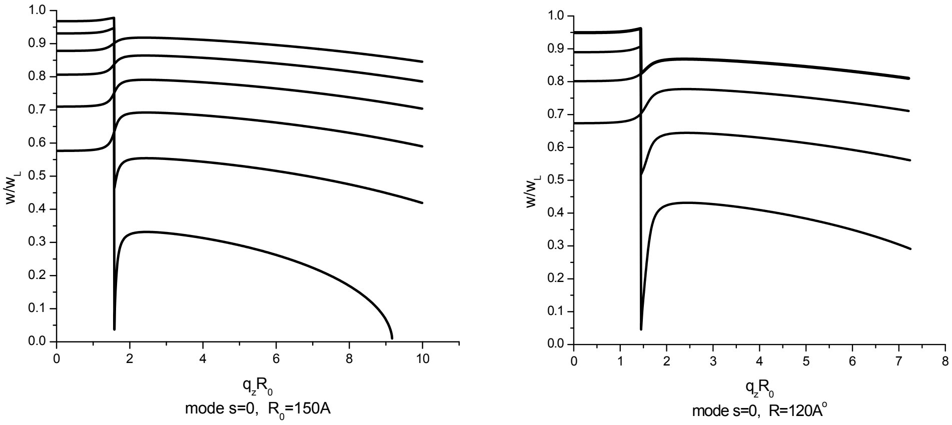

Figure 3

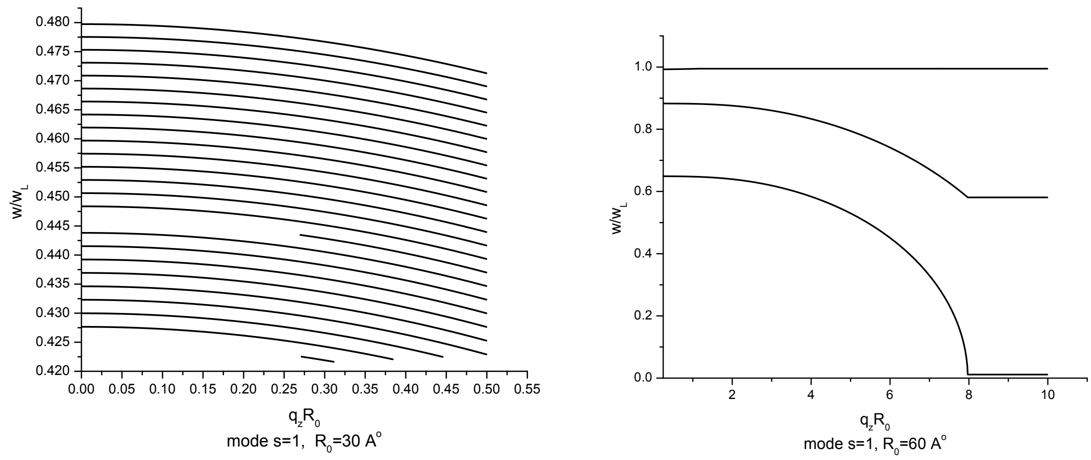

Figure 4

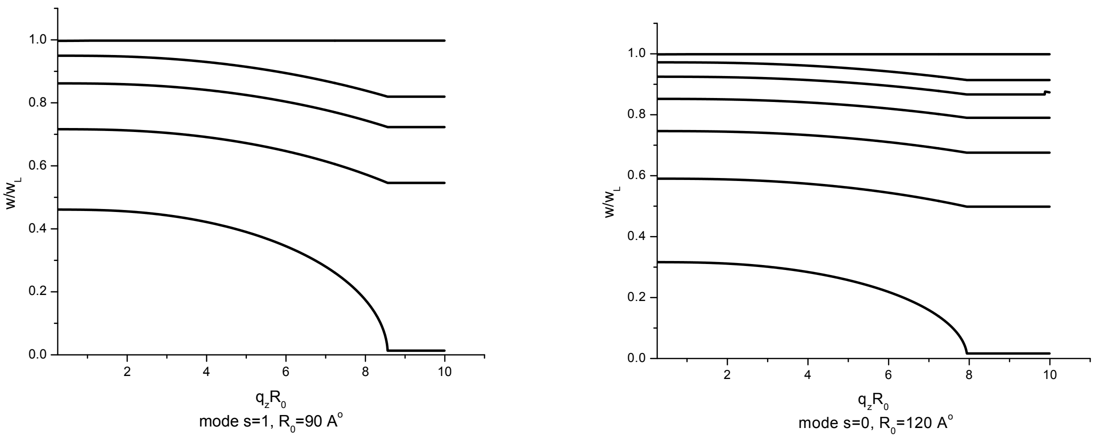

Figure 5

Dispersion graph showed the energy of hybridons in the wires. As can be seen from the figures, for the wires with radius smaller than 50 Å, the curves of dispersion graph has a high density and rapidly decrease when $\mathbf{q_z}R_0$ closed to 0.5. The high density of the despersion curves and the large spacing among them show that the quantization of hybrid modes is unclear. However, they resemble the dispersion curves of the LO mode in [4] but the curve of the hybrid mode more rapidly reach to zero. In the wires with radii bigger than 60Å, the density of the dispersion curves decreases. The flexure of the dispersion curves slowly decreases in the wires with bigger radius. These show that the quantization of the hybrid modes followed the Oz direction is clear.

3. CONCLUSION

Using continuous boundary conditions for a free quantum wire, we have found the equation of motion of the hybrid modes in the wires. Then using the second quantization theory, we obtained hybridons and found their dispersion patterns. The numerical results for a free GaAs wire show that the energy of the electrons is a function of the **q**z wave vector. It decreases rapidly to zero for those with a smaller radius. For larger ones, the speed is slower. For the wires with radii less than 50Å, dispersive curves show that hybrid modes are quantized and their energy is bound to be closer to each other and split up to more levels than the wire that have a radius greater than 50Å. The dispersion of wires smaller than 50Å depends on the **q**z wave vector smoothly, linearly and rapidly decreases to 0 when $\mathbf{q}_z R$ is about 0.5. For larger wires, the dependence has some unlinearity points and the curves is suddenly altered when $\mathbf{q}_z R$ is between 1.5 and 2.

REFERENCES

1. B. K. Redley, *Electron –hybridon interaction interaction a quan tum well.* Department of physic, Univercity of Esex, Wivenhoe Park, Colchester, Esex CO4 3SQ, England. Rev, 1991: p. 4592.
2. A. P. Silin, *Semiconductors superlattice* Soviet Physics Uspekhi, 1995. **28**: p. 972.
3. Đặng Trần Chiến, N.A., Nguyễn Sỹ Hải, Tạ Anh Tấn, *Optical modes in a free standing quantum wire.* Tạp chí Khoa học, 2016. **8**: p. 5-13.
4. N. C. Constantinou and B.K. Redley, *Interaction of Electron the confined LO phonons of a free-standing GaAs quantum wire* Phys. Rev. B. (1989). 1989. **41**: p. 10627

APPENDIX CALCULATION OF THE DISPERSIVE RELATION

To find the dispersion mode of mode, replace the coefficients A and C from expressions (3) and (4) into equation (2c).

$$\begin{aligned} &-B\frac{1}{\mathbf{q}_z R_0}\frac{1}{\mathbf{q}_z R_0}\frac{\left[\boldsymbol{\eta}^2 - s^2\mathbf{I}_s^2\left(\mathbf{q}_z R_0\right)\right]}{\boldsymbol{\eta}\mathbf{J}_s\left(\mathbf{q}_{sp}^L R_0\right)}\boldsymbol{\xi} + B\mathbf{I}_s(\mathbf{q}_z R_0) + \\ &\quad + Bs^2\frac{\left[\boldsymbol{\eta}^2 - s^2\mathbf{I}_s^2\left(\mathbf{q}_z R_0\right)\right] - \mathbf{q}_Z^2 R_0^2\mathbf{I}_s^2\left(\mathbf{q}_z R_0\right)}{\mathbf{q}_Z^2 R_0^2\boldsymbol{\eta}^2}\mathbf{I}_s(\mathbf{q}_z R_0) = 0 \end{aligned} \tag{D.1}$$

Transform this equation to get

$$\begin{aligned} &\frac{1}{\mathbf{q}_Z^2 R_0^2}\frac{\left[\boldsymbol{\eta}^2 - s^2\mathbf{I}_s^2\left(\mathbf{q}_z R_0\right)\right]}{\boldsymbol{\eta}^2\mathbf{J}_s\left(\mathbf{q}_{sp}^L R_0\right)}\boldsymbol{\xi}\boldsymbol{\eta} - \frac{\mathbf{q}_Z^2 R_0^2}{\mathbf{q}_Z^2 R_0}\boldsymbol{\eta}^2\mathbf{I}_s(\mathbf{q}_z R_0)\frac{\mathbf{J}_s\left(\mathbf{q}_{sp}^L R_0\right)}{\mathbf{J}_s\left(\mathbf{q}_{sp}^L R_0\right)} - \\ &-\frac{\left\{s^2\left[\boldsymbol{\eta}^2 - s^2\mathbf{I}_s^2\left(\mathbf{q}_z R_0\right)\right] - s^2\mathbf{q}_Z^2 R_0^2\mathbf{I}_s^2\left(bq_z R_0\right)\right\}}{\mathbf{q}_Z^2 R^2\boldsymbol{\eta}^2}\mathbf{I}_s(\mathbf{q}_z R)\frac{\mathbf{J}_s\left(\mathbf{q}_{sp}^L R_0\right)}{\mathbf{J}_s\left(\mathbf{q}_{sp}^L R_0\right)} = 0 \end{aligned}$$

$$\left[\boldsymbol{\eta}^2 - s^2\mathbf{I}_s^2\left(\mathbf{q}_z R_0\right)\right]\boldsymbol{\xi\eta} - \mathbf{q}_Z^2 R^2 \boldsymbol{\eta}^2 \mathbf{I}_s(\mathbf{q}_z R_0)\mathbf{J}_s\left(\mathbf{q}_{sp}^L R_0\right) -$$
$$-\left\{s^2\left[\boldsymbol{\eta}^2 - s^2\mathbf{I}_s\left(\mathbf{q}_z R_0\right)\right] - s^2\mathbf{q}_Z^2 R_0^2 \mathbf{I}_s^2\left(\mathbf{q}_z R_0\right)\right\}\mathbf{I}_s(\mathbf{q}_z R_0)\mathbf{J}_s\left(\mathbf{q}_{sp}^L R_0\right) = 0$$

$$\left[\boldsymbol{\eta}^2 - s^2\mathbf{I}_s^2\left(\mathbf{q}_z R_0\right)\right]\boldsymbol{\xi\eta} - \mathbf{q}_Z^2 R_0^2 \boldsymbol{\eta}^2 \mathbf{I}_s(\mathbf{q}_z R_0)\mathbf{J}_s\left(\mathbf{q}_{sp}^L R_0\right) -$$
$$-s^2\left[\boldsymbol{\eta}^2 - s^2\mathbf{I}_s^2\left(\mathbf{q}_z R_0\right)\right]\mathbf{I}_s(\mathbf{q}_z R_0)\mathbf{J}_s\left(\mathbf{q}_{sp}^L R_0\right) + s^2\mathbf{q}_Z^2 R_0^2 \mathbf{I}_s^2\left(\mathbf{q}_z R_0\right)\mathbf{I}_s(\mathbf{q}_z R_0)\mathbf{J}_s\left(\mathbf{q}_{sp}^L R_0\right) = 0$$

$$\left[\boldsymbol{\eta}^2 - s^2\mathbf{I}_s^2\left(\mathbf{q}_z R_0\right)\right]\left[\boldsymbol{\xi\eta} - s^2\mathbf{I}_s(\mathbf{q}_z R_0)\mathbf{J}_s\left(\mathbf{q}_{sp}^L R_0\right) - \mathbf{q}_Z^2 R_0^2 \mathbf{I}_s(\mathbf{q}_z R_0)\mathbf{J}_s\left(\mathbf{q}_{sp}^L R_0\right)\right] = 0$$

$$\left[\boldsymbol{\eta} - s^2\mathbf{I}_s^2\left(\mathbf{q}_z R_0\right)\right]\left[\boldsymbol{\xi\eta} - \left(\mathbf{q}^2 + \mathbf{q}_Z^2 R_0^2\right)\mathbf{I}_s(\mathbf{q}_z R_0)\mathbf{J}_s\left(\mathbf{q}_{sp}^L R_0\right)\right] = 0 \qquad \text{(D.2)}$$

From this equation, there are two cases:

$$\left[\begin{array}{l}\left[\boldsymbol{\eta}^2 - s^2\mathbf{I}_s^2\left(\mathbf{q}_z R_0\right)\right] = 0 \\ \boldsymbol{\xi\eta} - \left(s^2 + \mathbf{q}_Z^2 R_0^2\right)\mathbf{I}_s(\mathbf{q}_z R_0)\mathbf{J}_s\left(\mathbf{q}_{sp}^L R_0\right) = 0\end{array}\right. \qquad \text{(D.3)}$$

From (D.3), we obtain the dispersion relation for the hybrid mode as follows:

$$\boldsymbol{\xi\eta} - \left(s^2 + \mathbf{q}_Z^2 R_0^2\right)\mathbf{I}_s(\mathbf{q}_z R_0)\mathbf{J}_s\left(\mathbf{q}_{sp}^L R_0\right) = 0 \qquad \text{(D.4)}$$

or
$$\begin{bmatrix} s\mathbf{J}_s\left(\mathbf{q}_{sp}^L R_0\right) - \\ -\mathbf{q}_{sp}^L R_0 \mathbf{J}_{s+1}\left(\mathbf{q}_{sp}^L R_0\right)\end{bmatrix}\begin{bmatrix}\left(s+1\right)\mathbf{I}_s\left(\mathbf{q}_z R_0\right) - \\ -R_0\mathbf{q}_z\mathbf{I}_{s+1}\left(\mathbf{q}_z R_0\right)\end{bmatrix} - \left(s^2 + \mathbf{q}_Z^2 R_0^2\right)\mathbf{I}_s(\mathbf{q}_z R_0)\mathbf{J}_s\left(\mathbf{q}_{sp}^L R_0\right) = 0 \qquad \text{(D.5)}$$

In the framework of this problem we calculate the dispersion mode of hybrid mode for some simple modes with s=0,1,2,.

With s=0, we have

$$-\sqrt{\left(\omega_L^2 - \omega_{sp}^2\right)\beta^{-2} - \mathbf{q}_z^2}\, R_0 \mathbf{J}_1\left(\mathbf{q}_{sp}^L R_0\right)\left[\mathbf{I}_0\left(\mathbf{q}_z R_0\right) - R_0\mathbf{q}_z\mathbf{I}_1\left(\mathbf{q}_z R_0\right)\right] - \mathbf{q}_Z^2 R_0^2 \mathbf{I}_0(\mathbf{q}_z R_0)\mathbf{J}_0\left(\mathbf{q}_{sp}^L R_0\right) = 0$$

$$\begin{aligned}&\sqrt{\left(\omega_L^2 - \omega_{sp}^2\right)\beta^{-2} - \mathbf{q}_z^2}\, R_0 \mathbf{J}_1\left(\sqrt{\left(\omega_L^2 - \omega_{sp}^2\right)\beta^{-2} - \mathbf{q}_z^2}\, R_0\right)\left[\mathbf{I}_0\left(\mathbf{q}_z R_0\right) + R_0\mathbf{q}_z\mathbf{I}_1\left(\mathbf{q}_z R_0\right)\right] - \\ &\quad + \mathbf{q}_Z^2 R_0^2 \mathbf{I}_0(\mathbf{q}_z R_0)\mathbf{J}_0\left(\sqrt{\left(\omega_L^2 - \omega_{sp}^2\right)\beta^{-2} - \mathbf{q}_z^2}\, R_0\right) = 0\end{aligned} \qquad \text{(D.6)}$$

with s=1

$$\begin{bmatrix}\mathbf{J}_1\left(k_L R_0\right) - \\ -\sqrt{\left(\omega_L^2 - \omega_{sp}\right)\beta^{-2} - \mathbf{q}_z^2}\, R_0 \mathbf{J}_2\left(\mathbf{q}_{sp}^L R_0\right)\end{bmatrix}\begin{bmatrix}2\mathbf{I}_1\left(\mathbf{q}_z R_0\right) - \\ -R_0\mathbf{q}_z\mathbf{I}_2\left(\mathbf{q}_z R_0\right)\end{bmatrix} - \left(1 + \mathbf{q}_Z^2 R_0^2\right)\mathbf{I}_1(\mathbf{q}_z R_0)\mathbf{J}_1\left(\mathbf{q}_{sp}^L R_0\right) = 0$$

ta có

$$\mathbf{J}_2\left(\mathbf{q}_{sp}^L r\right)=\frac{2}{\mathbf{q}_{sp}^L r}\mathbf{J}_1\left(\mathbf{q}_{sp}^L r\right)-\mathbf{J}_0\left(\mathbf{q}_{sp}^L r\right)$$
$$\mathbf{I}_2\left(\mathbf{q}_z r\right)=\frac{2}{\mathbf{q}_z r}\mathbf{I}_1\left(\mathbf{q}_z r\right)-\mathbf{I}_0\left(\mathbf{q}_z r\right) \tag{D.7}$$

We obtained the dispersion relation for mode s=2

$$\left[\mathbf{J}_1\left(\mathbf{q}_{sp}^L R_0\right)-\sqrt{\left(\omega_L^2-\omega_{sp}^2\right)\beta^{-2}-\mathbf{q}_z^2}R_0\left(\frac{2}{\mathbf{q}_{sp}^L R_0}\mathbf{J}_1\left(\mathbf{q}_{sp}^L R_0\right)-\mathbf{J}_0\left(\mathbf{q}_{sp}^L R_0\right)\right)\right]\times$$
$$\times\left[\mathbf{I}_1\left(\mathbf{q}_z R_0\right)-R_0\mathbf{q}_z\left(\frac{2}{\mathbf{q}_z r_1}\left(\mathbf{q}_z R_0\right)-\mathbf{I}_0\left(\mathbf{q}_z R_0\right)\right)\right]-\left(1+\mathbf{q}_Z^2 R_0^2\right)\mathbf{I}_1(\mathbf{q}_z R_0)\mathbf{J}_1\left(\mathbf{q}_{sp}^L R_0\right)=0$$

HẠT LAI TRONG DÂY LƯỢNG TỬ TỰ DO

Tóm tắt: *Sự lai hoá của các mode quang bằng cách tổ hợp tuyến tính của cả 3 dao động phonon quang dọc (LO), các mode polariton bề mặt 1 (IP1) và polariton bề mặt 2 (IP2). Chúng thoả mãn đồng thời các điều kiện biên cơ và điện từ. Ở dây lượng tử tự do thì điều kiện biên liên tục của mọi độ dịch chuyển tiến đến 0 tại biên của dây. sử dụng lý thuyết lượng tử hoá lần thứ 2, chúng tôi thu được các hạt lai và tìm được các hệ thức tán sắc của chúng. Từ các kết quả tính số cho thấy năng lượng của electron là một hàm của véc tơ sóng* $\mathbf{q}_z$ *và nó giảm rất nhanh về không đối với những dây có bán kính nhỏ còn đối với những dây lớn hơn thì tốc độ giảm chậm hơn.*

Từ khóa: *Hạt lai, LO, IP1, IP2 véc tơ sóng* $\mathbf{q}_z$

H_1 DECAYS INTO A_1 AND A_1 IN THE NMSSM

[1]Nguyen Chinh Cuong, [2]Vu Dang Luat
[1]*Faculty of Physics, Ha Noi National University of Education,*
[2]*Thai Binh College of Education and Training.*

Abstract: *To solve the μ problem of the Minimal Supersymmetric Standard Model (MSSM), a single field S is added to build the Next Minimal Supersymmetric Standard Model (NMSSM). Vacuum enlarged with non-zero vevs of the neutral-even CP is the combination of H_u, H_d and S. In the NMSSM, the higgs sector is increased to 7 (compared with 5 higgs in the MSSM), including three higgs – which are the even-CP $h_{1,2,3}$ ($m_{h1}< m_{h2}< m_{h3}$), two higgs – which are odd-CP $a_{1,2}$ ($m_{a1}< m_{a2}$) and a couple of charged higgs $H^{\pm}$. The decay of higgs into higgs is one of the remarkable new points of the NMSSM. In this paper we study the decay ofh$_3$ into $a_1$and a_1, which is the main decay branch of the lightest neutral scalar higgs boson. The decay width is calculated to one loop vertex correction. The numerical calculation resultson the influence of CP violationare also givenfor discussion.*

Keywords: *Higgs boson, Decay, CP violation, NMSSM.*

Email: cuongnc@hnue.edu.vn
Received 14 May 2018
Accepted for publication 25 May 2018

1. INTRODUCTION

The simplest version of supersymmetry is the Minimal Supersymmetric Standard Model (MSSM). This version is limited by two problems: the μ and the hierarchy [1,3,4,7]. The simple supersymmetry, which is beyond the MSSM, is the Next Minimal Supersymmetric Standard Model (NMSSM). The special characteristic of Higgs boson in the NMSSM is the decay of Higgs into Higgs. It is remarkable that the lightest state a_1 of the odd-CP Higgs can play a role of a pseudo-goldstone, which has small mass and can lead to the predominated decay of the even-CP $h \to a_1 a_1$ [2].The even-CP Higgs and the heavy odd-CP Higgs can be generated at LEP in $e^+e^- \to ha$, but they may not be discovered because the dominant h decay were not searched for. There are different ways to make the mass of Higgs boson increased in the MSSM and in the beyond MSSM. One simple way is to study the beyond singlet of the MSSM which contains one term $\lambda\hat{S}\hat{H}_u\hat{H}_d$ in the super-potential, this is the term that contributes $\lambda^2 v^2 \sin^2 2\beta$ at v = 174 GeV to the squared mass of even-CP Higgs [10]and therefore, it can make the mass of Higgs boson increased over the limit of independent decay state.

The charged Higgs makes up more than 40% in the top-quark decay at Tevatron; the products of this decay are charged Higgs and bottom-quark ($t \to H^+ b$). The decay method of charged Higgs is $H^\pm \to W^\pm a_1$, with $a_1 \to \overline{cc}, gg$.

The neutral Higgs sector in the NMSM includes the following states: three even-CP and two odd-CP. Many analysis on Higgs sector in the NMSSM [5] have shown that, in the specific physical state of the even-CP Higgs, there is a strong mix between the doublet state and the singlet SU(2) with the reduction in the interaction of gauge boson. The study on light Higgs contributes to the discovery of one or more Higgs states at LEP, at LHC [5] and at large energy accelerators.

In the NMSSM, the terms of the super-potential $W_{\text{Higgs}}$are dependent on superfieldHiggs $\hat{H}_d$, $\hat{H}_u$ and $\hat{S}$ (here, we follow the SLHA2 regulations, however $\hat{H}_u$ is also written as $\hat{H}_d$ and $\hat{H}_d$ is also written as $\hat{H}_1$):

$$\boldsymbol{W}_{\text{Higgs}} = \left(\mu + \lambda\hat{S}\right)\hat{H}_u.\hat{H}_d + \xi_F\hat{S} + \mu'\hat{S}^2 + \frac{\kappa}{3}\hat{S}^3 \tag{1}$$

with: λ, κ is the non-dimension coupling Yukawa

μ, μ' is the supersymmetry mass,

ξ_F is the square supersymmetry mass parameter.

From (1), Yuakawa interaction of quark and lepton superfield are added to

$$W_{\text{Yukawa}} = h_u\hat{H}_u.\hat{Q}\hat{U}_R^c + h_d\hat{H}_d.\hat{Q}\hat{D}_R^c + h_e\hat{H}_d.\hat{L}\hat{E}_R^c \tag{2}$$

The soft breaking supersymmetry sector is regulated in SLHA2:

$$\begin{aligned} -L_{\textit{soft}} = {} & m_{Hu}^2\left|H_u\right|^2 + m_{Hd}^2\left|H_d\right|^2 + m_s^2\left|S\right|^2 + m_Q^2\left|Q^2\right| + m_U^2\left|U_R^2\right| \\ & + m_D^2\left|D_R^2\right| + m_L^2\left|L^2\right| + m_E^2\left|E_R^2\right| \\ & + (h_uA_uQ.H_uU_R^c - h_dA_dQ.H_dD_R^c - h_eA_eL.H_dE_R^c \\ & + \lambda A_\lambda H_u.H_dS + \frac{1}{3}\kappa A_\kappa S^3 + m_3^2H_u.H_d + m_s^{2\prime}S^2 + \xi_sS + hc) \end{aligned} \tag{3}$$

As any supersymmetry theory with invariant super-potential sector (ternary), the Lagrangians,which contain the soft supersymmetry violation conditionsspecified by (3), have one symmetry Z_3 randomly, which is corresponding to the multiplication of all chiral superfields with $e^{2\pi i/3}$. The non-dimension terms in the super-potential (1) will break the symmetry Z_3. The model with super-potential (1) is the NMSSM. The invariant Z_3 Higgs sector isdefined by the seven parameters $\lambda, \kappa, m_{H_d}^2, m_{H_u}^2, m_S^2, A_\lambda, A_\kappa$. The expression of Higgs mass matrix in the invariant Z_3 of the NMSSM shows that invariant Z_3 is obtained when:

$$m_3^2 = m_S^{2\prime} = \xi_S = \mu = \mu' = \xi_F = 0. \tag{4}$$

From the supersymmetry gauge interaction and soft supersymmetry breaking conditions, we obtainthe Higgs potential:

$$\begin{aligned} V_{Higgs} &= \left|\lambda(H_u^+H_d^- - H_u^0H_d^0) + \kappa S^2 + 2\mu' S + \xi_F\right|^2 \\ &+ (m_{H_u}^2 + |\mu + \lambda S|^2(|H_u^0|^2 + |H_u^+|^2) + (m_{H_d}^2 + |\mu + \lambda S|^2(|H_d^0|^2 + |H_d^-|^2) \\ &+ \frac{g_1^2 + g_2^2}{8}(|H_u^0|^2 + |H_u^+|^2 - |H_d^0|^2 - |H_d^-|^2)^2 + \frac{g_2^2}{2}\left|H_u^+H_d^{0*} + H_u^0H_d^{0*}\right|^2 \\ &+ m_S^2|S|^2 + (\lambda A_\lambda(H_u^+H_d^- - H_u^0H_d^0)S + \frac{1}{3}\kappa A_\kappa S^3 + m_3^2(H_u^+H_d^- - H_u^0H_d^0) \\ &+ m_S'^2S^2 + \xi_S S + h.c \end{aligned} \tag{5}$$

where g_1 and g_2 present gauge interaction U(1) and SU(2) .

The Higgs doublets H_1 and H_2 can be developed in the form:

$$H_1 = \begin{pmatrix} v_1 + S_1 + iA\sin\beta \\ H^{+*}.\sin\beta \end{pmatrix},\ H_2 = \begin{pmatrix} H^+.\cos\beta \\ v_2 + S_2 + iA\cos\beta \end{pmatrix},\ S = (x + X + iY) \tag{6}$$

In case the CP violation is considered, the x parameter will be considered as the complex number.

In the year 2012, the Higgs boson was found out with the mass approximatesto 125GeV, which could be considered as the $h_2$in the NMSSM.The decay of Higgs into Higgs in the NMSSMis being researched in the experiment. The research on the decay of the new particles in the model will bring usthe hope of finding out these particles as well as verifying the correctness of the model [6]. In this paper, we have studied the decay $h_1 \to a_1 + a_1$ and calculated the decay width of this process to one loop vertex correction. The numerical calculation results arealso presented in charts to evaluate the influence of CP violation onthe decay width and the lifetime of h_1.

2. THEFEYNMAN DIAGRAM FOR CORRECTION SUSY – QCD IN DECAY$H_1 \to A_1 + A_1$

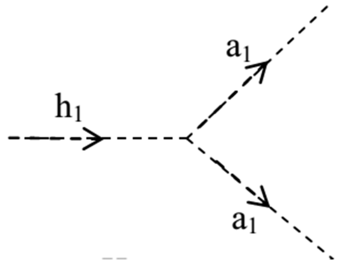

Figure 1: Feyman diagram for Tree levvel of decay$h_1 \to a_1 + a_1$.

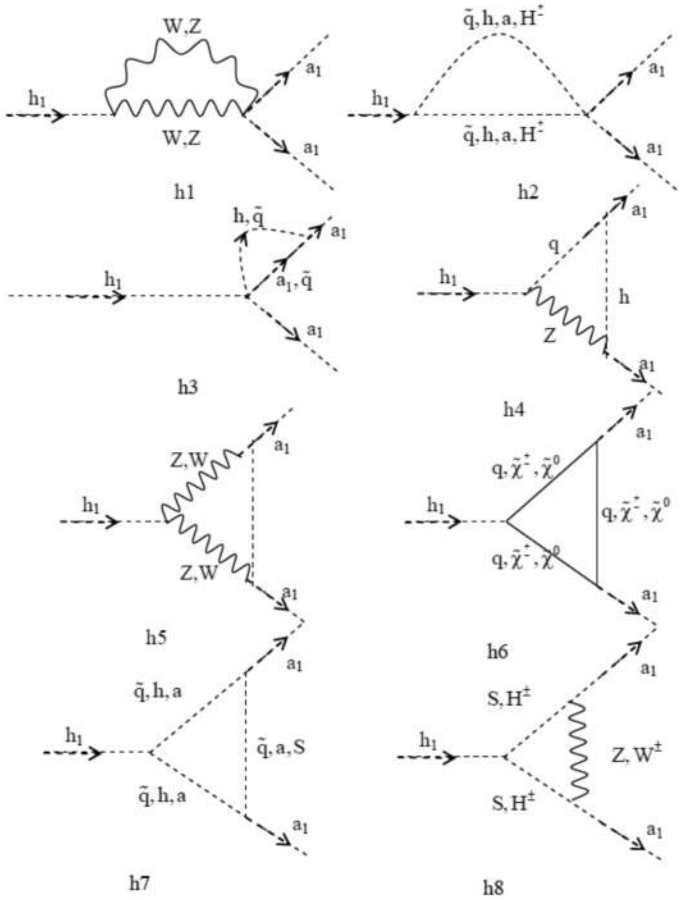

Figure 2: Feyman diagram for one loop vertex correction SUSY – QCD in decay$h_1 \to a_1 + a_1$.

3. NUMERICAL RESULTS

To study the influence of the mass $m_{a1}$and the CP violation phaseϕon the decay process $h_1 \to a_1 a_1$, we have used two set of parameters [5, 6, 8, 9] for programming numerical calculation on the Maple version 17.0. The results are calculated to the one loop vertex correction as in Fig.2 and Fig.3.

* The 1st parameter set: $\lambda = 0{,}8$; $x = 200.e^{i\phi}$; $k = 0{,}1$; m_{h1}= 98GeV; $\tan\beta = 3$; $\sin\alpha = -0{,}58$; $A_k = 6$; $A_\lambda = 486$. From the results obtained, we have found that the influence of ϕ on the decay $h_3 \rightarrow Za_1$is relatively significant (Figure.3 and Figure.4).

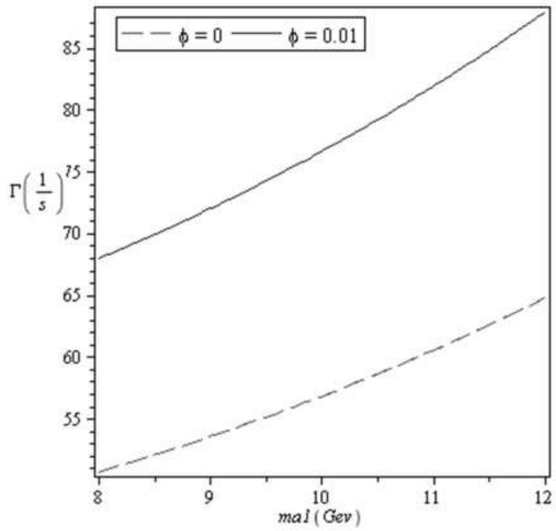

Figure 3: The influence of ma_1 on the decay width of the decay $h_1 \rightarrow a_1a_1$.

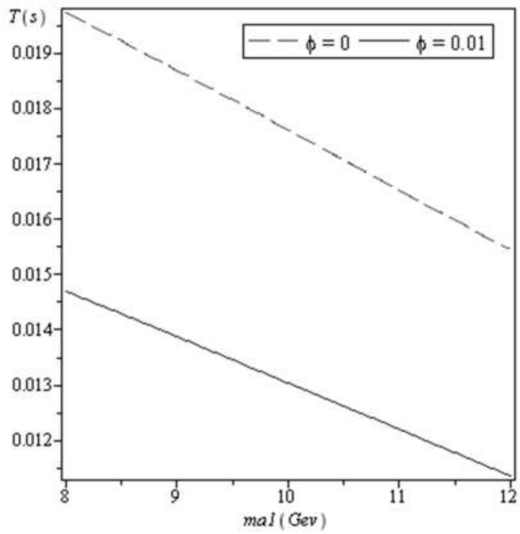

Figure 4:The influence of ma_1 on the lifetime of $h_1$of the decay $h_1 \rightarrow a_1a_1$.

Specifically, the influence of odd-CPHiggs mass a_1 (ma_1)and CP violation phase parameter (ϕ) on the decay width and on the lifetime of h_1 in the decay $h_1 \rightarrow a_1a_1$is relatively significant. When ma_1changesfrom 8GeVto12GeV, it can make thedecay width increased about 25% and make the lifetime of h_1 decreased about 26%. When ϕ= 0.01rad, the decay width increases about 35% andthe lifetime of h_1 decreasesabout 36% in comparision with the cases without CP violation. With the 1st parameter set, when the CP violation is taken into account, we have obtained the results as follows: the decay width $h_1 \rightarrow a_1a_1$**is** around 67 – 87 (1/s) and the lifetime of $h_1$is around0.011–0.0147 (s).

* The 2nd parameter set: $\lambda = 0.8$; $x = 200e^{i\phi}$; $k = 0.1$; m_{h1} = 98GeV; $\tan\beta = 10$; $\sin\alpha = -0.726$; $A_k = 7$; $A_\lambda = 492$.. We have obtained the results as in Fig. 5 and Fig. 6.

From the results in the graphs for the 2nd parameter set, we can see that the contribution of ma_1 andϕ in this case is relatively significant. When ma_1changes from 8GeV to 12GeV, it can make the decay width increased about 31% and make the lifetime of h_1 decreased about 30%. When ϕ= 0.01rad, the decay width decreases about 5% and the lifetime of $h_1$increases about 5% in comparision with the cases without CP violation. With the 2nd parameter set, when the CP violation is taken into account, we have obtained the results as follows: the decay width $h_1 \to a_1a_1$is around60 – 82 (1/s) and the lifetime of $h_1$is around0.012 – 0.016 (s).

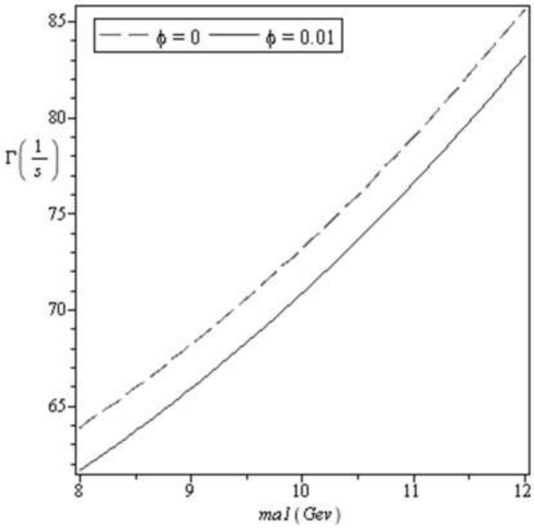

Figure 5: The influence of ma_1 on the decay width of the decay $h_1 \to a_1a_1$.

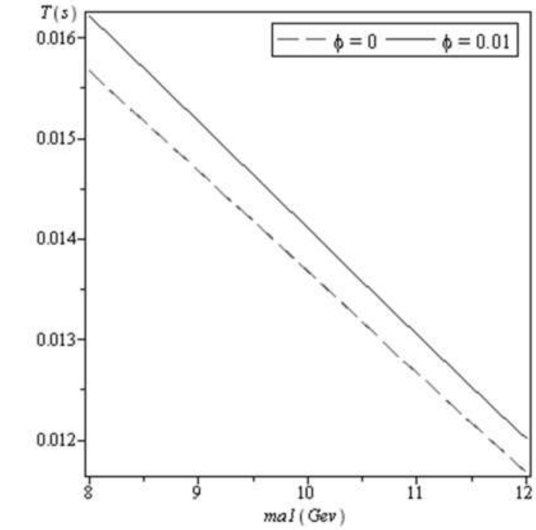

Figure 6: The influence of ma_1 on the lifetime of $h_1$of the decay $h_1 \to a_1a_1$.

4. CONCLUSION

In the NMSSM, a single superfield is added with complex scalar field components, this leads to the appearance of seven Higgs in the NMSSM (including three even-CP Higgs $h_{1,2,3}$ ($m_{h1}< m_{h2}< m_{h3}$), two odd-CP Higgs $a_{1,2}$ ($m_{a1}< m_{a2}$) and a pair of charged Higgs $H^{\pm}$).

The influence of CP violation on the decay width and the life time of h_1 is relatively significant in case the 1st set of parameter is used (the results can be changed up to 35%).

The influence of ma_1on the decay width and the life time of h_1 is relatively significant, about 25%-31% on the decay width and about 26%-30% on the lifetime of h_1.

The numerical calculation results have shown that the lifetime of $h_1$is around0.012 – 0.016 (s) and the decay with is around60 – 82 (1/s).

From these results,we need to pay attention to the above two elementsin studying theories as well as to the decay experiments of h_1.These results bring us the hope that we can find the other Higgsbosons soon.

Acknowledgements. This research is supported by the National Foundation for Scienceand Technology Development (NAFOSTED) of Vietnam. Grant number: 103.01-2016.44.

REFERENCES

1. Radovan Demi'senk and John F. Gunion, hep-ph/0811.3537.
2. M.M. Almarashi anh S.moretti, hep-ph/1109.1735.
3. M.M. Almarashi anh S.moretti, hep-ph/1105.4191.
4. H. E. Haber and G.L. Kane.Phys. Rep. 117 (1985) 75.
5. Ulrich Ellwanger, hep-ph/1108.0157.
6. U. Ellwanger, C. Hugonie and A. M. Teixeira, Phys. Rept. 496 (2010) 1.
7. W. Bernrenther and M. Suzuki, Rev. Mod. Phys. 63 (1991) 3-13.
8. N. C. Cuong, P. X. Hung, L. H. Thang, Scientific Journal of HMU, 2 (2016), 22-30.
9. Radovan Dermisek (2010), hep-ph/1012.3487vl.
10. A. Barlt, et. al., Phys. Lett.B419 (1998) 243.

PHÂN RÃ H_1 THÀNH A_1 VÀ A_2 TRONG NMSSM

Tóm tắt: *Để giải quyết vấn đề μ trong mô hình chuẩn siêu đối xứng tối thiểu (MSSM), một trường đơn S được đưa vào khi xây dựng mô hình chuẩn siêu đối xứng gần tối thiểu (NMSSM).Trong NMSSM sẽ có 7 boson Higgs (còn trong MSSM có 5 boson Higgs), với ba Higgs vô hướng - CP chẵn $h_{1,2,3}$ ($mh_1 < mh_2 < mh_3$) cùng hai Higgs giả vô hướng - CP lẻ $a_{1,2}$ ($ma_1 < ma_2$) và một cặp Higgs mang điện $H^{\pm}$. Phân rã Higgs thành Higgs là một điểm mới đáng chú ý của NMSSM.Trong bài báo này chúng tôi nghiên cứu phân rã $h_1 \rightarrow a_1\, a_1$ là kênh phân rã chủ yếu của boson higgs vô hướng trung hòa nhẹ nhất.Độ rộng phân rã được tính tính tới hiệu chỉnh đỉnh một vòng. Các kết quả tính số về ảnh hưởng của vi phạm CP cũng được đưa ra để thảo luận.*

Từ khóa: *Higgs boson, phân rã, vi phạm CP, NMSSM.*

UNPARTICLE PRODUCTION IN e^+e^- COLLISION WHEN e^+e^- ARE POLARIZED

Nguyen Thi Hau[1], Dao Thi Le Thuy[2], Le Nhu Thuc[2]
[1]Hanoi University of Mining and Geology, [2]Hanoi National University of Education
[1]email: nguyenthihau@humg.edu.vn; [2]email: thuydtl@hnue.edu.vn

Abstract: *In this paper, we studied detail the process* $e^+e^- \to \gamma \mathcal{U}(\mathcal{U}^\mu)$ *and* $e^+e^- \to Z\mathcal{U}(\mathcal{U}^\mu)$. *In each process, we calculated the differential cross section and total cross section when* e^+, e^- *beams are unpolarized and polarized. The results show that, the cross-section depends strongly on the polarization of the initial beams and can observe the unparticle in the low energy domain.*

Keywords: *Unparticle physics, polarized, cross section.*

Email: nguyenthihau@humg.edu.vn
Received 24 May 2018
Accepted for publication 7 June 2018

1. INTRODUCTION

The Standard Model (SM) has brought a lot of success, but it still has many existing problems. For example, it could not explain neutrinos to be massive, does not include gravity, has no dark matter candidate, subsumes the so-called hierarchy problem, etc. One of the extended models of the SM is unparticle physics, which is Georgy proposed since 2007 [1]. Until now, unparticle effects have been explored in many areas spanning Collider physics [2–7], cosmology and astrophysics [8], black holes [9-11]. Also, many papers have studied the presence of unparticle in CP violation, such as [12-16]. Unparticles have been proposed to explain some anomalies in currents flowing in super-conductors [17-19] and the scientists are trying to find unparticle at the LHC [4-6, 9, 20]. We are notice to the issue about "Interactions of Unparticles with Standard Model Particles" [21]. In this paper, the authors analyzed interactions of scalar $\mathcal{U}$, vector $\mathcal{U}^\mu$ and spinor $\mathcal{U}^s$ unparticles with SM fields. They listed possible operators involving interactions of scalar $\mathcal{U}$, vector $\mathcal{U}^\mu$ and spinor $\mathcal{U}^s$ unparticles with the SM fields and derivatives up to dimension four and discussed some phenomenology related to these operators. They concentrated on the possibility of distinguishing whether an O_{u} and an O_{u}^{μ} is produced through e^+e^- collider through $e^+e^- \to \gamma \mathrm{u}(\mathrm{u}^{\mu})$, $e^+e^- \to Z\mathrm{u}(\mathrm{u}^{\mu})$. However, they did not analyze e^+e^- collider when e^+, e^- beams are polarized. In this work, we continue to evaluate the scalar $\mathcal{U}$ and vector $\mathcal{U}^{\mu}$ unparticle production in e^+e^- collisions when e^+, e^- beams are unpolarized and polarized.

At high energy the theory of unparticles contains the SM fields and the fields of the scale invariant sector, called BZ fields [22]. The interactions between the SM particles and BZ sector occur through the exchange of heavy particles at a very high energy $M_{\mathcal{U}}$. Once those heavy fields are integrated out, the effective Lagrangian that describes the interactions between the SM particles and unparticles is obtained. The corresponding effective Lagrangian that respects $SU(3)_C \times SU(2)_L \times U(1)_Y$ gauge invariance can be written as [1, 23]:

$$L_{\mathcal{U}} = C_{O_{\mathcal{U}}} \frac{\Lambda_{\mathcal{U}}^{d_{BZ}-d_{\mathcal{U}}}}{M_{\mathcal{U}}^{d_{SM}+d_{BZ}-4}} O_{SM} O_{\mathcal{U}} \tag{1}$$

Where $d_{\mathcal{U}}$ is the scale dimension of the unparticle operator $O_{\mathcal{U}}$, O_{SM} is an operator with mass dimension d_{SM} built out of SM fields and $C_{O_{\mathcal{U}}}$ is a coefficient function fixed by the matching. For instance, the effective interactions of spin-0 and spin-1 unparticles with SM fermions are as follows [1], [3].

$$\lambda_0 \frac{1}{\Lambda_{\mathcal{U}}^{d_{\mathcal{U}}-1}} \bar{f} f O_{\mathcal{U}}, \lambda_0 \frac{1}{\Lambda_{\mathcal{U}}^{d_{\mathcal{U}}-1}} \bar{f} i\gamma^5 f O_{\mathcal{U}}, \lambda_0 \frac{1}{\Lambda_{\mathcal{U}}^{d_{\mathcal{U}}}} \bar{f} \gamma^{\mu} f (\partial_{\mu} O_{\mathcal{U}}), \lambda_0 \frac{1}{\Lambda_{\mathcal{U}}^{d_{\mathcal{U}}}} G_{\alpha\beta} G^{\alpha\beta} O_{\mathcal{U}} \tag{2}$$

$$\lambda_1 \frac{1}{\Lambda_{\mathcal{U}}^{d_{\mathcal{U}}-1}} \bar{f} \gamma_{\mu} f O_{\mathcal{U}}^{\mu}, \lambda_1 \frac{1}{\Lambda_{\mathcal{U}}^{d_{\mathcal{U}}-1}} \bar{f} \gamma_{\mu} \gamma_5 f O_{\mathcal{U}}^{\mu} \tag{3}$$

In this paper, we are interested in the production of the scalar $\mathcal{U}$ and vector $\mathcal{U}^{\mu}$ unparticle in e^+e^- collider when the e^+, e^- beams are unpolarized and polarized. The Feynman diagrams for this collider are shown in Fig.1.

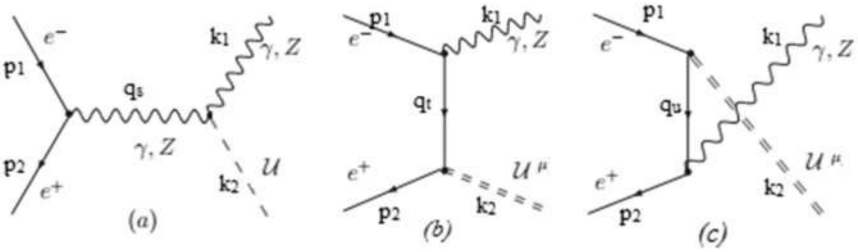

Figure 1: *The Feynman diagrams for the process* $e^+e^- \to \gamma(Z)\mathrm{u}(\mathrm{u}^{\mu})$

Next, in section II, III we evaluate the number and discuss dependence of the differential cross-section (DCS) on cosθ, and the total cross-section fully follows $\sqrt{s}$ for $e^+e^- \to \gamma \mathcal{U}(\mathcal{U}^\mu)$, $e^+e^- \to Z\mathcal{U}(\mathcal{U}^\mu)$ process, respectively. Finally, the conclusions are presented in Sec.IV.

2. CROSS SECTION FOR THE PROCESS $e^+e^- \to \gamma \mathcal{U}(\mathcal{U}^\mu)$

For unpolarized e^+,e^- beams, using Feynman rules, the matrix element for process $e^+e^- \to \gamma \mathcal{U}(\mathcal{U}^\mu)$ is given as following.

+ For $\mathcal{U}$ production, the matrix element only through by s-channel:

$$M_{s\gamma} = -\frac{4ie\lambda_0}{\Lambda_u^{du} q_s^2}\overline{v}(p_2)\gamma^\mu u(p_1) g_{\mu\nu}\varepsilon_\alpha^*(k_1)\left(-(k_1 q_s)g^{\alpha\nu} + k_1^\nu q_s^\alpha\right) \tag{4}$$

+ For $\mathcal{U}^\mu$ production, the matrix element through by u, t-channels:

$$M_{t\gamma} = \frac{e\lambda_1}{\Lambda_u^{du-1}\left(q_t^2 - m_e^2\right)}\overline{v}(p_2)\gamma^\nu(1+\gamma^5)\varepsilon_\nu(k_2)\left(\hat{q}_t + m_e\right)\varepsilon_\mu(k_1)\gamma^\mu u(p_1) \tag{5}$$

$$M_{u\gamma} = \frac{e\lambda_1}{\Lambda_u^{du-1}\left(q_u^2 - m_e^2\right)}\overline{v}(p_2)\gamma^\nu\varepsilon_\nu(k_2)\left(\hat{q}_u + m_e\right)\varepsilon_\mu(k_1)\gamma^\mu(1+\gamma^5)u(p_1) \tag{6}$$

where $q_s = p_1 + p_2 = k_1 + k_2$; $q_t = p_1 - k_1 = k_2 - p_2$; $q_u = k_1 - p_2 = p_1 - k_2$.

Similarly, we obtained the matrix element of the process of $e^+e^- \to \gamma \mathcal{U}(\mathcal{U}^\mu)$ when the e^+,e^- beams are polarized by substituting $u(k)$ into $P_L u(k)$ or $P_R u(k)$ and $v(k)$ into $P_L v(k)$ or $P_R v(k)$.

Here $k = p_1, p_2, k_1, k_2$ and

$$P_L = \frac{1-\gamma_5}{2}, P_R = \frac{1+\gamma_5}{2} \tag{7}$$

By using this matrix elements, we evaluated the DCS of the process $e^+e^- \to \gamma \mathcal{U}(\mathcal{U}^\mu)$ by the expression:

$$\frac{d\sigma}{d\cos\theta} = \frac{1}{64\pi s}\frac{\left|\vec{k}_1\right|}{\left|\vec{p}_1\right|}\left|M\right|^2 \tag{8}$$

where M is the matrix element, $s = (p_1 + p_2)^2$, $\sqrt{s}$ is the center-of-mass energy and θ is angle between $\vec{p}_1$ and $\vec{k}_1$.

We chose $d_u = 1.5$, $\Lambda_u = 1000$ and $\lambda_0 = \lambda_1 = 1$ to evaluate the number of the dependence of the DCS on cosθ. We obtained some results for the cross-section as following:

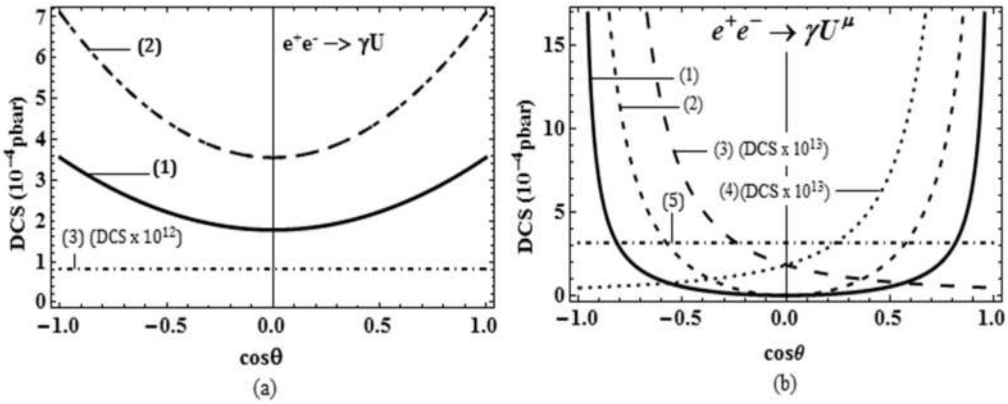

Figure 2: *The DCS of* $e^+e^- \to \gamma\mathcal{U}$ *(a) and* $e^+e^- \to \gamma\mathcal{U}^\mu$ *(b) as a function of* $\cos\theta$ *when the* e^+, e^- *beams are unpolarized and polarized. In Fig.2a, (1), (2), (3) are* e^+e^-, $e^+_Re^-_R$ *or* $e^+_Le^-_L$ *and mix* $(e^+_Re^-_R; e^+_Le^-_L)$, *respectively. In Fig.2b, (1), (2), (3), (4), (5) are* e^+e^-, $e^+_Re^-_R$, $e^+_Le^-_R$, $e^+_Re^-_L$ *and mix* $(e^+_Re^-_R; e^+_Re^-_L; e^+_Le^-_R)$, *respectively.*

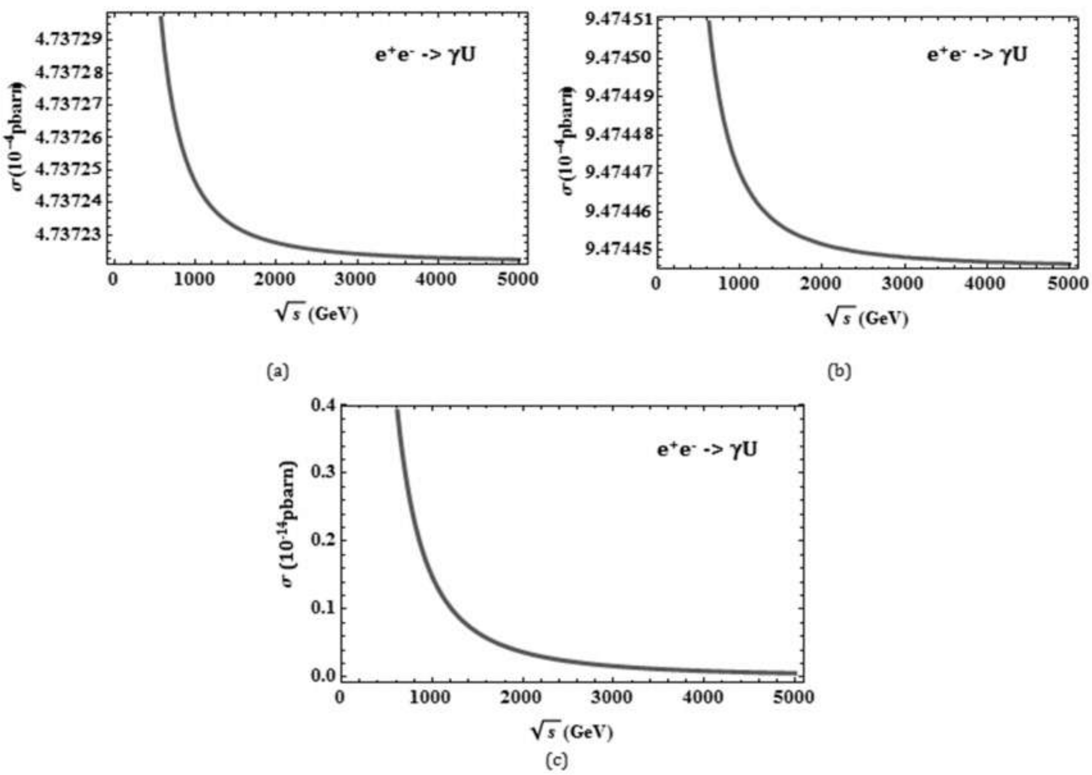

Figure 3: *The total cross-section of* $e^+e^- \to \gamma\mathcal{U}$ *as a function of the collision energy* $\sqrt{s}$ *when the* e^+, e^- *beams are unpolarized (a),* $(e^+_Re^-_R)$ *or* $(e^+_Le^-_L)$ *(b) and mix* $(e^+_Re^-_R; e^+_Le^-_L)$ *(c).*

In the Figure 2 shows that, the behavior of DCS at fixed collision energy $\sqrt{s}$ = 3000GeV (CLIC). For $\mathcal{U}$ production, the DCS when the e^+, e^- beams right-right polarized or left-left polarized are largest and the DCS equals zero when the e^+, e^- beams are right-left polarized or left-right polarized. For $\mathcal{U}^\mu$ production, the DCS equals zero when the e^+, e^- beams are left-left polarized, the DCS when the e^+, e^- beams right-right polarized are largest.

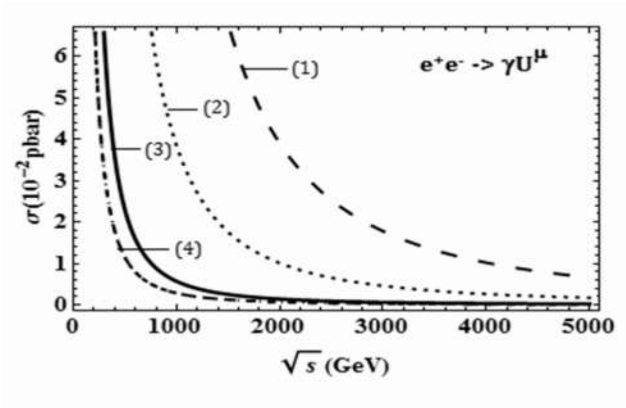

Figure 4: *The total cross-section of $e^+e^- \to \gamma\mathcal{U}^\mu$ as a function of the collision energy $\sqrt{s}$ when the e^+, e^- beams are unpolarized and polarized. Here (1), (2), (3), (4) are $e_R^+e_R^-$, e^+e^-, $mix(e_R^+e_R^-; e_R^+e_L^-; e_L^+e_R^-)$, and $e_L^+e_R^-$ or $e_R^+e_L^-$, respectively.*

Next, we plotted the total cross-section as a function of the collision energy $\sqrt{s}$. The $\sqrt{s}$ dependence of the $e^+e^- \to \gamma\mathcal{U}$ cross section is shown in Fig. 3 and of the $e^+e^- \to \gamma\mathcal{U}^\mu$ cross section is shown in Fig. 4. The figures show that the total cross-section decreases when $\sqrt{s}$ increases for the $\mathcal{U}^\mu$ production.

3. CROSS SECTION FOR THE PROCESS $e^+e^- \to Z\mathcal{U}(\mathcal{U}^\mu)$

By using Feynman rules, the matrix element for process $e^+e^- \to Z\mathcal{U}(\mathcal{U}^\mu)$ is givens as following:

+ For $\mathcal{U}$ production, the matrix element only through by s-channel:

$$M_{sz} = \frac{i\lambda_0 g}{\Lambda_u^{du} c_W \left(q_s^2 - m_z^2\right)} \overline{v}(p_2)\gamma^\mu \left(-1 + 4s_W^2 + \gamma^5\right) u(p_1) \left(g_{\mu\nu} - \frac{q_{s\mu} q_{s\nu}}{m_z^2} \right) \varepsilon_\alpha^*(k_1) \left(-k_1 q_s . g^{\alpha\nu} + k_1^\nu q_s^\alpha\right) \quad (9)$$

+ For $\mathcal{U}^\mu$ production, the matrix element through by u, t-channels:

$$M_{tz} = -\frac{\lambda_1 g}{\Lambda_u^{du-1} 4c_W \left(q_t^2 - m_e^2\right)} \overline{v}(p_2)\gamma^\nu (1+\gamma^5) \varepsilon_\nu(k_2) \left(\hat{q}_t + m_e\right) \varepsilon_\mu(k_1) \gamma^\mu \left(-1 + 4s_W^2 + \gamma^5\right) u(p_1) \quad (1)$$

$$M_{uz} = -\frac{\lambda_1 g}{\Lambda_u^{du-1} 4c_{\mathrm{w}}\left(q_u^2 - m_e^2\right)} \bar{v}(p_2)\gamma^{\nu}\left(-1+4s_{\mathrm{w}}^2+\gamma^5\right)\varepsilon_{\nu}(k_2)\left(\hat{q}_u + m_e\right)\varepsilon_{\mu}(k_1)\gamma^{\mu}\left(1+\gamma^5\right)u(p_1) \quad (2)$$

After substituring $u(k)$ into $P_L u(k)$ or $P_R u(k)$ and $v(k)$ into $P_L v(k)$ or $P_R v(k)$, we obtained the matrix element of the process $e^+e^- \to \gamma U(U^{\mu})$ when the e^+, e^- beams are polarized.

Similarly, we evaluated the $\cos\theta$ dependence of the DCS and the $\sqrt{s}$ dependence of the total cross-section. We have obtained some results for the cross-section as following:

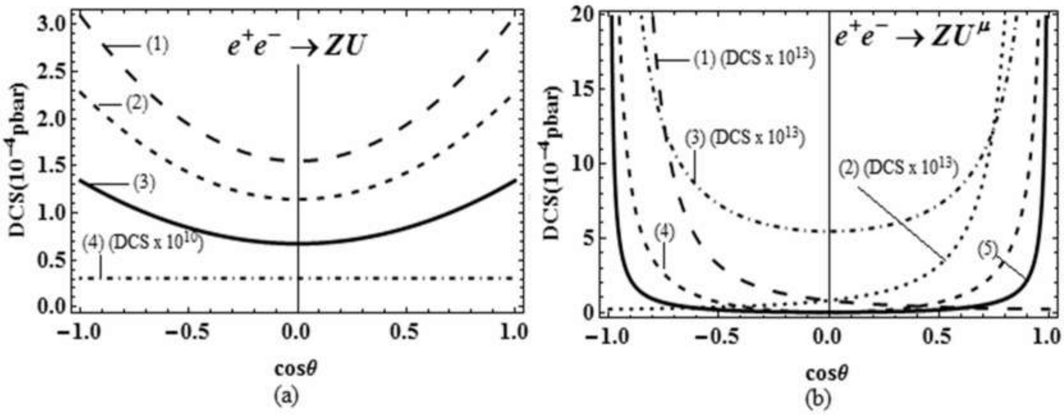

Figure 5: *The DCS of $e^+e^- \to ZU$ (a) and $e^+e^- \to ZU^{\mu}$ (b) as a function of $\cos\theta$ when the e^+, e^- beams are unpolarized and polarized. In Fig.5a, (1), (2), (3), (4) are $e_L^+e_L^-$, $e_R^+e_R^-$, e^+e^-, and mix($e_R^+e_R^-$, $e_L^+e_L^-$), respectively; in Fig.5b, (1), (2), (3), (4), (5) are $e_L^+e_R^-$, $e_R^+e_L^-$, mix($e_R^+e_R^-$, $e_L^+e_L^-$, $e_R^+e_R^-$), $e_R^+e_R^-$, and e^+e^-, respectively.*

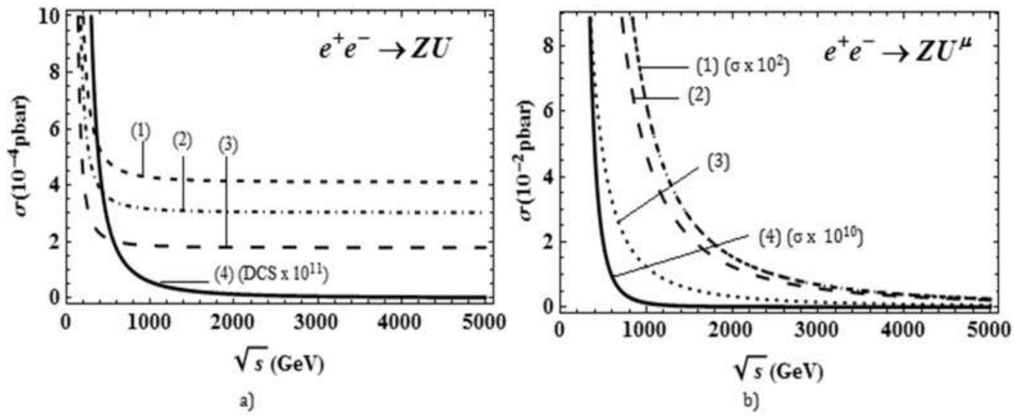

Figure 6: *The total cross-section of $e^+e^- \to ZU$ (a) and $e^+e^- \to ZU^{\mu}$ (b) as a function of the collision energy $\sqrt{s}$ when the e^+, e^- beams are unpolarized and polarized. In Fig.6a, (1), (2), (3), (4) are $e_L^+e_L^-$, $e_R^+e_R^-$, e^+e^- and mix($e_L^+e_L^-$, $e_R^+e_R^-$), respectively; In Fig.6b, (1), (2), (3), (4) are $e_R^+e_L^-$ or $e_L^+e_R^-$, $e_R^+e_R^-$, e^+e^- and mix($e_R^+e_L^-$, $e_L^+e_R^-$, $e_R^+e_R^-$), respectively.*

+ In Fig. 5a, the DCS when the e^+e^- beams left-left polarized are largest. In Fig. 5b, the DCS when the e^+e^- beams right-right polarized are largest.

+ In Fig. 6, the total cross-section decreases when $\sqrt{s}$ increases. The cross-section of the process $e^+e^- \to ZU^\mu$ are larger than the cross-section of the process $e^+e^- \to ZU$.

+ Furthermore, we caculated for the $\mu^+\mu^- \to \gamma(Z)U(U^\mu)$ and obtained the same results.

4. CONCLUSION

In this paper, we have calculated the DCS and total cross-sections of the process $e^+e^- \to \gamma(Z)U(U^\mu)$ in unparticle physics when the e^+,e^- beams are unpolarized and polarized. The results show that the cross-section depends strongly on the polarization of the initial beams; The cross-section of the process $e^+e^- \to \gamma(Z)U^\mu$ is larger than the cross-section of the process $e^+e^- \to \gamma(Z)U$; For the process $\mu^+\mu^- \to \gamma(Z)U(U^\mu)$, we obtained the results as for the process $e^+e^- \to \gamma(Z)U(U^\mu)$; and can observe the unparticle in the low energy domain.

Acknowledgements. The work is supported in part by National Foundation for Science and Technology Development of VietNam (NAFOSTED) under grand No. 103.01-2016.44.

REFERENCES

1. H. Georgi, "Unparticle Physics", Phys. Rev. Lett. 98, (2007) 221601.
2. K. Cheung, W. Y. Keung and T. C. Yuan, “collider signals of unparticle physics”, Phys. Rev. Lett. 99: 051803, 2007.
3. K. Cheung, W. -Y. Keung, and T. -C. Yuan, “Collider phenomenology of unparticle physics”, Phys. Rev. D76 (2007) 055003.
4. CMS Collaboration, “Search for dark matter, extra dimensions, and unparticles in monojet events in proton-proton collisions at $\sqrt{s} = 8TeV$ ”, Eur. Phys. J. C75 (2015) 235.
5. CMS Collaboration, “Search for dark matter and unparticles produced in association with a Z boson in proton - proton collisions at $\sqrt{s} = 8TeV$ ”, Phys. Rev. D93, 052011 (2016).
6. CMS Collaboration, “Search for dark matter and unparticles in events with a Z boson and missing transverse momentum in proton-proton collisions at $\sqrt{s} = 13TeV$ ”, JHEP 03 (2017) 061, [arxiv: 1701.02042].

7. S. Kathrein, S. Knapen, and M. J. Strassler, "Bounds from LEP on unparticle interactions with electroweak bosons", Phys. Rev. D84 (2011) 015010.
8. H. Davoudiasl, "Constraining unparticle physics with cosmology and astrophysics", Phys. Rev. Lett. 99 (2007) 141301.
9. J. R. Mureika, "Unparticle-enhanced black holes at the LHC", Phys. Lett. B660 (2008) 561–566.
10. [10] J. R. Mureika, "Differentiating unparticles from extra dimensions via mini black hole thermodynamics", Phys. Rev. D79 (2009) 056003.
11. J. R. Mureika and E. Spallucci, "Vector unparticle enhanced black holes: Exact solutions and thermodynamics", Phys. Lett. B693 (2010) 129–133.
12. C. H. Chen and C. Q. Geng, "Unparticle physics effects on direct CP violation", Phys. Rev. D 76 (2007) 115003.
13. C.S. Huang, and X.H. Wu, "Direct CP violation of $B \to lv$ in unparticle physics", Phys. Rev. D 77 (2008) 075014.
14. R. Zwicky, "Unparticles and CP -violation", Journal of Physics: Conference Series 110 (2008) 072050.
15. M. Ettefaghi, R. Moazzemi, and M. Rousta, "Constraining unparticle physics from CP violation in Cabibbo-favored decays of D mesons", Phys. Rev. D95, 095027 (2017).
16. H. Bagheri, M. Ettefaghi, and R. Moazzemi, "On the difference of time-integrated CP asymmetries in $D^0 \to K^+K^-$ and $D^0 \to \pi^+\pi^-$ decays: unparticle physics contribution", Phys. Lett, B771 (2017), 309-312.
17. J. P. F. LeBlanc and A. G. Grushin, "Unparticle mediated superconductivity", New J. Phys. 17 (2015) 033039.
18. P. W. Phillips, B. W. Langley, J. A. Hutasoit, 2013, "*Un-Fermi Liquids: Unparticles in Strongly Correlated Electron Matter*", Phys. Rev. B vol. 88, 115129.
19. K. Limtragool, P. Phillips, 2015, "*Power-law Optical Conductivity from Unparticles: Application to the Cuprates*", Phys. Rev. B 92, 155128.
20. T.M. Aliev, S. Bilmis, M. Solmaz, and I. Turan, "Scalar Unparticle Signals at the LHC", Phys. Rev.D95, 095005 (2017).
21. S. L. Chen, X. G. He, "Interactions of Unparticles with Standard Model Particles", Phys. Rev. D76:091702, 2007.
22. T. Banks and A. Zaks, "On the phase structure of vector-like gauge theories with massless fermions", Nucl. Phys. B 196, 189 (1982).
23. J. Barranco, "Tensorial NSI and Unparticle physics in neutrino scattering**"**, Int. J. Mod. Phys. A27 (2012) 1250147 arXiv: 1108.1220 [hep-ph].

SỰ SINH U-HẠT TRONG TÁN XẠ e^+e^- KHI CHÙM e^+e^- PHÂN CỰC

Tóm tắt: *Trong bài báo này, chúng tôi nghiên cứu các quá trình tán xạ* $e^+e^- \rightarrow \gamma \mathrm{U}(\mathrm{U}^\mu)$ *và* $e^+e^- \rightarrow Z\mathrm{U}(\mathrm{U}^\mu)$. *Trong mỗi quá trình tán xạ, chúng tôi đã tính toán tiết diện tán xạ vi phân và tiết diện tán xạ toàn phần khi chùm* e^+, e^- *không phân cực và phân cực. Kết quả cho thấy, tiết diện tán xạ phụ thuộc vào sự phân cực của chùm* e^+, e^- *và có thể quan sát thấy* U *– hạt trong miền năng lượng thấp.*

Từ khóa: *U-hạt, phân cực, tiết diện tán xạ.*

THE SM GAUGE BOSONS IN $SU(2)_1 \otimes SU(2)_2 \otimes U(1)_Y$ MODEL WITH VECTOR-LIKE QUARKS

[1]Hoang Ngoc Long, [2]Tran Thi Hong Anh, [3]Bui Thi Gam,
[4]Nguyen Van Tam, [5]Pham Thanh Thuy
[1]*Institute of Physics, VAST, 10 Dao Tan, Ba Dinh, Hanoi, Vietnam*
[2,3,4,5]*Graduate School, Can Tho University, Can Tho, Vietnam*

Abstract: *We present gauge states and masses of the SM gauge bosons (the Z and W bosons) in the $SU(2)_1 \otimes SU(2)_2 \otimes U(1)_Y$ model with vector-like quarks. Studying branching ratio $Z \rightarrow b\bar{b}$ as a function of θ, we have derived limit for the $Z - Z'$ mixing angle. This result is helpful for fixing parameter space of the G(221) model.*

Keywords: *Standard Model, SM, gauge bosons, vector-like quark.*

Received 22 April 2018
Accepted for publication 25 May 2018

1. INTRODUCTION

The Standard Model (SM) is one of the greatest triumph of Physics in the 20th Century. However the SM has some problems such as neutrino mass and mixing, Dark Matter, etc. This leads to need in extension of the SM. Among the extended models, the models based on the $SU(2)_1 \otimes SU(2)_2 \otimes U(1)_Y$ gauge group (called G(221) model for shot) [1–4] play an important role. In the [4] the G(221) the vector-like extra quarks and leptons are introduced to solve the family lepton number non-universality, while in [3] the vector-like quarks play a role of new physics at the LHC. In this paper we are concerned on the couplings of the Z boson with fermions in order to get constraints on the $Z - Z'$ mixing angle.

2. MODEL

The model is based on $SU(2)_1 \times SU(2)_2 \times U(1)_Y$, where the SM particles belong to the representations of $SU(2)_1 \times U(1)_Y$ and are singlets of $SU(2)_2$. The ordinary fermions are assigned under $SU(2)_1 \times U(1)_Y$ the same as in the SM [3]

$$L_{aL} = \begin{pmatrix} \nu_a \\ l_a \end{pmatrix}_L \sim (1,2,1,-1)\ , \quad l_{aR} \sim (1,1,1,-2) \tag{1}$$

where $a = e,\mu,\tau$. Similarly for ordinary quarks

$$q_{aL} = \begin{pmatrix} u_a \\ d_a \end{pmatrix}_L \sim \left(3,2,1,\frac{1}{3}\right)\ , \quad u_{aR} \sim \left(3,1,1,\frac{4}{3}\right),\quad d_{aR} \sim \left(3,1,1,-\frac{2}{3}\right), \tag{2}$$

where $a = 1,2,3$ is family index.

New exotic vector-like quark doublet (as *the fourth quark generation*) are in doublet of $SU(2)_2$ but are singlet of the $SU(2)_1$ as follows

$$Q'_{L/R} = \begin{pmatrix} U' \\ D' \end{pmatrix}_{L/R} \sim \left(3,1,2,\frac{1}{3}\right) \tag{3}$$

Ordinary quarks are the same as in the SM

$$q_{aL} = \begin{pmatrix} u_a \\ d_a \end{pmatrix}_L \sim \left(3,2,1,\frac{1}{3}\right)\ , \quad u_{aR} \sim \left(3,1,1,\frac{4}{3}\right),\quad d_{aR} \sim \left(3,1,1,-\frac{2}{3}\right), \tag{4}$$

where $a = 1,2,3$ is family index.

The electric charge operator is defined as

$$Q = T_3^{(1)} + T_3^{(2)} + \frac{Y}{2} \tag{3}$$

Higgs sector contains two scalar doublets and one singlet with the Vacuum Expectation Values (VEV) as follows

$$\begin{aligned} H'_1 &= \begin{pmatrix} H_1^+ \\ H_1^{0'} \end{pmatrix} = \begin{pmatrix} 0 \\ \frac{v_1}{\sqrt{2}} \end{pmatrix} + \begin{pmatrix} H_1^+ \\ H_1^0 \end{pmatrix} \equiv \langle H'_1\rangle + H_1 \sim (1,2,1,1)\ , \\ H'_2 &= \begin{pmatrix} H_2^+ \\ H_2^{0'} \end{pmatrix} = \begin{pmatrix} 0 \\ \frac{v_2}{\sqrt{2}} \end{pmatrix} + \begin{pmatrix} H_2^+ \\ H_2^0 \end{pmatrix} \equiv \langle H'_2\rangle + H_2 \sim (1,1,2,1)\,, \\ S' &= v_s + S \sim (1,1,1,0). \end{aligned} \tag{6}$$

The representations and charge assignments of particles under the gauge symmetry of $SU(3)_C \times SU(2)_1 \times SU(2)_2 \times U(1)_Y$ are expressed in **Table 1**.

The Yukawa couplings for the ordinary leptons are given by

$$-\mathcal{L}^{SM}_{Yukawa} = h^u_{ab}\overline{q_{aL}}\widetilde{H'_1}u_{bR} + h^d_{ab}\overline{q_{aL}}H'_1 d_{bR} + h^l_{ab}\overline{L_{aL}}H'_1 l_{bR} + H.c.\,, \tag{7}$$

where the leptons get masses by the same way as in the SM. For the new quarks interacting *only with quarks of third generation (t and b)* we have

$$
\begin{aligned}
-\mathcal{L}^{exotic} &= y_F\overline{Q'_L}Q'_RS' + y_b\overline{Q'_L}H'_2b_R + y_t\overline{Q'_L}\widetilde{H'_2}t_R \\
&+ m_\Psi\bar{Q}'_LQ'_R + H.c.\,.
\end{aligned} \tag{8}
$$

Table 1. Representations and charge assignments of particles in the G(221)

	Fermions						Scalars		
	q_L	u_R	d_R	L_L	l_R	$Q'_{L(R)}$	H'_1	H'_2	S'
$SU(3)_C$	**3**	**3**	**3**	**1**	**1**	**3**	**1**	**1**	**1**
$SU(2)_1$	**2**	**1**	**1**	**2**	**1**	**1**	**2**	**1**	**1**
$SU(2)_2$	**1**	**1**	**1**	**1**	**1**	**2**	**1**	**2**	**1**
$U(1)_Y$	$\frac{1}{3}$	$\frac{4}{3}$	$-\frac{2}{3}$	-1	-2	$\frac{1}{3}$	1	1	0

The model give lepton mass and coupling the same as in the SM. Let us expand the Yukawa couplings for quarks

$$
\begin{aligned}
-\mathcal{L}^{SM}_{Yukawa} &\subset h^u_{ab}\overline{q_{aL}}\widetilde{H'_1}u_{bR} + h^d_{ab}\overline{q_{aL}}H'_1d_{bR} + H.c. \\
&= \frac{h^u_{ab}v_1}{\sqrt{2}}\bar{u}_{aL}u_{bR} + \frac{h^d_{ab}v_1}{\sqrt{2}}\bar{d}_{aL}d_{bR} \\
&+ h^u_{ab}(\bar{u}_{aL},\bar{d}_{aL})\begin{pmatrix} H^{0*}_1 \\ -H^-_1 \end{pmatrix}u_{bR} + h^d_{ab}(\bar{u}_{aL},\bar{d}_{aL})\begin{pmatrix} H^+_1 \\ H^0_1 \end{pmatrix}d_{bR} + H.c. \\
&= \frac{h^u_{ab}v_1}{\sqrt{2}}\bar{u}_{aL}u_{bR} + \frac{h^d_{ab}v_1}{\sqrt{2}}\bar{d}_{aL}d_{bR} && (9) \\
&+ h^u_{ab}(\bar{u}_{aL}H^{0*}_1 - \bar{d}_{aL}H^-_1)u_{bR} + h^d_{ab}(\bar{u}_{aL}H^+_1 + \bar{d}_{aL}H^0_1)d_{bR} + H.c. && (10) \\
&= \text{mass terms for } u \text{ and } d \text{ and Yukawa couplings.}
\end{aligned}
$$

For new exotic quarks, only the quarks of the third generation can couple with the exotic ones:

$$
\begin{aligned}
-\mathcal{L}^{exotic} &= y_F\overline{Q'_L}Q'_RS' + y_b\overline{Q'_L}H'_2b_R + y_t\overline{Q'_L}\widetilde{H'_2}t_R \\
&+ m_\Psi\bar{Q}'_LQ'_R + H.c. \\
&= (y_Fv_s + m_\Psi)(\overline{U'}_LU'_R + \overline{D'}_LD'_R) + \frac{y_bv_2}{\sqrt{2}}\overline{D'}_Lb_R + \frac{y_tv_2}{\sqrt{2}}\overline{U'}_Lt_R && (11) \\
&+ S(\overline{U'}_LU'_R + \overline{D'}_LD'_R) + y_b(\overline{U'}_LH^+_2 + \overline{D'}_LH^0_2)b_R + y_t(\overline{U'}_LH^{0*}_2 - \overline{D'}_LH^-_2)t_R + H.c \\
&= \text{mass terms for } U' \text{ and } D' \text{ and Yukawa couplings.} && (12)
\end{aligned}
$$

From (10) and (11) we get mass matrix for up-quark in the base (u_L, c_L, t_L, U_L') as follows

$$M_u = \begin{pmatrix} m_u & 0 \\ m_{tU'} & m_{U'} \end{pmatrix} = \begin{pmatrix} \frac{v_1}{\sqrt{2}}h^u_{uu} & \frac{v_1}{\sqrt{2}}h^u_{uc} & \frac{v_1}{\sqrt{2}}h^u_{ut} & 0 \\ \frac{v_1}{\sqrt{2}}h^u_{cu} & \frac{v_1}{\sqrt{2}}h^u_{cc} & \frac{v_1}{\sqrt{2}}h^u_{ct} & 0 \\ \frac{v_1}{\sqrt{2}}h^u_{tu} & \frac{v_1}{\sqrt{2}}h^u_{tc} & \frac{v_1}{\sqrt{2}}h^u_{tt} & 0 \\ 0 & 0 & \frac{y_t v_2}{\sqrt{2}} & y_F v_s + m_\Psi \end{pmatrix} \quad (13)$$

where $m_u = \frac{h^u_{ab} v_1}{\sqrt{2}}$, $m_{tU'} = \frac{y_t v_2}{\sqrt{2}}$ and $m_{U'} = y_F v_s + m_\Psi$.

According Ref.[3], we can choose the basis for which the first two generations of quarks (i.e., quarks *u* and *c*) are in the mass eigenstates, however, the Dirac mass matrix for $t-U'$ and $b-D'$ quarks can be formulated by.

Between $h^u_{ut} = h^u_{ct} = 0$, we get

$$M_t = \begin{pmatrix} m_t & 0 \\ m_{tU'} & m_{U'} \end{pmatrix} \quad (14)$$

Similarly for down-quarks

$$M_b = \begin{pmatrix} m_b & 0 \\ m_{bD'} & m_{D'} \end{pmatrix}, \quad (15)$$

where $m_b = \frac{h^d v_1}{\sqrt{2}}$, $m_{bD'} = \frac{y_b v_2}{\sqrt{2}}$ and $m_{D'} = m_{U'} = y_F v_s + m_\Psi$.

Let us write mass term in the form

$$\begin{aligned} (\bar{t}_L, \overline{U'}_L) M_t \begin{pmatrix} t_R \\ U'_R \end{pmatrix} &= (\bar{t}_L, \overline{U'}_L) \left(V^{t\dagger}_L V^t_L\right) M_u \left(V^{t\dagger}_R V^t_R\right) \begin{pmatrix} t_R \\ U'_R \end{pmatrix} \\ &= (\bar{t}_L, \overline{U'}_L) V^{t\dagger}_L \left(V^t_L M_t V^{t\dagger}_R\right) V^t_R \begin{pmatrix} t_R \\ U'_R \end{pmatrix} \\ &\equiv (\overline{t^{mass}_L}, \overline{U'^{mass}_L}) M^{diag}_t \begin{pmatrix} t^{mass}_R \\ U'^{mass}_R \end{pmatrix}, \end{aligned} \quad (16)$$

where M_u^{diag} is diagonal matrix, the mass states relate with weak states as

$$M_t^{diag} = V_L^t M_t V_R^{t\dagger},$$
$$\begin{pmatrix} t_L^{mass} \\ U_L'^{mass} \end{pmatrix} = V_L^t \begin{pmatrix} t_L \\ U_L' \end{pmatrix}, \begin{pmatrix} t_R^{mass} \\ U_R'^{mass} \end{pmatrix} = V_R^t \begin{pmatrix} t_R \\ U_R' \end{pmatrix}. \quad (17)$$

Diagonalized matrix is determined by

$$M_t^{diag} M_t^{diag\dagger} = V_L^t M_t M_t^\dagger V_L^{t\dagger}, \quad (18)$$

$$M_t^{diag\dagger} M_t^{diag} = V_R^t M_t^\dagger M_t V_R^{t\dagger}, \quad (19)$$

Where

$$V_L^t = \begin{pmatrix} c_L^t & s_L^t \\ -s_L^t & c_L^t \end{pmatrix}, \quad (20)$$

and similarly for $V_R{}^t$. It follows that

$$M_t M_t^\dagger = \begin{pmatrix} m_t & 0 \\ m_{tU'} & m_{U'} \end{pmatrix} \begin{pmatrix} m_t^\dagger & m_{tU'}^\dagger \\ 0 & m_{U'}^\dagger \end{pmatrix} = \begin{pmatrix} m_t^2 & m_t m_{tU'}^\dagger \\ m_{tU'} m_t^\dagger & m_{tU'}^2 + m_{U'}^2 \end{pmatrix}, \quad (21)$$

$$M_t^\dagger M_t = \begin{pmatrix} m_t^\dagger & m_{tU'}^\dagger \\ 0 & m_{U'}^\dagger \end{pmatrix} \begin{pmatrix} m_t & 0 \\ m_{tU'} & m_{U'} \end{pmatrix} = \begin{pmatrix} m_t^2 + m_{tU'}^2 & m_{U'} m_{tU'}^\dagger \\ m_{tU'} m_{U'}^\dagger & m_{U'}^2 \end{pmatrix}, \quad (22)$$

where $m_t^2 \equiv m_t m_t^\dagger, m_{U'}^2 \equiv m_{U'} m_{U'}^\dagger, \ldots$

From (18) and (21), one gets

$$\tan 2\theta_L^t = \frac{2 m_t m_{tU'}^\dagger}{m_{tU'}^2 + m_{U'}^2 - m_t^2} \approx \frac{2 m_t m_{tU'}^\dagger}{m_{U'}^2} \to \tan\theta_L^t \approx \frac{m_t m_{tU'}^\dagger}{m_{U'}^2} \quad (23)$$

Similarly, from (19) and (22), it follows

$$\tan 2\theta_R^t = \frac{2 m_{U'} m_{tU'}^\dagger}{m_{U'}^2 - m_t^2 - m_{tU'}^2} \approx \frac{2 m_{tU'}^\dagger}{m_{U'}} \to \tan\theta_R^t \approx \frac{m_{tU'}^\dagger}{m_{U'}} \quad (24)$$

We will denote $C_L^t \equiv cos\theta_L^t, S_L^t \equiv sin\theta_L^t$ and so forth. From (23) and (24), it follows that the right-handed quark mixing angle is larger than that of left-handed quarks.

In practical calculation, we have to use mass (physical) states. So from (17) and (20) we have

$$\begin{pmatrix} t_L \\ U'_L \end{pmatrix} = \left(V_L^t\right)^{-1} \begin{pmatrix} t_L^{mass} \\ U_L^{\prime mass} \end{pmatrix} = \begin{pmatrix} c_L^t & -s_L^t \\ s_L^t & c_L^t \end{pmatrix} \begin{pmatrix} t_L^{mass} \\ U_L^{\prime mass} \end{pmatrix} \tag{25}$$

Similarly for other quarks

$$\begin{pmatrix} t_R \\ U'_R \end{pmatrix} = \begin{pmatrix} c_R^t & -s_R^t \\ s_R^t & c_R^t \end{pmatrix} \begin{pmatrix} t_R^{mass} \\ U_R^{\prime mass} \end{pmatrix}, \tag{26}$$

$$\begin{pmatrix} b_L \\ D'_L \end{pmatrix} = \begin{pmatrix} c_L^b & -s_L^b \\ s_L^b & c_L^b \end{pmatrix} \begin{pmatrix} b_L^{mass} \\ D_L^{\prime mass} \end{pmatrix}, \tag{27}$$

$$\begin{pmatrix} b_R \\ D'_R \end{pmatrix} = \begin{pmatrix} c_R^b & -s_R^b \\ s_R^b & c_R^b \end{pmatrix} \begin{pmatrix} b_R^{mass} \\ D_R^{\prime mass} \end{pmatrix}. \tag{28}$$

However, in the final result, the subscript ^{mass} will be removed.

The Lagrangian of Higgs fields is

$$L_{Higgs} = \sum_i \left(D^\mu H'_i\right)^\dagger D_\mu H'_i + \frac{1}{2}\partial^\mu S' \partial_\mu S' - V(H'_1, H'_2, S') \tag{29}$$

where

$$\begin{aligned} V(H'_1, H'_2, S') \ = \ & \sum_{i=1,2} \left[\mu_i^2 H_i'^\dagger H'_i + \lambda_i \left(H_i'^\dagger H'_i\right)^2\right] + \frac{1}{2}\mu_S^2 S'^2 + \lambda_S S'^4 \\ & +\mu_3 S'^3 + S'(\mu_{1S} H_1'^\dagger H'_1 + \mu_{2S} H_2'^\dagger H'_2) + \lambda_{12} H_1'^\dagger H'_1 H_2'^\dagger H'_2 \\ & +\lambda_{1S} S'^2 H_1'^\dagger H'_1 + \lambda_{2S} S'^2 H_2'^\dagger H'_2 \,. \end{aligned} \tag{30}$$

3. GAUGE BOSON SECTOR

Let us consider gauge boson masses, which arise from the part

$$L_{Gaugemass} = \sum_i \left(D^\mu \langle H'_i \rangle\right)^\dagger D_\mu \langle H'_i \rangle \tag{31}$$

where

$$D_\mu = \partial_\mu - ig_1 A_{\mu a} t_a - ig_2 A'_{\mu a} t'_a - \frac{i}{2} g_Y B_\mu \tag{32}$$

After some manipulations, ones get mass Lagrangian in the form

$$L_{Gaugemass} = L^1_{Gauge\ mass} + L^2_{Gauge\ mass},$$

Where

$$\begin{aligned} L^1_{Gauge\ mass} &= \left(D^\mu\langle H_1'\rangle\right)^\dagger D_\mu\langle H_1'\rangle \\ &= \frac{g_1^2v_1^2}{4}W_\mu^+W^{-\mu} + \frac{g_1^2v_1^2}{8}(-A_{\mu3} + \frac{g_Y}{g_1}B_\mu)(-A_3^\mu + \frac{g_Y}{g_1}B^\mu), \end{aligned} \tag{33}$$

and

$$\begin{aligned} L^2_{Gauge\ mass} &= \left(D^\mu\langle H_2'\rangle\right)^\dagger D_\mu\langle H_2'\rangle \\ &= \frac{g_2^2v_2^2}{4}W_\mu'^+W'^{-\mu} + \frac{g_2^2v_2^2}{8}(-A'_{\mu3} + \frac{g_Y}{g_2}B_\mu)(-A_3'^\mu + \frac{g_Y}{g_2}B^\mu). \end{aligned} \tag{34}$$

From (33) and (34) it follows

$$m_W^2 = \frac{g_1^2v_1^2}{4}, \quad m_{W'}^2 = \frac{g_2^2v_2^2}{4} \tag{35}$$

Hence, the W is identified with the SM W boson; and this leads to replace g_1 with g and $v_1 = v = 246$ GeV.

Let us deal with neutral gauge boson mixing. The mass matrix for neutral gauge bosons in base ($A'_{\mu3}, A_{\mu3}, B_\mu$)

$$\mathcal{L}_M = \frac{1}{8}\begin{pmatrix} A'_{\mu3} \\ A_{\mu3} \\ B_\mu \end{pmatrix}^T \begin{pmatrix} v_2^2g_2^2 & 0 & -v_2^2g_2g_Y \\ 0 & v_1^2g_1^2 & -v_1^2g_1g_Y \\ -v_2^2g_2g_Y & -v_1^2g_1g_Y & (v_1^2+v_2^2)g_Y^2 \end{pmatrix} \begin{pmatrix} A_3'^\mu \\ A_3^\mu \\ B^\mu \end{pmatrix} \tag{36}$$

This means that the mass mixing matrix of neutral gauge bosons is given by

$$M_{NG}^2 = \frac{1}{4}\begin{pmatrix} v_2^2g_2^2 & 0 & -v_2^2g_2g_Y \\ 0 & v^2g^2 & -v^2gg_Y \\ -v_2^2g_2g_Y & -v^2gg_Y & (v^2+v_2^2)g_Y^2 \end{pmatrix} \equiv M_1^2 + M_2^2 \tag{37}$$

with $g = g_1, v = v_1$ and M_1^2 contains mass term arising at the first SSB and depending only on v_2, while M_1^2 depends only on v.

The diagonalization of this matrix can be done through three steps. The first step: when $\langle H_2'\rangle = v_2 \neq 0$ and $v = 0$, we have matrix

$$M_1^2 = \frac{v_2^2}{4}\begin{pmatrix} g_2^2 & 0 & -g_2 g_Y \\ 0 & 0 & 0 \\ -g_2 g_Y & 0 & g_Y^2 \end{pmatrix} \tag{38}$$

The matrix (38) is diagonalized by the matrix

$$C_1 = \begin{pmatrix} c_\theta & 0 & -s_\theta \\ 0 & 1 & 0 \\ s_\theta & 0 & c_\theta \end{pmatrix}, \tag{39}$$

.

where $\tan\theta = \frac{gY}{g2}$. Then we have

$$M_{1diag}^2 = C_1.M_1^2.C_1^T = \mathrm{diag}\left(\frac{v_2^2}{4}(g_2^2+g_Y^2),0,0\right), \tag{40}$$

and

$$M_{NG1}^2 = C_1.M_{NG}^2.C_1^T = \frac{1}{4}\begin{pmatrix} \frac{(g_3^2+g'^2)^2 v_2^2 + g'^4 v^2}{g_3^2} & \frac{gg'^2 v^2}{g_3} & -\frac{g'^3 v^2}{g_3} \\ \frac{gg'^2 v^2}{g_3} & g^2 v^2 & -gg' v^2 \\ -\frac{g'^3 v^2}{g_3} & -gg' v^2 & g'^2 v^2 \end{pmatrix} \tag{41}$$

where we have denoted $g_3 = g_2 c_\theta$, $g = g_1$, $g' = g_Y c_\theta$.

At this step, the original gauge fields $Z_{1\mu}, A_{3\mu}^3, B'_\mu$ transform to $A'_{3\mu}, A_{3\mu}^3, B_\mu$ by

$$\begin{pmatrix} Z_{2\mu} \\ A_{3\mu}^3 \\ B'_\mu \end{pmatrix} = C_1 \begin{pmatrix} A'_{3\mu} \\ A_{3\mu}^3 \\ B'_\mu \end{pmatrix} = \begin{pmatrix} c_\theta & 0 & -s_\theta \\ 0 & 1 & 0 \\ s_\theta & 0 & c_\theta \end{pmatrix}\begin{pmatrix} A'_{3\mu} \\ A_{3\mu}^3 \\ B_\mu \end{pmatrix} \tag{42}$$

Here, we have denoted

$$c_\theta = \frac{g_2}{\sqrt{g_2^2+g_Y^2}} = \frac{g_2}{\sqrt{g_2^2+g'^2/c_\theta^2}} \Rightarrow g_2 = c_\theta\sqrt{g_2^2+g'^2/c_\theta^2} \tag{43}$$

Hence

$$c_\theta = \frac{\sqrt{g_2^2-g'^2}}{g_2}; \quad s_\theta = \frac{g'}{g_2} \tag{44}$$

In the second step: when $\langle H_1' \rangle = v_1 \neq 0$ and $v_2 = 0$ we diagonalize the right-bottom 2×2 matrix in (41), namely

$$M_{SM}^2 = \frac{v^2}{4}\begin{pmatrix} 0 & 0 & 0 \\ 0 & g^2 & -gg' \\ 0 & -gg' & g'^2 \end{pmatrix} \tag{45}$$

The matrix (45) is diagonalized by the matrix

$$C_2 = \begin{pmatrix} 1 & 0 & 0 \\ 0 & c_W & -s_W \\ 0 & s_W & c_W \end{pmatrix}, \tag{46}$$

where $\tan\theta_W = \frac{g'}{g}$

We have then

$$M_{SMdiag}^2 = C_2.M_2^2.C_2^T = \text{diag}\left(0, \frac{v^2}{4}(g^2+g'^2), 0\right) \tag{47}$$

Hence, the matrix in (41) is transformed to

$$M_F^2 = C_2.M_{NG1}^2.C_2^T = \begin{pmatrix} M_{Z_2}^2 & m_{Z_1Z_2}^2 & 0 \\ m_{Z_1Z_2}^2 & m_{Z_1}^2 & 0 \\ 0 & 0 & 0 \end{pmatrix}, \tag{48}$$

where

$$M_{Z_2}^2 = \frac{1}{4}\left(1+\frac{g'^2}{(g_2c_\theta)^2}\right)^2 g_2^2c_\theta^2v_2^2 + \frac{g'^4}{4(g_2c_\theta)^2}v^2 = \frac{v_2^2g_2^4+v^2g'^4}{4(g_2^2-g'^2)}, \tag{49}$$

$$m_{Z_1Z_2}^2 = \frac{g'(g^2+g'^2)s_Wv^2}{4g_2c_\theta} = \frac{v^2g'^2}{4}\sqrt{\frac{g^2+g'^2}{g_2^2-g'^2}}, \tag{50}$$

$$m_{Z_1}^2 = \frac{1}{4}(g^2+g'^2)v^2. \tag{51}$$

Note that our formulas (49) and (50) *coincide* with Eq. (19) in [3]. At the second step, the gauge fields $Z_{2\mu}, Z_{1\mu}, A_\mu$ transform to $Z_{2\mu}, A_{3\mu}^3, B'_\mu$ by

$$\begin{pmatrix} Z_{2\mu} \\ Z_{1\mu} \\ A_\mu \end{pmatrix} = C_2\begin{pmatrix} Z_{2\mu} \\ A_{3\mu} \\ B'_\mu \end{pmatrix} = \begin{pmatrix} 1 & 0 & 0 \\ 0 & c_W & -s_W \\ 0 & s_W & c_W \end{pmatrix}\begin{pmatrix} Z_{2\mu} \\ A_{3\mu} \\ B'_\mu \end{pmatrix}.$$

Therefore we have

$$\begin{pmatrix} Z_{2\mu} \\ Z_{1\mu} \\ A_\mu \end{pmatrix} = C_2 \begin{pmatrix} Z_{2\mu} \\ A_{3\mu} \\ B'_\mu \end{pmatrix} = C_2 C_1 \begin{pmatrix} A'_{3\mu} \\ A_{3\mu} \\ B_\mu \end{pmatrix}$$
$$= \begin{pmatrix} 1 & 0 & 0 \\ 0 & c_W & -s_W \\ 0 & s_W & c_W \end{pmatrix} \cdot \begin{pmatrix} c_\theta & 0 & -s_\theta \\ 0 & 1 & 0 \\ s_\theta & 0 & c_\theta \end{pmatrix} \begin{pmatrix} A'_{3\mu} \\ A_{3\mu} \\ B_\mu \end{pmatrix} \tag{52}$$

In practice, it is useful

$$\begin{pmatrix} A'_{3\mu} \\ A_{3\mu} \\ B_\mu \end{pmatrix} = (C_2 C_1)^T \begin{pmatrix} Z_{2\mu} \\ Z_{1\mu} \\ A_\mu \end{pmatrix}$$
$$= \begin{pmatrix} c_\theta & 0 & s_\theta \\ 0 & 1 & 0 \\ -s_\theta & 0 & c_\theta \end{pmatrix} \cdot \begin{pmatrix} 1 & 0 & 0 \\ 0 & c_W & s_W \\ 0 & -s_W & c_W \end{pmatrix} \begin{pmatrix} Z_{2\mu} \\ Z_{1\mu} \\ A_\mu \end{pmatrix}$$
$$= \begin{pmatrix} c_\theta & -s_\theta s_W & s_\theta c_W \\ 0 & c_W & s_W \\ -s_\theta & -c_\theta s_W & c_\theta c_W \end{pmatrix} \begin{pmatrix} Z_{2\mu} \\ Z_{1\mu} \\ A_\mu \end{pmatrix}. \tag{53}$$

The last step, matrix in (55) is diagonalized by matrix C3

$$C_3 = \begin{pmatrix} c_Z & -s_Z & 0 \\ s_Z & c_Z & 0 \\ 0 & 0 & 1 \end{pmatrix}, \tag{54}$$

where $c_Z = \cos\theta_Z$, $s_Z = \sin\theta_Z$ and the mixing angle Z_2, Z_1 is determined

$$\tan 2\theta_Z = -\frac{2m^2_{Z_1Z_2}}{M^2_{Z_2} - m^2_{Z_1}}. \tag{55}$$

It is emphasized that our $\tan 2\theta_Z$ is *opposite* with that in Ref. [3].

Let us summarize the above procedure. The physical gauge bosons relate with original ones by matrix

$$\begin{pmatrix} Z_{2\mu} \\ Z_{1\mu} \\ A_\mu \end{pmatrix} = C_3. \begin{pmatrix} Z'_\mu \\ Z_\mu \\ A_\mu \end{pmatrix}. \qquad (56)$$

The physical states Z' and Z get masses

$$m^2_{Z/Z'} = \frac{M^2_{Z_2} + m^2_{Z_1}}{2} \pm \frac{1}{2}\sqrt{(M^2_{Z_2} - m^2_{Z_1})^2 + 4m^4_{Z_1Z_2}}. \qquad (57)$$

It follows that

$$\begin{aligned} C_F &= C_3.C_2.C_1, \\ M^2_{NGdiag} &= C_F.M^2_{NG}.C_F^T = \mathrm{diag}\left(M^2_{Z'}, m^2_Z, 0\right) \end{aligned} \qquad (58)$$

The gauge bosons transform accordingly

$$\begin{aligned} \begin{pmatrix} A'_{3\mu} \\ A_{3\mu} \\ B_\mu \end{pmatrix} &= (C_3C_2C_1)^T \begin{pmatrix} Z'_\mu \\ Z_\mu \\ A_\mu \end{pmatrix} \\ &= \begin{pmatrix} c_\theta & 0 & s_\theta \\ 0 & 1 & 0 \\ -s_\theta & 0 & c_\theta \end{pmatrix} . \begin{pmatrix} 1 & 0 & 0 \\ 0 & c_W & s_W \\ 0 & -s_W & c_W \end{pmatrix} . \begin{pmatrix} c_Z & s_Z & 0 \\ -s_Z & c_Z & 0 \\ 0 & 0 & 1 \end{pmatrix} \begin{pmatrix} Z'_\mu \\ Z_\mu \\ A_\mu \end{pmatrix} \\ &= \begin{pmatrix} c_\theta & -s_\theta s_W & s_\theta c_W \\ 0 & c_W & s_W \\ -s_\theta & -c_\theta s_W & c_\theta c_W \end{pmatrix} \begin{pmatrix} c_Z & s_Z & 0 \\ -s_Z & c_Z & 0 \\ 0 & 0 & 1 \end{pmatrix} \begin{pmatrix} Z'_\mu \\ Z_\mu \\ A_\mu \end{pmatrix} \end{aligned} \qquad (59)$$

4. CURRENTS

The main Lagrangian:

$$L_f = i\sum_F \bar{F}\gamma^\mu D_\mu F = i\sum_F \bar{F}\gamma^\mu \partial_\mu F + J^{em}_\mu A^\mu + J^Z_{1\mu} Z^\mu_1 + J^Z_{2\mu} Z^\mu_2 + J^W_\mu W^\mu + J^{W'}_\mu W'^\mu. \qquad (60)$$

The covariant derivative is given by

$$
\begin{aligned}
D_\mu &= \partial_\mu - ig_2 T_a^{(2)} A'_{\mu a} - igT_a^{(1)} A_{\mu a} - i\frac{g_Y}{2} Y B_\mu \\
&= \partial_\mu - ig_2 \sum_{i=1}^{2} T_i^{(2)} A'_{\mu i} - ig \sum_{i=1}^{2} T_i^{(1)} A_{\mu i} \\
&- ig_2 T_3^{(2)} A'_{\mu 3} - igT_3^{(1)} A_{\mu 3} - i\frac{g_Y}{2} Y B_\mu \\
&= \partial_\mu - iP_\mu^{CC} - iP_\mu^{NC},
\end{aligned} \tag{61}
$$

where P_μ^{CC} and P_μ^{NC} are parts responsible for charged and neutral currents.

4.1. Neutral currents

The part *(for neutral currents)* is given by

$$P_\mu^{NC} = g_2 T_3^{(2)} A'_{\mu 3} + gT_3^{(1)} A_{\mu 3} - i\frac{g_Y}{2} Y B_\mu. \tag{62}$$

Using (53), the neutral currents are given by

$$
\begin{aligned}
P_\mu^{NC} &= \left(g_2 T_3^{(2)} s_\theta c_W + gT_3^{(1)} s_W + \frac{g_Y}{2} Y c_\theta c_W\right) A_\mu \\
&+ \left(g_2 T_3^{(2)}(-s_\theta s_W) + gT_3^{(1)} c_W + \frac{g_Y}{2} Y(-c_\theta s_W)\right) Z_{1\mu} \\
&+ \left(g_2 T_3^{(2)} c_\theta + \frac{g_Y}{2} Y(-s_\theta)\right) Z_{2\mu} \\
&= \left(T_3^{(2)} g s_W + gT_3^{(1)} s_W + \frac{Y}{2} g s_W\right) A_\mu \\
&+ \frac{g}{c_W}\left(-T_3^{(2)} s_W^2 + T_3^{(1)} c_W^2 - \frac{Y}{2} s_W^2\right) Z_{1\mu} \\
&+ \frac{g}{c_W} t \left(T_3^{(2)}(1 - s_\theta^2) - s^2\theta(Q - T_3^{(1)} - T_3^{(2)})\right) Z_{2\mu} \\
&= g s_W \left(T_3^{(2)} + T_3^{(1)} + \frac{Y}{2}\right) A_\mu \\
&+ \frac{g}{c_W}\left(T_3^{(1)} - s_W^2 (T_3^{(1)} + T_3^{(2)} + \frac{Y}{2})\right) Z_{1\mu} \\
&+ \frac{g}{c_\omega} t \left(T_3^{(2)} + s_\theta^2 T_3^{(1)} - s_\theta^2 Q\right) Z_{2\mu} \\
&= eQA_\mu + \frac{g}{c_W}\left(T_3^{(1)} - s_W^2 Q\right) Z_{1\mu} && (63) \\
&+ \frac{g}{c_\omega} t \left(T_3^{(2)} + s_\theta^2 T_3^{(1)} - s_\theta^2 Q\right) Z_{2\mu}, && (64)
\end{aligned}
$$

where $e = gs_W$ as in the SM.

Notice: To get Z_2 couplings, the following replacements: $g \Rightarrow g_2, s_W \Rightarrow s_\theta, c_W \Rightarrow c_\theta$.

The neutral currents interacting with the Z_1 boson

$$\mathcal{L}_f^{NC} = \frac{g}{c_W} Z_1^\mu J_{1\mu}^0 . \tag{65}$$

From (63) one has

$$\begin{aligned} J_{1\mu}^0 &= \bar{f}^u \gamma_\mu \left[T_3^{(1)}(f_L^u) P_L - s_W^2 Q(f^u) \right] f^u \\ &+ \bar{f}^d \gamma_\mu \left[T_3^{(1)}(f_L^d) P_L - s_W^2 Q(f^d) \right] f^d \\ &\equiv J_{1\mu}^0(f^u) + J_{1\mu}^0(f^d) \end{aligned} \tag{66}$$

The neutral currents are usually written in the left-handed (L) and right-handed (R) forms

$$J_{1\mu}^0(f) = \frac{1}{2}\left[g_{1L}^f \bar{f}\gamma_\mu(1-\gamma_5)f + g_{1R}^f \bar{f}\gamma_\mu(1+\gamma_5)f \right]. \tag{67}$$

Comparison of (67) with (66) yields

$$g_{1L,R}^f = T_3^{(1)}(f_{L,R}) - s_W^2 Q(f). \tag{68}$$

For completeness, ones give out the $V-A$ form of neural currents

$$J_{1\mu}^0(f) = \frac{1}{2}\left[g_{1V}^f \bar{f}\gamma_\mu f - g_{1A}^f \bar{f}\gamma_\mu\gamma_5 f \right]. \tag{69}$$

Relation among two kinds of coefficients are as follows

$$g_{1V}^f = g_{1L}^f + g_{1R}^f, \quad g_{1A}^f = g_{1L}^f - g_{1R}^f.$$

The neutral currents are usually written in the left-handed (L) and right-handed (R) forms

$$J_{2\mu}^0(f) = \frac{1}{2}\left[g_{2L}^f \bar{f}\gamma_\mu(1-\gamma_5)f + g_{2R}^f \bar{f}\gamma_\mu(1+\gamma_5)f \right]. \tag{70}$$

Comparison of (64) with (70) yields

$$g_{2L,R}^f = T_3^{(2)}(f_{L,R}) + s_\theta^2 T_3^{(1)}(f) - s_\theta^2 Q(f). \tag{71}$$

For completeness, ones give out the $V-A$ form of neural currents

$$J_{2\mu}^0(f) = \frac{1}{2}\left[g_{2V}^f \bar{f}\gamma_\mu f - g_{2A}^f \bar{f}\gamma_\mu\gamma_5 f \right]. \tag{72}$$

Relation among two kinds of coefficients are as follows

$gVf = gLf + gRf,\ gAf = gLf - gRf$.

From (64) ones get non-vanishing couplings of the Z_2 are given in Table **??.**

To deal with physical fields Z and Z' we change as follows

$$\begin{pmatrix} Z_{2\mu} \\ Z_{1\mu} \end{pmatrix} = \begin{pmatrix} c_Z & s_Z \\ -s_Z & c_Z \end{pmatrix} \begin{pmatrix} Z'_\mu \\ Z_\mu \end{pmatrix} \tag{73}$$

Then, Eq. (75) is rewritten as

$$\begin{aligned} \mathcal{L}_f^{NC} &= \frac{g}{c_W} J^0_{1\mu} Z_1^\mu = \frac{g}{c_W} J^0_{1\mu}(c_Z Z^\mu + s_Z Z'_\mu) \\ &= \frac{g}{c_W} \bar{f}\gamma_\mu \left[T_3^{(1)}(f) - s_W^2 Q(f)\right] f(c_Z Z^\mu - s_Z Z'_\mu) \end{aligned} \tag{74}$$

For physical Z and Z' we have to associate c_Z for Z_1 and s_Z for Z_2 as follows The neutral currents interacting with the Z boson

$$\begin{aligned} \mathcal{L}_f^{NC} &= \frac{g}{c_W} Z^\mu J^0_\mu \\ &= \frac{g}{2c_W} \bar{f}\gamma_\mu \left[g_L^f(1-\gamma_5) + g_R^f(1+\gamma_5)\right] f \\ &= \frac{g}{2c_W} \bar{f}\gamma_\mu \left[g_V^f - g_A^f \gamma_5\right] f, \end{aligned} \tag{75}$$

where

$$g^f_{L,R} = c_Z \left[T_3^{(1)}(f) - s_W^2 Q(f)\right] + s_Z t \left[T_3^{(2)}(f) + s_\theta^2 T_3^{(1)}(f) - s_\theta^2 Q(f)\right].$$

Coupling constants given in Table II

Table 2. Non-zero coupling constant of Z

f	g_L	g_R	g_V	g_A
ν	$\frac{1}{2}\left[c_z + s_z t s_\theta^2\right]$	0	$\frac{1}{2}\left[c_z + s_z t s_\theta^2\right]$	$\frac{1}{2}\left[c_z + s_z t s_\theta^2\right]$
l	$\left[c_z(-\frac{1}{2} + s_w^2) + \frac{1}{2}s_z t s_\theta^2\right]$	$c_z s_w^2 + s_z t s_\theta^2$	$-\frac{1}{2}c_z\left(1-4s_w^2\right) + \frac{3}{2}s_z t s_\theta^2$	$-\frac{c_z}{2} - \frac{1}{2}s_z t s_\theta^2$
u	$\frac{1}{2}\left[c_z(1-\frac{4}{3}s_w^2) - \frac{1}{3}s_z t s_\theta^2\right]$	$-\frac{2}{3}\left(c_z s_w^2 + s_z t s_\theta^2\right)$	$c_z\left(\frac{1}{2} - \frac{4}{3}s_w^2\right) - \frac{5}{6}s_z t s_\theta^2$	$\frac{1}{2}c_z + \frac{1}{2}s_z t s_\theta^2$
d	$\frac{1}{2}\left[c_z(-1+\frac{2}{3}s_w^2) - \frac{1}{3}s_z t s_\theta^2\right]$	$\frac{1}{3}\left(c_z s_w^2 + s_z t s_\theta^2\right)$	$c_z\left(-\frac{1}{2} + \frac{2}{3}s_w^2\right) + \frac{1}{6}s_z t s_\theta^2$	$-\frac{1}{2}c_z - \frac{1}{2}s_z t s_\theta^2$
U'	$-\frac{2}{3}c_z s_w^2 + s_z t\left(\frac{1}{2} - \frac{2}{3}s_\theta^2\right)$	$-\frac{2}{3}c_z s_w^2 + s_z t\left(\frac{1}{2} - \frac{2}{3}s_\theta^2\right)$	$-\frac{4}{3}c_z s_w^2 + s_z t\left(1 - \frac{4}{3}s_\theta^2\right)$	0
D'	$\frac{1}{3}c_z s_w^2 - s_z t\left(\frac{1}{2} - \frac{1}{3}s_\theta^2\right)$	$\frac{1}{3}c_z s_w^2 - s_z t\left(\frac{1}{2} - \frac{1}{3}s_\theta^2\right)$	$\frac{2}{3}c_z s_w^2 - s_z t\left(1 - \frac{2}{3}s_\theta^2\right)$	0

$$\begin{aligned}\mathcal{L}_f^{\prime NC} &= \frac{g}{c_W} Z'^{\mu} J'^{0}_{\mu} \\ &= \frac{g}{2c_W}\bar{f}\gamma_\mu\left[g_L'^f(1-\gamma_5)+g_R'^f(1+\gamma_5)\right] f Z'^{\mu} \\ &= \frac{g}{2c_W}\bar{f}\gamma_\mu\left[g_V'^f - g_A'^f\gamma_5\right] f Z'^{\mu}\end{aligned} \tag{76}$$

where

$$g^f_{L,R} = s_Z\left[-T_3^{(1)}(f)+s_W^2 Q(f)\right] + tc_Z\left[T_3^{(2)}(f)+s_\theta^2 T_3^{(1)} - s_\theta^2 Q(f)\right]$$

4.2. Charged currents

This part is common for the doublets.

$$P^{CC}_\mu = g_2\sum_{i=1}^{2} T_i^{(2)} A'_{\mu i} + g\sum_{i=1}^{2} T_i^{(1)} A_{\mu i}. \tag{77}$$

Let us consider the charged currents for $SU(2)_1$ doublets

$$P^{CC1}_\mu = g\sum_{i=1}^{2}\frac{\sigma_i}{2}A_{\mu i} = \frac{g}{\sqrt{2}}\begin{pmatrix} 0 & W^+_\mu \\ W^-_\mu & 0\end{pmatrix}, . \tag{78}$$

where $W^\pm_\mu \equiv \frac{1}{\sqrt{2}}(A_{\mu 1} \mp A_{\mu 2})$. Therefore for SM doublets q_L and L_L we get couplings the same as in the SM, namely

$$\begin{aligned} L^{CC1} &= \sum_{F=q_L,L_L} \bar{F}\gamma_\mu P^{CC1}_\mu F \\ &= \frac{g}{\sqrt{2}}\left[\bar{l}\gamma^\mu\frac{(1-\gamma_5)}{2}\nu_l W^-_\mu + \bar{\nu}_l\gamma^\mu\frac{(1-\gamma_5)}{2} l W^+_\mu\right] \\ &+ \frac{g}{\sqrt{2}}\left[\bar{u}\gamma^\mu\frac{(1-\gamma_5)}{2} d W^+_\mu + \bar{d}\gamma^\mu\frac{(1-\gamma_5)}{2}\ u W^-_\mu\right]\end{aligned} \tag{79}$$

The charged currents for $SU(2)_2$ doublets

$$P^{CC2}_\mu = g_2\sum_{i=1}^{2}\frac{\sigma_i}{2}A'_{\mu i} = \frac{g_2}{\sqrt{2}}\begin{pmatrix} 0 & W'^+_\mu \\ W'^-_\mu & 0\end{pmatrix}, . \tag{80}$$

where $W'^\pm_\mu \equiv \frac{1}{\sqrt{2}}(A'_{\mu 1} \mp A'_{\mu 2})$. Therefore for SM doublets q_L and L_L we get couplings the same as in the SM, namely

$$\begin{aligned} L^{CC2} &= \sum_{F=Q'_L,Q'_R} \bar{F}\gamma^\mu P_\mu^{CC2} F \\ &= \frac{g_2}{\sqrt{2}}\left[\overline{U'}\gamma^\mu \overline{D'}W'^{+}_\mu + \overline{D'}\gamma^\mu\,\overline{U'}W'^{-}_\mu\right]. \end{aligned} \tag{81}$$

The total Lagrangian is

$$\begin{aligned} L^{CC} &= L^{CC1} + L^{CC2} \\ &= \frac{g}{\sqrt{2}}\left[\bar{l}\gamma^\mu\frac{(1-\gamma_5)}{2}\nu_l W_\mu^- + \bar{\nu}_l\gamma^\mu\frac{(1-\gamma_5)}{2} l W_\mu^+\right] \\ &+ \frac{g}{\sqrt{2}}\left[\bar{u}\gamma^\mu\frac{(1-\gamma_5)}{2} d W_\mu^+ + \bar{d}\gamma^\mu\frac{(1-\gamma_5)}{2}\, u W_\mu^-\right] \\ &+ \frac{g_2}{\sqrt{2}}\left[\overline{U'}\gamma^\mu \overline{D'}W'^{+}_\mu + \overline{D'}\gamma^\mu\,\overline{U'}W'^{-}_\mu\right]. \end{aligned} \tag{82}$$

5. PHENOMENOLOGY

The Z decay has the form [5]

$$\Gamma(f\bar{f}) = \frac{\rho G_F M_Z^3}{6\sqrt{2}} N_c^f \left(\beta^2(|g_A^f|^2 + \frac{3\beta-\beta^2}{2}|g_V^f|^2\right)(1+n_f)R_{EW}R_{QCD}, \tag{83}$$

where $\beta = \sqrt{1-4\frac{m_f^2}{M_Z^2}}$. β is very small and we present a result which is correct up to terms of order $\alpha\alpha_s$:

$$\Gamma(f\bar{f}) = \frac{\rho G_F M_Z^3}{6\sqrt{2}} N_c^f \left(|g_V^f|^2 R_V^f + |g_A^f|^2 R_A^f\right)(1+n_f), \tag{84}$$

where N_c^f is the color factor and other parameters are given in [5]

$$\begin{aligned} \rho &= 1+\delta_\rho, \delta_\rho(f\neq b) = \frac{3G_F m_t^2}{8\sqrt{2}\pi^2}, \\ \delta_\rho(f=b) &= -\frac{G_F m_t^2}{2\sqrt{2}\pi^2}, n_b = 10^{-2}\left(\frac{1}{5}-\frac{m_t^2}{2M_Z^2}\right), n_{f\neq b}\sim 0. \end{aligned} \tag{85}$$

The non-factorial electroweak corrections is given by [6]

$$R_V^f = 1+\frac{3\alpha(M_Z)}{4\pi}, \quad R_A^f = 1-6\frac{m_f^2}{M_Z^2}+\frac{3\alpha(M_Z)}{4\pi}, \tag{86}$$

where $\alpha(M_z) = \frac{1}{128} = 0.1182$. The QCD correction is given by

$$R_V^f(s) = R_A^f(s) = 1 + \frac{3\alpha_s}{4\pi}Q_f^2 + \frac{\alpha_s}{\pi} + \mathcal{O}(\alpha^2) \quad (87)$$

For the special channel decay $Z \to b^{-}b$, one obtains

$$\Gamma(Z \to b\bar{b}) = \frac{\rho_b G_F M_Z^3}{2\sqrt{2}}\left(|g_V^b|^2 R_V^b + |g_A^b|^2 R_A^b\right) \times 10^{-2}\left(\frac{1}{5} - \frac{m_t^2}{2M_Z^2}\right), \quad (88)$$

with

$$\begin{aligned} \rho_b &= 1 - \frac{G_F m_t^2}{2\sqrt{2}\pi^2},\ R_V^b = \left(1 + \frac{3\alpha(M_Z)}{4\pi}\right)\left(1 + \frac{\alpha_s}{12\pi} + \frac{\alpha_s}{\pi}\right) \\ R_A^b &= \left(1 - 6\frac{m_t^2}{M_Z^2} + \frac{3\alpha(M_Z)}{4\pi}\right)\left(1 + \frac{\alpha_s}{12\pi}Q_q^2 + \frac{\alpha_s}{\pi}\right). \end{aligned} \quad (89)$$

In the G(221), the coupling of the Z boson also depends on two parameters such as s_θ and s_z in mass states. In Fig. 1 we have plotted branching decay $Z \to b^{-}b$ as function of $Z - Z'$ mixing angle θ for three values of $s_z = 0.04, 0.06, 0.08$. Comparing with experimental data $Br(Z \to b^{-}b) = 0.37727 \pm 0.0005$ one gets limit for the $Z - Z'$ mixing angle θ as follows

$$\begin{aligned} s_z &= 0.004 \quad \Rightarrow \quad \theta \in [0 - 0.1], \\ s_z &= 0.006 \quad \Rightarrow \quad \theta \in [0.05 - 0.15], \\ s_z &= 0.008 \quad \Rightarrow \quad \theta \in [0.12 - 0.17]. \end{aligned} \quad (90)$$

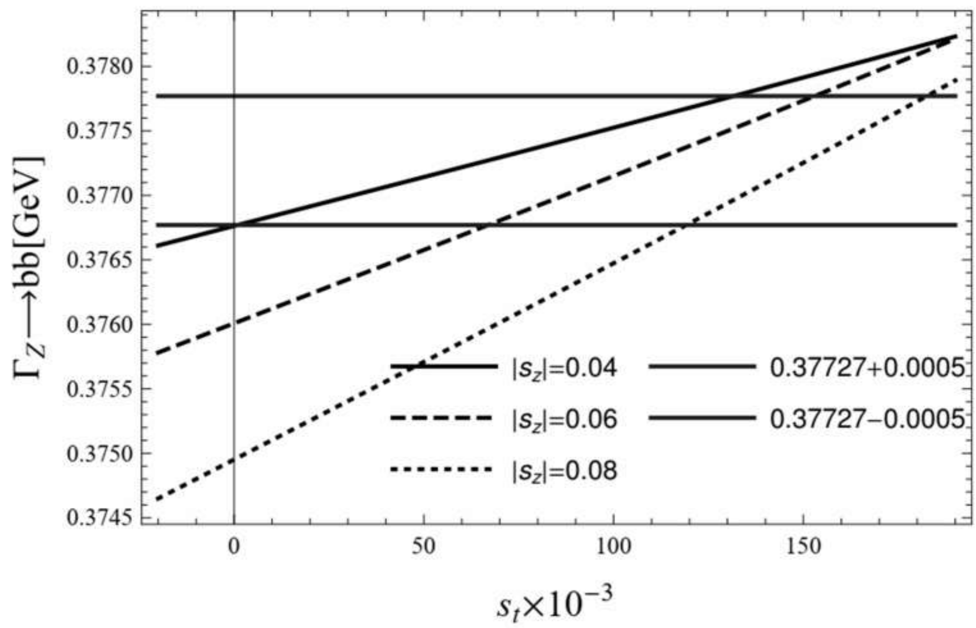

Figure 1. *Br() of ΓZ as function of |sz| in the G(221)*

6. CONCLUSION

In this paper we present in details diagonalization of neutral gauge boson sector. This procedure consists of three steps and two first steps are consistent with result in Ref.[3]. However, at the last step, our result is opposite with that in Ref. [3]. Studying branching ratio $Z \to \bar{b}b$ as a function of θ, we have derived limit for the $Z - Z'$ mixing angle.

REFERENCES

1. S. M. Boucenna, A. Celis, J. Fuentes-Martin, A. Vicente and J. Virto, JHEP **1612**, 059 (2016), arXiv: 1608.01349 [hep-ph]; S. M. Boucenna, A. Celis, J. Fuentes-Martin, A. Vicente and J.Virto, Phys. Lett. **B 760** (2016) 214.
2. K. Hsieh, K. Schmitz, J-H Yu, C-P Yuan, Phys. Rev. D **82**, 035011 (2010).
3. C. H. Chen and T. Nomura, Phys. Rev. D **95**, 015015 (2017), [arXiv:1606.03804 [hep-ph]].
4. L. T. Hue, A. B. Arbuzov, N. T. K. Ngan, and H. N. Long, *Eur. Phys. J.* **C 77**, No 5, (2017) 346
5. D. A. Gutierrez, W. A. Ponce and L. A. Sanchez, Eur. Phys. J. C, 46 497 (2006); For more details, see A. Carcamo, R. Martinez, R. and F. Ochoa, Phys. Rev. D73, 035007 (2006).
6. D. Bardin and G. Passarino, *The Standard Model in the Making*, Clarendon Press, Oxford (1999).
7. C. Patrignani et al. (Particle Data Group), Chin. Phys. C, 40, 100001 (2016)

MÔ HÌNH CHUẨN CỦA CÁC LOẠI HẠT CƠ BẢN TRONG MÔ HÌNH $SU(2)_1 \otimes SU(2)_2 \otimes U(1)_Y$ VỚI MÔ HÌNH VÉC TƠ KIỂU HẠT QUARKS

Tóm tắt: *Bài báo trình bày về trạng thái và khối lượng của hạt gauge trong mô hình chuẩn của các loại hạt cơ bản giữa mô hình $SU(2)_1 \otimes SU(2)_2 \otimes U(1)_Y$ với mô hình vec tơ kiểu hạt Quark. Khi nghiên cứu tỷ lệ phân nhánh $Z \to bb$ theo hàm của θ, chúng ta chuyển đổi giới hạn từ góc bàn tay trộn Z – Z'. Kết quả mang lại giúp cố định vùng tham số trong mô hình G (221).*

Từ khóa: *Mô hình chuẩn, SM, các loại hạt cơ bản, mô hình vec tơ kiểu hạt quark.*

DISCUSSION ON THERMOELECTRIC ECONOMY AND RESEARCH OF BISMUTH TELLURIDE

Nguyen Bich Ngoc[1], Tran Van Quang [2]
[1]*Graduate University of Science and Technology, Vietnam Academy of Science and Technology*
[2]*Department of Physics, University of Transport and Communications, Hanoi, Vietnam*

Abstract: *The thermoelectric effect, first discovered by Seebeck, has been known for a long time. Its practical applications can be found in thermocouples, thermoelectric generators and thermoelectric refrigeration modules used in electronic devices, etc. However, current applications for the energy issue are limited and not come into daily life due to the poor performance and cost demanded. Improving thermal efficiency is still a difficult task. In this article, we select to introduce thermoelectric effect in economy and provide discussion on research of* Bi_2Te_3*, the favorite thermoelectric material. We used density functional theory and Bolzmann transport equation for the calculations. The results are consistent with experiment and other calculations.*

Keywords: *Thermoelectric effect, Bolzmann transport equation, density functional theory, and thermoelectric cost.*

Email: tranquang@utc.edu.vn
Received 2 May 2018
Accepted for publication 20 May 2018

1. THERMOELECTRIC EFFECT

Thermoelectric effect has been investigated long time ago which allows direct conversion of heat into electricity. When the temperature gradient applied at a junction of two different conductors, the electric field is generated, $\vec{E} = S\nabla T$, where S is the Seebeck coefficient or the thermopower. This effect is called Seebeck effect. In contrast, when there is an external current in the corresponding circuit, the temperature gradient occurs. This effect is also called the Peltier effect. The Peltier effect is much more widely used than the Seebeck effect in refrigeration modules. Today's typical thermoelectric materials are chalcogenide compounds such as Bi_2Te_3, Sb_2Te_3, PbTe or other materials such as skutterudites, clathrates, half-heapslers, and related oxides, and etc [1–3].

The thermoelectric efficiency of a device or a material is [4]

$$\eta = \left(1 - \frac{T_c}{T_h}\right)\frac{\sqrt{1+ZT}-1}{\sqrt{1+ZT}+\frac{T_c}{T_h}}, \tag{1}$$

where T_c is cold-source temperature, T_h is hot-source temperature, and *ZT* is the dimensionaless figure of merit. *ZT* strongly depends on materials and it is usally used to qualify the thermoelectric performance. It is defined as

$$ZT = S^2\sigma T/\kappa, \tag{2}$$

where σ is electrical conductivity, κ the thermal conductivity and T the temperature.

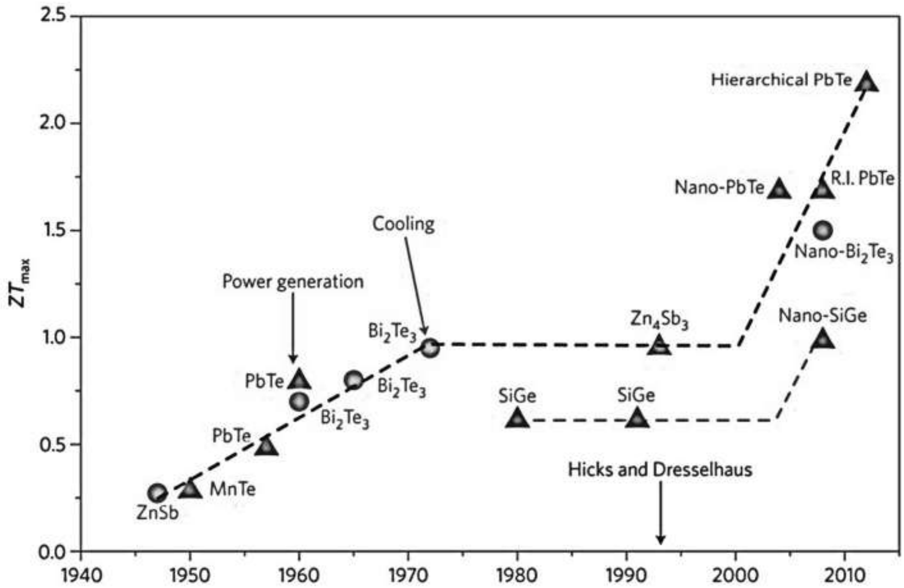

Fig. 1*. Development of improving ZT [5]*

Table 1*. Typical ZT values of materials and their cost used now aday [6]*

Compound	*ZT*	T (°C)	η	Cost ($/kg)
Cobalt Oxide	1.4	727	12%	$345
Clathrate	1.4	727	12%	$5,310
SiGe	0.86	727	9%	$6,033
Chalcogenide	2.27	727	16%	$730
Half -Heusler	1.42	427	17%	$1,988
Skutterudite	1.5	427	18%	$562
Silicide	0.93	727	9%	$151

Improving *ZT* encountered many obstacles due to conflicting requirements. Highly conductive metal is accompanied by very small S and very large κ. In contrast, the dielectric material gives large S while the electrical conducting is poor. Today, in order to develop the field, one focuses on semiconductors to seek. However, the value of *ZT* is still low. In addition to the scientifically-found-high-*ZT* materials, their price is expensive. Table 1 presents the *ZT* values, operating temperatures, performance and cost of some common compounds today. Such obstacles have made thermoelectric technology to be difficult to implement in practical applications.

Despite these limitations, the TE application is still noticeable due to its stability and ease of design. The diagram describing the application of the TE effect is illustrated in Fig. 1. In order to increase the power, one must pair the semiconductor components together to form a sequence for generating electricity. A hot surface works as heat absobtion taken from the heat source (such as in a car, a motorbike or a machine). A cold surface is exposed to a normal embient environment, i.e. heat sink or coolant. Such generated electricity as mentioned above, is costly. Table 2 shows the cost of electricity generated by TE generation compared to the electricity produced by other methods. Basically using electricity from theTE generator is very expensive which is not found frequently in our practical component in Vietnam.

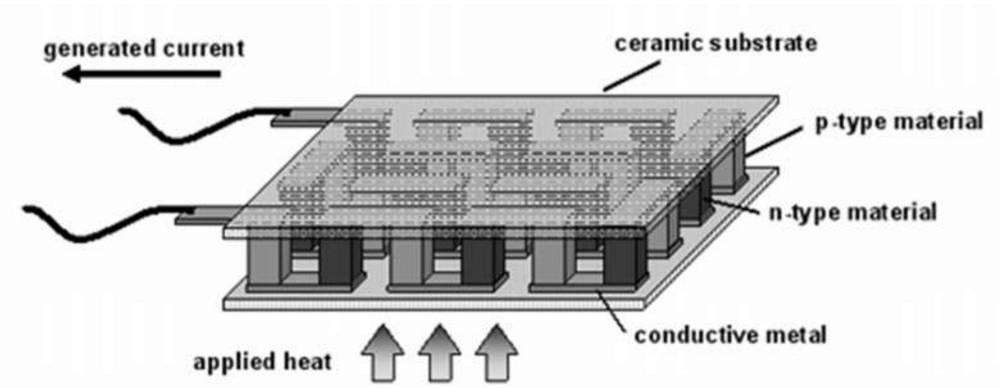

***Fig. 2.** The diagram depicts a TE module as an actual equipment of the Lairdtech company (*https://www.digikey.com*)*

***Table 2.** Electricity costs at various temperature ranges [6]*

Operating temperatures	Electricity	Cost ($/W)
Low (T_h~100°C)	Geoelectric	$4.14
	Half-Heusler Thermoelectric (Bulk $Zr_{0.25}Hf_{0.25}Ti_{0.5}NiSn_{0.994}Sb_{0.006}$)	$125.05

Operating temperatures	Electricity	Cost ($/W)
	Silicon Quantym Wire, Thermoelectric	$104.18
	Chalcogenide Thermoelectric (Nanobulk $Bi_{0.52}Sb_{1.48}Te_3$)	$62.44
Medium (T_h~250°C)	Rankine Circle	$4.00
	Solar Cell	$3.60
	PV Target	$1.00
	Skutterudite Thermoelectric (Bulk $Yb_{0.2}In_{0.2}Co_4Sb_{12}$)	$19.02
	Half-Heusler Thermoelectric (Bulk $Zr_{0.25}Hf_{0.25}Ti_{0.5}NiSn_{0.994}Sb_{0.006}$)	$14.45
	Chalcogenide Thermoelectric (Nanobulk $Bi_{0.52}Sb_{1.48}Te_3$)	$11.92
High (~500°C)	Nuclear	$5.34
	Coal	$2.84
	Gas	$0.98
	Silicide Thermoelectric (Bulk $Mg_2Si_{0.6}Sn_{0.4}$)	$5.56
	Chalcogenide Thermoelectric (Bulk $AgPb_{18}SbTe_{20}$)	$5.06
	Half-Heusler Thermoelectric (Bulk $Zr_{0.25}Hf_{0.25}Ti_{0.5}NiSn_{0.994}Sb_{0.006}$)	$4.48

2. METHOD OF CALCULATION

The development of science searching for promising materials to overcome these obstacles is one of the great challenges of science today [2]. One of the most important materials are the alloys of chalcogenides [3,7–11]. New effects among these materials are being explored. One of the most cost-effective practical approaches today is the research based on calculus ultilizing density functional theory [12,13].

For any particle system, the Schrodinger equation for the description is given by

$$H\left|\Psi\right\rangle = i\frac{\partial\left|\Psi\right\rangle}{\partial t} \quad (3)$$

in which H is Hamintonian. In fact, this leads to a system of unknown Avogadro size equations (10^{23} particles per gram). Solving this problem even with the help of the most modern supercomputers is impossible. In the simplified approach of using the principle of variation, the energy expectation is gradually leading to the formation of density functional theory. The fundamental quantity in the theory is the electronc density function. The foundation is based on two Hohenberg-Kohn theorems [12,13]. The first statement states that the electron density is uniquely determined by the external potential (with the difference of an additional constant). Thus, it shows that the density functional theory is clearly expressed in term of electron density (and not necessary to consider the wave function of the system in the usual way). The second theorem allows us to work with trial densities, i.e. the minimum energy density is the density of the real system [2]. Accordingly, the total energy is electron density functional

$$E[\rho]=F[\rho]+\int v(\vec{r})\rho(\vec{r})d\vec{r}\,, \tag{4}$$

where $F[\rho]=T[\rho]+V_{ee}[\rho]$ is a universal Kohn-Sham functional. It is generally transferable for any system. The electron density is synthesized by Kohn-Sham orbital ψ

$$\rho(\vec{r})=\sum_{i=1}^{N} n_i\langle\psi_i|\psi_i\rangle, \tag{5}$$

in which n is occupation number. The Kohn-Sham orbital ψ obeys Kohn-Sham equation

$$H_{KS}\psi_i=\varepsilon_i\psi_i\,, \tag{6}$$

where $H_{KS}=-\dfrac{\Delta}{2}+v(\vec{r})+\int\dfrac{\rho(\vec{r}')}{|\vec{r}-\vec{r}'|}d\vec{r}'+v_{xc}[\rho(\vec{r})]$ is Kohn-Sham Halmintonian; $v_{xc}[\rho]=\delta E_{xc}[\rho]/\delta\rho$ is exchange-colleration potential. Equation (6) is solved self-consistently as following

$$\rho_{in}\rightarrow V\rightarrow H_{KS}\rightarrow\psi_i\rightarrow\rho_{out}\rightarrow\rho_{conv} \tag{7}$$

This means that Halminton H_{KS} is determined from a trial density. Thus, ψ is obtained by solving (6). Next, ρ synthesized and one cirles is completed. The self-consistent solution is achieved until ρ is converved. The central difficulty here is v_{xc}. This is approximated in different ways such as by using local density approximation (LDA), generalized gradient approximation (GGA), etc. [13]

3. RESULTS AND DISCUSSION

The solution of Eq. (6) above gives the total energy of the crystal system. For new materials, this is also the way to search for the most stable structure. Therefore, the ground state of the relevant material is analyzed. The density of state (DOS) and band structure around the Fermi level play a crutial role to determine transport properties of a compound [14,15]. The steep DOS at bandeges gives rise to the large Seebeck coefficient and therefore the high power factor. This is main feature of Bi_2Te3 leading it to be a potential TE material. From ground state, we utize the solution of Boltzmann Transport Equation (BTE) [10,11,16] to determine the TE coefficients [17], i.e. the Seebeck coefficient and the power factor [18,19]. Accordingly, S is estimated through the solution of BTE equation as follow [16,20].

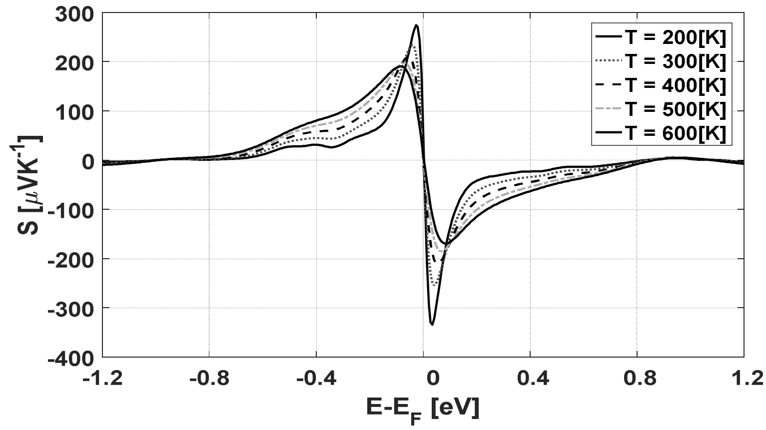

Fig 3. Seebeck coefficient, S (μV/K) at various temperatures as a function of chemical potential.

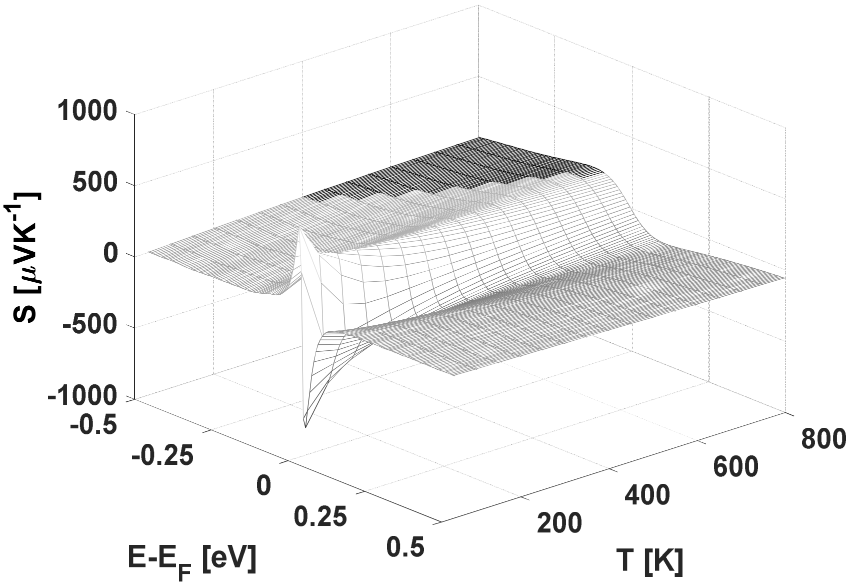

Fig 4. Two-dimensional representation of thermopower S (μV / K) as a function of temperature and chemical potential.

$$S = -\frac{1}{eT}\left(\Lambda^{(0)}\right)^{-1}\Lambda^{(1)}$$

where

$$\Lambda_{ij}^{(\alpha)} = \int d\varepsilon \sum_{\vec{k}} \frac{\partial f}{\partial \varepsilon}(\varepsilon-\mu)^{\alpha} e^2 \tau_{ik}(\vec{k})\delta(\varepsilon-\varepsilon(\vec{k}))\vec{v}_k(\vec{k})\vec{v}_j(\vec{k})$$

in which ε is eigenvalues obtained from Eq. (6), f is Fermi-Dirac distribution function, e the elementary charge, δ Dirac-Delta function, v the group velocity determined form $\varepsilon(\vec{k})$, and $\vec{k}$ the wave vector.

The result calculation of S as a function of the chemical potential at different temperatures are presented in FIG. 3. At low temperatures, the chemical potential dependence of S is altered strongly. This is due to the bipolar effect and the Pisarenko effect [1,21]. This somehow demonstrates that Bi_2Te_3 is a narrow band semiconductor. The resulting transport coefficient derived from the contribution to transport properties comes mainly from the p states of the elements Bi and Te [22]. But when we do n-doping, we get the main contribution of the remaining Te, but the slope of the DOS in the case decreased slightly [3,23]. For the detail, we present in FIG. 4 the temperature and chemical potential dependence of S as 2D functions. As can be seen, the highest S is obtained when the chemical is small, and the temperature is low. This is consistent with previous calculations and results published by empirical and other calculations in which the maximum S is of about 200~300 μV/K [3,7,23–25].

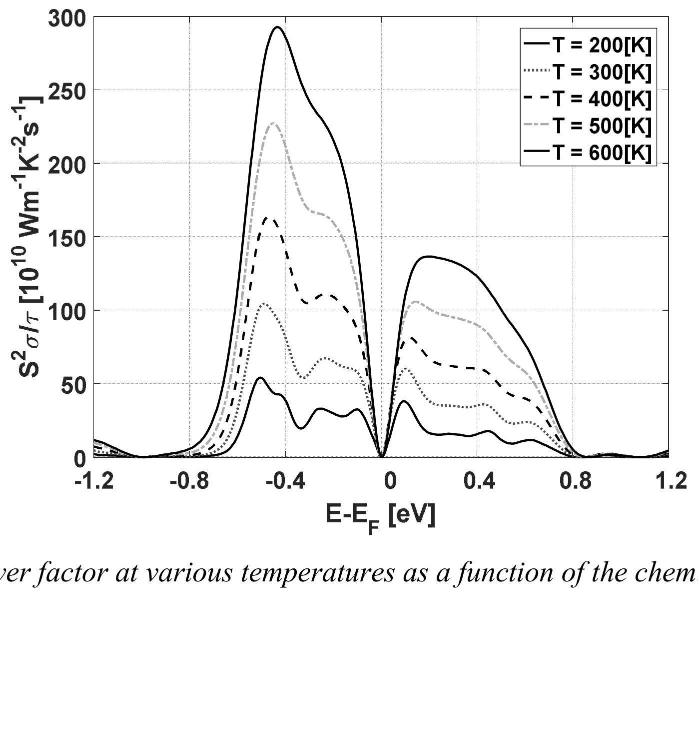

Fig 4. Power factor at various temperatures as a function of the chemical potential.

Next we examine the power factor, $S^2\sigma$, as a function of the chemical potential at various temperatures. Since σ is the relaxation time dependence, i.e. σ is proportional to relaxation time parameter τ. The value of τ is about 10^{-14}s for the chalcogenide compounds [23,24,26,27]. To generalize, we estimate $S^2\sigma/\tau$ which is relaxation time independence to make discussion. We present the calculation results in FIG. 5. It is clearly seen that in the too small or too large doping levels, the power factor is very small. For the low doping level, S is very large while σ is small. Therefore, σ plays important role in this area while in large doping level, σ is very large while S is very low leading to a decrease in power factor. In other words, in this region the coefficient S determines the TE properties of the material. These results suggest that to improve power factor, the doping level must be optimized. The value of the optimal doping level depends on the temperature. To substabtiate the point, we present in FIG. 6 the power factor as two variables dependence of the power factor, i.e. as a function of temperature and chemical potential. The peak of power factor is occurred at around -0.5eV (for p-type doping) and 0.2 eV (for n-type doping). These doping levels is desired to improve the power factor. Moreover, p-type doping level with optimized doping level gives higher power factor compared with that of n-type doping.

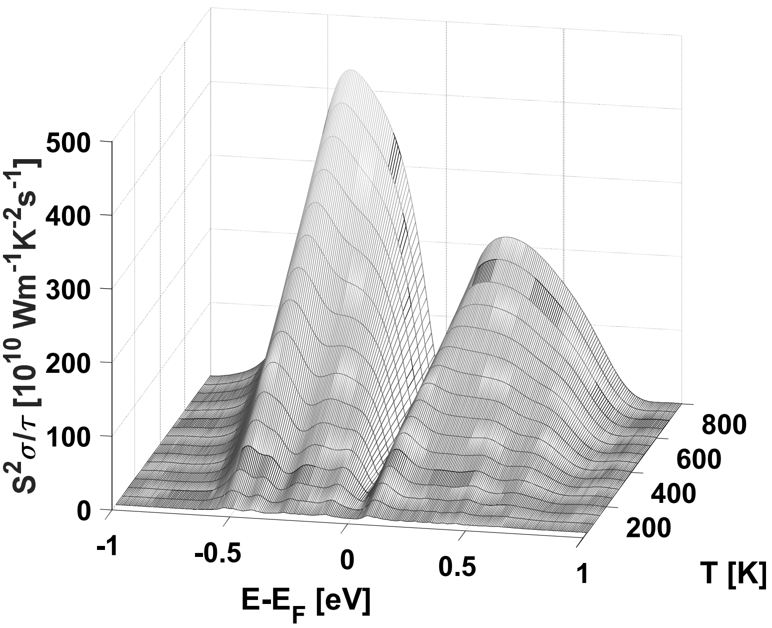

Fig 5. Two-dimensional representation of power factir a function of temperature and chemical potential.

4. CONCLUSION

TE effect is important in the current demand for green energy resource. The study of thermoelectric effects in Vietnam is a hot topic. This paper deals with issues related to: thermoelectric effects, typical applications, cost and one aspect of scientific calculations of thermoelectric materials research. We also performed a real calculation for Bi2Te3 and provide relative discussion using density funtional theory combined with Boltzmann Transport Equation to estimate the Seebeck coefficient and the thermal power factor for Bi2Te3 as a function of chemical potential and discussion. Calculated results are consistent with previous experiments and calculations.

Acknowledgments. This research is funded by Vietnam National Foundation for Science and Technology Development (NAFOSTED) under grant number 103.01-2015.11. The authors also thank the program for science and technology development of University of Transport and Communications.

REFERENCES

1. X. Zhang, L.-D. Zhao, Thermoelectric materials: Energy conversion between heat and electricity, J. Mater. 1 (2015) 92–105. doi:10.1016/j.jmat.2015.01.001.
2. G.J. Snyder, E.S. Toberer, Complex thermoelectric materials, Nat. Mater. 7 (2008) 105–114. doi:10.1038/nmat2090.
3. T. Van Quang, M. Kim, The metal-insulator phase transition in the strained GdBiTe3, J. Appl. Phys. 113 (2013) 17A934. doi:10.1063/1.4795743.
4. A. Bulusu, D.G. Walker, Review of electronic transport models for thermoelectric materials, Superlattices Microstruct. 44 (2008) 1–36. doi:10.1016/j.spmi.2008.02.008.
5. J.P. Heremans, M.S. Dresselhaus, L.E. Bell, D.T. Morelli, When thermoelectrics reached the nanoscale, Nat. Nanotechnol. 8 (2013) 471–473. doi:10.1038/nnano.2013.129.
6. S. Leblanc, S.K. Yee, M.L. Scullin, C. Dames, K.E. Goodson, Material and manufacturing cost considerations for thermoelectrics, Renew. Sustain. Energy Rev. 32 (2014) 313–327. doi:10.1016/j.rser.2013.12.030.
7. C.B. Satterthwaite, R.W. Ure, Electrical and Thermal Properties of Bi2Te3, Phys. Rev. 108 (1957) 1164–1170. doi:10.1103/PhysRev.108.1164.
8. J.N. Kim, M. Kaviany, J.-H. Shim, Optimized ZT of Bi2Te3-GeTe compounds from first principles guided by homogeneous data, Phys. Rev. B. 93 (2016) 075119. doi:10.1103/PhysRevB.93.075119.
9. H. Osterhage, J. Gooth, B. Hamdou, P. Gwozdz, R. Zierold, K. Nielsch, Thermoelectric properties of topological insulator Bi2Te3, Sb2Te3, and Bi2Se3 thin film quantum wells, Appl. Phys. Lett. 105 (2014). doi:10.1063/1.4896680.

10. T. Van Quang, M. Kim, Role of O and Se defects in the thermoelectric properties of bismuth oxide selenide, J. Appl. Phys. 120 (2016) 195105. doi:10.1063/1.4967989.
11. T. Van Quang, K. Miyoung, Electronic Structures and Thermoelectric Properties of Layered Chalcogenide PbBi4Te7 from First Principles, J. Korean Phys. Soc. 68 (2016) 393–397. doi:10.3938/jkps.68.393.
12. P. Hohenberg, W. Kohn, Inhomogeneous Eelectron gas, Phys. Rev. 136 (1964) B864-871. doi:10.1103/PhysRev.136.B864.
13. W. Kohn, L.J. Sham, Self-Consisten Equations Including Exchange and Correlation Effects, Phys. Rev. 140 (1965) A1134–A1138. doi:http://dx.doi.org/10.1103/PhysRev.140.A1133.
14. T.J. Scheidemantel, C. Ambrosch-Draxl, T. Thonhauser, J. V. Badding, J.O. Sofo, Transport coefficients from first-principles calculations, Phys. Rev. B. 68 (2003) 125210. doi:10.1103/PhysRevB.68.125210.
15. G.D. Mahan, J.O. Sofo, The best thermoelectric., Proc. Natl. Acad. Sci. 93 (1996) 7436–7439. doi:10.1073/pnas.93.15.7436.
16. G.D. Mahan, J.O. Sofo, The best thermoelectric., Proc. Natl. Acad. Sci. U. S. A. 93 (1996) 7436–7439. doi:10.1073/pnas.93.15.7436.
17. P. Giannozzi, S. Baroni, N. Bonini, M. Calandra, R. Car, C. Cavazzoni, D. Ceresoli, G.L. Chiarotti, M. Cococcioni, I. Dabo, A.D. Corso, S. Fabris, G. Fratesi, S. de Gironcoli, R. Gebauer, U. Gerstmann, C. Gougoussis, A. Kokalj, M. Lazzeri, L. Martin-Samos, N. Marzari, F. Mauri, R. Mazzarello, S. Paolini, A. Pasquarello, L. Paulatto, C. Sbraccia, S. Scandolo, G. Sclauzero, A.P. Seitsonen, A. Smogunov, P. Umari, R.M. Wentzcovitch, Quantum ESPRESSO: a modular and open-source software project for quantum simulations of materials, J. Phys. Condens. Matter. 21 (2009) 395502. doi:10.1088/0953-8984/21/39/395502.
18. T. Van Quang, K. Miyoung, Spin-orbit Coupling Effect on the Structural Optimization; Bismuth Telluride in First-principles, J. Korean Magn. Soc. 23 (2013) 1.
19. T. Van Quang, M. Kim, Effect on the Electronic, Magnetic and Thermoelectric Properties of by the Cerium Substitution, IEEE Trans. Magn. 50 (2014) 1000904. doi:10.1109/TMAG.2013.2279854.
20. N.W. Ashcroft, N.D. Mermin, Solid State Physics, 1976. doi:10.1016/0038-1101(66)90069-4.
21. T. Van Quang, M. Kim, Enhancement of the thermoelectric performance of oxygen substituted bismuth telluride, J. Appl. Phys. 122,. 122 (2017) 245104.
22. P. Larson, S. Mahanti, M. Kanatzidis, Electronic structure and transport of Bi2Te3 and BaBiTe3, Phys. Rev. B. 61 (2000) 8162–8171. doi:10.1103/PhysRevB.61.8162.
23. M.S. Park, J.H. Song, J.E. Medvedeva, M. Kim, I.G. Kim, A.J. Freeman, Electronic structure and volume effect on thermoelectric transport in p -type Bi and Sb tellurides, Phys. Rev. B. 81 (2010) 155211. doi:10.1103/PhysRevB.81.155211.
24. G.K.H. Madsen, D.J. Singh, BoltzTraP. A code for calculating band-structure dependent quantities, Comput. Phys. Commun. 175 (2006) 67–71. doi:10.1016/j.cpc.2006.03.007.

25. G. Pizzi, D. Volja, B. Kozinsky, M. Fornari, N. Marzari, An updated version of BOLTZWANN: A code for the evaluation of thermoelectric and electronic transport properties with a maximally-localized Wannier functions basis, Comput. Phys. Commun. 185 (2014) 2311–2312. doi:10.1016/j.cpc.2014.05.004.

26. T. Thonhauser, T.J. Scheidemantel, J.O. Sofo, Improved thermoelectric devices using bismuth alloys, Appl. Phys. Lett. 85 (2004) 588–590. doi:10.1063/1.1775286.

27. T. Quang, H. Lim, M. Kim, Temperature and carrier-concentration dependences of the thermoelectric properties of bismuth selenide dioxide compounds, J. Korean Phys. Soc. 61 (2012) 1728–1731. doi:10.3938/jkps.61.1728.

VẤN ĐỀ KINH TẾ NHIỆT ĐIỆN VÀ NGHIÊN CỨU TÍNH CHẤT NHIỆT ĐIỆN BISMUTH TELLURIDE

Tóm tắt: *Hiệu ứng nhiệt điện, phát hiện đầu tiên bởi Seebeck, đã được biết đến từ lâu. Hiệu ứng này ngày nay được biết đến rộng rãi trong khoa học và đời sống. Các ứng dụng trong thực tiễn có thể thấy là cặp nhiệt điện dùng cho các đầu đo nhiệt độ, pin nhiệt điện, modun làm lạnh cho các thiết bị điện tử, ... Tuy vậy, các ứng dụng hiện tại cho vấn đề năng lượng vẫn bị giới hạn và chưa đi vào đời sống thường ngày do hiệu suất của các thiết bị còn thấp và giá thành còn cao. Việc cải tiến hiệu suất nhiệt điện cho đến nay vẫn là một bài toán khó. Trong bài báo cáo này, chúng tôi giới thiệu về hiệu ứng nhiệt điện từ thực tiễn ứng dụng đơn giản đến khoa học hiện đại và chỉ ra những vấn đề còn tồn đọng. Chúng tôi thực hành nghiên cứu bằng lý thuyết phiếm hàm mật độ và lý thuyết vận chuyển Boltzmann trên vật liệu kinh điển Bi_2Te_3. Kết quả thu được phù hợp với thực nghiệm và các tính toán khác.*

Từ khóa: *Hiệu ứng nhiệt điện, phương trình vận chuyển Boltzmann, lý thuyết phiếm hàm mật độ, và giá thành nhiệt điện.*

STUDY OF FOURIER TRANSFORM AND APPLICATION TO SOLVE PROBLEMS OF CIRCUIT AC AND THERMAL TRANSFER

Nguyen Vu Nhan[1*], Quang Thi Thuy[2]
Nguyen Huyen Trang[2], Nguyen Thu Huyen[3]
1. Center of Science and Technology, Hanoi Metropolitan University.
2. Pedagogic of Physics CLC K41, Hanoi Metropolitan University.
3. Pedagogic of Physics K41, Hanoi Metropolitan University.
** E-mail: nvnhan@daihocthudo.edu.vn*

Abstract: *The mathematical-physics equation is a application subject, requires students of pedagogic of physics and mathematic must understand the methods and techniques to calculate. There are many methods applied in mathematical-physics equations such as Laplace transform, Fourier transform. In this paper, we introduce the Fourier transform and applied to solving the problems of circuit AC and thermal transfer (diffusion equation). The illustrative exercises show the advantages of this method in comparison with other methods for the above problems. However, that the application of Fourier transforms is more limited than that of using Laplace transforms as it requires the absolute conditions for integrals.*

Keywords: *Teaching methods, teaching innovation, teaching theory.*

Email: nvnhan@daihocthudo.edu.vn
Received 2 May 2018
Accepted for publication 20 May 2018

1. INTRODUCTION

In advanced mathematics as well as in mathematical-physical equations, students have been studying thematic sequences, including Fourier series and some applications of the Fourier series. However, the Fourier transform and its applications to solve differential equations in circuit problems, thermal transfer, wave propagation, diffusion, etc. have not been considered due to the time condition of the course subject. These problems belong to a class of exercises that are very useful for students of pedagogic of physics and mathematic in depth research in solving problems in electrical circuits, wave propagation and thermal transfer... Addressed directly to this problem by analytical methods usually very cumbersome and complex, so physicists have developed several methods of efficiency and fully resolve the problem as Laplace transform, Fourier transform ...

Today, with the help of computers, solving these problems with the above method proved to be effective quickly. This article briefly introduces the Fourier transform and focuses its attention on the application of the Fourier transform in solving a number of AC circuit problems and specific diffusion problems.

2. SUMMARY OF FOURIER TRANSFORM

Fourier transform applications effectively solve the problems of circuit AC, diffusion as well as many other problems such as integrals, solutions of differential equations, diffusion problems, mathematical-physics equation ...

Consider the set L 'of the functions f(x) satisfying the Dirichlet conditions in any finite interval. In that range, continuous function f, or a number of finite discontinuity (type one), and absolutely integrable in the range (-∞, + ∞), ie exist the integral $\int_{-\infty}^{\infty} |f(x)| dx$.

Then, for all $f \in L'$, we have:

$$f(x) = \frac{1}{2\pi} \int_{-\infty}^{\infty} d\omega \int_{-\infty}^{\infty} f(t) e^{i\omega(x-t)} dt. \quad (1)$$

We can write (1) in the following form:

$$f(x) = \frac{1}{2\pi} \int_{-\infty}^{\infty} G(\omega) e^{i\omega x} d\omega, \quad (2)$$

$$G(\omega) = \int_{-\infty}^{\infty} f(t) e^{-i\omega t} dt. \quad (3)$$

The function G(ω) defined by formula (3) is called the Fourier image of the function f(x). Sign:

$$\phi[f(t),\omega] = G(\omega). \quad (4)$$

The mapping ϕ is called the Fourier transform of the function f.

Let $f \in L'$ and Fourier of function f:

$$f(x) = \frac{1}{2\pi} \int_{-\infty}^{\infty} G(\omega) e^{i\omega x} d\omega, \quad (5)$$

$$G(\omega) = \int_{-\infty}^{\infty} f(t) e^{-i\omega t} dt. \quad (6)$$

First of all, we consider the special case of the Fourier (5) and (6) formulas because they have many applications for studying non-stop phenomena in electrical circuits.

Suppose the function f(x) is zero with x <0. Then the formulas (5), (6) are of the form:

$$f(x) = \frac{1}{2\pi}\int_{-\infty}^{\infty} G(\omega)e^{i\omega x}d\omega, \tag{7}$$

$$G(\omega) = \int_{0}^{\infty} f(t)e^{-i\omega t}dt. \tag{8}$$

Formulas (7), (8) are construed as follows: If f(x) satisfies the Dirichlet conditions in finite intervals within (0, + ∞) and absolute integrates in (0, + ∞), then integral in the right-hand side of the equation (7) equal f(x) with x> 0 and equal zero with x <0; when x = 0, that integral is $\frac{1}{2}\lim_{x\to 0} f(x)$. Note that the opposite is not true.

We have a relation between the Laplace transform:

$$F(\alpha+i\omega) = \int_{0}^{\infty} e^{-(\alpha+i\omega)x}f(x)dx, \ (\alpha>0), \tag{9}$$

and Fourier transform:

$$G(\omega) = \int_{0}^{\infty} e^{-i\omega x}f(x)dx, \tag{10}$$

in that, f(x) satisfies the Dirichlet conditions in finite intervals, and the integral is in (0, + ∞). We have:

$$G(\omega) = \lim_{\alpha\to 0} F(\alpha + i\omega) = F(i\omega) \tag{11}$$

Thus, the Fourier image G(ω) of a given function to equal the Laplace image F(p) of that function if set to p = iω. For example, if f(x) = e^{-ax} (a> 0) then F(p) = $\frac{1}{p+a}$ and according to formula (11) then G(ω) = $\frac{1}{i\omega+a}$. However, if f(x) = C, then F(p) = $\frac{C}{p}$, and G (ω) does not exist because f(x) = C does not have absolute integral at (0,+∞).

The relationship between the Fourier transform and the Laplace of a function given by Equation (11) demonstrates that, when solving differential equations and mathematical-physics equations, we can also use Fourier transforms. It should be noted, the application of Fourier transforms is more limited than that of using Laplace transforms, since it requires the function must to be absolute integral. The application of the Fourier transform of functions to solve differential equations and mathematical-physics equations is the same as applying the Laplace transform. Indeed, if G(ω) is the Fourier image of the function f(x) with the assumption f(0) = 0, from expression (11) and the formula for the Laplace image of $f'(x) \risingdotseq pF(p)$, we have the Fourier transform of derivative f '(x):

$$i\omega F(i\omega) = i\omega G(\omega). \tag{12}$$

In addition, from the formula for the Laplace image of the integral $\int_0^x f(t)dt \risingdotseq \frac{1}{p}F(p)$, Fourier transform of $\int_0^x f(t)dt$ is calculated by the following expression:

$$\frac{F(i\omega)}{i\omega} = \frac{G(\omega)}{i\omega}. \tag{13}$$

Thus, when solving differential equations and mathematical-physics equations, the formulas of the Laplace transform can be used by replacing F(p) by G(ω) and putting p = iω. If G(ω) is the Fourier transform of the function f(x), then f(x) can be found by the formula (7).

In particular, if Fourier transform G(ω) is a form of $G(\omega) = \frac{N(\omega)}{M(\omega)}$, where N(ω) and M(ω) are polynomials of ω, and the degree of the polynomial N(ω) is lower than that degree of the polynomials M(ω), provided that the following equation:

$$M(\omega) = 0, \tag{14}$$

only single solutions. Then, the function f(x) can be defined by the formula:

$$f(x) = \sum_{k=1}^{m} \frac{iN(\omega_k)}{M'(\omega_k)} e^{i\omega_k x}, \tag{15}$$

here, the index k of total in (15) takes all the solutions of equation (14).

We know that in electrical engineering and radio technology the intensity of current is usually indicated by the letter i, so to avoid confusion, we will denote the virtual unit by j.

3. APPLICATION OF FOURIER TRANSFORM TO SOLVE THE AC CIRCUIT PROBLEM

Following, we apply the Fourier transform to solve some specific problems.

3.1. Problem 1

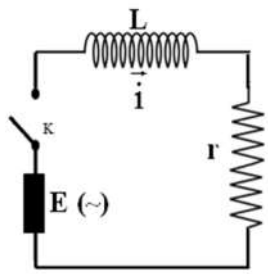

Fig. 1

For the rLC circuit (Fig. 1), the power source E has a constant electromotive force. Assume that when t = 0, the current i(0) = 0. Determine the instantaneous current i(t) in the circuit.

The answer:

When there is current i(t), the voltage of the circuit consists of the offset voltage for a power of electrical inductance $L\dfrac{di}{dt}$, and the voltage r.i caused by the resistance of the circuit. So we have the equation:

$$L\frac{di}{dt} + r.i = E\,. \tag{16}$$

Since the constant E does not have absolute integral over the range (0, + ∞), it is not possible to apply the Fourier transform to each term of the equation. Then, the derivative of the two sides of equation (16), and applying the Fourier transform. Let i(ω) be the Fourier picture of i(t), we obtain:

Since the constant E does not have absolute integral over the range (0, + ∞), it is not possible to apply the Fourier transform to each term of the equation. Then, the derivative of the two sides of equation (16), and applying the Fourier transform. Let i(ω) be the Fourier picture of i(t), we obtain:

$$L[(j\omega)^2 I(\omega) - i'(0)] + j\omega r.I(\omega) = 0, \tag{17}$$

because $i'(0) = \dfrac{E}{L}$ should be:

$$L[-\omega^2 I(\omega) - \frac{E}{L}] + j\omega r.I(\omega) = 0, \tag{18}$$

so:

$$I(\omega) = \frac{E}{-\omega^2 L + j\omega r}\,. \tag{19}$$

Let N(ω) = E, M(ω) = $-\omega^2 L + j\omega r$, where M'= - 2ωL + jr, from formula (15), we obtain the solution of the problem, or get the expression of the current intensity in the circuit:

$$i(t) = \frac{E}{r}\left[1 - e^{-\frac{r}{L}t}\right]. \tag{20}$$

3.2. Problem 2

The rLC serial circuit (Fig. 2) has a voltage source $Ee^{-\alpha t}$ ($\alpha > 0$). Determine the instantaneous intensity i(t) in the circuit knowing that at the initial time i(0) = 0.

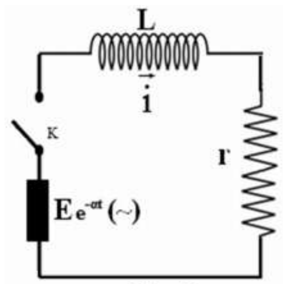

Fig. 2

The answer:

Similar to problem 1, calling I (ω) is the Fourier image of i(t). Applying Fourier transforms to each term of the equation, we obtain:

$$j\omega L.I(\omega) + r.I(\omega) = \frac{E}{j\omega + \alpha}.$$

So: $$I(\omega) = \frac{E}{(j\omega + \alpha)(j\omega L + r)}.$$

Let N(ω) = E and M(ω) = (jω + α) (jωL + r), M'(ω) = -2ωL + (r + (r + αL)j. Applying the formula (11), we obtain the expression of the electric current running in the written circuit in the following form:

$$i(t) = \frac{E}{r - \alpha L}\left(e^{-\alpha t} - e^{-\frac{r}{L}t}\right). \tag{21}$$

3.3. Problem 3

A capacitor to has capacitance C. The capacitoris charged to voltage E, then capacitor discharges into a circuit consisting of an inductance L and a resistor r connected as shown in Fig. 3. Find the instantaneous current i(t) with initial condition i(0) = 0.

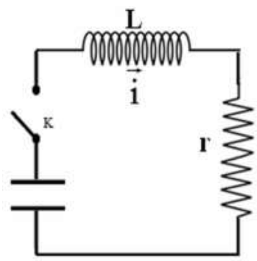

Fig. 3

The answer:

The intensity of current i(t) is the solution of the equation:

$$L\frac{di}{dt} + r.i + \frac{1}{C}\int_0^t i(s)ds = E. \tag{22}$$

First, the derivative of the two sides of above equation:

$$L\frac{d^2i}{dt^2} + r\frac{di}{dt} + \frac{i}{C} = 0. \tag{23}$$

Calling I(ω) be the Fourier image of i(t), applying the Fourier transform to Equation (22), we obtain:

$$L[(j\omega)^2 I(\omega) - i'(0)] + j\omega r.I(\omega) + \frac{1}{C}I(\omega) = 0, \tag{24}$$

Since $i'(0) = \frac{E}{L}$, from here we have:

$$I(\omega) = \frac{E}{-\omega^2 L + j\omega r + \frac{1}{C}}. \tag{25}$$

Let $N(\omega) = E$, $M(\omega) = -\,\omega^2 L + j\omega r + \frac{1}{C}$. Applying the formula (15), we find:

$$i(t) = \frac{E}{2\beta L}e^{-\alpha t}\left(e^{\beta t} - e^{-\beta t}\right) = \frac{E}{\beta L}e^{-\alpha t}\mathrm{sh}\beta t\,, \tag{26}$$

here: $\alpha = \frac{r}{2L}$; $\beta = \sqrt{\alpha^2 - \frac{1}{LC}}$.

4. APPLICATION OF FOURIER TRANSFORM SOLVING THERMAL TRANSFER PROBLEM

Fourier transforms are also used in solving mathematical - physics equations. The thermal transfer (diffusion) problem below is an example.

Consider the fundamental problem: Find the temperature distribution T (x,t) in an infinite solid, knowing that T(x,0) = f (x).

To solve this problem, we derive from the equation of heat transfer:

$$\frac{\partial^2 T}{\partial x^2} = \frac{1}{k}\frac{\partial T}{\partial t}. \tag{27}$$

Applying the Fourier transform by the variable x, we have:

$$T(x,t) = \frac{1}{2\pi}\int_{-\infty}^{\infty} G(\omega,t)e^{i\omega x}d\omega, \tag{28}$$

with $G(\omega,t) = \int_{-\infty}^{\infty} T(x,t)e^{-i\omega x}dx$. After the transformation, we have the equation:

$$-\omega^2 G(\omega, t) = \frac{1}{k}\frac{\partial G(\omega, t)}{\partial t}. \quad (29)$$

This equation has the solution:

$$G(\omega,t) = C(\omega)\, e^{-\omega^2 kt}. \quad (30)$$

Under initial conditions:

$$G(\omega,0) = \int_{-\infty}^{\infty} T(x,0)e^{-i\omega x}dx = \int_{-\infty}^{\infty} f(x)e^{-i\omega x}dx, \quad (31)$$

so: $$C(\omega) = G(\omega,0) = \int_{-\infty}^{\infty} f(x)e^{-i\omega x}dx, \quad (32)$$

and $$G(\omega,t) = \int_{-\infty}^{\infty} f(x)e^{-i\omega x}e^{-\omega^2 kt}dx. \quad (33)$$

Obtaining the reverse Fourier transform, we obtain:

$$T(x,t) = \int_{-\infty}^{\infty} \frac{d\omega}{2\pi}e^{i\omega x}\int_{-\infty}^{\infty} dx' f(x')e^{-i\omega x'}e^{-\omega^2 kt} = \int_{-\infty}^{\infty} dx' f(x')\int_{-\infty}^{\infty} \frac{d\omega}{2\pi}e^{i\omega(x-x')}e^{-\omega^2 kt}. \quad (34)$$

Integral in Eq. (34), we obtain the solution of the diffusion equation (or thermal equation) in the solid:

$$T(x,t) = \int_{-\infty}^{\infty} dx' f(x')\sqrt{\frac{1}{4\pi kt}}\, e^{-\frac{(x-x')^2}{4kt}}, \quad (35)$$

here, $G(x,t;x') = \sqrt{\frac{1}{4\pi kt}}\, e^{-\frac{(x-x')^2}{4kt}}$ is called the Green function of the problem.

5. CONCLUSIONS

Applied the Fourier transform to solving the three problems of the AC circuit and a heat transfer problem in the above solid, we have some remarks as follows:

In this method, calculus is fast, simple and easy to build algorithms to solve problems on the circuit AC, radio waves, thermal transfer as well as wave transmission problems in the environment.

Get the expression in analytical form, which is convenient for evaluating, graphing, analyzing and discussing results.

Fourier transform, along with Laplace transform, are effective methods for solving homogeneous and non-homogeneous differential equations, as well as other mathematical-physics equations.

These methods, good support in the study of mathematics, physics, applied physics, engineering physics ... and scientific research for students as well as for teachers.

Here, we introduce two problems that students can solve by applying the Fourier transform. Readers should also uses with other methods for comparing, evaluating and discussing the results obtained, thereby drawing their own conclusions about the optimal method and scope of application.

Problem 01. Using the Fourier transform, solve the following equations:

a) $y'' - y = \sin x + \cos 2x$.

b) $L\dfrac{di}{dt} + Ri = a\cos\omega t$.

Problem 02. Plug in a power source that has a constant electromotive force on the rLC circuit. Know that $r=2\sqrt{\dfrac{L}{C}}$, and at time t = 0 in the circuit there is no intensity of current, and capacitor is uncharged. Determine the intensity i(t) of the current in the circuit after the capacitor is charged.

REFERENCES

1. Tran Ngoc Hoi, Pham Van Thieu (2006), *General Physics - Principles and Applications,* Vol. 1, - Education Publishing House.
2. Nguyen Van Hung, Le Van Truc (2004), *Mathematical Methods for Physics,* Vol. 1, 2, - *National University Publishing House, Hanoi.*
3. Đo Đinh Thanh (2002), *Methods of Mathematics-Physics,* - Education Publishing House.
4. Le Van Truc (2007), *Mathematical Analysis,* Vol. 1, 2, - National University Publishing House, Hanoi.
5. Jon Matheus, R. L Walker (1971), *Mathematics for Physics* (Vietnamese translation), - Hanoi Science and Technology Publishing House.

NGHIÊN CỨU PHÉP BIẾN ĐỔI FOURIER VÀ ỨNG DỤNG GIẢI BÀI TOÁN MẠCH ĐIỆN XOAY CHIỀU, BÀI TOÁN TRUYỀN NHIỆT

Tóm tắt: *Phương trình toán -lý là một môn học ứng dụng, đòi hỏi sinh viên ngành sư phạm vật lý và sư phạm toán phải nắm chắc phương pháp giải cũng như phải có kỹ thuật làm toán. Có nhiều phương pháp được áp dụng trong phương trình toán lý như phép biến đổi Laplace, phép biến đổi Fourier. Trong bài báo này chúng tôi giới thiệu phép biến đổi Fourier và ứng dụng trong giải một số bài toán mạch điện xoay chiều và phương trình truyền nhiệt (hay phương trình khuếch tán). Các bài toán minh họa cho thấy những ưu điểm trong tính giải tích của phương pháp này so với các phương pháp khác đối với các bài toán kể trên. Tuy nhiên, cần chú ý rằng việc áp dụng biến đổi Fourier gặp nhiều hạn chế hơn việc dùng biến đổi Laplace vì nó đòi hỏi hàm số phải khả tích tuyệt đối.*

Từ khóa: *Phương pháp giảng dạy, đổi mới dạy học, lý luận dạy học bậc đại học.*

PRESENT 3-3-1 MODELS AND IMPLICATION FOR NEW PHYSICS

Phung Van Dong[1], Dang Quoc Phong[2], Dang Van Soa[3], Nguyen Chi Thao[4]
[1]*Institute of Physics, Vietnam Academy of Science and Technology, 10 Dao Tan, Ba Dinh, Hanoi, Vietnam*
[2]*Department of Physics, Hanoi Architectural University, 10 Nguyen Trai, Ha Dong, Hanoi, Vietnam*
[3]*Department of Physics, Hanoi Metropolitan University, 98 Duong Quang Ham, Cau Giay, Hanoi, Vietnam*
[4]*Graduate University of Science and Technology, Vietnam Academy of Science and Technology, 18 Hoang Quoc Viet, Cau Giay, Hanoi, Vietnam*
(Dated: April 26, 2018)

Abtrast: *In this work, we give a brief review of the latest 3-3-1 extensions, called the simple 3-3-1 model and 3-3-1-1 model, which address a number of the important experimental issues. We present the fundamental features of the models as well as providing the physical masses, states, and interactions, which are necessary for the searches at colliders.*

PACS numbers: 12.60.-i

Keywords: *3-3-1-1 model, experiment, new physics, interaction.*

Email:: pvdong@iop.vast.ac.vn
Received 26 April 2018
Accepted for publication 10 May 2018

1. INTRODUCTION

The leading experimental problems of particle physics and cosmology, that our fundamental theories as the standard model and general relativity leave out unsolved, include neutrino oscillation, matter-antimatter asymmetry, dark matter, and cosmological inflation. Additionally, the LHC experiments have recently pointed out new physics resonances with high statistic significances [1]. Furthermore, the traditional proposals (supersymmetry, extradimension, and grand unification) may solve only some of the questions separately.

In this work, we briefly review the latest developments of the 3-3-1 models, known as the simple 3-3-1 model and the 3-3-1-1 model, which can provide potential solutions for numerous important issues, for instances, small neutrino masses, dark matter candidates and stability, leptogenesis, and inflation. Another aim of this note is to supply necessary materials in order for probing such models in near future at the current and projected colliders. The rest of this note is organized as follows: Sections II and III are devoted to present the 3-3-1-1 and 3-3-1 models, respectively, where the tables of the fermion–gauge boson (vector and axial-vector) couplings are achieved. Lastly, we give a concluding remark in Sec. IV.

2. THE 3-3-1-1 MODEL

The 3-3-1-1 model was proposed in [2]. Its theoretical and phenomenological aspects were extensively studied in [3–5]. The generalization of the model as well as the inclusion of the kinetic mixing e‹ect were further investigated in [6] and [7], respectively. In this work, we take the most general form of the model into account.

Let $SU(2)_L$ extend to $SU(3)_L$. Generally, the electric charge (Q) and the baryon-minus-lepton charge ($B\ L$) neither commute nor close algebraically with $SU(3)_L$. To have a closed algebra that encompasses all these charges, the smallest group is $SU(3)_L \boxtimes U(1)_X \boxtimes U(1)_N$. Here, the new charges X and N correspondingly determine Q and $B\ L$, such that

$$Q = T_3 + T_8 + X,$$

$$BL = 0T_8 + N, \qquad (1)$$

where and 0 are the embedding coe cients, and T_i (i = 1,2,3,...,8) are $SU(3)_L$ charges. The nontrivial commutation relations for Q and $B\ L$ are

$$[Q, T_1 \pm iT_2] = \pm(T_1 \pm iT_2),\ [Q, T_4 \pm iT_5] = \mp q(T_4 \pm iT_5),$$

$$[Q, T_6 \pm iT_7] = \mp(1+q)(T_6 \pm iT_7),$$

$$[B\text{-}L, T_4 \pm iT_5] = \mp(1+n)(T_4 \pm iT_5),$$

$$[BL, T_6 \pm iT_7] = \mp(1+n)(T_6 \pm iT_7), \qquad (2)$$

where $\beta(1+2q)/\sqrt{3}$ andb $\beta' \equiv -2(1+n)/\sqrt{3}$. Thus, (q,n) directly define the $(Q, B\ \ L)$ values of component fields in representations (as shown below and in Tab. I), respectively. Further, the hypercharge (Y) and W-parity (P) are identified as

$$Y = \beta T_8 + X,\ P = (\ 1)^{3(\beta' T_8 + N) + 2s}, \qquad (3)$$

where s is spin, and "W" means the wrong ($B\ L$) particles having nontrivial P (see Tab. I). Including the color group, the full gauge symmetry is $SU(3)_C \otimes SU(3)_L \otimes U(1)_X \otimes U(1)_N$, called

Table 1. (Q,B L) charges and W-parity for the model particles, where $P^{\pm} \equiv (\ 1)^{\pm(3n+1)}$ are nontrivial for $n \neq \frac{2m-1}{3}, m = 0, \pm 1, \pm 2, \ldots$ Specially, the wrong particles become odd particles, i.e. $P^{\pm} = 1$, if $n = \frac{2m}{3}$. The other particles including the standard model ones are called normal particles. Additionally, the corresponding antiparticles have opposite (Q,B L) charges and conjugated W-parity.

Particle	ν_a	e_a	u_a	d_a	γ	W	Z_1	Z_2	Z_3	$\eta_{1,2}$	$\rho_{1,2}$	χ_3	ϕ	k_a	j_α	j_3	X	Y	η_3	ρ_3	$\chi_{1,2}$
Q	0	-1	$\frac{2}{3}$	$-\frac{1}{3}$	0	1	0	0	0	$0,-1$	$1,0$	0	0	q	$-\frac{1}{3}-q$	$\frac{2}{3}+q$	$-q$	$-1-q$	q	$1+q$	$-q,-1-q$
$B-L$	-1	-1	$\frac{1}{3}$	$\frac{1}{3}$	0	0	0	0	0	0	0	0	2	n	$-\frac{2}{3}-n$	$\frac{4}{3}+n$	$-1-n$	$-1-n$	$1+n$	$1+n$	$-1-n$
P	1	1	1	1	1	1	1	1	1	1	1	1	1	P^+	P^-	P^+	P^-	P^-	P^+	P^+	P^-

3-3-1-1. It yields that the electroweak and BL interactions are nontrivially unified, analogous to the Glashow-Weinberg-Salam theory. It is broken down to,

$$SU(3)_C \otimes SU(3)_L \otimes U(1)_X \otimes U(1)_N \rightarrow SU(3)_C \otimes U(1)_Q \otimes P,$$

where the last ones are conserved by the vacuum.

The fermion content which is anomaly free is given by

$$\psi_{aL} \equiv \begin{pmatrix} \nu_{aL} \\ e_{aL} \\ k_{aL} \end{pmatrix} \sim \left(1, 3, \frac{1+q}{3}, \frac{2+n}{3}\right), \tag{4}$$

$$\nu_{aR} \sim (1,1,0,\ \ 1), \quad e_{aR} \sim (1,1,\ \ 1,\ \ 1), \quad k_{aR} \sim (1,1,q,n), \tag{5}$$

$$Q_{3L} \equiv \begin{pmatrix} u_{3L} \\ d_{3L} \\ j_{3L} \end{pmatrix} \sim \left(3, 3, \frac{1+q}{3}, \frac{2+n}{3}\right), \quad Q_{\alpha L} \equiv \begin{pmatrix} d_{\alpha L} \\ u_{\alpha L} \\ j_{\alpha L} \end{pmatrix} \sim \left(3, 3^*, \ \ \frac{q}{3}, \ \ \frac{n}{3}\right), \tag{6}$$

$$u_{aR} \sim \left(3, 1, \frac{2}{3}, \frac{1}{3}\right), \quad d_{aR} \sim \left(3, 1, \ \ \frac{1}{3}, \frac{1}{3}\right), \tag{7}$$

$$j_{3R} \sim \left(3, 1, \frac{2}{3} + q, \frac{4}{3} + n\right), \quad j_{\alpha R} \sim \left(3, 1, \ \ \frac{1}{3} \ \ q, \ \ \frac{2}{3} \ \ n\right), \tag{8}$$

where a = 1,2,3 and α = 1,2 are generation indices. We might also have two minimal versions by excluding $k_{aL,R}$, while the positions of k_{aL} are occopied by either ν_{aR}^c or e_{aR}^c, respectively.

The scalar content suitable for the 3-3-1-1 breaking and mass generation is given by

$$\eta = \begin{pmatrix} \eta_1 \\ \eta_2 \\ \eta_3 \end{pmatrix} \sim \left(1, 3, \frac{q-1}{3}, \frac{n+1}{3}\right), \quad \rho = \begin{pmatrix} \rho_1 \\ \rho_2 \\ \rho_3 \end{pmatrix} \sim \left(1, 3, \frac{q+2}{3}, \frac{n+1}{3}\right), \tag{9}$$

$$\chi = \begin{pmatrix} \chi_1 \\ \chi_2 \\ \chi_3 \end{pmatrix} \sim \left(1, 3, -\frac{2q+1}{3}, -\frac{2}{3}(n+1)\right), \quad \phi \sim (1, 1, 0, 2), \tag{10}$$

with the corresponding vacuum expectation values (VEVs),

$$\langle\eta\rangle = \frac{1}{\sqrt{2}} \begin{pmatrix} u \\ 0 \\ 0 \end{pmatrix}, \quad \langle\rho\rangle = \frac{1}{\sqrt{2}} \begin{pmatrix} 0 \\ v \\ 0 \end{pmatrix}, \quad \langle\chi\rangle = \frac{1}{\sqrt{2}} \begin{pmatrix} 0 \\ 0 \\ w \end{pmatrix}, \quad \langle\phi\rangle = \frac{1}{\sqrt{2}}\Lambda \tag{11}$$

The VEVs ϖ, Λ break the 3-3-1-1 group down to the standard model and define W-parity as well as generating the masses for the new particles, while u,v break the standard model symmetry and give the masses for ordinary particles. For consistency, we impose $\varpi, \Lambda \gg u,v$.

Apart from the gauge fixing and ghost terms, the total Lagrangian contains,

$$\begin{aligned} \mathcal{L} = & \sum_F \bar{F} i\gamma^\mu D_\mu F + \sum_S (D^\mu S)^\dagger (D_\mu S) + \mathcal{L}_{\text{Yukawa}} - V(\eta, \rho, \chi, \phi) \\ & -\frac{1}{4} G_{i\mu\nu} G_i^{\mu\nu} - \frac{1}{4} A_{i\mu\nu} A_i^{\mu\nu} - \frac{1}{4} B_{\mu\nu} B^{\mu\nu} - \frac{1}{4} C_{\mu\nu} C^{\mu\nu} - \frac{\delta}{2} B_{\mu\nu} C^{\mu\nu}, \end{aligned} \tag{12}$$

where F and S stand for fermion and scalar multiplets, respectively, and the covariant derivative is $D_\mu = \partial_\mu + ig_s t_i G_{i\mu} + igT_i A_{i\mu} + ig_X X B_\mu + ig_N N C_\mu$. Moreover, $\{g_s, g, g_X, g_N\}$, $\{t_i, T_i, X, N\}$, $\{G_i, A_i, B, C\}_{\mu\nu}$ denote the coupling constants, generators, gauge bosons, and field strength tensors of the 3-3-1-1 groups, respectively. The δ term presents the kinetic mixing of the two $U(1)$ gauge bosons, satisfying $|\delta| < 1$ to have a definitely positive kinetic energy.

The Yukawa Lagrangian and scalar potential are given by

$$\begin{aligned} \mathcal{L}_{\text{Yukawa}} = & h^\nu_{ab} \bar{\psi}_{aL} \eta \nu_{bR} + h^e_{ab} \bar{\psi}_{aL} \rho e_{bR} + h^k_{ab} \bar{\psi}_{aL} \chi k_{bR} + h'^\nu_{ab} \bar{\nu}^c_{aR} \nu_{bR} \phi \\ & + h^j_{33} \bar{Q}_{3L} \chi j_{3R} + h^j_{\alpha\beta} \bar{Q}_{\alpha L} \chi^* j_{\beta R} + h^u_{3a} \bar{Q}_{3L} \eta u_{aR} \\ & + h^u_{\alpha a} \bar{Q}_{\alpha L} \rho^* u_{aR} + h^d_{3a} \bar{Q}_{3L} \rho d_{aR} + h^d_{\alpha a} \bar{Q}_{\alpha L} \eta^* d_{aR} + H.c., \end{aligned} \tag{13}$$

$$\begin{aligned}V(\eta,\rho,\chi,\phi) \;=\; & \mu_1^2\eta^\dagger\eta+\mu_2^2\rho^\dagger\rho+\mu_3^2\chi^\dagger\chi+\mu_4^2\phi^\dagger\phi+\lambda_1(\eta^\dagger\eta)^2+\lambda_2(\rho^\dagger\rho)^2\\ & +\lambda_3(\chi^\dagger\chi)^2+\lambda_4(\phi^\dagger\phi)^2+\lambda_5(\eta^\dagger\eta)(\rho^\dagger\rho)+\lambda_6(\eta^\dagger\eta)(\chi^\dagger\chi)\\ & +\lambda_7(\rho^\dagger\rho)(\chi^\dagger\chi)+\lambda_8(\phi^\dagger\phi)(\eta^\dagger\eta)+\lambda_9(\phi^\dagger\phi)(\rho^\dagger\rho)+\lambda_{10}(\phi^\dagger\phi)(\chi^\dagger\chi)\\ & +\lambda_{11}(\eta^\dagger\rho)(\rho^\dagger\eta)+\lambda_{12}(\eta^\dagger\chi)(\chi^\dagger\eta)+\lambda_{13}(\rho^\dagger\chi)(\chi^\dagger\rho)+(\mu\eta\rho\chi+H.c.). \qquad (14)\end{aligned}$$

Particularly, the seesaw mechanism and charge quantization condition can be derived from the Yukawa interactions after the symmetry breaking. The Higgs and Goldstone fields can be identified from the scalar potential, where the standard model ones are consistently recognized.

The non-Hermitian gauge bosons W, X, and Y can be identified as

$$W=\frac{A_1 \quad iA_2}{\sqrt{2}},\qquad X=\frac{A_4 \quad iA_5}{\sqrt{2}},\qquad Y=\frac{A_6 \quad iA_7}{\sqrt{2}}, \qquad (15)$$

with corresponding masses,

$$m_W^2=\frac{g^2}{4}(u^2+v^2),\qquad m_X^2=\frac{g^2}{4}(w^2+u^2),\qquad m_Y^2=\frac{g^2}{4}(w^2+v^2). \qquad (16)$$

The fields X and Y are new gauge bosons with masses in w scale due to $w\ u,v$, while W is identical to that of the standard model, which implies $u^2 + v^2 = (246\ \text{GeV})^2$. The neutral gauge bosons A_3, A_8, B, and C mix by themselves, which are related to the physical states as

$$(A_3\, A_8\, B\, C)^T = U\, U_{\checkmark} U_{\varnothing} U_{\leftarrow}(A\, Z_1\, Z_2\, Z_3)^T, \qquad (17)$$

where

$$U_\delta=\begin{pmatrix}1&0&0&0\\0&1&0&0\\0&0&1&\frac{\delta}{\sqrt{1\quad\delta^2}}\\0&0&0&\frac{1}{\sqrt{1\quad\delta^2}}\end{pmatrix},\quad U_\theta=\begin{pmatrix}s_W&c_W&0&0\\ \beta s_W&\beta s_W t_W&\sqrt{1\quad\beta^2t_W^2}&0\\ c_W\sqrt{1\quad\beta^2t_W^2}&s_W\sqrt{1\quad\beta^2t_W^2}&\beta t_W&0\\0&0&0&1\end{pmatrix}$$

$$U_\epsilon\simeq\begin{pmatrix}1&0&0&0\\0&1&\epsilon_1&\epsilon_2\\0&\epsilon_1&1&0\\0&\epsilon_2&0&1\end{pmatrix},\quad U_\xi=\begin{pmatrix}1&0&0&0\\0&1&0&0\\0&0&c_\xi&s_\xi\\0&0&s_\xi&c_\xi\end{pmatrix}, \qquad (18)$$

which present the kinetic mixing, (B C) ! (B0 C0), the 3-3-1 type mixing, (A_3 A_8 B0) ! (A Z Z0), the seesaw type mixing, (Z Z0 C0) ! (Z_1 Z^0 C0), and the heavy field mixing

(Z^0 C0) ! (Z_2 Z_3), respectively. The parameters □$_{1,2}$ are negligible as $(u^2,v^2)/(w^2,\Lambda^2)$ suppressed, which yields $U_{□}$ ' 1, thus Z_1 ' Z, Z^0 ' $Z0$, and C^0 ' $C0$. The Z0-C0 mixing angle and physical masses are given by

$$t_{2\xi} \simeq \frac{2\sqrt{1 \quad \delta^2}t_W t_X\,(\delta\beta t_X \quad \beta' t_N)\,w^2}{12(1 \quad \delta^2)t_W^2 t_N^2\Lambda^2 + \left[t_W^2(\delta\beta t_X \quad \beta' t_N)^2 \quad (1 \quad \delta^2)t_X^2\right]w^2}, \tag{19}$$

$$m_A = 0,\ m_{Z_1}^2 \simeq \frac{g^2}{4c_W^2}(u^2+v^2),\ m_{Z_2,Z_3}^2 \simeq \frac{1}{2}\left[m_{Z'}^2 + m_{C'}^2 \mp \sqrt{(m_{Z'}^2 \quad m_{C'}^2)^2 + 4m_{Z'C'}^4}\right], \tag{20}$$

where

$$t_N \equiv \frac{g_N}{g},\ t_X \equiv\ g_X/g\ = t_W/\sqrt{1-\beta^2 t_W^2}$$

identified from electromagnetic couplings, and

$$\begin{aligned}
m_{Z'}^2 &= \frac{g^2}{12(1 \quad \beta^2 t_W^2)}\left[(1+\sqrt{3}\beta t_W^2)^2u^2 + (1 \quad \sqrt{3}\beta t_W^2)^2 v^2 + 4w^2\right],\\
m_{Z'C'}^2 &= \frac{g^2}{12\sqrt{(1 \quad \delta^2)(1 \quad \beta^2 t_W^2)}}\left\{(1+\sqrt{3}\beta t_W^2)\left[\delta t_X(\sqrt{3}+\beta) \quad \beta' t_N\right]u^2\right.\\
&\quad (1 \quad \sqrt{3}\beta t_W^2)\left[\delta t_X(\sqrt{3} \quad \beta) + \beta' t_N\right]v^2 + 4\left[\delta\beta t_X \quad \beta' t_N\right]w^2\Big\},\\
m_{C'}^2 &= \frac{g^2}{12(1 \quad \delta^2)}\left\{\left[\delta t_X(\sqrt{3}+\beta) \quad \beta' t_N\right]^2u^2 + \left[\delta t_X(\sqrt{3} \quad \beta) + \beta' t_N\right]^2 v^2\right.\\
&\quad +4\left[\delta\beta t_X \quad \beta' t_N\right]^2 w^2 + 48(1 \quad \delta^2)t_N^2\Lambda^2\Big\}.
\end{aligned}$$

The fields A and Z_1 are identical to those of the standard model, while Z_2 and Z_3 are new neutral gauge bosons having masses in ϖ, Λ scales due to ϖ, $\Lambda \gg u,v$. Additionally, $Z0$ and $C0$ finitely mix given that ϖ □ Λ, where they decouple only if the mixing e↵ects due to the kinetic mixing and the symmetry breaking cancel out, i.e. $= \delta = (\beta'_{gN})/(\beta_{gX})$.

Further, the above gauge coupling matching implies $s^2_W < 1/(1+\beta^2)$, which yields 2.08011 < q < 1.08011, provided that $s^2_W = 0.231$. Taking only integer values, we have q = 2, 1, 0, 1 corresponding to $\beta = \sqrt{3}, 1/\sqrt{3}, -1/\sqrt{3}, -\sqrt{3}$. Additionally, this model automatically provides dark matter candidates as the lightest wrong particle (LWP), which is stabilized by W-parity for $n = \frac{2m-1}{3}$. The candidates must be electrically neutral and colorless, which yields two dark matter versions: (i) The q = 0 model has candidates as some k_a fermion, X boson, or some η_3, χ_1 scalar, which was investigated in [2]; (ii) The q = -1 model includes candidates as Y boson or some ρ_3, χ_2 scalar. Motivated for dark matter, we only take the models with q = 0 and q = 1 into account. For simplicity, we also use some initial values of $n = \frac{2m}{3} = 0, \pm 1, \pm 2/3, \ldots$ Lastly, note that due to W-parity conservation, the scalar fields η_3, ρ_3, $\chi_{1,2}$ cannot develop VEVs when they are electrically neutral, and the unwanted interactions for quarks disappear. The exotic and ordinary quarks as well as the non-Hermitian and neutral gauge bosons do not mix. The dangerous FCNCs and CP-asymmetries due to the mixings are suppressed.

The interactions of the non-Hermitian gauge bosons with fermions are

$$\mathcal{L}_{\mathrm{CC}} \; = \; J_W^{\ \mu} W_\mu^+ + J_X^{q\mu} X_\mu^{\ q} + J_Y^{(1+q)\mu} Y_\mu^{\ 1 \quad q} + H.c., \tag{21}$$

where the charged currents are obtained by

$$\begin{aligned} J_W^{\ \mu} \; &= \; \frac{g}{\sqrt{2}}\left(\bar{\nu}_{aL}\gamma^\mu e_{aL} + \bar{u}_{aL}\gamma^\mu d_{aL}\right), \\ J_X^{q\mu} \; &= \; \frac{g}{\sqrt{2}}\left(\bar{\nu}_{aL}\gamma^\mu k_{aL} + \bar{u}_{3L}\gamma^\mu j_{3L} \quad \bar{j}_{\alpha L}\gamma^\mu d_{\alpha L}\right), \\ J_Y^{(1+q)\mu} \; &= \; \frac{g}{\sqrt{2}}\left(\bar{e}_{aL}\gamma^\mu k_{aL} + \bar{d}_{3L}\gamma^\mu j_{3L} + \bar{j}_{\alpha L}\gamma^\mu u_{\alpha L}\right) \end{aligned} \tag{22}$$

.The interactions of the neutral gauge bosons with fermions take the form,

$$\mathcal{L}_{\mathrm{NC}} = \quad eQ(f)\bar{f}\gamma^\mu f A_\mu \quad \frac{g}{2c_W}\bar{f}\gamma^\mu[g_V^I(f) \quad g_A^I(f)\gamma_5] f I_\mu \; , \tag{23}$$

where the couplings, $g_{V,A}{}^I = a^I{}_L \pm a^I{}_R$ for $I = Z_1$, Z_2, and Z_3, are defined by

$$\begin{aligned} a^{Z_1} &= T_3 \quad s_W^2 Q, \\ a^{Z_2} &= c_W\left[c_\xi\sqrt{1 \quad \beta^2 t_W^2}\,T_8 + t_X\left(\frac{\delta s_\xi}{\sqrt{1 \quad \delta^2}} \quad \beta c_\xi t_W\right)X \quad \frac{s_\xi t_N}{\sqrt{1 \quad \delta^2}}N\right] \\ a^{Z_3} &= a^{Z_2}(c_\xi \to s_\xi; s_\xi \to -c_\xi). \end{aligned} \; , \tag{24}$$

The $Z_{1,2}$ couplings are listed in Tabs. 1 and 2, respectively. For the Z_3 couplings, one can read off from Tab. III by replacements: $c_\xi \to s_\xi$, $s\xi \to - c\xi$.

***Table 2.** The couplings of Z_1 with fermions.*

f	$g_V^{Z_1}(f)$	$g_A^{Z_1}(f)$
ν_a	$\frac{1}{2}$	$\frac{1}{2}$
e_a	$-\frac{1}{2}+2s_W^2$	$-\frac{1}{2}$
k_a	$-2qs_W^2$	0
u_a	$\frac{1}{2}-\frac{4}{3}s_W^2$	$\frac{1}{2}$
d_a	$-\frac{1}{2}+\frac{2}{3}s_W^2$	$-\frac{1}{2}$
j_3	$-2(2/3+q)s_W^2$	0
j_α	$2(1/3+q)s_W^2$	0

Table 3. The couplings of Z_2 with fermions

f	$g_V^{Z_2}(f)$	$g_A^{Z_2}(f)$
ν_a	$\frac{c_\xi\sqrt{1-\delta^2}(1+\sqrt{3}\beta t_W^2)+s_\xi[t_N(4\sqrt{3}+\beta')\sqrt{1-\beta^2t_W^2}-\delta(\sqrt{3}+\beta)t_W]}{2\sqrt{3}c_W^{-1}\sqrt{1-\delta^2}\sqrt{1-\beta^2t_W^2}}$	$\frac{c_\xi\sqrt{1-\delta^2}(1+\sqrt{3}\beta t_W^2)+s_\xi[t_N\beta'\sqrt{1-\beta^2t_W^2}-\delta(\sqrt{3}+\beta)t_W]}{2\sqrt{3}c_W^{-1}\sqrt{1-\delta^2}\sqrt{1-\beta^2t_W^2}}$
e_a	$\frac{c_\xi\sqrt{1-\delta^2}(1+3\sqrt{3}\beta t_W^2)+s_\xi[t_N(4\sqrt{3}+\beta')\sqrt{1-\beta^2t_W^2}-\delta(3\sqrt{3}+\beta)t_W]}{2\sqrt{3}c_W^{-1}\sqrt{1-\delta^2}\sqrt{1-\beta^2t_W^2}}$	$\frac{c_\xi\sqrt{1-\delta^2}(1-\sqrt{3}\beta t_W^2)+s_\xi[\delta(\sqrt{3}-\beta)t_W+t_N\beta'\sqrt{1-\beta^2t_W^2}]}{2\sqrt{3}c_W^{-1}\sqrt{1-\delta^2}\sqrt{1-\beta^2t_W^2}}$
k_a	$\frac{c_\xi\sqrt{1-\delta^2}(3\beta^2t_W^2+\sqrt{3}\beta t_W^2-1)+s_\xi[2t_N(\sqrt{3}+\beta')\sqrt{1-\beta^2t_W^2}-\delta(\sqrt{3}+2\beta)t_W]}{\sqrt{3}c_W^{-1}\sqrt{1-\delta^2}\sqrt{1-\beta^2t_W^2}}$	$\frac{-c_\xi\sqrt{1-\delta^2}+s_\xi(\delta\beta t_W-t_N\beta'\sqrt{1-\beta^2t_W^2})}{\sqrt{3}c_W^{-1}\sqrt{1-\delta^2}\sqrt{1-\beta^2t_W^2}}$
u_α	$\frac{-c_\xi\sqrt{1-\delta^2}(\sqrt{3}+5\beta t_W^2)+s_\xi[\delta(5+\sqrt{3}\beta)t_W-t_N(4+\sqrt{3}\beta')\sqrt{1-\beta^2t_W^2}]}{6c_W^{-1}\sqrt{1-\delta^2}\sqrt{1-\beta^2t_W^2}}$	$\frac{-c_\xi\sqrt{1-\delta^2}(1-\sqrt{3}\beta t_W^2)-s_\xi[\delta(\sqrt{3}-\beta)t_W+t_N\beta'\sqrt{1-\beta^2t_W^2}]}{2\sqrt{3}c_W^{-1}\sqrt{1-\delta^2}\sqrt{1-\beta^2t_W^2}}$
d_α	$\frac{-c_\xi\sqrt{1-\delta^2}(\sqrt{3}-\beta t_W^2)-s_\xi[\delta(1-\sqrt{3}\beta)t_W+t_N(4+\sqrt{3}\beta')\sqrt{1-\beta^2t_W^2}]}{6c_W^{-1}\sqrt{1-\delta^2}\sqrt{1-\beta^2t_W^2}}$	$\frac{-c_\xi\sqrt{1-\delta^2}(1+\sqrt{3}\beta t_W^2)+s_\xi[\delta(\sqrt{3}+\beta)t_W-t_N\beta'\sqrt{1-\beta^2t_W^2}]}{2\sqrt{3}c_W^{-1}\sqrt{1-\delta^2}\sqrt{1-\beta^2t_W^2}}$
u_3	$\frac{c_\xi\sqrt{1-\delta^2}(\sqrt{3}-5\beta t_W^2)+s_\xi[\delta(5-\sqrt{3}\beta)t_W-t_N(4-\sqrt{3}\beta')\sqrt{1-\beta^2t_W^2}]}{6c_W^{-1}\sqrt{1-\delta^2}\sqrt{1-\beta^2t_W^2}}$	$\frac{c_\xi\sqrt{1-\delta^2}(1+\sqrt{3}\beta t_W^2)-s_\xi[\delta(\sqrt{3}+\beta)t_W-t_N\beta'\sqrt{1-\beta^2t_W^2}]}{2\sqrt{3}c_W^{-1}\sqrt{1-\delta^2}\sqrt{1-\beta^2t_W^2}}$
d_3	$\frac{c_\xi\sqrt{1-\delta^2}(\sqrt{3}+\beta t_W^2)-s_\xi[\delta(1+\sqrt{3}\beta)t_W-t_N(4-\sqrt{3}\beta')\sqrt{1-\beta^2t_W^2}]}{6c_W^{-1}\sqrt{1-\delta^2}\sqrt{1-\beta^2t_W^2}}$	$\frac{c_\xi\sqrt{1-\delta^2}(1-\sqrt{3}\beta t_W^2)+s_\xi[\delta(\sqrt{3}-\beta)t_W+t_N\beta'\sqrt{1-\beta^2t_W^2}]}{2\sqrt{3}c_W^{-1}\sqrt{1-\delta^2}\sqrt{1-\beta^2t_W^2}}$
j_α	$\frac{c_\xi\sqrt{1-\delta^2}(\sqrt{3}-\beta t_W^2-3\sqrt{3}\beta^2t_W^2)-s_\xi[2t_N(1+\sqrt{3}\beta')\sqrt{1-\beta^2t_W^2}-\delta(1+2\sqrt{3}\beta)t_W]}{3c_W^{-1}\sqrt{1-\delta^2}\sqrt{1-\beta^2t_W^2}}$	$\frac{c_\xi\sqrt{1-\delta^2}-s_\xi(\delta\beta t_W-t_N\beta'\sqrt{1-\beta^2t_W^2})}{\sqrt{3}c_W^{-1}\sqrt{1-\delta^2}\sqrt{1-\beta^2t_W^2}}$
j_3	$\frac{c_\xi\sqrt{1-\delta^2}(3\sqrt{3}\beta^2t_W^2-\beta t_W^2-\sqrt{3})+s_\xi[2t_N(\sqrt{3}\beta'-1)\sqrt{1-\beta^2t_W^2}+\delta(1-2\sqrt{3}\beta)t_W]}{3c_W^{-1}\sqrt{1-\delta^2}\sqrt{1-\beta^2t_W^2}}$	$\frac{-c_\xi\sqrt{1-\delta^2}+s_\xi(\delta\beta t_W-t_N\beta'\sqrt{1-\beta^2t_W^2})}{\sqrt{3}c_W^{-1}\sqrt{1-\delta^2}\sqrt{1-\beta^2t_W^2}}$

3. THE SIMPLE 3-3-1 MODEL

We have eventually been interested in some calculable 3-3-1 model which includes a minimal content of scalars and fermions. The first one was the economical 3-3-1 model [8] extracted from the 3-3-1 model with right-handed neutrinos. The second one first appeared as the reduced 3-3-1 model [9] deduced from the minimal 3-3-1 model. However, the latter was encountered with the problems of the ⇢-parameter, FCNCs constraints, and the Landau pole limit. The realistic theory for the second approach overcoming such issues was finally introduced, called the simple 3-3-1 model [10]. Its phenomenological aspects have been extensively studied in [11, 12].

The fermion content, which is anomaly free, is given by

$$\psi_{aL} \equiv \begin{pmatrix} \nu_{aL} \\ e_{aL} \\ (e_{aR})^c \end{pmatrix} \sim (1,3,0), \tag{25}$$

$$Q_{\alpha L} \equiv \begin{pmatrix} d_{\alpha L} \\ -u_{\alpha L} \\ J_{\alpha L} \end{pmatrix} \sim (3,3^*,-1/3), \tag{26}$$

$$Q_{3L} \equiv \begin{pmatrix} u_{3L} \\ d_{3L} \\ J_{3L} \end{pmatrix} \sim (3,3,2/3)\,, \tag{27}$$

$$u_{aR} \sim (3,1,2/3)\,, \quad d_{aR} \sim (3,1,-1/3)\,, \tag{28}$$

$$J_{\alpha R} \sim (3,1,-4/3)\,, \quad J_{3R} \sim (3,1,5/3)\,, \tag{29}$$

where $a = 1,2,3$ and $\alpha = 1,2$ are generation indices. The new quarks J_a have exotic electric charges such as $Q(J_\alpha) = 4/3$ and $Q(J_3) = 5/3$. The third generation of quarks has been arranged differently from the first two, in order to have a well-defined new physics scale below the Landau pole of around 5 TeV, due to the FCNCs constraints [10]. By contrast, if either the first or the second generation transforms differently, the FCNCs bound $w > 2.2 \times 10^3$ TeV, which is much beyond the Landau pole, and thus the model is incorrect.

The scalar content can be minimally introduced as

$$\eta = \begin{pmatrix} \eta_1^0 \\ \eta_2^- \\ \eta_3^+ \end{pmatrix} \sim (1,3,0), \quad \chi = \begin{pmatrix} \chi_1^- \\ \chi_2^{--} \\ \chi_3^0 \end{pmatrix} \sim (1,3,-1), \tag{30}$$

with corresponding VEVs,

$$\langle\eta\rangle = \frac{1}{\sqrt{2}}\begin{pmatrix} u \\ 0 \\ 0 \end{pmatrix}, \quad \langle\chi\rangle = \frac{1}{\sqrt{2}}\begin{pmatrix} 0 \\ 0 \\ w \end{pmatrix}. \tag{31}$$

This scalar sector is unique, given that it includes only two scalar triplets among others, the top quark gets a tree-level mass, and the ρ- parameter possibly coincides with the global fit. The VEV ϖ breaks the 3-3-1 symmetry and gives the new particle masses, while u breaks the standard model symmetry and provides the ordinary particle masses. To keep consistency, we impose $u \ll \varpi$.

Let us stress that another choice of two scalar triplets like ⇢ and often studied would lead to an unacceptably large contribution for the ρ-parameter due to the Landau pole limit [13]; additionally, it yields vanishing top-quark mass, which is unnaturally induced by radiative corrections or effective interactions [10]. By this proposal, the model can contain a dark sector denoted by ϕ, which is inert scalar multiplets, $\phi = \eta', \chi'$ or, protected by Z_2 symmetry $\phi \rightarrow -\phi$, which provides dark matter candidates [10] and governs the ρ-parameter appropriately to the bounds [12]. The model also realizes $B\ L$ as an approximate symmetry (otherwise, it is not self-consistent since the $B\ L$ and 3-3-1 symmetries are algebraically non-closed), which yields suitably small neutrino masses and makes dark matter candidates phenomenologically consistent. Further, the proton is stabilized due to lepton parity $(-)^L$ naturally embedded in this model.

The total Lagrangian, omitting the gauge fixing and ghost terms, is given by

$$\begin{aligned}\mathcal{L} \;=\; & \sum_F \bar{F} i\gamma^\mu D_\mu F + \sum_S (D^\mu S)^\dagger (D_\mu S) \\ & \frac{1}{4} G_{i\mu\nu} G_i^{\mu\nu} \quad \frac{1}{4} A_{i\mu\nu} A_i^{\mu\nu} \quad \frac{1}{4} B_{\mu\nu} B^{\mu\nu} \\ & + \mathcal{L}_Y \quad V, \end{aligned} \tag{32}$$

where the covariant derivative is $D_\mu = \delta_\mu + ig_s t_i G_{i\mu} + igT_i A_{i\mu} + ig_X X B_\mu$. The scalar potential contains $V = V$simple $+ V$inert, where

$$V_{\text{simple}} = \mu_1^2 \eta^\dagger \eta + \mu_2^2 \chi^\dagger \chi + \lambda_1 (\eta^\dagger \eta)^2 + \lambda_2 (\chi^\dagger \chi)^2 + \lambda_3 (\eta^\dagger \eta)(\chi^\dagger \chi) + \lambda_4 (\eta^\dagger \chi)(\chi^\dagger \eta) \tag{33}$$

is the potential for the normal scalars, while the second potential includes inert scalars which appropriately summarizes those supplied in [10] for = ℋ0, 0, or . The Higgs and Goldstone bosons as well as dark matter candidates can be deduced from the potential, which are phenomenologically consistent [12]. The Yukawa Lagrangian is

$$\begin{aligned}\mathcal{L}_Y \;=\; & h_{33}^J \bar{Q}_{3L} \chi J_{3R} + h_{\alpha\beta}^J \bar{Q}_{\alpha L} \chi^* J_{\beta R} + h_{3a}^u \bar{Q}_{3L} \eta u_{aR} + \frac{h_{\alpha a}^u}{\Lambda} \bar{Q}_{\alpha L} \eta \chi u_{aR} \\ & + h_{\alpha a}^d \bar{Q}_{\alpha L} \eta^* d_{aR} + \frac{h_{3a}^d}{\Lambda} \bar{Q}_{3L} \eta^* \chi^* d_{aR} + h_{ab}^e \bar{\psi}_{aL}^c \psi_{bL} \eta + \frac{h_{ab}^{\prime e}}{\Lambda^2} (\bar{\psi}_{aL}^c \eta \chi)(\psi_{bL} \chi^*) \\ & + \frac{s_{ab}^\nu}{\Lambda} (\bar{\psi}_{aL}^c \eta^*)(\psi_{bL} \eta^*) + H.c., \end{aligned} \tag{34}$$

where Λ is a new physical scale that induces the effective interactions. All the fermions including neutrinos can get suitable masses from these interactions [10].

Due to the Z_2 symmetry, the ϕ VEV vanishes. The gauge bosons can gain masses from the η, χ VEVs only. The charged gauge bosons are obtained,

$$W^\pm = \frac{A_1 \mp iA_2}{\sqrt{2}}, \quad m_W^2 = \frac{g^2}{4} u^2, \tag{35}$$

$$X^\mp = \frac{A_4 \mp iA_5}{\sqrt{2}}, \quad m_X^2 = \frac{g^2}{4} (w^2 + u^2), \tag{36}$$

$$Y^{\mp\mp} = \frac{A_6 \mp iA_7}{\sqrt{2}}, \quad m_Y^2 = \frac{g^2}{4} w^2. \tag{37}$$

W is identical to that of the standard model, which gives $u \simeq 246$ GeV. X and Y are new charged gauge bosons with masses in the w scale. The neutral gauge bosons are achieved as

$$A = s_W A_3 + c_W \left(-\sqrt{3}t_W A_8 + \sqrt{1-3t_W^2}B\right), \quad m_A = 0, \tag{38}$$

$$Z = c_W A_3 - s_W \left(-\sqrt{3}t_W A_8 + \sqrt{1-3t_W^2}B\right), \quad m_Z^2 = \frac{g^2}{4c_W^2}u^2, \tag{39}$$

$$Z' = \sqrt{1-3t_W^2}A_8 + \sqrt{3}t_W B, \quad m_{Z'}^2 = \frac{g^2[(1-4s_W^2)^2u^2 + 4c_W^4 w^2]}{12c_W^2(1-4s_W^2)}, \tag{40}$$

where $s_W = e/g = t/\sqrt{1+4t^2}$, with $t = g_X/g$.

The photon field A is massless and decoupled, whereas Z, Z' slightly mix via a mass term $m_{ZZ'}^{22} = \frac{g^2\sqrt{1-4s_w^2}}{4\sqrt{3}c_w^2} \cong 0.16m_Z^2 \ll m_{Z'}^2$, and a mixing angle

$$t_{2\varphi} = m_{ZZ'}^2/\left(m_{Z'}^2 - m_Z^2\right) \cong 1.4 \times 10^{-4} \times \frac{3.6TeV}{w}.$$

This leads to mass shifts, $\Delta m_Z^2/m_Z^2 \cong -1.14 \times 10^{-5} \times \left(\frac{3.6TeV}{w}\right)^2$, $\Delta m_{Z'}^2/m_{Z'}^2 \cong 5.1 \times 10^{-9} \times \left(\frac{3.6TeV}{w}\right)^4$ and ρ-parameter deviation, $(\Delta\rho)_{\text{tree}} \simeq \Delta m^2_Z/m^2_Z$. All such mixing e↵ects are negligible due to w > 3.6 TeV from the FCNCs bound [10]. Z is physical, identical to that of the standard model, while Z0 is a new neutral gauge boson with mass in the w scale. The ρ parameter bounds can be solved by the loop e↵ect of inert scalar ϕ [12], where note that the loop e↵ect of X, Y is negligible [13].

The charged current with fermions takes the form,

$$\mathcal{L}_{\text{CC}} = \quad gJ_W^\mu W_\mu^+ \quad gJ_X^\mu X_\mu \quad gJ_Y^\mu Y_\mu \quad + H.c., \tag{41}$$

where

$$J_W^\mu = \frac{1}{\sqrt{2}}\left(\bar{\nu}_{aL}\gamma^\mu e_{aL} + \bar{u}_{aL}\gamma^\mu d_{aL}\right), \tag{42}$$

$$J_X^\mu = \frac{1}{\sqrt{2}}\left(\bar{\nu}_{aL}\gamma^\mu e_{aR}^c - \bar{J}_{\alpha L}\gamma^\mu d_{\alpha L} + \bar{u}_{3L}\gamma^\mu J_{3L}\right), \tag{43}$$

$$J_Y^\mu = \frac{1}{\sqrt{2}}\left(\bar{e}_{aL}\gamma^\mu e_{aR}^c + \bar{J}_{\alpha L}\gamma^\mu u_{\alpha L} + \bar{d}_{3L}\gamma^\mu J_{3L}\right). \tag{44}$$

The neutral current with fermions takes the form,

$$\begin{aligned}\mathcal{L}_{\text{NC}} = \quad & eQ(f)\bar{f}\gamma^\mu f A_\mu \quad \frac{g}{2c_W}\bar{f}\gamma^\mu\left[g_V^Z(f) \quad g_A^Z(f)\gamma_5\right]fZ_\mu \\ & \frac{g}{2c_W}\bar{f}\gamma^\mu\left[g_V^{Z'}(f) \quad g_A^{Z'}(f)\gamma_5\right]fZ'_\mu,\end{aligned} \tag{45}$$

where

$$g_V^Z(f) = T_3(f_L) - 2s_W^2 Q(f), \quad g_A^Z(f) = T_3(f_L), \tag{46}$$

$$g_V^{Z'}(f) = \sqrt{1-4s_W^2}\,T_8(f_L) + \frac{\sqrt{3}s_W^2}{\sqrt{1-4s_W^2}}(X+Q)(f_L), \tag{47}$$

$$g_A^{Z'}(f) = \frac{c_W^2}{\sqrt{1-4s_W^2}}T_8(f_L) - \frac{\sqrt{3}s_W^2}{\sqrt{1-4s_W^2}}T_3(f_L), \tag{48}$$

which are listed in Tables IV and V for *Z* and *Z*0, respectively.

Table 4. *The couplings of Z with fermions.*

f	g_V^Z	g_A^Z
ν_e, ν_μ, ν_τ	$\frac{1}{2}$	$\frac{1}{2}$
e, μ, τ	$\frac{1}{2}\left(4s_W^2 - 1\right)$	$-\frac{1}{2}$
u, c, t	$\frac{1}{2}\left(1 - \frac{8}{3}s_W^2\right)$	$\frac{1}{2}$
d, s, b	$\frac{1}{2}\left(\frac{4}{3}s_W^2 - 1\right)$	$-\frac{1}{2}$
J_1, J_2	$\frac{8}{3}s_W^2$	0
J_3	$-\frac{10}{3}s_W^2$	0

Table 5. *The couplings of Z' with fermions.*

f	$g_V^{Z'}$	$g_A^{Z'}$
ν_e, ν_μ, ν_τ	$\frac{1}{2}\sqrt{\frac{1-4s_W^2}{3}}$	$\frac{1}{2}\sqrt{\frac{1-4s_W^2}{3}}$
e, μ, τ	$\frac{\sqrt{3}}{2}\sqrt{1-4s_W^2}$	$-\frac{1}{2}\sqrt{\frac{1-4s_W^2}{3}}$
u, c	$-\frac{1}{2}\frac{1-6s_W^2}{\sqrt{3(1-4s_W^2)}}$	$-\frac{1}{2}\frac{1+2s_W^2}{\sqrt{3(1-4s_W^2)}}$
t	$\frac{1}{2}\frac{1+4s_W^2}{\sqrt{3(1-4s_W^2)}}$	$\frac{1}{2}\sqrt{\frac{1-4s_W^2}{3}}$
d, s	$-\frac{1}{2}\frac{1}{\sqrt{3(1-4s_W^2)}}$	$-\frac{1}{2}\sqrt{\frac{1-4s_W^2}{3}}$
b	$\frac{1}{2}\frac{c_{2W}}{\sqrt{3(1-4s_W^2)}}$	$\frac{1}{2}\frac{1+2s_W^2}{\sqrt{3(1-4s_W^2)}}$
J_1, J_2	$\frac{1}{\sqrt{3}}\frac{1-9s_W^2}{\sqrt{1-4s_W^2}}$	$\frac{1}{\sqrt{3}}\frac{c_W^2}{\sqrt{1-4s_W^2}}$
J_3	$-\frac{1}{\sqrt{3}}\frac{\left(1-11s_W^2\right)}{\sqrt{1-4s_W^2}}$	$-\frac{1}{\sqrt{3}}\frac{c_W^2}{\sqrt{1-4s_W^2}}$

4. CONCLUDING REMARKS

We have given a review of the latest features of the simple 3-3-1 model and 3-3-1-1 model. The identification of particles and their interactions have been appropriately provided, and they are ready for the collider searches as the LHC and ILC.

Acknowledgments. This research is funded by Vietnam National Foundation for Science and Technology Development (NAFOSTED) under grant numbers 103.01-2016.77 (PVD) and 103.01-2016.44 (DVS).

REFERENCES

1. C. Patrignani *et al.* (Particle Data Group), Chin. Phys. C **40**, 100001 (2016), with partial updates at http://pdg.lbl.gov.
2. P. V. Dong, T. D. Tham, and H. T. Hung, Phys. Rev. D **87**, 115003 (2013).
3. P. V. Dong, D. T. Huong, F. S. Queiroz, and N. T. Thuy, Phys. Rev. D **90**, 075021 (2014).
4. D. T. Huong, P. V. Dong, C. S. Kim, and N. T. Thuy, Phys. Rev. D **91**, 055023 (2015).
5. D. T. Huong and P. V. Dong, arXiv:1605.01216 [hep-ph].
6. P. V. Dong, Phys. Rev. D **92**, 055026 (2015).
7. P. V. Dong and D. T. Si, Phys. Rev. D **93**, 115003 (2016).
8. W. A. Ponce, Y. Giraldo and L. A. Sanchez, Phys. Rev. D **67**, 075001 (2003); P. V. Dong, H. N. Long, D. T. Nhung and D. V. Soa, Phys. Rev. D **73**, 035004 (2006).
9. J. G. Ferreira Jr, P. R. D. Pinheiro, C. A. de S. Pires, and P. S. Rodrigues da Silva, Phys. Rev. D **84**, 095019 (2011).
10. P. V. Dong, N. T. K. Ngan, and D. V. Soa, Phys. Rev. D 90, 075019 (2014).
11. P. V. Dong, C. S. Kim, N. T. Thuy, and D. V. Soa, Phys. Rev. D 91, 115019 (2015).
12. P. V. Dong and N. T. K. Ngan, arXiv:1512.09073 [hep-ph].
13. P. V. Dong and D. T. Si, Phys. Rev. D **90**, 117703 (2014).

CÁC MÔ HÌNH 3-3-1 HIỆN THỜI VÀ HỆ QUẢ CHO VẬT LÍ MỚI

Tóm tắt: *Trong bài báo này, chúng tôi tổng quan về các mở rộng 3-3-1 mới nhất, gọi là mô hình 3-3-1 đơn giản và mô hình 3-3-1-1, cho giải quyết một số vấn đề thực nghiệm quan trọng. Chúng tôi trình bầy các yếu tố cơ sở, đồng thời cung cấp các khối lượng vật lý, trạng thái vật lý và các tương tác, cần thiết cho nghiên cứu các mô hình này ở máy gia tốc đang hoạt động và trong tương lai.*

Từ khóa: *Mô hình 3-3-1, thực nghiệm, vật lý mới, tương tác.*

THE APPLICATIONS OF q-DEFORMED STATISTICS IN PHENOMENON OF BOSE-EINSTEIN CONDENSATION FOR THE q- GASES

Luu Thi Kim Thanh
Hanoi Pedagogical University no.2

Abstract: *In this paper, we consider the q-deformed statistics and their applications in phenomenon of Bose-Einstein condensations. The expression for the Bose-Einstein condensation temperature of the q-gas is derived.*

Keywords: *q deformed oscillators, q-deformed statistics, Bose-Einstein condensation.*

Email: luuthikim.thanh888@gmail.com
Received 16 April 2018
Accepted for publication 12 May 2018

1. INTRODUCTION

Recently, the interest in the quantum deformation of the Lie algebra (quantum group) has been growing in the physical and mathematical wold [1-3]. The idea of quantum Lie algebras originated in the study of the solution of the quantum Yang-Baxter equation for integrable lattice models. Generally speaking in the context of these deformation the quantum Lie algebra is the universal enveloping algebra deformed by one parameter (q-deformation) and possesses the structure of Holf algebra. However, the essential reason for the name “quantum” algebra is that it become the Lie algebra in the $q\rightarrow1$ limit (classical limit). The study of such kind of oscillators has been stimulated by the increasing interest in particles obeying statistics different from Bose and Fermi [4, 5].

In this paper, we would like to consider the statistics of q-oscillators and their applications in phenomenon of -Einstein condensations. The expressions for the Bose-Einstein condensation temperature of the q-gas is derived.

2. CONTENTS

2.1. q – deformed statistics

We start by defining the q deformed algebra through the commutation relations [4,5]

$$\hat{a}\hat{a}^{+} - q^{\mp 1}\,\hat{a}^{+}\hat{a} \;= q^{\pm \hat{N}} \tag{1}$$

$$[\hat{N}, \hat{a}^{+}] = \; -\hat{a}, \;\; [\hat{N}, \hat{a}] = \hat{a}^{+}$$

where q is a parameter; $\hat{a}, \hat{a}^{+}$ and $\hat{N}$ are the annihilation, creation and number operators respectively. One can construct the representation of (1) in the Fock space spanned by the or thonormalized eigenstates |n> of the operator $\hat{N}$

$$|n> = \frac{(\hat{a}^{+})^{n}}{\sqrt{[n]!}}\;|o>$$

$$\hat{a}\;|o> = 0 \tag{2}$$

where

$$[n]! \;\equiv [n][n-1]\ldots[1]$$

and the notation

$$[n] \equiv \frac{q^{n} - q^{-n}}{q - q^{-1}} \tag{3}$$

is used.

In this Fock space it is easy to prove that the following relations hold:

$$\hat{a}\hat{a}^{+} = \left[\hat{N} + 1\right], \hat{a}^{+}\hat{a} = [\hat{N}] \tag{4}$$

The action of the operators on the basis is given by

$$\hat{a}|n\rangle = \sqrt{[n]}|n-1\rangle \tag{5}$$

$$\hat{a}^{+}|n\rangle = \sqrt{[n+1]}|n+1\rangle$$

The matrix representation of annihilation and creation operators of the q deformed oscillators in the basic (2) have the expression:

$$\hat{a} = \begin{pmatrix} 0 & \sqrt{[1]} & 0 & \cdots \\ 0 & 0 & \sqrt{[2]} & \cdots \\ 0 & 0 & 0 & \cdots \\ \cdots & \cdots & \cdots & \cdots \end{pmatrix} \tag{6}$$

$$\hat{a}^{+} = \begin{pmatrix} 0 & 0 & 0 & \cdots \\ \sqrt{[1]} & 0 & 0 & \cdots \\ 0 & \sqrt{[2]} & 0 & \cdots \\ \cdots & \cdots & \cdots & \cdots \end{pmatrix} \tag{7}$$

In order to study the properties of q deformed oscillators, let us consider now the statistical averages and calculate the deformed "distributions" which follow from the "q-algebras" defined in (1)

As in well known the thermodynamic properties are determined by the partition function Z, which in the grand canonical ensemble is defined by

$$Z = Tr(e^{-\beta(\hat{H}-\mu\hat{N})} \tag{8}$$

where

$$\beta = \frac{1}{kT}$$

$\hat{H}$ is Hamiltonian, which is usually taken of the form $\hat{H} = \varepsilon\hat{N}$, ε being one particle - oscillator energy, μ is the chemical potential. The trace must be taken over a complete set of states. For any operator $\hat{F}$, the statistical average is the obtained with the prescription

$$< \hat{F} >= \frac{1}{Z} Tr(e^{-\beta(\hat{H}-\mu\hat{N})}\hat{F}) \tag{9}$$

The calculations based on the equation (1), we recover the q-deformed statistics:

$$< \hat{a}^+\hat{a} > \equiv < [\hat{N}] >= \frac{e^{\beta(\varepsilon-\mu)}-1}{e^{2\beta(\varepsilon-\mu)}-(q+q^{-1})e^{\beta(\varepsilon-\mu)}+1} \tag{10}$$

2.2. The Bose-Einstein condensation temperature of the q-gas

By an ideal q – gas we understand a system defined by the Hamiltonian

$$H = \sum_i \varepsilon_i(\hat{a}_i\hat{a}_i{}^+ + \hat{a}_i{}^+\hat{a}_i) = \sum_i \varepsilon_i([\hat{N}_i] + [\hat{N}_i + 1])$$

We shall interpret $\hat{a}_i$, $\hat{a}_i{}^+, \hat{N}_i$ as annihilation, creation and occupation number operators, respectively, of particles in the state i and ε_i as the energy of the level i.

The ideal q – gas obeys q – deformed statistics (10), we obtain the total number of particles in the gas:

$$N = \frac{g(2m)^{\frac{3}{2}}V}{4\pi^2\hbar^3}\int_0^\infty \frac{e^{\frac{\varepsilon-\mu}{kT}}-1}{e^{\frac{2(\varepsilon-\mu)}{kT}}-(q+q^{-1})e^{\frac{\varepsilon-\mu}{kT}}+1}\sqrt{\varepsilon}d\varepsilon \tag{11}$$

where g$= 2s + 1$ (s being the spin of the particle), V is the total volume of the gas. The chemical potential μ must satisfy conditions

$$\mu \leq 0, \quad \frac{\partial\mu}{\partial T} \leq 0 \tag{12}$$

So that, if the temperature of the gas is lowered at constant density $\frac{N}{V}$, the chemical potential μ will increase, i.e. its apsolute magnitude will decrease. It reaches the value $\mu = 0$ at a temperature T_c determined by equation

$$N = \frac{g(2m)^{\frac{3}{2}}V}{4\pi^2\hbar^3}\int_0^{\infty}\frac{e^{\frac{\varepsilon}{kT_c}}-1}{e^{\frac{2\varepsilon}{kT_c}}-(q+q^{-1})e^{\frac{\varepsilon}{kT_c}}+1}\sqrt{\varepsilon}d\varepsilon \tag{13}$$

In terms of a new variable of integration $x = \frac{\varepsilon}{kT_c}$, the equation (13) can be written

$$N = \frac{g(2mkT_c)^{\frac{3}{2}}V}{4\pi^2\hbar^3} I_{q,\frac{1}{2}} \tag{14}$$

where

$$I_{q,\frac{1}{2}} = \int_0^{\infty}\frac{e^x-1}{e^{2x}-(q+q^{-1})e^x+1}x^{\frac{1}{2}}dx \tag{15}$$

From equation (14), we obtain the expression for the Bose-Einstein condensation temperature

$$T_c = \frac{2^{\frac{1}{3}}\pi^{\frac{4}{3}}\hbar^2}{I^{\frac{2}{3}}_{q,\frac{1}{2}}mkg^{\frac{2}{3}}}(\frac{N}{V})^{\frac{2}{3}} \tag{16}$$

In reality, therefore, the situation for $T < T_c$ is as follows: The chemical potential $\mu = 0$, the total number of particles with energy $\varepsilon > 0$ will thus be

$$N_{\varepsilon>0} = \frac{g(2mkT)^{\frac{3}{2}}V}{4\pi^2\hbar^3} I_{q,\frac{1}{2}} = N\left(\frac{T}{T_c}\right)^{\frac{3}{2}} \tag{17}$$

The remaining

$$N_{\varepsilon=0} = N\left[1-\left(\frac{\mathrm{T}}{\mathrm{T_c}}\right)^{\frac{3}{2}}\right] \tag{18}$$

the particles are in the lowest state, i.e. have energy $\varepsilon = 0$. The steady increase of particles in the state with $\varepsilon = 0$ is often called Bose- Einstein condensation.

3. CONCLUSIONS

1. The Bose-Einstein condensation temperature T_c (16) of the q – gas not only depends on density of the q- gas but also depends on the q- deformation parameter.

2. When q=1, we recover the familiar formulae of the Bose-Einstein condensation temperature for ideal bose gas.

3. From these results and comparison with experimental results, we can determine the q- deformation parameters.

Acknowledgments. We would like to thank Prof. Dao Vong Duc for useful discussions and the valuable comments. Thanks are due to the colleagues at Hanoi Pedagogical University No.2.

REFERENCES

1. A. J. Macfarlane (1989), "On q-analogues of the quantum harmonic oscillators and the quantum group SU($2_{q,}$)", *J. Phys. A: Math*. Gen. **22**, pp.4581-4587.
2. L. C. Biedenharn (1971), "In Group Theory and its applications", *Edited by E. H. Lieb, New York*, pp.157-192.
3. O. W. Greenberg (1990), "Exemple of infinite statistics", *Phys. Rev*. lett. **64**, pp.705-709.
4. Dao Vong Duc and Nguyen Ba An (1998), "Coherent states for oscillators of non-coventional statistics", *ICTP. Report IC/IR/98/25.*
5. Luu Thi Kim Thanh (2007), "Coherent states for two parametters p, q- deformed oscillators', *Comm. in Phys*. **17**, pp. 9-12.

ÁP DỤNG THỐNG KÊ BIẾN DẠNG Q VÀO HIỆN TƯỢNG NGƯNG TỤ BOSE-EINSTEIN ĐỐI VỚI Q-KHÍ

Tóm tắt: *Trong bài viết này, chúng tôi quan tâm đến thống kê biến dạng – q và áp dụng thống kê này vào hiện tượng ngưng tụ Bose-Einstein, kết quả là chúng tôi thu được biểu thức về nhiệt độ ngưng tụ Bose-Einstein của q-khí.*

Từ khóa: *Dao động biến dạng q, thống kê biến dạng q, ngưng tụ Bose-Einstein.*

INFLUENCE OF Co CONCENTRATION AND TEMPERATURE TREATMENT ON THE STRUCTURAL AND OPTICAL PROPERTIES OF TiO_2 FILMS

Pham Van Vinh[1], **Ha Thi Hang**[2]
[1]*Hanoi National University of Education*
[2]*Hanoi community college*

Abstract: *TiO_2 and Co-doped TiO_2 films were deposited on the glass substrate by a spin coater. The solution used to deposit the films were prepared by sol-gel method from $TiCl_3$ precursor. The structural and optical properties of the films as a function of cobalt concentration and temperature treatment were studied by X-ray diffraction and UV-vis analysis. The XRD showed the presence of TiO_2 anatase phase in the films. However, no XRD peaks related with Co was found. The SEM images showed that Co dopant influenced negligibly on the surface morphology of the films. The transmittance spectra showed that the films were good transparent in the visible region and the band gap of the films tended to narrow with the increase of cobalt dopant concentration. Besides, the band gap is also varied with different temperature treatment.*

Keywords: *TiO_2; Co-doped TiO_2, sol-gel, spin coater, $TiCl_3$ precursor*

Email: vinhpv@hnue.edu.vn
Received 27 March 2018
Accepted for publication 24 April 2018

1. INTRODUCTION

TiO_2 material, specially, TiO_2 in nano structure has been known as the material which promises a great number of applications in many fields. Due to their novel physical and chemical properties, TiO_2 thin films have been widely used for many applications such as photocatalytic purifier, air purification, self sterilization, optical thin film devices like antireflection coating for solar cell, multilayer optical coating, and also as a sensor material …etc [1-4]. Almost applications were base on the physical and chemical effect which related to the dopant and grain size. Among them, photocatalyst effect has been attractive to study. However, the application of TiO_2 films has been limited due to the large band gap of TiO_2. The band gap energy is around 3.2eV, only allows anatase TiO_2 to absorb ultraviolet light, which accounts for about 4% of the whole sunlight spectrum. In order to narrow the band gap, a great deal of effort has been made to prepare doped TiO_2 films by various methods [5]. Therefore, studying the properties of TiO_2 doped with transition metal to reduce band gap is still an interesting object. Although TiO_2 was prepared by many methods, the methods were complicated and required the expensive equipments or chemical precursor. Some groups used $TiCl_3$, the cheap chemical, to prepare TiO_2. However, almost of research were only done on TiO_2 powder. A few TiO_2 films prepared using this chemical have been found [6-13]. In this study, the TiO_2 films and TiO_2 deposited by spin coater from $TiCl_3$ precursor were carried out to investigate the influence of Co concentration on the optical properties of the films.

2. EXPERIMENTAL

$TiCl_3$ salt was dissolved into C_2H_5OH and IPA solution with the predetermined ratios. Subsequently, the solution was stirred for 30 min at 60^oC. Then, an appropriated amount of H_2O was dropped slowly into the solution. The solution would slowly change to be opalescent color. The stirring process was continued for 180 min to get sol for depositing pure films. The solution for doped films was prepared like to which for the doped films but the predetermined $Co(CH_3COO)_2.4H_2O$ salt was put before adding H_2O in to solution. Both of doped and undoped films were deposited by a spin coater. Amount of solution was dropped on the rotating substrate in order that the solution spread uniformly on it. After that, the sample was annealed to obtain the TiO_2 films.

An X-ray diffractometer, SEM and UV-vis spectroscopy were used to determine the crystalline phases, observe the surface morphology and investigate the optical properties of the films.

3. RESULT AND DISCUSSION

X-ray XRD diffractograms of the Co-doped TiO_2 films deposited by spin coater on glass substrate were shown in Fig. 1. All the films were the single anatase phase of TiO_2. Although the considerable amount of Co doped, no XRD peaks related with other secondary phases and impurities were presented. Besides, the XRD peaks tended to shift toward the higher angles with the increase of Co concentrations. Since the ionic radius of Ti^{2+} (100pm) is larger than that of Co^{2+} (83.8pm) and Co^{3+} (71.8pm), Co ions substituted to Ti^{2+} in the TiO_2 lattice the XRD peaks could shift toward higher angles. The averaged crystalline size of the films were estimated by Scherrer's formula from X-ray diffraction pattern. The results showed that the crystalline size of samples with Co-dopant in the range of 0% to 15% decreased in increasing Co concentration. The average crystalline sizes approximated is in the range from 7 nm to13 nm.

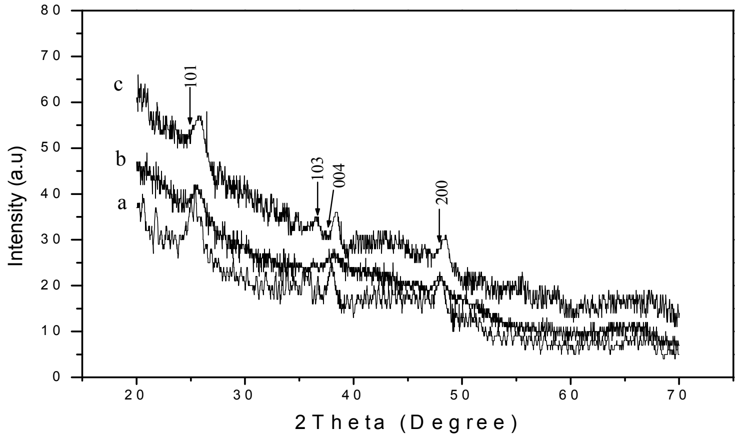

***Fig 1**. XRD diffractograms of TiO_2 and Co-doped TiO_2 films deposited with different Co concentrations (a: 0% Co; b: 10%Co; c: 15 %Co).*

The surface morphology of the films deposited with different Co concentration were showed in Fig.2. The crystals were agglomerated into grain with the sizes ranging from 20 nm to 100 nm. The effect of Co-dopant on the morphology was negligible. The grain size was slightly increase with the increase of the Co concentration.

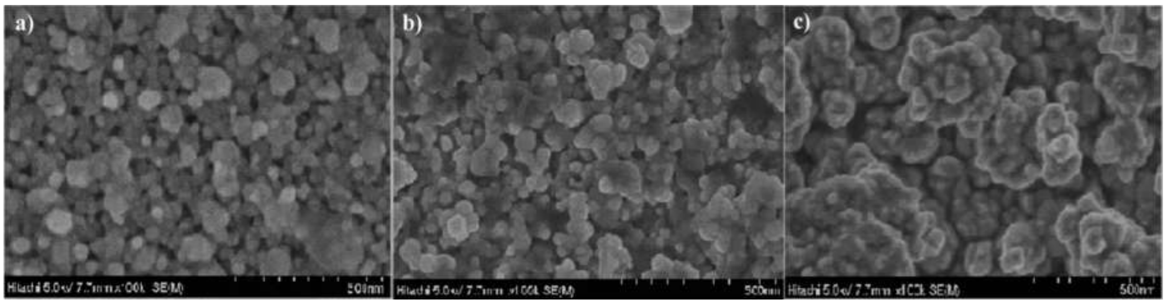

***Fig 2**. SEM images of TiO_2 and Co-doped TiO_2 films deposited with different Co concentrations (a: 0% Co; b: 10%Co; c: 15 %Co).*

Fig. 3 is the transmittance spectra of Co-Doped thin films with different solution concentration. The transmittance increases with the decrease of solution concentration. Indeed, the thickness of the films should be decreased when they were deposited by low solution concentration. The thinner films allowed light to transfer easier, resulting in improving the transparence of samples. The best transparence was found on the samples that deposited using the solution concentration of 0.86M. The absorption edge of the samples deposited with high solution concentration was bended. The bended absorption edge was believed to be caused by defects. In general, the thick films should limit the solution evaporation and the pyrolysis reaction during temperature treatment to form the films. Uncompleted pyrolysis reaction left the defects in the films. The samples deposited with solution concentration of 0.86M shown better transparent and less defect. Therefore, they were chosen to subsequent experiments.

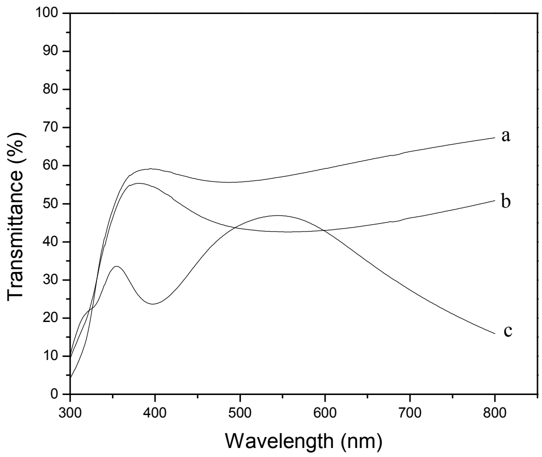

Fig 3. Transmittance spectra of Co-Doped thin films with different solution concentration a: 0.86M; b:0.91M; c: 1.36M

Fig. 4 shows the transmittance spectra of TiO_2 thin films deposited with different temperature. The optical transmission of TiO_2 films in the visible wavelength region seems to be stable with the change of temperature treatment. However, the absorption edge was a little shift to short wavelength. This means that the band gap was broaden with the increase of temperature treatment. The shift of absorption edge toward the shorter wavelength with an increase in the increase of deposition temperature was attributed to the Burstein-Moss shift and the reduction of defect [14]. Indeed, at high temperature treatment, the crystallization becomes perfect resulting in perfect crystal.

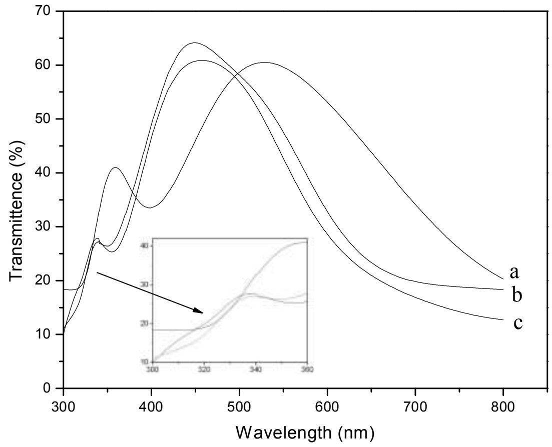

Fig 4. Transmittance spectra of TiO_2 thin films deposited with different temperature a: 300^oC; b: 400^oC; c: 550^oC

The transmittance spectra of Co-Doped thin films with different dopant concentration in fig. 5 shows that the transmittance of the films in the wavelength region higher than 500nm increased with the increase of Co concentration from 0% to 10%. Further increase of Co concentration decreased of transmittance. Besides, the transparent band broadened and the absorption edges were shifted toward higher wavelength with the increase of Co concentration. In addition, the absorption edges were bended at high Co concentration. This referred the narrow of band gap at high Co concentration. This event was attributed to the impurity defect sites in the vicinity of the valence.

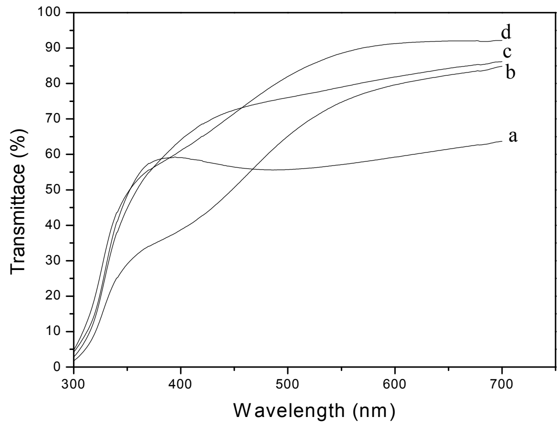

Fig 5. Transmittance spectra of Co-Doped thin films with different Co concentration a: 0%; b: 15%; c: 5%; d:10%.

4.CONCLUSION

TiO_2 and Co-Doped TiO_2 were deposited successfully on glass substrate by spin coater. The transmittance increases with the decrease of solution concentration. The band gap was broadened with the increase in temperature treatment while it was reduced with the increase in Co-dopant concentration. The crystalline size of the films was decrease with the increase of concentration of Co-dopant. In contrast, the grain size was slightly increase with the increase of Co-dopant. The transmittance of the films in the wavelength region higher than 500 nm increased with the increase of Co concentration from 0% to 10%. Further increase of Co concentration decreased of transmittance.

Acknowledgments: This research is funded by Vietnam National Foundation for Science and Technology Development (NAFOSTED) under grant number of 103.02-2013.50

REFERENCES

1. H.P. Deshmukh, P.S. Shinde, P.S. Patil, (2006), "Structural, optical and electrical characterization of spray-deposited TiO_2 thin films", Volume 130, Issues 1–3, Materials Science and Engineering, PP. 220-227
2. Adawiya J. Haider, Riyad Hassan AL- Anbari, Ghadah Rasim Kadhim, Chafic Touma Salame (2017), "Exploring potential Environm ental applications of TiO_2Nanoparticles" *Energy Procedia, Volume 119*, pp.332-345.
3. Mohammad BagherAskari, ZohaTavakoli Banizi, MajidSeifi, SedighehBagheri Dehaghi, PayamVeisi (2017), "Synthesis of TiO2 nanoparticles and decorated multi-wall carbon nanotube (MWCNT) with anatase TiO2 nanoparticles and study of optical properties and structural characterization of TiO2/MWCNT nanocomposite", *Optik - International Journal for Light and Electron Optics, Volume 149*, pp. 447-454
4. Stephen A.Diamond, Alan J.Kennedy, Nicholas L.Melby, Robert, D.Moser, A.R.Poda, C.A.WeissJr, J.A.Brame (2017), "Assessment of the potential hazard of nano-scale TiO2 in photocatalytic cement: application of a tiered assessment framework" NanoImpact, Volume 8, pp 11-19
5. L. Wan, J.F. Li, J.Y. Feng, W. Sunb, Z.Q. Mao (2007), "Anatase TiO2 films with 2.2 eV band gap prepared by micro-arc oxidation" Materials Science and Engineering, Volume 139, Issues 2–3, pp. 216-220
6. Hyeon-Ju An, Song-Rim Jang, R. Vittal, Jiwon Lee, Kang-Jin Kim (2005), "Cationic surfactant promoted reductive electrodeposition of nanocrystalline anatase TiO2 for application to dye-sensitized solar cells", Electrochimica Acta, Volume 50, Issue 13, pp 2713-2718
7. Y. Lei, L.D. Zhang, J.C. Fan, Fabrication (2001), "characterization and Raman study of TiO2 nanowire arrays prepared by anodic oxidative hydrolysis of TiCl3", Chemical Physics Letters, Volume 338, Issues 4–6, pp 231-236
8. Sophie Cassaignon, Magali Koelsch, Jean-Pierre Jolivet (2007), "From TiCl3 to TiO2 nanoparticles (anatase, brookite and rutile): Thermohydrolysis and oxidation in aqueous medium", Journal of Physics and Chemistry of Solids, Volume 68, Issues 5–6, pp 695-700.
9. Xiangping Huang, Chunxu Pan (2007), "Large-scale synthesis of single-crystalline rutile TiO2 nanorods via a one-step solution route Journal of Crystal Growth", Volume 306, Issue 1, Pages 117-122.
10. Katrin Wessels, Miyuki Maekawa, Jiri Rathousky, Torsten Oekermann (2007), "One-step electrodeposition of TiO2/dye hybrid films", Thin Solid Films, Volume 515, Issue 16, pp 6497-6500.
11. Aditi R. Gandhe a, Sajo P. Naik b, Julio B. Fernandes (2005), "Selective synthesis of N-doped mesoporous TiO2 phases having enhanced photocatalytic activity", Microporous and Mesoporous Materials, Volume 87, Issue 2, pp 103-109.

12. Huanxin Gao, Wenkui Lu, Qingling Chen (2000), "Characterization of titanium silicalite-1 prepared from aqueous TiCl3", Microporous and Mesoporous Materials, Volume 34, Issue 3, pp 307-315.

13. Keita Kakiuchia, Eiji Hosonob, Hiroaki Imaia, Toshio Kimuraa, Shinobu Fujihara (2006), "{1 1 1}-faceting of low-temperature processed rutile TiO2 rods", Journal of Crystal Growth, Volume 293, pp 541-545

14. Mingsong Wang, Ka Eun Lee, Sung Hong Hahn, Eui Jung Kim, Sunwook Kim, Jin Suk, Chung, Eun Woo Shin, Chinho Park (2007), "Optical and photoluminescent properties of sol-gel Al-doped ZnO thin films" Materials Letters, Volume 61, Issues 4–5, pp 1118-1121

ẢNH HƯỞNG CỦA NỒNG ĐỘ TẠP CHẤT CO VÀ NHIỆT ĐỘ XỬ LÝ MẪU LÊN CẤU TRÚC VÀ TÍNH CHẤT QUANG CỦA MÀNG MỎNG TIO$_2$

Tóm tắt: *Màng mỏng TiO_2 và TiO_2 pha tạp Co đã được phủ thành công trên đế kính bằng máy quay phủ li tâm. Dung dịch được sử dụng để phủ màng được chế tạo bằng phương pháp Sol-Gel từ tiền chất $TiCl_3$. Ảnh hưởng của nồng độ tạp chất Co và nhiệt độ xử lý mẫu lên các tính chất về cấu trúc và tính chất quang của màng được nghiên cứu bằng phương pháp nhiễu xạ tia X và phép phân tích phổ hấp thụ UV-vis. Giản đồ nhiễu xạ tia X cho thấy có sự xuất hiện của các pha tinh thể TiO_2 ở dạng anatase. Tuy nhiên, không có đỉnh nhiễu xạ nào liên quan đến Co xuất hiện. Ảnh SEM cho thấy tạp chất Co ảnh hưởng không đáng kể lên hình thái bề mặt của màng. Phổ truyền qua đã chứng tỏ màng mỏng có khả năng cho ánh sáng truyền qua tốt trong vùng khả kiến và bề rộng vùng cấm có xu hướng thu hẹp khi tăng nồng độ tạp chất Co. Bên cạnh đó, bề rộng vùng cấm cũng thay đổi khi mẫu được xử lý ở các nhiệt độ khác nhau.*

Từ khóa: *TiO_2, TiO_2 pha tạp Co, sol-gel, quay phủ, tiền chất $TiCl_3$*

ISOLATE AND DETERMINE THE STRUCTURED SUBSTANCES FROM ETHYL ACETATE EXTRACT LEAVES OF VÚ BÒ SPECIES (*FICUS HIRTA* VAHL.) INVIETNAM

Nguyen Thi Lieu[1], Ta Vu Quynh Trang
[1] *Hanoi Metropolitan university, 98 Duong Quang Ham street, Cau Giay district, Ha noi, Viet nam.*

Abstract: *From 30 grams of Ethyl acetate (EtOAc) the leaf of Vu bo species (Ficus hirta Vahl.) chromatographs isolated two clean compounds are β-Sitosterol and Bergapten. Their structure is determined by the H^1NMR, C^{13}NMR and MS spectra combined with data search.*

Keywords: *Ficus hirta Vahl., sterol, furanocoumarine*

Email: ntlieu@daihocthudo.edu.vn
Received 6 April 2018
Accepted for publication 21 May 2018

1. INTRODUCTION

The scientific name of Vu bo species is *Ficus hirta* Vahl., the mulberry family (Moraceae).

Vu bo 1-2 meters high. Soft feathers. Stems less branch, with thick feathers. Leaves are sparse, usually in the tops of the body, oval, round or slightly rounded, with tapering head, 3-5 lobes (usually 3), upper armor, small furry, teeth, tendon 3; petiole with thick, hard feathers; leaf with spear. Flowering blossoms in the interstitium include male and female flowers; males without stem, leaf 4, resolution, stick together in the root, double 2, flowers with stem, leaves 4, prison, oval. Compound spherical, when ripe yellow. The tree grows in the mountains of our country [1÷4].

Vu bo is a spicy, sweet, warm, spicy, low-gas, sprout. People see this as a tonic, used for people with tuberculosis, eczema, bad breath, diarrhea, rheumatism, hepatitis [1÷4].

The results of chemical studies show that cow breeds contain alkaloids, flavonoids, cumarin, terpenoids, benzoic acid derivatives.

In Vietnam, there is only one research on the chemical composition of the cow breed (*Ficus hirta*Vahl.) by Tran Duc Dai et al. [5]

Picture of Vu bo (Ficus hirtaVahl.)

2. CONTENT

2.1. Materials and Methods

i) Plant material

Leaves of Vu bo were collected in October 2014 in Yen Son district, Tuyen Quang province. Do Huu Thu (Institute of Ecology and Biological Resources - Vietnam Academy of Science and Technology) identifies the scientific name (Ficus hirta Vahl.) Of the Moraceae family. Samples are stored at the Natural Research Institute, Institute of Chemistry - Vietnam Academy of Science and Technology.

ii) Equipment, chemicals

• Nuclear NMR spectrum recorded by Bruker Avance 500 [499.84 MHz (^{1}H-) and 125 MHz (^{13}C-); TMS (δ = 0.0); CD_3OD (δ = 49.0); $CDCl_3$ (δ = 77.0)] at the Institute of Chemistry, Vietnamese Academy of Science and Technology.

• ESI-MS mass spectrum was measured on the Agilent LC-MSD-Trap SL machine at the Institute of Chemistry, Vietnamese Academy of Science and Technology.

• Chemicals include ethyl acetate, dichlorormane, methanol, n-hexane, silica gel, sephadex ...

iii) Research methodology

- Extraction method

Total extraction: Leaf samples were leached with methanol (repeatedly) to obtain total methanol residue. Total residue is added to distilled water (about 100-200 g of distilled water in 1 liter of distilled water). Water-based liquid-liquid extraction with less soluble organic solvents and gradually increasing polarization from *n*-hexane, chloroform, ethyl acetate and *n*-butanol. Then store the solvent under reduced pressure to extract the extracts of *n*-hexane, chloroform, ethyl acetate and *n*-butanol respectively.

- Method of isolation and purification

The materials were separated and purified by column chromatography combined with thin layer chromatography with appropriate solvent systems. For polarizers, use Sephadex LH-20. Examine the segments and cleanliness of the substances as well as monitor the separation process on the column by thin layer chromatography with appropriate solvent system.

- Methods to determine the chemical structure of substances

The chemical structure of clean substances is determined by combining modern spectral methods such as mass spectrometry (MS), 1D NMR spectra of NMR such as ^{1}H-NMR, ^{13}C-NMR.

2.2. Isolation of clean substances from Ethyl acetate extracts

30 g of EtOAc (VBLE) was isolated on the column chromatography with silica gel adsorbent, solvent system (CH2Cl2: MeOH: H2O) at the appropriate solubilization ratio of (90%: 10%: 0 % -> 30%: 10%: 1%) obtained 10 segments (VBLE1 → VBLE10).

VBLE3 (6g) column chromatography with silica gel, solvent (CH_2Cl_2 / MeOH 8: 2) obtained 6 fractions (VBLE3.1 →VBLE3.6). From VBLE3.1 (580 mg) further isolation on column chromatography of LH-20 / MeOH sephadex yielded the **VB1** clean compound. From VBLE3.4 (830 mg) further isolated on silica gel column chromatography (CH_2Cl_2 / MeOH 9: 1) obtained a clean substance denoted **VB2**.

2.3. Research results and discussion

2.3.1. Define the VB1 structure

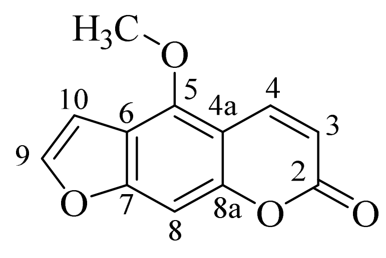

VB1. Bergapten

VB1 is solid, white. The FT-IR / KBr spectra exhibit covalent oscillation signals of ʋmax (cm-1): 3088-3013 (weak,> C = CH), 2959 (weak, -OCH3), 1732 (> C = O), 1606-1542 (C = C benzene ring).

^{1}H-NMR spectra exhibit characteristic signals for the furanocoumarine frame. In the weak field there appear two pairs of doublet signals having the same separation characteristic for conjugated olefin protons (-CH = CH-), each of which signals with 1 proton at δH 8.16 (1H, d, J = 10.0 Hz, H-4) and 6.27 (1H, d, J = 10.0 Hz; 7.6 (1H, d, J = 2.5 Hz, H-9) and 7.02 (1H, d, J = 2.5 Hz; A single resonant signal of the aromatic proton was also observed at 7.1 (1H; s; H-8). A single strong-signal singularity characteristic of the three methoxy-protons was shifted towards the weak field at 4.27 (3H; s; 5-OCH_3). Signals resonating on the ^{13}C-NMR spectrum show 12 signals of carbon atoms including a conjugated carbon carbonyl atom (> C = O) at δ_C161.34; 5 methylene groups (> CH-), of which 4 olefinic carbon at δ_C 112.73 (C-3), 139.36 (C-4), 144.92 (C-9), 105.15 1 aromatic carbon at δC 94.02 (C-8); Fourth-order resonant of carbon tetrahedron at C 112.86 (C-6), 158.53 (C-7), 149.72 (C-8a), 106.59 (C-4a), 1 signal resonance of the carbon-3 bond with oxygen at 152.87 (C-5) and 1 resonance signal of the methyl group carbon at δ_C of 60.2 (5-OCH_3).

***Table 1**. NMR spectra of compounds **VB1** and Bergapten [6]*

C	VB1		Bergapten [6]	
	^{1}H-, ^{13}C-NMR (500 MHz, 125 MHz) / CD_3OD		^{1}H-, ^{13}C-NMR (400 MHz, 110 MHz) / $CDCl_3$	
	δ_H, J (Hz)	δ_C	δ_H, J (Hz)	δ_C
2	-	161.3	-	161.2
3	6.27 (1H, d, J = 10)	112.7	6.27 (1H, d, J = 9.8)	112.5
4	8.16 (1H, d, J = 10)	139.5	8.15 (1H, d, J = 9.8)	139.2
4a	-	106.6	-	106.4
5	-	149.7	-	149.5
6	-	112.9	-	112.6
7	-	158.5	-	158.4
8	7.14 (1H, s)	94.0	7.12 (1H, s)	93.8
8a	-	152.9	-	152.7
9	7.59 (1H, d, J = 2.5)	144.9	7.59 (1H, d, J = 2.4)	144.8
10	7.02 (1H, d, J = 2.5)	105.2	7.02 (1H, dd, J = 2.4; 1.0)	105.0
OCH_3	4.27 (3H, s)	60.24	4.27 (3H, s)	60.1

Comparison of the ^{1}H-NMR and ^{13}C-NMR spectra of the **VB1** compound with the published NMR data of the bergapten compound [6] found good fit. Thus the **VB1** compound is identified as ***bergapten***. Bergapten is widely distributed in the canopy family. Plant flowers are capable of synthesizing and storing bergapten. Bergapten has the ability to slow cell division by interacting with DNA, fungal pathogens against plants, treating leukemia, psoriasis, inflammatory diseases such as pyelonephritis, nephritis [7] .

2.3.2. Define the VB2 structure

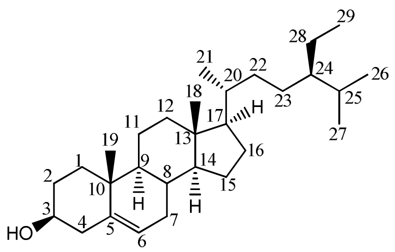

VB2. β-Sitosterol

^{1}H-NMR spectrum showed the presence of two methyl singlet groups at δ_H 1.07 (3H, s) and 0.70 (3H, s), a methyl triplet group at δH 0.87 (3H, t, J = 7, 1 Hz) together with three other methyl groups at δ_H 1.00 (3H, d, J = 6.7) and 0.86 (6H, br s). Effect of an olefin proton at δ_H 5.38-5.36 (1H, m) and a oxymethine proton signal at δ_H of 3.56-3.52 (1H, m). Signals of the remaining protons overlap in the range of δ_H 2.33-1,11ppm. The ^{13}C-NMR spectrum indicates the signal of two olefinic carbon (δ_C 140.79; 121.72) and a group of oxymethine at δ_C 71.82. Signals of six methyl groups appear at δC 19.82; 19,41; 19.06; 18.80; 12.00; 11,87. The remaining six methane groups and nine methylene groups are within the range of δ_C 21,11 ÷ 56,80 ppm. Comparison of NMR data with reference [8], identified as β-sitosterol.

3. CONCLUSIONS

From 30 grams of ethyl acetate extracts (EtOAc) of Vu bo leaves (*Ficus hirta*Vahl.) Through silica gel column chromatography and sephadex repeatedly with suitable solvent systems were isolated two clean substances Bergapten (**VB1**) and β-Sitosterol (**VB2**). The structure of the two compounds was determined by the NMR spectrometry method in combination with standard document comparisons.

REFERENCES

1. Many authors (2004), *Medicinal plants and animal medicine in Vietnam*, Science and Technology Publishing, Hanoi, Vol.1, p.716.
2. Multiple authors (2003), *List of Plants of Vietnam*, Agricultural Publishing, Volume II, pp.180-203.
3. La Dinh Moi, Tran Minh Hoi, Duong Duc Huyen, Tran Huy Thai, Ninh Khac Ban (2005), *Plant resources in Vietnam - Plants containing bioactive compounds*, Agricultural Publishing, T. I, pp.127-129.
4. Liu, L.L. Wang, T. Wang, X. Liu, and X. Yang (2008), *Phytochemical and pharmacological research progress in Ficus microcarpa L. f.*Shizhen Guoyi Guoyao, 19, p.390.
5. Tran Duc Dai (2018), *Study on chemical composition and biological activity of two species of ngoc cau* (*Balanophora laxiflora* Hemsl.) And Vu bo (*Ficus hirta* Vahl.), PhD thesis, Academy of Sciences Vietnam
6. Shinsuke Marumoto, Mitsuo Miyazawa (2011), *Microbial reduction of coumarin, psoralen, and xanthyletin by Glomerella cingulata*. Tetrahedron, 67, pp.495-500.
7. Takahiro Masuda, Mitsuo Takasugi and masaki Anetai (1998), *Psoralen and other linear furanocoumarins as phytoalexins in Glehnia littoralis*. Phytochemistry, 47(1), pp.13-16.
8. Mellick R., Porter C., Rossetto M. (2009), *Isolation and characterisation of polymorphic microsatellite loci from Podocarpus elatus (Podocarpaceae)*, Molecular Ecology Resources, 9(6), pp.1460-1466.

PHÂN LẬP VÀ XÁC ĐỊNH CẤU TRÚC CÁC CHẤT TỪ DỊCH CHIẾT ETHYL ACETATE CỦA LÁ LOÀI VÚ BÒ (*FICUS HIRTA* VAHL.) Ở VIỆT NAM

Tóm tắt: *Từ 30g cao chiết Ethyl acetate (EtOAc) lá loài Vú bò (Ficus hirta Vahl.), tiến hành sắc kí cộtđã phân lập được hai hợp chất sạch là β-Sitosterol và Bergapten. Cấu trúc của chúng được xác định bằng phương pháp phổ H^1NMR, C^{13}NMR và MS kết hợp với tra cứu dữ liệu.*

Từ khóa: *Lá loài Vú bò, chất sterol, hoạt tính furanocoumarine.*

RESEARCH ON CHARACTERISTICS OF HUMAN LANESCAPES IN ORDER TO PROVIDE ENVIRONMENTAL PROTECTING ORIENTATIONIN VAN DON DISTRICT, QUANG NINH PROVINCE

Bui Minh Tuyen[1], Mai Huong Lam[2], Nguyen Thi Nhan[3]
[1] *Ha Noi Metropolitan university*
[2]*Ha Noi university of natural resources and environment.*
[3]*VNU university of science.*

Abstract: The human landscape theory is an approach that links natural and social values to solve territorial development issues, especially in the orientation of environmental protection. This article presents the territorial divisions of 04 landscape types and 35 landscape types, creating a premise for the establishment of 07 landscape subregions of Van Don district, Quang Ninh province. On the basis of determining: (i) landscape characteristics, (ii) environmental and biodiversity issues, (iii) developing conflicts; The study proposes specific environmental protection guidelines for each sub-region. Accordingly, the landscape approach to humanity not only provides a scientific basis for the sustainable development of the territory, but also allows applicating of the socio-economic contradictions arised in the past in territorial exploitating processes.

Keywords: Human landscape, subregion, environmental protection, Van Don district, Quang Ninh province.

Email: bmtuyen@daihocthudo.edu.vn
Received 21 May 2018
Accepted for publication 1 June 2018

1. SET THE PROBLEM

The theory of sustainable development or environmentally-friendly development is difficult to achieve (Mawere M. et al., 2012). The term “sustainability”, although be applied to different fields, lacks the scientific basis to apply them (Temple, 1992); then arising many conflicts among environmental protection and socio-cultural development in the process of resource exploitation and using (Kiriama et al., 2010). Thus, the coming out of the society of a cultural landscape becomes the perfect solution to resolve conflicts as: (i) the definition is “... a landscape created by human culture” (James & Martin, 1981); (ii) reconstruct the relationship among natural and human factors and the interrelationships among them (Priore, 2001; Fowler, 2001); (iii) demonstrate human evolution under the limited influence of natural or socio-cultural or cultural development (World Heritage Committee, 2008); (iv) spatial and temporal variations are highly dependent on cultural horizons (Sauer, 1925; Guilfoyle, 2006). The fact that the cultural landscape represents the synergistic effect of many variables, then this approach becomes a solution for proposing management direction appropriate to each region (ICCROM, 2009). In particular, resolving thoroughly the conflicts in the invironmentally integrated planning (Lain J.K., 2003, Nguyen Cao Huan, 2005), is the premise for "sustainable development".

Van Don district, Quang Ninh province has achieved many economic achievements, total production value in 2015 reached 2684 billion, average income per capita reached 36.7 million, rising 2.3 times in the period from 2010 to 2015. However, environmental issues are changing in the negative direction, the activities of aquaculture in cages on the sea are increasing (reaching over 4,000 cages in 2015), livestock breeding activities accounted for more than 50% the amount of waste from agricultural activities, daily solid waste was more than 100m3. The studied area environment is increasingly polluted according to the current economic growth and had a great impact on people's lives. Therefore, the theory of human landscape application in the orientation of environmental protection will become a effective solution of the existing environmental problem, *the study of the characteristics of human landscape to serve the orientation of protection Van Don District, Quang Ninh Province* will be conducted.

The aim of the study is to address the shortcomings of environmental protection according economic development. The structure of the study consists of (i) identifying the characteristics of the type group and landscape type, (ii) the human landscape zoning, (iii) identifying environmental issues and developmental contradictions in each sub-region (iv) proposed environmental protection.

2. THERORETICAL BASES AND RESEARCH METHODS

2.1. Theory of human landscape and landscape divisions.

From a variety of perspectives, the landscape of humanity is broadly defined as "natural landscapes in which any component is altered or preserved by human activities" (Nguyen Cao Huan, 2002). By this point of view, the theory of human lanscape is consisted by the following contents.

Each Unit of human landscape contains two groups that are natural and human attributes. Corresponding to this structure, human landscape has two functions which are natural and social functions (the ability to ensure economic, social and living values).

The role of the human factor in the formation and development of the research of human landscape has a direct or indirect impact (indirectly through developingpolicies towards the landscape). Over time, human landscapes constantly changes. Especially in periods of economic developing, it can be changed positively or negatively, depending on the perception, the culture of the community of the subject, and when we stop exploiting; landscapes tend to return to their original state depending on the level of human impact. Man with his right understanding by means of legal tools, policy impact positively create the cultural landscape with economic, social, ecological and environmental values.

In the history of development, the landscape changes in stages from the past to the present and in the future. Man can not abolish the laws of nature, but only obey them. Knowing the type of landscape in the past, we will adjust the direction of their development or conservate that type of landscape or develop in a positive way to form a new landscape type compared with the original type of landscape. This is the basis of the direction in using resources and protecting environment landscapes in a given territory.

The landscape classification process is based on three principles: (i) Principle of Identifying the developmental process of landscape units, comparing them with the current status as a basis for predicting trends of future transformation; (ii) Relativistic Principle: Each hierarchy landscape level is defined by one or several criterias, reflecting the relationship among components (geology, geomorphology, climate, plants, human impact); (iii) Synthesis Principle: According to this principle, when analyzing landscape boundaries, it is necessary to analyze some main components. Based on the analysis and overlapping of components, the map of Van Don District is structured into two levels: type and group of landscapes.

Table 1. *Unit system and criteria for landscape classification of Van Don district, Quang Ninh province*

Classification	Classification criteria	Example
Group of human landscape	Main land using type and resource using	- Group type of natural forest concludes: - Agricultural group - Group of residents
Type of human landscape	Uniformity of land using types with specific technical characteristics, natural conditions and types of resource exploitation	Group of residents includes: +Type of urban population. + Form of rural population

According to various approaches, zoning can be interpreted as "dividing territory or maritime zones into zones or sections, distinguished by their homogeneous levels" (Le Ba Thao, 1988). The key principles in the Van Don District landscape include: (i) Principle of Analyzing the differentiation rules that form the partitioning unit and their evolution in the development process. It anticipates the trend of future development and help people use them appropriately and effectively. (ii) Relativistic Principles: Natural geographic regions have very complex structures but also uniform in certain indicators; (iii) Principle of common territory: Each natural geographical area has a closed boundary, distinct from other neighboring areas.

Thus, partitioning the landscape of human life in Van Don District, is one of the scientific basis of the integration among natural conditions and human activities. The result of the assessment is the foundation for effective use of natural resources and environmental protection for Van Don District.

2.2. Research Methods

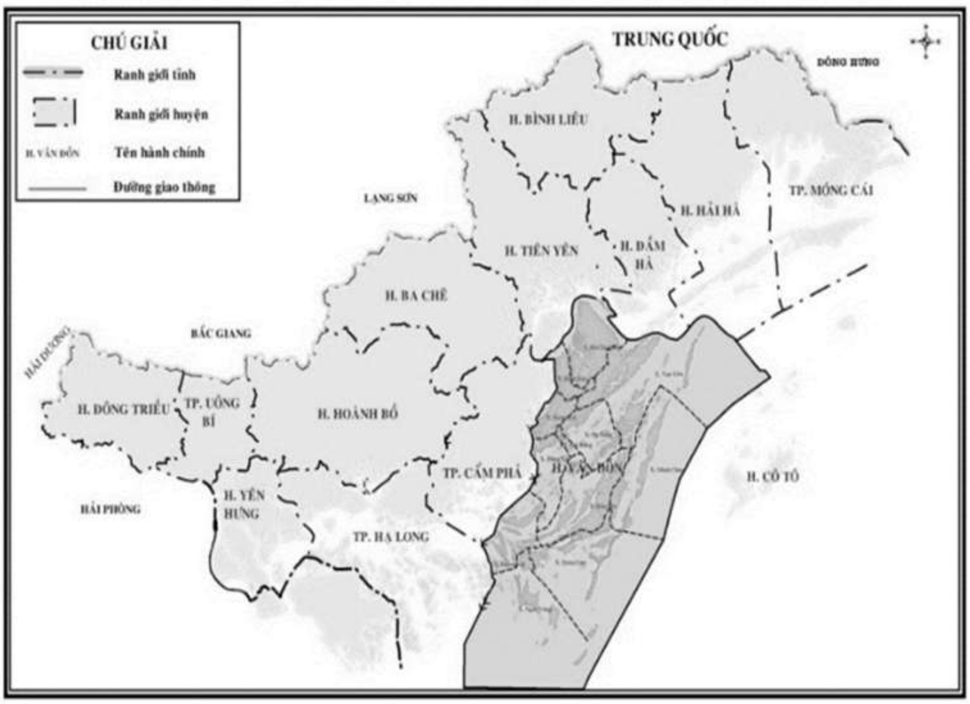

Picture 1: *Map of Van Don District, Quang Ninh Province*

The study consists of three main methods: (i) synthesis data analysised that enables the analysis and synthesis of documents from sources collected through books, newspapers, the internet, reports, planning of studied areas, the duplication in the study was inherited, resulting in the results of previous studies. From there, it is possible to determine the right direction of the study of the thesis; *(ii) the field survey method-GIS* is one of the most important methods in the study to collect additional data on natural, economic, social, environmental and environmental conflicts arised. In addition, interviews with local people in the area enable the study have a better understand about emerging environmental issues, affecting people's lives. At the survey sites, take sampling and observation of environmental parameters; (*iii) Mapping - GIS* is the most important method for mapping research results. In the study, Van Don District's geological maps, Van Don District's geomorphological maps, Van Don District's soil maps, land use map of 2015 in Van Don District, a map of Van Don District and a map of space for environmental management and protection in Van Don District are used.

2.3. Overview of the study area

Van Don is a mountainous district located in the east and southeast of Quang Ninh province with geographic coordinates from 20^{o}40’ 21^{o}16’ north latitude and from 107^{o}15’ to 108^{o}00’ east. With a total natural area of 55,320.23 ha including Cai Rong Town and 11 communes. *For geological features*, Van Don is composed of solid bases of the formation: Bai Chay (P3bc), Bai Chay (P3bc), D3-C1ph, Cat Ba (C2cb), Ha (J1-2 hc) (Nguyen Cao Hung, 2016*). For terrain-geomorphologic features*, the geological formations of the area have led to the formation of diverse terrain types and a distinct division from low mountains (distributed in island communes). The topography of the delta is mixed with the valley topography to the terrain of the river and the origin of the sea, creating many beautiful landscapes and valuable tourism development. These are two of the most important factors in the formation of landscapes because they are the first to be directly affected by the laws of terrain and non-terrain, affecting the differentiation of natural conditions according to space and in the formation of landscape boundaries. For climatic characteristics, Van Don is dominated by coastal climate, influence and impact of the sea, creating coastal mixed coastal ecosystems. During the year usually divided into two distinct seasons: hot humid summer often rain heavily from April to October; Cold, dry winter with North East winds from November to March next year. The annual average temperature is 24,4 ^{O}C, the average annual rainfall is about 2090 - 2380 mm, the rains are divided into two distinct seasons. In addition, Van Don is an island mountainous district, thus it is directly affected by the storms landing from the sea and usually appear in June to October (General Statistics Office, 2015). Climatic mode involved in the formation and transformation of the landscape through the movement of matter in the air is the basis for the division of landscape units.

The soil of Van Don district is diverse and is the result of the geothermal heat base on different terrain types including 6 main soil groups: red soil (F) distributed throughout the district with an area of 34,081.32ha; sandy soil (C) with total area of 5551.67 ha distributed mainly in coastal communes and island communes; Saline soil (M) has an area of 4533.41 ha, distributed mainly in the coastal areas of Binh Dan, Thang Loi, Ngoc Vung, Quan Lan, Ban Sen and Minh Chau communes; Alum soil (S) covers an area of 85.70 ha, distributes almost in the district, alluvial soil (P) with an area of 76.2 ha distributed into narrow strips running along the river in the area of Dai Xuyen, Binh Dan, Doan Ket; gray grays (X) of the area of 443.1 ha, formed and developed mainly on ancient silt and sandy soils, distributed in hilly terrain with the height from 25 to 175m (Institute of Planning and Design Survey agriculture, 2005). The earth is a special constituent of the landscape due to its regenerative nature, which clearly shows the interaction among nature and creatures.

On socio-economic development conditions, the population of Van Don District in 2014 is 43,400 people with the average population density of 79 people/km^2. However, the population is unevenly distributed, with high population density such as Cai Rong town with 2,223 people/km^2 ..., low population density in Van Yen commune with 14 persons / km2. In the period of 2010 - 2015, the structure of labor in the economic sectors tends to shift towards the proportion of agriculture-forestry-fishery labor decreased 10.2%, industrial increased 0.6%, labor trade and services increased 10.1% (Van Don District People's Committee, 2015, Socio-Economic Report). Along with the economic development of the district, the consequences for the environment, agricultural activities, aquaculture, mineral exploitation, tourism trade ... caused the degradation of land and water resources, environmental pollution and landscape change. Therefore, environmental management planning and protection in Van Don district is not affected by the characteristics of socio-economic development.

3. RESEARCH RESULTS

3.1. Characteristics of Van Don District's landscape

Based on the analysis of the classification system of published researches by many authors at home and abroad, the combined analysis of the natural and socio-economic components of the research area, Van Don District shown on the *map 1*: 25.000 scale, including 2 levels: group landscape ->landscape. Each level of landscapeis represented as a subgroup of landscape sub-zones as a prerequisite for environmental protection planning and rational use of land. The study area was divided into 4 groups of landscape and 35 types of landscape:

Group of agricultural landscapes: landscape12 types of agricultural crops: 354.60 ha (0.64%); Annual crop (landscape13, landscape17) covers an area of 315.16 ha (0.57%); landscape rice farming on alkaline soil (landscape27) with an area of 92 ha (0.17%); landscape34 aquaculture has an area of 159.08 ha (0.29%).

Upland populations: formed by human settlement, distributed along the Van Don peninsula and on three main island clans which are Tra Ban, Ngoc Vung - Van Canh and Quan Lan - Minh Chau. Group landscape includes: landscape9, landscape14, landscape18, landscape20, landscape21, landscape26, landscape28, landscape30, landscape32, landscape35 with an area of 11,487.41 ha (20.77%). This type of group is likely to expand in the future, putting pressure on the environment.

Group of landscapes of forest, grassland and shrubs: including landscape2, landscape3, landscape4, landscape6, landscape8, landscape11, landscape16, landscape22 and landscape25 with an area of 24005.69 ha (43.39%). Plantation forest area is 23497.7 ha, the rest is the area of hills and grassland, distributed mainly in mountainous areas in the communes of Dai Xuyen, Van Yen, Binh Dan, Ban Sen, Quan Lan.

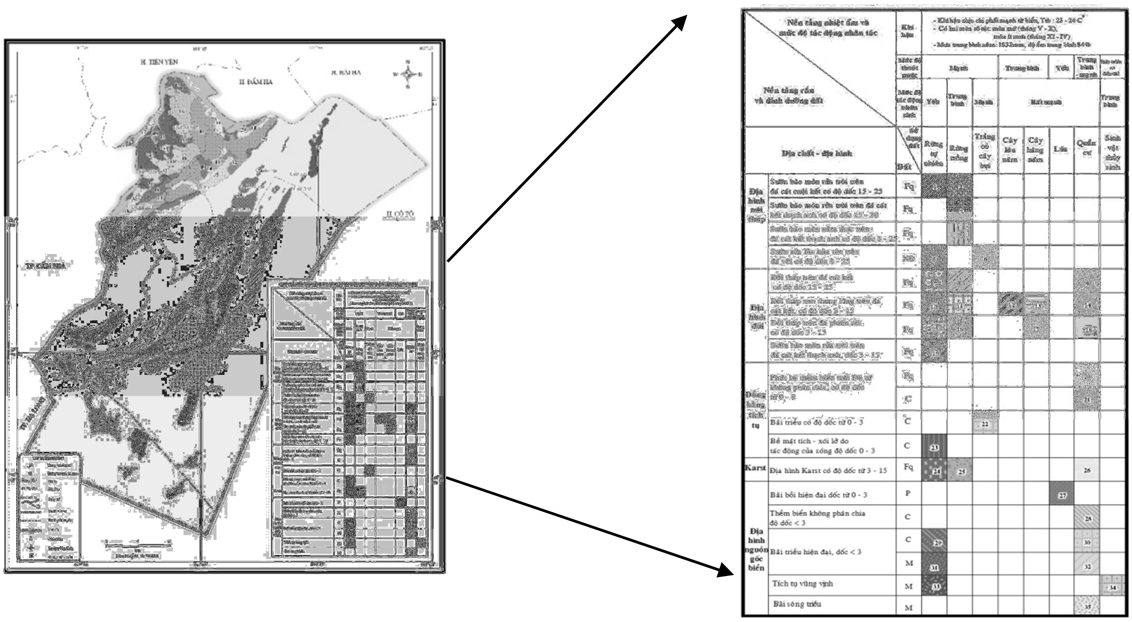

***Picture 2.** Map of Van Don District's human landscape*

Group of natural forest landscape: including landscape1, landscape5, landscape7, landscape10, landscape15, landscape19, landscape23, landscape24, landscape29, landscape31, landscape33 with an area of 18906.28 ha (34.18%). The watershed protection forest is concentrated in the dam area and coastal protection forest (Ngoc Vung, Quan Lan, Thang Loi, Dien Xuyen).It is the second largest landscape group, but it plays the most important role in biodiversity conservation, mitigating the negative impacts of nature (storms, landslides.

3.2. Identify environmental issues in each sub-region

Based on the analysis and aggregation of landscape and landscape groups, the study area was divided into seven sub-zones with landscape characteristics and specific environmental problems:

The production forest area of Dai Xuyen (subregion 1) accounts for 2.99% of the natural area (1653,114 ha), especially landscape4, landscape14 and landscape15. The current environmental problem is biodiverse decrese, production forest in the area of Dai Xuyen: water environment indicators are in the standard allowed: DO (6.46mg/l), pH (7.59), total suspended solids TSS (11.5 mg/l), salinity (0.34 ‰). These conflicts arise from the exploitation of production forests by local people and the development orientation of surface coating.

The landscape of Dong Xa - Van Yen coastal sub-area (subregion 2) accounts for 4.39% of the natural area (2427.609 ha), the landscape of the community (landscape28, landscape30, landscape35), the natural forest (landscape10) plantation forest (landscape11). Fishery processing activities cause environmental problems in the sub-region: DO content (2.43 mg/l) is outside the standard, the surface water level index (0.92 ‰) is higher than permitted standards. Aquatic product processing and port operations bring high economic benefits, however, putting pressure on environmental protection and management.

The protection forest area along the Voi Lon river (subregion3) accounts for 7.63% (4221.992 ha), the type of natural forest (landscape4, landscape15, landscape17, landscape31), landscape 4, landscape17. Landscape population (landscape14, landscape18, landscape32). The environmental problem is the risk of deterioration in the quantity and quality of protection forest along the Voi Lon river, the dust content of 1,861 mg/m^3 exceeds QCVN (0.3 mg/m^3), the amount of dissolved oxygen in water 4, 78 - 5.41 mg/l below QCVN (> 6 mg/l), salinity in surface water was 0.57 ‰ in excess of QCVN (0.5‰). The conflicts in this development arise due to the orientation of industrial, service and tourism expansion with forest restoration and environmental protection.

The Van Don sub-zone (subregion4) is 12.29% (6800.522 ha), characterized by the landscape of the sub-region being service, exploitation and tourism. Water pollution (pH level 9) exceeds QCVN for surface water, air is affected by waste from ship's activities, the content of organic matter in water is increased. The conflicts arise because of the benefits from fishing activities, wharves, tourism which is increasing, and the water and air environment is increasingly affected.

The forest of the special use forest on the island of Sau Nam, Ba Mun (subregion5) accounts for 23.65% (13082.47 ha), including natural forest landscape types (landscape5, landscape7, landscape23, landscape24), and plantation forest (landscape6). Surface water is polluted due to aquaculture activities: the content of lead (Pb) reaches 7.21 μg/l beyond the allowable limits, and storms, thunderstorms, flash floods and landslides are also a potential cause of environmental pollution. Contradictions in this sub-region due to natural disasters (storms, tornadoes and sea level rise) have implications for biodiversity conservation in the SUF on Cai Lim and Cong Ngo.

Aquaculture production on Tra Ban Island, Cong Tay (subregion6) accounts for 16.59% (9177.53ha), including landscape production forests landscape2, landscape3, landscape4, landscape8, landscape11, landscape25, landscape28 and landscape28. Sea water pollution and air pollution caused by the aquaculture of the people around the island, salinity (1.32‰) is higher than that of QCVN. These confilcts arise from the direction of expanding cage culture, raft with biotechnology development orientation to preserve the ecosystem.

Subregion7 (sub-area of sea tourism and aquaculture on Canh Cuoc - Ha Mai island): occupies 32.46% (17956.99 ha), including habitat types (landscape20, landscape 21, landscape28); natural forest (landscape7, landscape24), plantation forest (landscape22). Environmental problems occur in water, air and soil: the total dust content is 0.741mg / m^3), 2.47 times as much as QCVN, the processing of jellyfish on the island is increasing. Environmental contamination arises when the mollusk culture (seagulls...), seafood processing is increasingly interested and expanded.

Thus, the characteristics of each subregion are analyzed, the environmental problem is addressed and the cause of the environmental problem is expressed. This result is the basis of implementing space orientation for sustainable development in Van Don District.

3.3. Spatial orientation on the basis of legal and practical basis

Spatial aspects of environmental protection in Van Don District are proposed including 7 subregions: (1) spatial sub-region to prioritize the development of production forest in combination with eco-tourism; (2) The priority space will be developed into an administrative, economic, cultural, medical and education center of Van Don combining marine tourism and environmental protection; (3) Preferential space develops to an airport and becomes a high-class trade and service center catering to tourists' shopping and accommodation needs; (4) Priority space should be given to marine tourism and eco-tourism in combination with high-end aquaculture; (5) priority protected areas of special-use forests of the core zone of Bai Tu Long National Park; (6) Priority space should be given to develop production forests in combination with advanced aquaculture; (7) Space for tourism development, aquaculture combined with Tram biodiversity conservation.

Table 2. Developmental space orientation

Space	Orientation in using	Environmental managing and protecting solutions
Subregion 1	- Developing and expansing of production forests. - Improving the quality of production forests. - Developing Ecotourism.	- Planting additional forest to prevent bank erosion in the north of Dai Xuyen commune, along the Voi Lon river. - Encouraging people to actively care for and protect forests;
Subregion 2	-Developing administrative, economic and cultural centers in combination with tourism and environmental protecting solutions.	- Creating green space along the provincial road on Cai Bau island; - Managing the construction of urban garbage and garbage collection and treatment system; - Making detailed quarterly environmental status report for each coastal zone; - Strictly handling establishments dealing in motels, hotels and processing aquatic products causing environmental pollution; - Upgrading and renovating Cai Rong port (tourism development area, anchorage area).
Subregion 3	- Developing of airports and commercial centers. - Avoiding damaging the estuarine ecosystem.	- Detailed planning of airports for environmental protection; - Building waterway links linking the adjacent areas; - Raising the capacity of management and administration of local authorities;
Subregion 4	Planning to separate the aquaculture area with tourism development along Cai Rong town. - Organizing tours associated with available resources (national park, beach).	- Identifying tourist routes that exploit the advantages of Bai Tu Long Bay; - Planning aquaculture areas far from wharf area; - Strengthening and supplementing mangroves in the area of Van Don bridge (I, II, III) in combination with aquaculture.

Space	Orientation in using	Environmental managing and protecting solutions
Subregion 5	- Preserving core zone of Bai Tu Long National Park. - Protectngof living space for red book animals: white-headed langur;	- Training forest rangers and villagers about the importance of the core zone of Bai Tu Long NP, - Assessing, inventoring and planning of biodiversity conservation; - Developing ecotourism, combining local people with diversified protection; - Establishing sustainable ecotourism models (bathing, sightseeing, exploration, ecology).
Subregion 6	- Planting, exploiting and protecting forests in accordance with current status; - Completing policies to encourage households to plant production forests on the large island of Tra Ban. - Zoning off aquaculture, ensure water in the ponds to meet standards;	- Detailed planning for development of production forests, aquaculture zones; - Developing a communication strategy on environmental protection law for tourism companies and communities; - Organizing the environmental inspection and examination according to the plan.
Subregion 7	Forming a marine eco-tourism area - Cac Can Island, eco-tourism in Bai Tu Long National Park.	- Detailed tourism development planning: sea ecotourism (Ngoc Vung), island eco-tourism (Nui Dat). - Zoning for protection - preserving the area of forest Chien (Tram); - Using economic sanctions for polluting establishments, especially jellyfish processing.

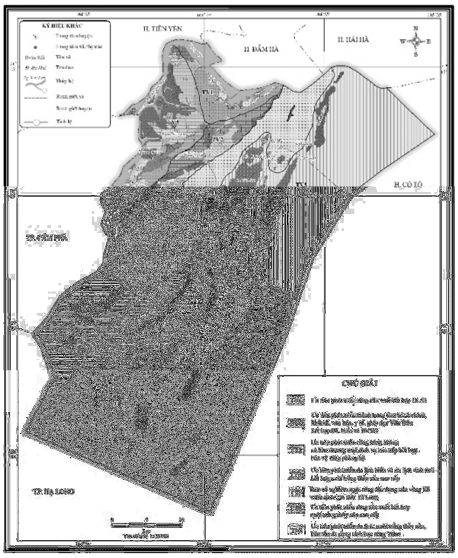

Picture 3*. Map of protection of Van Don District*

Thus, each sub-landscape of human life has its own characteristics, the direction of using and protecting of the environment is to built on the basis of those characteristics. These orientations may be applied to areas with similar human landscapes characteristics, but for the most effective, we need to base on the particular characteristic of each region.

4. CONCLUSION

Human landscape is one of the approaches to solve environmental problems in the sea area. This approach analyzes natural features, human activities and future environmental change trends in the study area. Van Don is an island district of Quang Ninh province with relatively good economic developing status. However, the environment is under pressure from human activities and needs to be paid attention. Based on the analysisof four types and 35 types of research papers, the study identified seven sub-areas: (i) (ii) Dong Xa - Van Yen coastal sub-area; (iii) sub-area of protection forest along the Voi Lon river; (iv) Van Don sub-zone for tourism and aquaculture; (v) Sub-area of special-use forest on the South Island, Ba Mun Island; (vi) sub-zones of production and tourism forests, aquaculture on Tra Ban Island, Cong Tay; (vii) marine tourism and aquaculture on Canh Coc Island - Ha Mai. Since then, specific orientations have been developed for seven subregions to raise awareness of resource using and environmental protecting, and to provide appropriate policies for each territorial unit.

REFERENCES

1. A.G. Ixatsenko (1976), *Natural Landscape and Natural Geographical Base*, (Vu Tu Lap, Trinh Sanh, Nguyen Phi Hanh, Le Trong Tuc), - Science Publishing House, Hanoi
2. Armand (1982), *Landscape Science*, - Science & Engineering Publishing house, Hanoi
3. Dinh Thi Bao Hoa (2005), "Assessing human landscapes in Thanh Tri district, Hanoi serving the orientation of territorial planning", - *Topic QTN05_28 Hanoi University of Science*.
4. Nguyen Cao Huan (2008), "Planning for Environmental Protection in the direction of Sustainable Development at the Provincial and District Levels - Case Study of Uong Bi Town, Quang Ninh Province, Viet Nam", - *The third Viet Nam International Conference "Vietnam: Integration and Development"*, pp.543-555 (Volume IV).
5. Nguyen Cao Huan, Tran Anh Tuan (2002), "Vietnam Classification of Scientific and Technological Citation", - *Scientific Notification of Universities*, Department of Geographic Sciences, Ministry of Education and Training.
6. Nguyen Dang Hoi (2004), "Research and assessment of Kon Tum territorial area for the rational use of land and forest resources", - *PhD thesis*, Hanoi
7. Anne China, Li Anb, Joan L. Florsheimc, Laura R. Laurencioa, Richard A. Marstond, Anna P. Solversona, Gregory L. Simona, Emily Stinsona, Ellen Whole (2016), "Investigating

feedbacks in human–landscape systems: Lessons following a wildfire in Colorado, USA", - Geomorphology Volume 252, 1 January 2016, pp.40-50.

8. Candido A. Cabrido (2009), "Ecological zoning as a policy tool for sustainable development at the local level", - *The East Asian Seas Congress 2009*, Partnerships at Work: Local Implementation and Good Practices" Manila, Philippines, 23-27 November 2009.
9. Çiğdem CanbayTürkyılmaz (2016), "Interrelated Values of Cultural Landscapes of Human Settlements: Case of Istanbul", - *Procedia - Social and Behavioral Sciences*, Volume 222, 23 June 2016, pp.502-509.
10. Justice, Susanne and etc (2018), "Suitability of different landscape metrics for the assessments of patchy landscapes in West Africa", - *Ecological Indicators*, Volume 85, February 2018, Pages 117-127.
11. Gabriel, Santiago.R, Llorenç. P, Paola.M, Yolanda.L (2018), "The onset of islandscapes in the Balearic Islands: A study-case of Addaia (northern Minorca, Spain)", - *Palaeoecology Available online*, 21 February 2018.
12. Lubo G., Lei Y., Yi R., Zhewei C. Huaxing B. (2011), "Spatial and Temporal Change of Landscape Pattern in the Hilly-Gully Region of Loess Plateau", - *Procedia Environmental Sciences* (8), pp.103-111.
13. Mawere, M. etal (2012), *Memoirs of an unsung legend, Langaa RPCIG: Bamenda.*
14. World Heritage Committee (2008), *Cultural Landscape: The Challenges of Conservation.* Published in 2003 by UNESCO World Heritage Centre.

NGHIÊN CỨU ĐẶC ĐIỂM PHÂN HÓA CẢNH QUAN NHÂN SINH PHỤC VỤ ĐỊNH HƯỚNG BẢO VỆ MÔI TRƯỜNG HUYỆN VÂN ĐỒN, TỈNH QUẢNG NINH

Tóm tắt: *Lý luận về cảnh quan nhân sinh là một cách tiếp cận nhằm kết nối các giá trị của tự nhiên và xã hội trong giải quyết các vấn đề phát triển của lãnh thổ; đặc biệt trong xây dựng định hướng bảo vệ môi trường. Bài báo trình bày sự phân hóa lãnh thổ của 04 nhóm dạng và 35 dạng cảnh quan, tạo tiền đề cho xác lập 07 tiểu vùng cảnh quan cho khu vực huyện Vân Đồn, tỉnh Quảng Ninh. Trên cơ sở xác định: (i) đặc trưng cảnh quan nhân sinh, (ii) vấn đề môi trường và đa dạng sinh học, (iii) mâu thuẫn phát triển; nghiên cứu đã đưa ra những đề xuất định hướng bảo vệ môi trường cụ thể cho từng tiểu vùng. Theo đó, cách tiếp cận cảnh quan nhân sinh không chỉ cung cấp cơ sở khoa học phục vụ định hướng phát triển bền vững của lãnh thổ, mà còn cho phép ứng dụng giải quyết các mâu thuẫn kinh tế-xã hội phát sinh trong quá trình khai thác lãnh thổ.*

Từ khóa: *Cảnh quan nhân sinh, tiểu vùng, bảo vệ môi trường, huyện Vân Đồn, tỉnh Quảng Ninh.*

USING AHP METHOD TO EVALUATE AND RANK THE IMPLEMENTATION OF SUSTAINABLE DEVELOPMENT GOALS IN EAST NORTHERN, VIETNAM.

Mai Huong Lam[1], Bui Minh Tuyen[2], Nguyen Thi Quynh Dung[3]
[1] Ha Noi university of natural resources and environment.
[2,3] Ha Noi Metropolitan university

Abstract: *Performing the United Nations' Sustainable Development Goals is necessary because it helps countries reducing poverty, developing the economy and improving the environment (The Global Goals, 2015). However, there is no evaluation tool to implement the United Nations Sustainable Development Goals at the scale of province. The ranking implementation of Sustainable Development Goals is necessary. The nations are attention about peace and security in recent times; climate change has many affect on people and the environment; The aims to develop comprehensively in the present society but must ensure the continued development in the distant future and more.The Sustainable Development Goals have a response that demand. (The United Nations, 2015). Viet Nam is considered to be implementing some of its National Sustainable Development Goals (The United Nations, 2015). If Vietnam is to earnestly implement its national objectives, a tool that can monitor its performance in smaller units. Therefore, the paper select the Northeast region is a particular example of this. The provinces affected by topography, weather, and ethnic diversity. In this paper, we use ten sub-criteria and use the analytic hierarchy process (AHP) technique to calculate the provincial indexes. The study showed Cao Bang, Thai Nguyen, and Yen Bai is performed well the objectives of sustainable development and Bac Giang is facing many difficulties in implementing. That output will be used by the policymakers to adjust plans and decisions in the future.*

Keywords: *Sustainable development goals, AHP, North East region, Viet Nam.*

Email: bmtuyen@daihocthudo.edu.vn
Received 21 May 2018
Accepted for publication 1 June 2018

1. INTRODUCTION

The United Nations Sustainable Development Goal are from 2015 to 2030 identifies issues facing people more and more. The countries need to have a system for monitoring the implementation of the United Nations Sustainable Development Goals (The United Nations, 2015). The development objective was previously called Millennium Development Goals (MDGs). The results are very positive, the particularly as extreme poverty has halved; 2.3 billion people have access to clean drinking water; Gender inequality among boys and girls are eliminated day by day;...(Prokop, 2015). However, apart from the results, at the global level, many indicators have not been completed. Currently, there are still about 1 billion people living below $ 1.25 a day, 800 million people do not have enough food (World Bank, 2015). Humanity is still facing many challenges such as environmental degradation, resource depletion, climate change, disease, employment, territorial disputes, terrorism, ethnic conflicts, and religion (The United Nations, 2015). It can be said that economic, social and environmental issues continue to be priorities in the SDGs, reflected in the presence of all targets and targets. According to a report by the Ministry of Planning and Investment (MPI), Vietnam has achieved significant results in the implementation of the Millennium Development Goals (MDGs), especially for the objectives of poverty reduction, gender equality, and education. In particular, Vietnam has eliminated extreme poverty and hunger since 2002 (MDG 1). Vietnam has also primarily fulfilled the goal of gender equality and empowerment for women; some dangerous epidemics have initially prevented the spread of HIV and are on the verge of achieving the MDG goals of reducing child mortality (MPI, 2014). With such results, Vietnam is considered a good country to achieve the goals of sustainable development (World Bank, 2015). However, these results are limited to the national level, and studies on the assessment of sustainable development goals in smaller units are not available. Therefore, in this paper we use the AHP method to assess the assessment of sustainable development goals in the provinces. In the world there have been studies using AHP in evaluating the implementation of SDGs. Nana Poku and Jim Whitman (2011) believe the holistic of the goals will bring a standard and motivation to ensure the best implementation of the SDGs [7]. The results are a motivating force for future development [8]. In 2016, Casey Stevens and Norichika Kanie published a study " The transformative potential of the Sustainable Development Goals (SDGs)", they affirm the flexibility of the SDGs [9]. Moreover, a successful implementation policy on sustainability to rely on local conditions with a suitable model. In over the years, the implementation of SDGs in the region was evaluated and they (author) believes that important to the country's sustainable development [10], [11], [12]. In 2010, the study by Rajiv Bhatt and partner "Analytic Hierarchy Process Approach for Criteria Ranking of Sustainable Building Assessment: A Case Study" provide a formula for evaluating SDGs of the United Nations by the AHP method [13]. In 2012, Yağmur Kara and Aylin Çiğdem Köne announced the study name is

"The Analytic Hierarchy Process (AHP) for assessment of regional environmental sustainability" clarify of the AHP method superiority in the assessment and measurement SDGs [14]. Therefore, the assessment and ranking of SDGs using AHP method in the North East are necessary. The results of the assessment and ranking of SDGs in the North East will be: (i) Ranking the implementation of the United Nations Sustainable Development Goal in the region. (ii) Identify the problem area.

2. MATERIAL AND METHOD

2.1. Sustainable development goals

The UN's Sustainable Development Goals is like a leader's promise to all people in the world that all nations will work together to build a better world. The orientation "for a world without leaving behind" with 193 nations committed to seriously implementing the United Nations' Sustainable Development Goals. The UN's sustainable development goals include 17 bold targets over the next 15 years. There are 17 objectives and 169 sub-criteria to ensure economic, social and environmental sustainability. The countries need to make a great effort to build a better future for the people and for all nations to live in a cooperative, peaceful and prosperous environment. Sustainable development goals bring about social stability, a developed economy, and a clean environment. For Vietnam, the Sustainable Development Goals are bringing positive results, but that is not clarity at the smaller units. For the North East region, some indicators in the Sustainable Development Goals do not change. In this paper, we will study the ten most significant changes in the area. These are our selective targets.

We consider and propose three main groups: economic, social and environment. These are the groups that different between provinces in the region. We selected ten sub-criteria based on the performance of the region. In the economic group, we selected three sub-criteria with large differences across provinces. There are three sub-criteria for "sustaining economic growth in accordance", "achieving higher levels of economic productivity" and "promoting development-oriented policies that support productive activities". For the social group, we realize that poverty is under control but the risk of re-poverty of the provinces is high. We select four sub-criteria that can reduce the social burden of the area. For these four sub-criteria we have considered the possibility of achieving poverty reduction targets, improving education and social security of the provinces. And the environmental group selected by our three indicators clearly distinguishes the provinces. Finally, we evaluate and rank the implementation of the SDGs in the provinces.

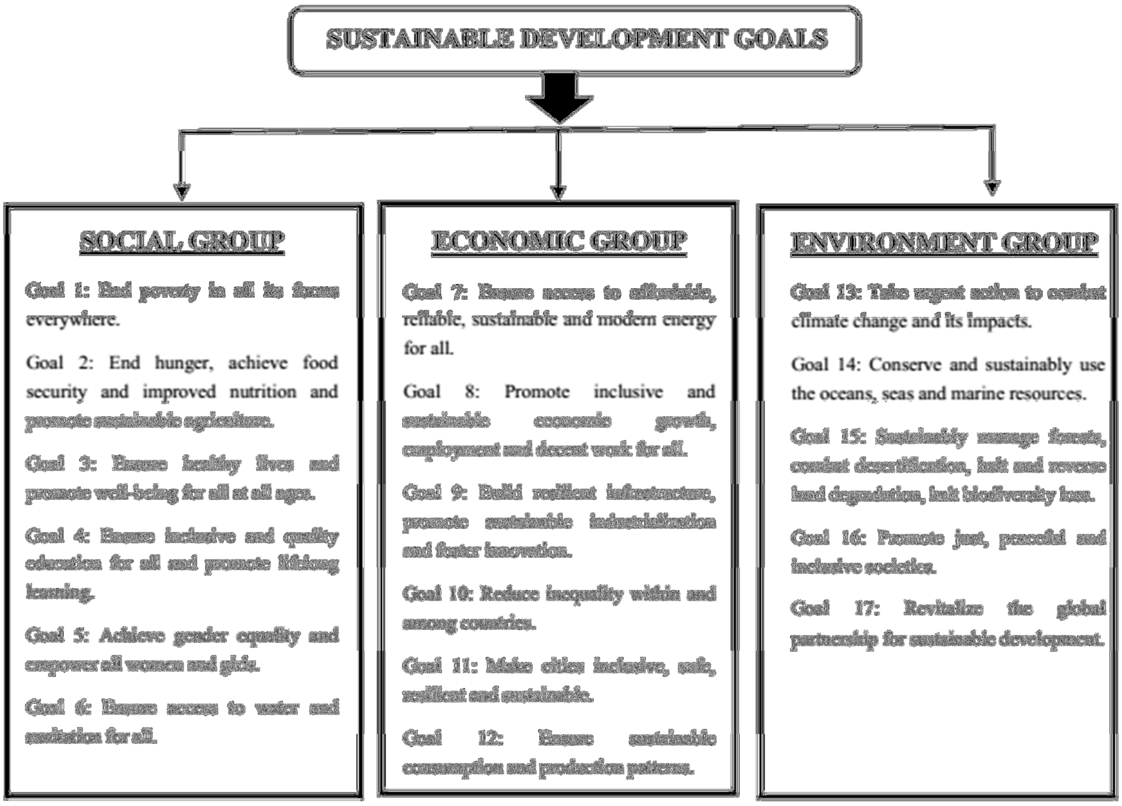

Figure 1: Location of selected area (MSc Blofeld)

2.2. Study area

We chose the Northeast as a research area. Northeast is one of the regions of Vietnam. It is at 21°42'5" North, 106°13'17" East [1]. The western side is limited by the Red River valley, the northern part junction with Vietnam-China border, the east is adjacent to the sea, the southwest is bordered by the Midwest. Although the mountains are low but the terrain here is very diverse [2]. Especially, the limestone karst topography is present in many places [3]. The terrain is low and the plains wide, creating conditions for the river system to develop and spread throughout the region [4]. The Northeast has many rivers flow through, including the major river of the Red, Chay, Lo, Gam (the Red rivers system), Cau, Thuong, Luc Nam (in Thai Binh river system), Bac Giang, Ky Cung...[5] The rivers usually have wide valleys, small slopes, relatively large amount of silt, two floods and dry seasons are very clear [6]. It includes the provinces of Phu Tho, Ha Giang, Tuyen Quang, Cao Bang, Bac Kan, Thai Nguyen, Lang Son, Bac Giang, Lao Cai, Yen Bai and Quang Ninh [7]. The most diverse ethnic group in the country with about 30 ethnic groups. The Northeast, which Kinh people for 66.1% of the total population; Tay people for 12.4%; the Nung group for 7.3%; The Dao group for 4.5%; The H'Mong group for 3.8% [8]. To a report by the General Statistics Office of Vietnam (2015), the provinces have tried to solve problems through SDGs. But it is not thoroughly. Here, the area is at risk of falling back into poverty in some provinces; the area of forest is preserved and restored to a limited extent [9]. However, the economic development potential of the region is huge, natural resources are diversity, marine tourism and seawards exploitation are developing.

2.3. Method

2.3.1. Analytical Hierarchy Process (AHP)

The Analytic Hierarchy Process (AHP) is a multi-criteria decision-making approach that can be used for solving complex opinions of the stakeholders on only one assessment but also considering the different criterion at the same time, which can not be done by normal decision- unstructured problems. It helps to capture both qualitative and quantitative aspects of a decision problem and provides a powerful yet simple way of weighing the decision criteria, thus reducing bias in decision-making (Saaty, the 1970s; Georgiou et al., 2012; Al-Abadi et al., 2016). To define the weight of layers target, the study used results of research works, expert's opinions and combined with Analytical Hierarchy Process (AHP) (Saaty T.L., 1980) method. The comparison of the criteria's importance was based on the actual density variation of the different indicators. The more significant variation is, the more critical these criteria affect perform SDGs. AHP method solves the problem with four necessary steps:

Step 1: Construction of Pairwise Comparison Matrices based on Experts opinion consultation. We can construct judgment matrices for each Selection criterion. This step evaluates the performance of each possible alternative to the other.

Selection criteria need to be related. This task is accomplished by employing the Scale Of Relative Importance (Saaty, 1980). Saaty's scale of relative importance is shown in the following table:

Table 1: *Experts opinion matrix (in case applying for 7 factors, A1, A2,… A7 is selection criterion) (Saaty, 1980)*

	A1	**A2**	**A3**	**A4**	**A5**	**A6**	**A7**
A1	1	A12	A13	A14	A15	A16	A17
A2	1/A8	1	A23	A24	A25	A26	A27
A3	1/A13	1/A23	1	A34	A35	A36	A37
A4	1/A14	1/A24	1/A34	1	A45	A46	A47
A5	1/A15	1/A25	1/A35	1/A45	1	A56	A57
A6	1/A16	1/A26	1/A36	1/A46	1/A56	1	A46
A7	1/A17	1/A27	1/A37	1/A47	1/A57	1/A67	1

Step 2: Extraction of Priority Vectors aims to give a Consistency Ratio matrix: Upon creating alternative judgment matrices for each selection criterion as well as the criteria judgment matrix, the analyst then proceeds to the next step in the analytic hierarchy process, which is to extract the relative importance implied by each matrix. The crudest method of principal eigenvector attainment is to merely sum the elements in each row and collum ($\sum_1^n a_{ij}$) of the matrix and then normalize them by dividing each sum by the total of all row sums.

Step 3: Consistency Evaluation. This step in the algorithm ensures that each matrix fits and therefore the comparison values do not violate intended by the analyst.

+ The maximum or principal eigenvalue (λmax) is estimated as the average of the entries inconsistency vector y and given by the formula (with n is the total number of selection criterion):

$$\lambda_{\max} = \frac{\sum_1^n y}{n}$$

+ This maximum eigenvalue is then used to compute the matrix's consistency index (CI) using:

$$CI = \frac{\lambda_{\max} - n}{n-1}$$

+ The final step in the consistency evaluation is to examine the ratio of the calculated consistency index. And the random index (RI) derived from the number of matrix activities. Random indices for varying matrix sizes are shown in the following table:

Table 2: *Random Indices (Saaty, 1980)*

n	1	2	3	4	5	6	7	8	9	10	11	12	13	14	15
RI	0	0	0.58	0.9	1.12	1.24	1.32	1.41	1.45	1.49	1.51	1.48	1.56	1.57	1.59

The ratio of CI to RI is the consistency ratio (CR):

$$CR = \frac{CI}{RI}$$

A consistency ratio of 0.10 or less is acceptable. If the consistency ratio is higher than 0.10, the weight assignments must be re-evaluated within the matrix violating the consistency limits.

Step 4: Determining weight by calculating the ratio of the components in rows and columns:

$$\mathrm{W}_{\mathrm{ij}} = \frac{a_{\mathrm{ij}}}{\sum_{1}^{n} a_{\mathrm{ij}}}$$

This value allows comparing the composition ratio of the plan, see the factors that accounted for what percentage ratio of the sum of the components.

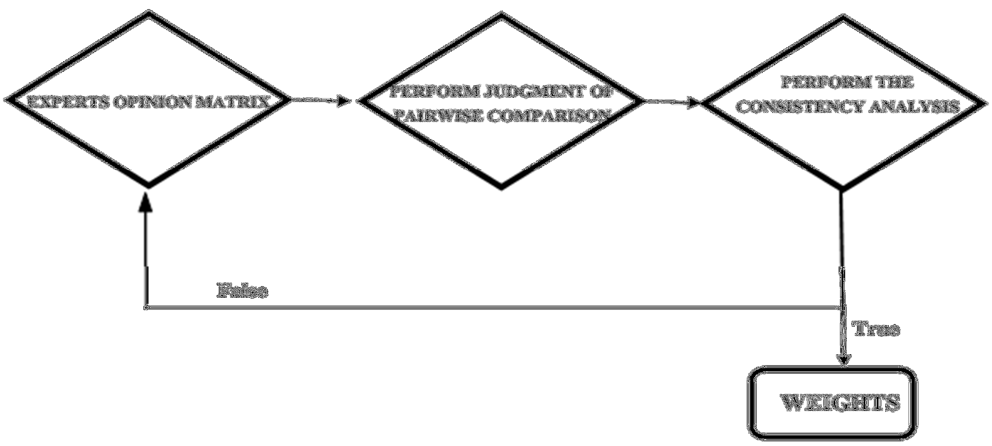

2.3.2. Framework

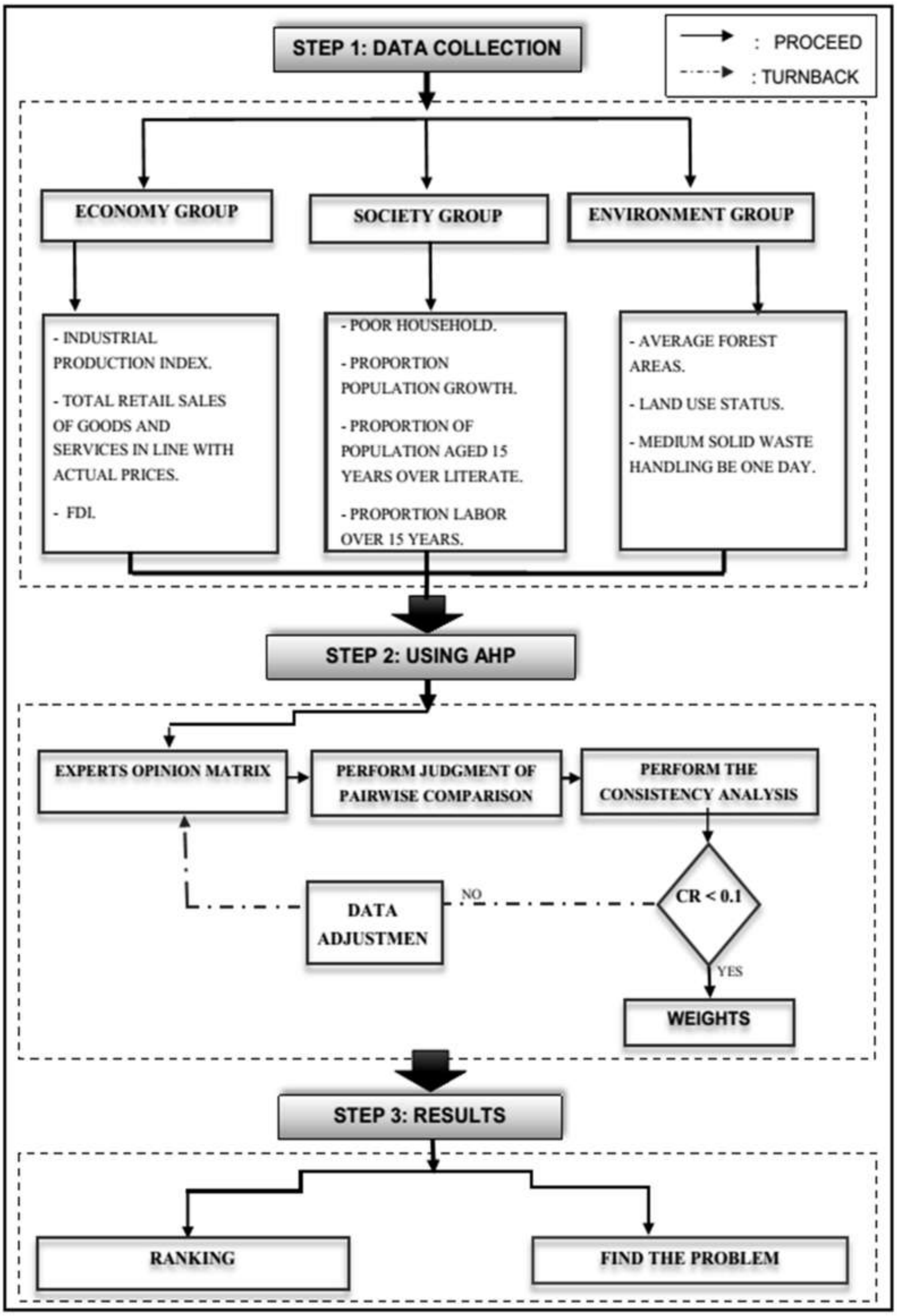

Figure 1: Framework of paper (Established by author)

The paper was carried out by following three main steps:

The first step in the assessment process is to gather information about the data source. The data are organized into three economic, social and environmental groups.

The second step's target was to find out the SDGs can be implemented in the Northeast. AHP approach was implemented as a multi-criteria decision-making to evaluate and ranking implement sub-criteria in SDGs. We find the comparative weight among the attribute of the decision elements by pairwise comparison matrix.

The third step aims to evaluate and rank. As a final result, evaluate and ranking implement SDGs in Northeast, Vietnam.

3. RESULTS

3.1. Identify the sub-criteria

In this paper, we have selected and focused on the ten sub-criteria that differ widely among provinces in the Northeast. This sub-criteria are broken down into three economic, social and environmental groups. These are three groups that directly affect the achievement of sustainable development goals in the provinces. The first is the industrial production index, we can consider the overview of industrial activity. It is not affected by price volatility and so we can evaluate purely industrial activity through it. If we evaluate this sub-criteria, there will be differences in the economic situation among the provinces. Second, the sub-criteria is total retail sales of goods and services in line with actual prices, which is an important indicator to assess the growth in the region - especially the service sector. The third is increase foreign direct investment (FDI), with this sub-criteria, we can see the regional attractiveness of foreign investment sources. The fourth sub-criteria is to reduce the proportion of poor households, society affected by poor households and the burden of society is higher. Fifth is the sub-criteria to reduce the proportion of population growth, the population is one of the factors constituting the society. The uncontrolled population increase will bring about many problems that are difficult to solve in society. The six of the sub-criteria is increased the literacy rate of the population aged 15 years and over. The seven, the sub-criteria is to reduce the rate of workers over 15 age. These are the two sub-criteria that best illustrate the social status of the provinces. The three sub-criteria in the environmental group best illustrate the province's dynamics for forest and land and the management of solid waste in the province. As a result, the assessment of the SDGs in the North East will be most general.

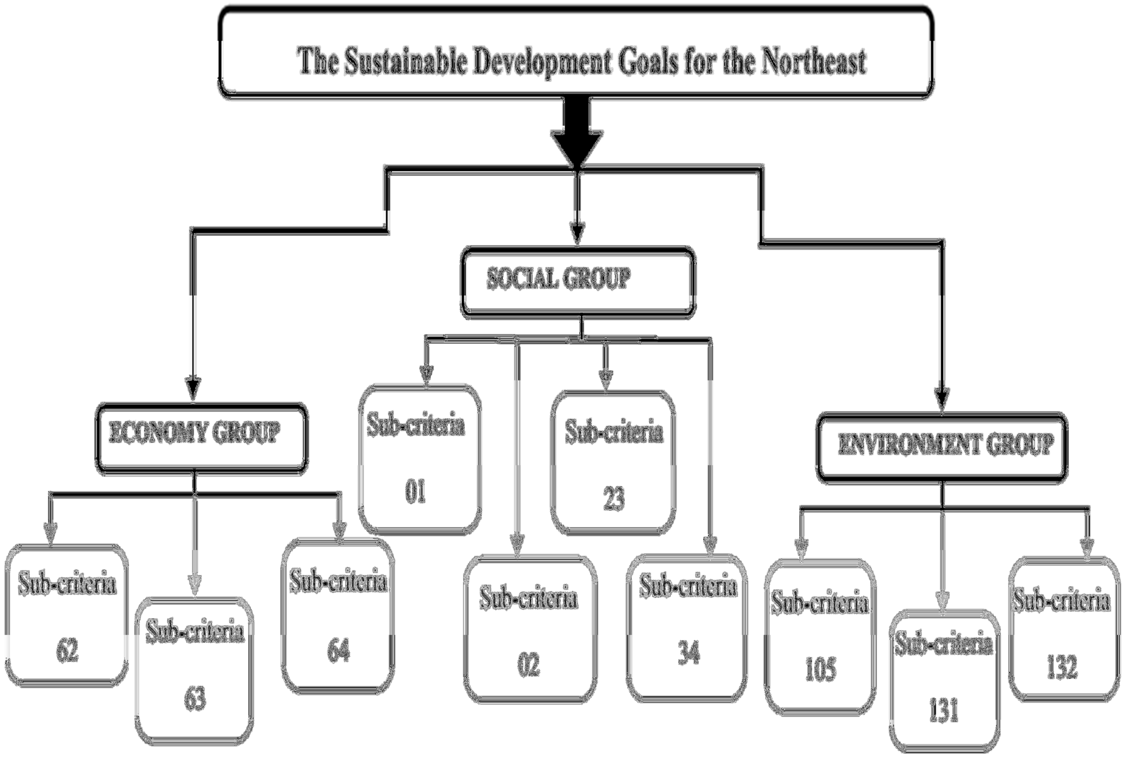

3.2. Creating chart ranking of provinces implementing the Sustainable Development Goals

Based on the appropriateness of the sub-criteria, the matrix to calculate the local weight and general weight of the area. Correlation matrix between economic, social and environmental factor. Thus, we have relationships between components.

	Economy	**Society**	**Environment**
Economy	1	$\frac{1}{5}$	$\frac{1}{2}$
Society	5	1	3
Environment	2	$\frac{1}{3}$	1

Figure 2: *The correlation of Economics, Society, and the Environment (Established by author)*

Local weight level I:

	Economy	Society	Environment
Local weight	0.122	0.648	0.230

Local weight level II:

	Industrial production index	GRDP	FDI
Industrial production index	1	1/8	1/3
GRDP	8	1	3
FDI	3	1/3	1

Figure 3*: The correlation of sub-criteria in Economics groups (Established by author)*

	Poor household	Population	Literate person	Young workers
Poor household	1	1/5	1/3	1/2
Population	5	1	2	3
Literate person	3	1/2	1	4
Young workers	2	1/3	1/4	1

Figure 4*: The correlation of sub-criteria in Society groups (Established by author)*

	Acreage forest	Acreage land used	Solid waste recycling
Acreage forest	1	1/5	1/3
Acreage land uses	5	1	3
Solid waste recycling	3	1/3	1

Figure 5*: The correlation of sub-criteria in Environment groups (Established by author)*

The calculation result of overall weight:

Industrial production index	GRDP	FDI	Poor Househol-d	Populatio-n	Literat-e person	Young worke-rs	Acreage forest	Acreage land uses	Solid waste recycli-ng
0.082	0.682	0.236	0.078	0.420	0.280	0.130	0.104	0.638	0.258

Figure 6: *The calculation result of overall weight (Established by author).*

We have established a table for assessing sub-criteria of provincial indicators based on collected data.

Criteria	Low	Medium	High
Industrial production index	< 50	50 -150	> 150
GRDP	< 10.000.000	10.000.000 –20.000.000	> 20.000.000
FDI	< 200	200 – 5.000	> 5.000
Poor household	< 10	10 - 20	> 20
Population	< 1	1 – 1.5	> 1.5
Literate person	< 80	80 - 90	> 90
Young worker	< 60	60 - 65	> 65
Acreage forest	< 5	5 - 10	> 10
Acreage land uses	< 500	500 - 700	> 700
Solid waste recycling	<100	100 - 200	> 200

Figure 07*: The determine the level of each sub-criteria based on the data of the region.*

Sub-criteria were classified based on the input data in the table. This study ranked 1 -5 indicating SDGs level of implementation in the province: 5 indicates high, 3 - medium, 1 - low.

We have a chart showing SDGs level of implementation in the province

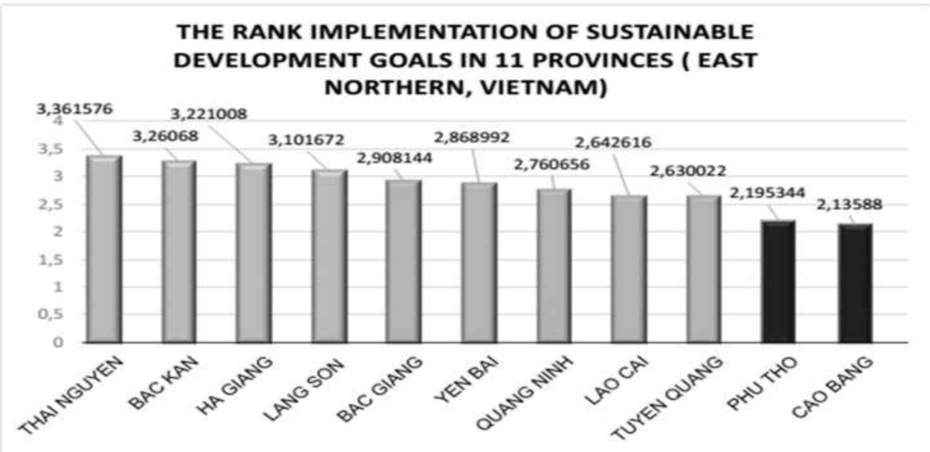

Table 01: The ranking implementation of Sustainable Development Goals in 11 provinces (East Northern, Vietnam)

The ranking results we get are generalized. It shows the situation that the area is experiencing. We recognize that the Thai Nguyen province is doing well of the United

Nations Sustainable Development Goals. Thai Nguyen is the center of education and training of the former North Vietnam and the northern midland today. The education and training system has 4 universities, 7 vocational schools, 6 technical workers schools, 19 laboratories, campuses, sub-institutes and research centers standards.The province has completed universal primary education at the right age and universal secondary education. The rate of raising children in the age group at all levels and levels is higher and higher than the national average. The size of general education, the network of schools continues to develop in accordance with the requirements of universal education, raising people's intellectual. The system of universities, colleges, vocational secondary schools, job training centers, vocational training centers, and continuing education centers have made important advances. Thai Nguyen is rich in mineral resources and has a number of industrial zones. Until now, the Thai Nguyen economy is still an economic structure of agriculture, forestry, and industry. The province is especially important as a traffic hub connecting the Northeastern provinces with the Red River Delta and the southern provinces.

We recognize that Cao Bang has not well implemented the Sustainable Development Goals. As a mountainous province in the highland border, far from the major economic centers of the Northeast and the country, Cao Bang has three border gates: Ta Lung, Hung Quoc, and Soc Ha. This is an important advantage, creating conditions for the province to exchange economic with outside, especially China. However, Guangxi (China) is a poor province, large population, strong in the consumer market but also fierce competition in the relationship of purchase, quality goods, prices into. In the country, Cao Bang can also exchange with some provinces of Lang Son, Bac Kan ... but due to mountainous terrain, traffic is poor so the level of development only to a certain extent. Moreover, the exchanges are mainly by road, so it also affects the socio-economic development of Cao Bang. The economy of Cao Bang goes up with a low starting point, many seriously unbalanced and facing great challenges. The main economic structure in agriculture, while the area of cultivated land is limited. The majority of food crops are a monoculture.The province adjacent to the northern critical economic region is very convenient for economic development and cultural exchange with other countries in the region. However, the population of the region is growing fast; the control is not good. As such, we have provided very objective assessment results to identify the issues that the region is facing. From here, strategic decision makers can make decisions that are appropriate for the province and country.

3.3. Conclusions and recommendations

3.3.1. Conclusions

The ranking implementation of Sustainable Development Goals are necessary. Vietnam is developing day by day. So, the SDGs are a suitable direction. The methodology used in this article is based on indicators for the economic, social and environmental factors of the provinces. This method is used in an effort to know the implementation of sustainable development goals in the provinces. From here, it is possible to find the difficulties that the province has encountered. Ten sub-criteria have been reviewed and researched to evaluate the implementation of SDGs in the provinces. The results of the present study clearly indicated that the implementation of SDG in the provinces is not good. We need more efforts in improving the difficulties from the provinces.

3.3.2. Recommendations

The AHP method clearly demonstrates the superiority of this paper. We have obtained accurate results and an overview. We recognize the problems that provinces need to address. Poverty issues influenced the development of society and the economy of the province. Some provinces already have actions to reduce poverty as Quang Ninh, Thai Nguyen. However, it should not the thorough risk of poverty is still high. General economic development of the province is not strong, it needs a capital investment from the state and abroad. For education, should promote the provision of teaching equipment. Risk forest area shrunk, it should be restored and preserved in the shortest time. The waste to collection and classification in order to meet reasonable safety handling. The problem of the area having no new but requires sustainable intervention. Therefore, we recommend using the AHP in evaluating and ranking the implementation of the UN Sustainable Development Goals in the provinces.

REFERENCES

1., 2., 3., 4., 5., 6., 7., 8., 9. Wikipedia (2017). Northeast (Vietnam). September 2017.

10. Institute of Anthropology, 2014
11. Wikipedia (2017). Economic. Northeast (Vietnam). September 2017
12. Dorine E Van Norren (2012). The Third World Quarterly. The Wheel of Development: the Millennium Development Goals as a communication and development tool (17 May 2012). Pages 825-836.
13. Nana Poku & Jim Whitman (2011). Third World Quarterly. The Millennium Development Goals: challenges, prospects, and opportunities (23 Feb 2011). Volume 32, Pages 3-8.
    http://www.tandfonline.com/doi/full/10.1080/01436597.2011.543808?src=recsys
14. SDG Funds UNDP (2017). Sustainable Development knowledge platform. Prosperity in Action: Results from the Sustainable Development Goals Fund (10 July 2017).
    https://sustainabledevelopment.un.org/index.php?page=view&type=20000&nr=2993&menu=2993
15. Casey Stevens (2016). The transformative potential of the Sustainable Development Goals (SDGs). International Environmental Agreements: Politics, Law and Economics, Volume 16 (June 2016), Issue 3, pp 393–396.

16. Vladimir Gurman (2000). Design of Sustainable Development Strategy for a Region. Implementing Ecological Integrity, NAIV, volume 1. (2000), pp 347-349.
17. MARC (2017). Serving the Kanas City Metropolitan Area. Regional Plan for Sustainable Development (March 2017).
18. The United Nations (2015). United Nations Regional Commissions New York Office. Regional Commissions and Climate Change (Wednesday, November 01, 2015).
19. The United Nations (2015). United Nations Regional Commissions New York Office. Regional Forums on Sustainable Development. (Wednesday, November 01, 2015).
20. Rajiv Bhatt, J.E.M. Macwan, Darshana Bhatt and Vipul Patel (2010). Analytic Hierarchy Process Approach for Criteria Ranking of Sustainable Building Assessment: A Case Study. World Applied Sciences Journal 8 (2010).
21. Yağmur Kara, Aylin Çiğdem Köne (2012). The analytic hierarchy process (AHP) approach for assessment of regional environment sustainability. Department of Economics, Muğla University, 48000, Muğla, Turkey.

* Worldbank (2017). Overview Vietnam. The World Bank In Vietnam (Apr 13, 2017).
http://www.worldbank.org/en/country/vietnam/overview

* The United Nations (2015)
http://www.un.org

SỬ DỤNG PHƯƠNG PHÁP AHP CHO CÔNG TÁC ĐÁNH GIÁ VÀ XẾP HẠNG CÁC MỤC TIÊU PHÁT TRIỂN BỀN VỮNG CỦA LIÊN HỢP QUỐC TẠI KHU VỰC ĐÔNG BẮC, VIỆT NAM

Tóm tắt: *Thực hiện Mục tiêu Phát triển Bền vững của Liên hợp quốc là cần thiết vì nó giúp các nước giảm đói nghèo, phát triển kinh tế và cải thiện môi trường (Mục tiêu Toàn cầu, năm 2015). Tuy nhiên, không có công cụ đánh giá để thực hiện Mục tiêu Phát triển Bền vững của Liên Hiệp Quốc ở quy mô của tỉnh. Việc thực hiện xếp hạng các Mục tiêu Phát triển Bền vững là cần thiết. Các quốc gia đang đặt chú ý của mình đến hòa bình và an ninh trong thời gian gần đây; biến đổi khí hậu có nhiều ảnh hưởng đến con người và môi trường; Mục tiêu phát triển toàn diện trong hiện tại mà phải đảm bảo sự phát triển liên tục trong tương lai xa và hơn nữa Các Mục tiêu Phát triển Bền vững có đáp ứng nhu cầu. (Sự đoàn kết Quốc gia, năm 2015). Việt Nam được coi là đang thực hiện một số Chiến lược Quốc gia Mục tiêu Phát triển Bền vững (Liên Hiệp Quốc, năm 2015). Nếu Việt Nam nghiêm túc thực hiện các mục tiêu quốc gia, một công cụ có thể giám sát hiệu quả hoạt động của nó các đơn vị. Do đó, bài báo chọn khu vực Đông Bắc là một ví dụ điển hình trong vấn đề này. Các tỉnh tại khu vực bị ảnh hưởng bởi địa hình, thời tiết, và sự đa dạng sắc tộc. Trong bài báo này, chúng tôi sử dụng mười tiêu chí phụ và sử dụng kỹ thuật phân cấp phân tích (AHP) để tính toán các chỉ số của tỉnh. Nghiên cứu cho thấy Cao Bằng, Thái Nguyên và Yên Bái đang thực hiện tốt các mục tiêu phát triển bền vững và Bắc Giang đang phải đối mặt rất nhiều khó khăn trong việc thực hiện. Kết quả này sẽ được các nhà hoạch định chính sách sử dụng điều chỉnh kế hoạch và quyết định trong tương lai.*

Từ khóa: *Mục tiêu phát triển bền vững, AHP, khu vực Đông Bắc, Việt Nam.*

THỂ LỆ GỬI BÀI

1. *Tạp chí Khoa học* là ấn phẩm của Trường ĐH Thủ đô Hà Nội, công bố các công trình nghiên cứu và bài viết tổng quan trong nhiều lĩnh vực khoa học. Tạp chí được xuất bản định kì, mỗi số về một lĩnh vực cụ thể: Khoa học Xã hội và Giáo dục; Khoa học Tự nhiên và Công nghệ.

2. Tác giả có thể gửi toàn văn bản thảo bài báo cho Tổng biên tập, Phó Tổng biên tập hoặc biên tập viên theo địa chỉ email ghi ở dưới. Tất cả bản thảo bài báo gửi công bố đều được thẩm định về nội dung khoa học bởi các nhà khoa học chuyên ngành có uy tín. Tạp chí không nhận đăng các bài đã công bố trên các ấn phẩm khác và không trả lại bài nếu không được duyệt đăng. Tác giả bài báo chịu hoàn toàn trách nhiệm về pháp lí đối với nội dung kết quả nghiên cứu được đăng tải.

3. Bố cục bài báo cần được viết theo trình tự sau: *tóm tắt* (nêu ý tưởng và nội dung tóm tắt của bài báo); *mở đầu* (tổng quan tình hình nghiên cứu, tính thời sự của vấn đề, đặt vấn đề); *nội dung* (phương pháp, phương tiện, nội dung nghiên cứu đã thực hiện); *kết luận* (kết quả nghiên cứu, hướng nghiên cứu tiếp theo) và *tài liệu tham khảo*.

   Bài báo toàn văn không dài quá 10 trang đánh máy trên khổ giấy A4, phông chữ Times New Roman (Unicode), cỡ chữ (Size) 12 thống nhất cho toàn bài, lề trái 3 cm, lề phải 2 cm, cách trên, cách dưới 2.5 cm, giãn dòng (Multiple) 1.25. Các thuật ngữ khoa học và đơn vị đo lường viết theo quy định hiện hành của Nhà nước; các công thức, hình vẽ cần được viết theo các ký hiệu thông dụng; tên hình vẽ đặt dưới hình, tên bảng, biểu đồ đặt trên bảng. Khuyến khích các bài sử dụng chương trình LaTex với khoa học tự nhiên, công thức hóa học có thể dùng ACD/Chem Sketch hoặc Science Helper for Word. Bài báo phải có tóm tắt bằng tiếng Việt và tiếng Anh. *Tóm tắt* viết không quá 10 dòng. *Tóm tắt tiếng Việt* đặt sau tiêu đề bài báo và tên tác giả, *tóm tắt tiếng Anh* gồm cả tiêu đề bài báo đặt sau *tài liệu tham khảo*. Các tên nước ngoài được ghi bằng kí tự Latinh. Cuối bài có ghi rõ cơ quan công tác, số điện thoại, địa chỉ email của tác giả.

4. Phần *Tài liệu tham khảo* xếp theo thứ tự xuất hiện trong bài báo và sắp xếp theo mẫu dưới đây:

   1. John Steinbeck (1994), *Chùm nho phẫn nộ* (Phạm Thủy Ba dịch, tập 2), - Nxb Hội nhà văn, H., tr.181.
   2. Bloom, Harold (2005), *Bloom's guides: John Steinbeck's The Grapes of Wrath*, New York: Chelsea House, pp.80-81.
   3. W.A Farag, V.H Quintana,. G Lambert-Torres (1998), "A Genetic-Based Neuro-Fuzzy Approach to odelling and Control of Dynamical Systems", *IEEE Transactions on neural Networks Volume*: 9 Issue: 5, pp.756-767.

Phòng Tạp chí - Trường Đại học Thủ đô Hà Nội
Số 98, Dương Quảng Hàm, Cầu Giấy, Hà Nội
Tel: 024.3.767.1409; Fax: 024.3. 833.5426
Email: tapchikhoahoc@daihocthudo.edu.vn